3.17 Assessment of CT Girder Load Distribution and Web Buckling through Field Load Testing and Finite-Element Analysis

Final Report
May 2024

Principal Investigator: William Davids

Department of Civil and Environmental Engineering
University of Maine

Authors
Jon Pinkham BS, EI
William Davids PhD, PE
Andrew Schanck PhD, PE

Sponsored By
Transportation Infrastructure Durability Center
MaineDOT

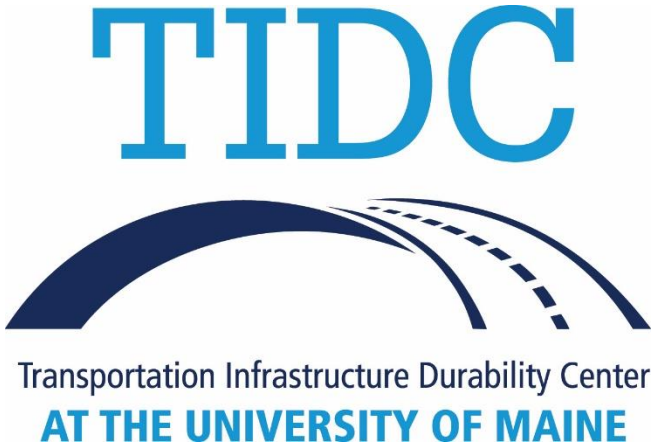

A report from
University of Maine
Department of Civil and Environmental Engineering
5711 Boardman Hall
Orono, ME 04469
Phone: 1-(207)-581-2171
Website: https://civil.umaine.edu/

About the Transportation Infrastructure Durability Center

The Transportation Infrastructure Durability Center (TIDC) is the 2018 US DOT Region 1 (New England) University Transportation Center (UTC) located at the University of Maine Advanced Structures and Composites Center. TIDC's research focuses on efforts to improve the durability and extend the life of transportation infrastructure in New England and beyond through an integrated collaboration of universities, state DOTs, and industry. The TIDC is comprised of six New England universities, the University of Maine (lead), the University of Connecticut, the University of Massachusetts Lowell, the University of Rhode Island, the University of Vermont, and Western New England University.

U.S. Department of Transportation (US DOT) Disclaimer

Acknowledgements

Funding for this research is provided by the Transportation Infrastructure Durability Center at the University of Maine under grant 69A3551847101 from the U.S. Department of Transportation's University Transportation Centers Program. The MaineDOT provided support for and assisted with all field live load testing documented herein.

Technical Report Documentation Page

1. Report No.	**2. Government Accession No.**	**3. Recipient Catalog No.**
4 Title and Subtitle 3.17 Assessment of CT Girder Load Distribution and Web Buckling through Field Load Testing and Finite-Element Analysis		**5 Report Date** 5/10/2024 **6 Performing Organization Code**
7. Author(s) Jon Pinkham https://orcid.org/0009-0000-6356-598X William Davids 0000-0002-9602-1046 Andrew Schanck https://orcid.org/0000-0002-1768-722X		**8 Performing Organization Report No.**
9 Performing Organization Name and Address University of Maine Department of Civil Engineering 5711 Boardman Hall Orono, ME 04469		**10 Work Unit No. (TRAIS)** **11 Contract or Grant No.** 69A3551847101
12 Sponsoring Agency Name and Address Transportation Infrastructure Durability Center, ASCC, University of Maine, 35 Flagstaff Rd., Orono, Maine		**13 Type of Report and Period Covered** Final Report 6/1/2022 through 5/31/2024 **14 Sponsoring Agency Code**

15 Supplementary Notes

16 Abstract

Bridges are vital nodes in the national transportation network, but many are reaching or have surpassed their usable lifespans. To help increase lifespan and durability of new construction, light weight and non-corrosive fiber reinforced polymers (FRPs) can be used to manufacture bridges' main structural members. The University of Maine has developed a a novel FRP composite tub (CT) girder system, which has been used in the construction of four bridges to-date. This study continues the development if the CT girder system by seeking to quantify the percentage of live load moment and shear apportioned to a single girder for design purposes. The American Association of State Highway and Transportation Officials (AASHTO) provides guidance on live load distribution in bridges constructed with steel, concrete, and wood girders, but not for FRP girders. First, live load distribution in CT girder bridges is assessed using four diagnostic field live load tests performed on two different, in-service CT girder bridges. Test results are then compared to existing AASHTO provisions to critically assess their applicability to CT girders. Subsequently, finite element (FE) models employing various levels of refinement were assessed for their ability to predict test results. Ultimately, two models that are computationally tractable and broadly applicable to CT girder bridges were implemented for predicting live load distribution, one for moment and another for shear. These models were used for a suite of parametric studies that provided insight into the effects of significant bridge geometric design on live load distribution factors (*DF*s). The results show that current AASHTO provisions for concrete box girders consistently predict higher *DF*s for both moment and shear carried by interior CT girders. New, CT-girder specific *DF* expressions for moment were then developed and proposed for use in future designs. For shear, initial parametric studies were completed to explore the limitations of current AASHTO expressions.

17 Key Words Live Load Distribution Finite-Element Modeling FRP Girder Diagnostic Load Test		**18 Distribution Statement** No restrictions. This document is available to the public through	
19 Security Classification (of this report) Unclassified	**20 Security Classification (of this page)** Unclassified	**21 No. of pages** 265	**22 Price** $0

Form DOT F 1700.7 (8-72)

Contents

List of Figures 8
List of Tables 11
Abstract 12
Chapter 1: Introduction 13
1.1 Background 13
1.2 FRPs In Infrastructure 13
1.3 FRP Composite Tub Girder: Prior Research and Current State of Knowledge 15
1.5 Research Goal and Objectives 17
1.6 Summary of Chapters 19
1.7 References 19
Chapter 2: Diagnostic Live Load Tests 22
2.1 Introduction 22
2.2 Test Bridges 23
2.3 Flexural Tests 27
2.3.1 Test Methods and Instrumentation 27
2.3.2 Results and Analysis 31
2.3.2.1 Flexural Strains 31
2.3.2.2 Girder End Restraint 33
2.3.2.3 Live Load Distribution 35
2.4 Shear Tests 37
2.4.1 Test Methods and Instrumentation 37
2.4.2 Results and Analysis 41
2.4.2.1 Shear Strains 41
2.4.2.2 Web Shear Differentiation 45
2.4.2.3 Live Load Shear Distribution Inferred From Measured Srains 46
2.5 Summary 48
2.6 References 49
Chapter 3: Finite Element Modeling 51
3.1 Introduction 51
3.2 High-Fidelity Finite Element Models 51
3.3.1 HGMB Nominal Model 53
3.3.1.1 Nominal Girder End Behavior 53
3.3.1.2 Nominal Live Load Distribution 54

3.3.2 HGMB Model Calibration 55
3.3.2.1 Calibration Parameters 55
3.3.2.2 Calibration Process 57
3.3.2.3 Calibrated Girder End Behavior 60
3.3.3 HGMB Simplified Moment Model 61
3.3.2.1 Model Description 61
3.3.2.2 Results Comparison 63
3.4 Shear Test Modeling 65
3.4.1 Baseline HGMB Model 65
3.4.2 HGMB Baseline Model Calibration 66
3.4.2.1 Calibration Parameter 66
3.4.2.2 Calibration Results 67
3.4.3 Twin Bridge Baseline Model 68
3.4.4 Twin Bridge Baseline Model Calibration 69
3.4.4.1 Calibration Parameter 69
3.4.4.2 Calibration Results 70
3.4.5 HGMB Simplified Shear Model 71
3.4.5.1 Model Description 72
3.4.5.2 Results Comparison 73
3.5 Summary 76
3.6 References 76
Chapter 4: Parametric Study 79
4.1 Introduction 79
4.2 Assumptions 79
4.2.1 Girder Design 80
4.2.2 Moment Model Implementation 81
4.2.3 Shear Model Implementation 83
4.2.4 Load Application 84
4.3.1 Moment Parametric Model Convergences 86
4.3.1.1 Mesh Convergence 86
4.3.1.2 Longitudinal Positioning Convergence 87
4.3.1.3 Transverse Positioning Convergence 89
4.3.2 Shear Parametric Model Convergences 90
4.3.2.1 Mesh Convergence 90

4.3.2.2 Longitudinal Positioning Convergence 91
4.3.2.3 Transverse Positioning Convergence 92
4.4 Moment Parametric Study 92
4.4.1 Effect of Spacing 93
4.4.2 Effect of Span Length 94
4.4.3 Effect of Span-to-Depth Ratio 95
4.4.4 Effect of Deck Thickness 96
4.4.5 Effect of Number of Girders 97
4.4.6 Effect of Deck Overhang on Exterior Girder *MDF* 98
4.4.7 Effect of Skew Angle 99
4.5 Shear Parametric Study 100
4.5.1 Effect of Spacing 101
4.5.2 Effect of Span Length 102
4.5.3 Effect of Bottom Flange Width 103
4.6 Summary 104
4.7 References 105
Chapter 5: Development of *MDF* Expressions 107
5.1 Introduction 107
5.2 Regression Analysis 107
5.3 Proposed Equations 109
5.3.1 Interior *MDF* 109
5.3.2 Exterior *MDF* 117
5.3.3 Skew *MDF* 120
5.4 Summary 122
5.5 References 125
Chapter 6: Summary and Conclusions 127
6.1 Summary 127
6.2 Conclusions 128
6.2.1 Conclusion 1: Finite Element Analysis Accurately Predict Live Load Distribution in CT Girder Bridges 128
6.2.2 Conclusion 2: Current Design Practices Tend to Over-Predict Moment Live Load Distribution to Interior Girders and Warrants Newly Developed *MDF* Expressions 129
6.2.3 Conclusion 3: Live Load Shear Distribution in CT Girders is Conservatively Predicted by AASHTO but Requires Additional Investigation 130
6.3 Future Work and Recommendations 130

Appendix A: Test Data 132
A.1 HGMB 2022 132
A.1.1 Instrumentation 132
A.1.2 Loading 133
A.1.3 Representative Data Plots 135
A.1.3.1 M41 Test 135
A.1.3.2 M42 Test 138
A.1.3.3 M43 Test 141
A.1.3.4 M21 Test 144
A.1.3.5 M22 Test 147
A.1.3.6 M23 Test 150
A.1.3.7 M24 Test 153
A.1.3.8 M25 Test 156
A.2 HGMB 2023 159
A.2.1 Instrumentation 159
A.2.2 Loading 160
A.2.3 Representative Data Plots 162
A.2.3.1 V41 Test 162
A.2.3.2 V42 Test 164
A.2.3.3 V43 Test 167
A.2.3.4 V21 Test 169
A.2.3.5 V22 Test 172
A.2.3.6 V23 Test 174
A.2.3.7 V24 Test 177
A.2.3.8 V25 Test 179
A.3 Twin Bridge 2023 182
A.3.1 Instrumentation 182
A.3.2 Loading 183
A.3.3 Representative Data Plots 185
A.3.3.1 V41 Test 185
A.3.3.2 V42 Test 188
A.3.3.3 V43 Test 191
A.3.3.4 V21 Test 194
A.3.3.5 V22 Test 197

A.3.3.6 V23 Test 200
A.3.3.7 V24 Test 203
A.3.3.8 V25 Test 206
Appendix B: Girder Design Scripts and Functions 209
Appendix C: Parametric Model Scripts and Functions 233
C.1 Moment Parametric Model 233
C.2 Shear Parametric Model 249

List of Figures

Figure 1.1. (a) HGMB Fully Constructed Looking Downstream, (b) During Construction with a Two-Girder System Being Set by an Individual Crane 16
Figure 1.2. Girder-Deck Friction Connector 17
Figure 2.1. (a) HGMB Looking Downstream. (b) Twin Bridge Looking North 24
Figure 2.2. HGMB Cross-Section 24
Figure 2.3. Typical HGMB Girder Cross-Section....26
Figure 2.4. Typical Twin Bridge Girder Cross-Section 26
Figure 2.5. HGMB Cross-Sectional Sensor Layout 29
Figure 2.6. (a) Typical Test Truck Configuration, (b) HL-93 Truck Configuration....30
Figure 2.7. HGMB M42 Truck Positioning Diagram 30
Figure 2.8. Typical Strain Transducer Output for Girder 3 at Midspan Test M42 (a) 2020 (b) 2022 32
Figure 2.9. Strain Measured Through the Depth of the Center Girder 32
Figure 2.10. As-Designed Girder End Detail 34
Figure 2.11. Twin Bridge Rosette Location on Girder....38
Figure 2.12. Typical Truck Dimensions and Wheel Weights for Shear Tests 39
Figure 2.13. (a) HGMB V42 Truck Positioning Diagram, (b) Four-Truck Two Lane Twin Bridge V41 Test 40
Figure 2.14. Shear Strains HGMB Girder 3 Webs Test V42 41
Figure 2.15. HGMB V41 Test Web Shear Strains vs Truck Position....42
Figure 2.16. HGMB V42 Test Web Shear Strains vs Truck Position....42
Figure 2.17. HGMB V43 Test Web Shear Strains vs Truck Position....43
Figure 2.18. Twin Bridge V41 Test Web Shear Strains vs. Truck Position 43
Figure 2.19. Twin Bridge V42 Test Web Shear Strains vs. Truck Position 44
Figure 2.20. Twin Bridge V43 Test Web Shear Strains vs. Truck Position 44
Figure 3.1. Nominal Deformed Model with Load Applied from Four Trucks Centered on the Bridge....53
Figure 3.2. *MGLF* M42 Calibrated and Nominal Model Prediction vs. Test *MGLF* (a) 2020 (b) 2022 55
Figure 3.3. Side Angle View of Paired Springs at One End 56
Figure 3.4. Calibration of Test M42 (a) 2020 (b) 2022....58
Figure 3.5. Simplified Model HGMB M42 2022....63
Figure 3.6. Comparison of M42 *MGLF* Results Test Data, Simplified Model, and Calibrated Model (a) 2020 (b) 2022 65
Figure 3.7. HGMB V42 Average Shear Strains....66
Figure 3.8. Twin Bridge Average Shear Strains Test V42....69
Figure 3.9. Fully Meshed Cross-Section Cut of Simplified HGMB FE Model....73

Figure 3.10. HGMB V42 *SGLF* Inferred from Model Reactions 75
Figure 4.1. Girder Axes 82
Figure 4.2. Polar Moment of Inertia Simplified Thin-Wall Cross Section 82
Figure 4.3. Girder Center Span Nodes Highlighted in Red for Girder 1.....83
Figure 4.4. Shear Model Girder End Partitions and Nodes for Boundary Conditions.....84
Figure 4.5. AASHTO HL-93 Load Applications to Model (a) Optimized on Exterior with Truck Axles (b) Interior Optimized Positioning with Tandem Axles 86
Figure 4.6. Simplified Moment Model Mesh Convergence.....87
Figure 4.7. Percent (%) Live Load Moment Achieved for Rear Axle Position from Support 88
Figure 4.8. Number of Transverse Load Runs Convergence (a) One Lane (b) Two Lanes 89
Figure 4.9. Shear Parametric Model Girder Mesh Convergence (a) 12.2 m Span Exterior *SDF* (b) 24.4 m Span Interior *SDF* 91
Figure 4.10. Interior *MDF* with Varying *S* (a) One Lane (b) Two Lanes 94
Figure 4.11. Interior *MDF* with Varying *L* (a) One Lane (b) Two Lanes.....95
Figure 4.12. Interior *MDF* with Varying Span-to-Total-Depth (a) One Lane (b) Two Lanes.....96
Figure 4.13. Interior *MDF* with Varying Deck Thickness *t* (a) One Lane (b) Two Lanes 97
Figure 4.14. Moment Exterior Correction Factor *e* with Varying Overhang (a) One Lane (b) Two Lanes 99
Figure 4.15. Interior Skew Correction Factor (a) One Lane (b) Two Lanes.....100
Figure 4.16. Effect of Girder Spacing S on Interior SDF 102
Figure 4.17. Effect of Span Length L on Interior SDF 103
Figure 4.18. Effect of Bottom Flange Width b_{bf} on Interior SDF 104
Figure 5.1. AASHTO vs. Model Interior *MDF* Regression Analysis (a) One Lane (b) Two Lanes 108
Figure 5.2. AASHTO vs. Model *e* Regression Analysis Two Lanes 109
Figure 5.3. Proposed Equation vs. Model Interior *MDF* Regression Analysis (a) Equation 5.3 (b) Equation 5.4.....112
Figure 5.4. Proposed Equation vs. Model Interior *MDF* Regression Analysis (a) Equation 5.7 (b) Equation 5.8.....114
Figure 5.5. Proposed Equation vs. Model Interior *MDF* Regression Analysis (a) Equation 5.9 (b) Equation 5.10.....115
Figure 5.6. AASHTO vs. Proposed Equation 5.10 Interior *MDF*.....116
Figure 5.7. Proposed Equation vs. Model Exterior *MDF* Regression Analysis (a) Equation 5.12 (b) Equation 5.13.....118
Figure 5.8. AASHTO vs. Proposed Equation 5.15 Exterior *MDF*.....119

Figure 5.9. Proposed Equation vs. Model Skewed *MDF* Regression Analysis
(a) Equation 5.17 (b) Equation 5.19.....121
Figure 5.10. Proposed Equation vs. Model Skewed *MDF* Regression Analysis
(a) Equation 5.18 (b) Equation 5.20.....122

List of Tables

Table 2.1. Nominal Lamina Material Properties....27
Table 2.2. HGMB Nominal Composite Section Properties....27
Table 2.3. Measured Midspan and Average End Strain (με)....34
Table 2.4. Two Lane AASHTO *MDF* vs. Maximum *MGLF* Calculated in Four-Truck Load Cases....36
Table 2.5. Ratio of Maximum Single Web Shear Strain to Average Shear Strain, r....46
Table 2.6. Nominal Girder Properties for *SGLF* Inference....47
Table 2.7. Test Inferred *SGLF*s Compared to AASHTO *SDF*s for Concrete Box Girder....48
Table 3.1. Nominal Model-Predicted Midspan and Average End Strains (με)....54
Table 3.2. Comparison of Measured and Model-Predicted Strains at Bottom of Girders at Midspan (με)....60
Table 3.3. Average End Strains Measured during Tests and Predicted by Models (με)....61
Table 3.4. Comparison of Maximum *MGLF*s Derived from all Field Tests with the Simplified Model....64
Table 3.5. Measured and Model-Predicted Shear Strains, γ (με) for HGMB....67
Table 3.6. Measured and Model-Predicted Shear Strains, γ (με) for Twin Bridge....71
Table 3.7. HGMB Maximum Model Predicted Two Lane *SGLF*s vs. AASHTO *SDF*s....76
Table 4.1. Transverse Elastic Modulus of Concrete for Certain Deck Thickness....83
Table 4.2. Longitudinal Position from Support to Rear Axle....88
Table 4.3. Interior *MDF* for Varying Girder Numbers....98
Table 5.1. Interior MDF Expressions Comparison....116
Table 5.2. Proposed CT Girder Live Load Moment Distribution Factors (S.I. Units)....124
Table 5.3. Proposed CT Girder Live Load Moment Distribution Factors (U.S. Units)....125

Abstract

Bridges are vital nodes in the national transportation network, but many are reaching or have surpassed their usable lifespans. To help increase life-span and durability of new construction, light weight and non-corrosive fiber reinforced polymers (FRPs) can be used to manufacture bridges' main structural members. The University of Maine has developed a a novel FRP composite tub (CT) girder system, which has been used in the construction of four bridges to-date. This study continues the development if the CT girder system by seeking to quantify the percentage of live load moment and shear apportioned to a single girder for design purposes. The American Association of State Highway and Transportation Officials (AASHTO) provides guidance on live load distribution in bridges constructed with steel, concrete, and wood girders, but not for FRP girders. First, live load distribution in CT girder bridges is assessed using four diagnostic field live load tests performed on two different, in-service CT girder bridges. Test results are then compared to existing AASHTO provisions to critically assess their applicability to CT girders. Subsequently, finite element (FE) models employing various levels of refinement were assessed for their ability to predict test results. Ultimately, two models that are computationally tractable and broadly applicable to CT girder bridges were implemented for predicting live load distribution, one for moment and another for shear. These models were used for a suite of parametric studies that provided insight into the effects of significant bridge geometric design on live load distribution factors (*DF*s). The results show that current AASHTO provisions for concrete box girders consistently predict higher *DF*s for both moment and shear carried by interior CT girders. New, CT-girder specific *DF* expressions for moment were then developed and proposed for use in future designs. For shear, initial parametric studies were completed to explore the limitations of current AASHTO expressions.

Chapter 1: Introduction

1.1 Background

As of 2020, the National Highway Administration reported that over 45,000 bridges in the United States were structurally deficient, with an estimated cost of replacement at nearly 50 billion USD (USDOT 2022). These bridges tend to be constructed from conventional materials such as steel and reinforced concrete (RC) which require significant maintenance and are prone to deterioration from corrosion. To increase design life and overall durability of newly constructed bridges, new materials and methods of minimizing corrosion are being developed that require less maintenance and are less prone to deterioration. In particular, fiber reinforced polymers (FRPs) show promise in bridge applications due to their non-corroding nature. A further benefit of FRPs is their light weight, which can reduce construction costs and logistics (Barbero, 2018).

1.2 FRPs In Infrastructure

Considerable research has been conducted into the use of FRPs in some aspects of highway bridge construction. Concrete-filled FRP tubes (CFFTs) have been used in over 30 short-span, buried bridges in multiple states since the early 2000s. These arches utilize a hybrid braided composite consisting of three layers, typically two outer layers of braided carbon fiber and an inner layer of braided E-glass fibers which confine the infilling concrete (Dagher et al. 2012; Walton et al. 2016). FRP reinforcing rod (rebar) has been used extensively as a corrosion-free alternative to steel rebar (Benmokrane et al. 2006; Kumar and GangaRao 1998) and is becoming typical for new construction in some states. For example, the Morristown bridge in Vermont, USA was constructed with a glass FRP (GFRP) rebar RC deck. It was field tested and

showed tensile strains well below ultimate for the rebar and tensile strains well below cracking in the concrete (Benmokrane et al. 2006). In addition, GFRP pultruded sheet pile was fabricated into stay-in-place concrete forms (Honickman and Fam, 2009) and box girders with a cast-in-place deck section (Fam and Honickman, 2010), both showing significant increases to strength and stiffness above the bare section. A numerical analysis of this girder-deck system showed that AASHTO's live load distribution paradigm could be applicable to girders manufactured from FRP (Kim and Fam, 2011). The success and popularity of FRPs in bridge construction has prompted the American Association of State Highway and Transportation Officials (AASHTO) to publish a number of guide specifications which set forth design guidelines under a uniform level of structural reliability. These specifications include guidelines for design of GFRP-reinforced concrete (AASHTO 2018), bonded FRP repair systems (AASHTO 2012a), and CFFTs (AASHTO 2012b).

Despite these successful usage cases of FRP in highway bridges, FRP girders have been deployed as the main structural members in very few highway bridge structures around the world. The Asturias bridge, constructed in Spain in 2004, uses carbon FRP (CFRP) in a trapezoidal box profile girder (Gutierrez et al. 2008; Mires et al. 2007). The CFRP laminates are wrapped around a foam core in the center to form a closed box section. Analysis of the bridge led to the conclusion that, although effective, the hand-laid pre-impregnated CFRP strips used in girder fabrication led to prohibitively expensive designs. The San Patricio hybrid FRP/RC bridge in Texas, USA was constructed in 2004 and uses twelve, U-shaped FRP girders that are closely spaced at 813 mm. Each girder has a constant 44 mm laminate thickness for all components including webs and flanges. Steel rods placed through the webs provide composite action with the RC deck that is partially cast into the girder depth (Ziehl et al. 2009). Ziehl et al. suggested

that, because of their linearity to failure, FRP materials used in bridge design should be subject to maximum design strains based on damage initiation rather than an ultimate strength. The Ryjak River bridge is a single span, 22 m long bridge constructed in Rzeszow, Poland in 2015 which is composed of four FRP girders. The girder cross sections are optimized for flexural strength by laying up stronger unidirectional CFRP in the bottom flange with GFRP in the webs and top flange where less tensile strength is required (Siwowski and Rajchel 2019; Siwowski et al. 2018). Due to the current lack of design guidance and experience, Siwowski et al. (2018) advocate for structural health monitoring of FRP bridge structures. This, they say, will help build confidence in FRP bridge structures and support their proliferation.

1.3 FRP Composite Tub Girder: Prior Research and Current State of Knowledge

In 2016, the University of Maine began development of a novel FRP girder system known as the composite tub (CT) girder, which is envisioned and designed to be a direct replacement for conventional steel and concrete girders in highway bridges with spans up to 30 m. The CT girder is a tub-shaped, GFRP-CFRP hybrid girder fabricated by the vacuum infusion process and is designed to work compositely with an overlying RC deck. A prototype, full-scale girder was subjected to four-point bend testing in 2018, resulting in a moment at failure 2.5 times a factored AASHTO Strength I load (Davids et al. 2022a). The first CT girder bridge, the Hampden Grist Mill Bridge (HGMB) pictured in Figure 1.1 (a), was constructed in Hampden, Maine on US Route 1A over Souadabscook stream in December of 2020. The HGMB is a 22.9 m, single span structure with five girders spaced at 2.46 m, which carries two lanes of traffic and a sidewalk. As shown in Figure 1.1 (b), the light weight of the CT girders allowed two girders and utilities to be assembled on the ground and subsequently lifted as a pair with a single crane. Another critical component of the success of the CT girders is the simplicity and effectiveness of

the girder-deck shear connection that ensures composite action. While the HGMB has bearing-type connectors, shown in Figure 1.2, that behave like traditional shear studs used in steel girder bridges (as did the original 2018 test girder), composite action between the RC deck and CT girders is now achieved with sinusoidal deformation pattern infused into the top surface of the top flange against which the deck is cast, providing frictional interlock. This connection was independently assessed for strength and fatigue resistance via shear block testing (Davids et al. 2022b), does not rely on any secondary bonding or infusion, and allows the use of widely-spaced stainless steel bolts or studs to maintain contact between the girder and concrete deck. Other recent research has focused on girder web shear strength and buckling capacity, which were characterized through a combination of in-place picture frame tests and extensive finite element (FE) analyses (Schanck et al. 2023). To-date, four highway bridges have been constructed in the United States using the CT girder as the main load-carrying structural system, including two bridges in Maine, one in Pasadena, Florida, and one ion Westerly, Rhode Island, and others are in the design phase.

(a) (b)

Figure 1.1: (a) HGMB Fully Constructed Looking Downstream, (b) During Construction with a Two-Girder System Being Set by an Individual Crane

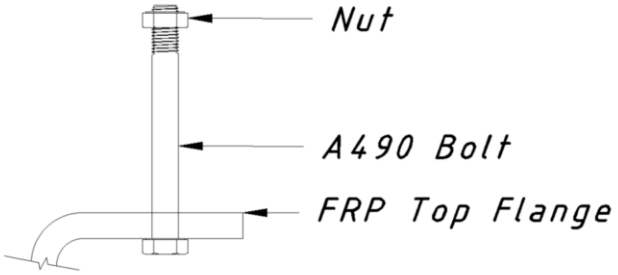

Figure 1.2: Girder-Deck Friction Connector

1.4 Live Load Distribution in CT Girder Bridges

The design and analysis of a slab-on-girder bridge requires the determination of the amount of live load moment and shear carried by individual girders. For conventional steel, concrete and timber girders, girder moments and shears can be quickly determined with of live load distribution factors (*DF*s*)* defined by AASHTO (2020). However, *DF*s are not defined for CT girders, and to-date there have been no detailed investigations into live load distribution for CT girder bridges, which is a barrier to their wider implementation. Current industry practice for CT girder design is to use the *DF*s prescribed by AASHTO (2020) for RC box beams to estimate live load distribution. However, the applicability of RC box girder *DF*s to CT girder bridges has not been verified and could lead to inefficient or inaccurate designs due to the much higher flexural stiffness of concrete girders relative to FRP girders.

1.5 Research Goal and Objectives

While previous research has established that the flexural and shear capacity of CT girder bridges can be accurately computed, and composite action between the CT girder and concrete deck can be reliably and efficiently achieved, the lack of information on the transverse distribution of live loads remains a barrier to their implementation. The goal of this research is to rigorously assess CT girder bridge live load distribution. This goal will be achieved through a

combination of field load testing, FE analysis, and a critical assessment of the current practice of using concrete box girder *DF*s for CT girder bridges.

The results of two diagnostic live load tests conducted on the HGMB – one in late December 2020 upon completion and commissioning of the structure and a second test conducted in early July 2022 – are used to experimentally assess moment live load distribution of a real bridge in the field. Measured flexural strains were used to assess composite action between the CT girders and concrete deck, end support rotational restraint, and moment live load distribution. For the distribution of live load shears, two additional diagnostic live load tests were performed on HGMB and Twin Bridge in the summer of 2023. These tests focused on maximizing shear effects to the CT girders and provide a data set for inferring shear live load distribution.

High-fidelity FE models of the two bridges incorporating a very precise representation of the bridges' actual geometry, laminate architecture and non-structural components were created and calibrated to match the flexural and shear strains recorded during the tests. Following calibration of the detailed models, simplified FE models were created and their ability to predict live load distributions similar to those of the detailed models and test data was evaluated. Using these validated, computationally efficient models, a larger set of typical bridge configurations with varying sectional and geometric parameters are analyzed under AASHTO HL-93 loading (AASHTO 2020), allowing an initial comparison with AASHTO *DF*s used for design. Comparisons between load distribution inferred from field testing and the FE analyses are used to critically assess the applicability of existing AASHTO *DF*s for the design of CT girders and make recommendations regarding new *DF* expressions for CT bridge girders.

1.6 Summary of Chapters

This report is organized into six Chapters where each describes the actions taken to perform this research, introduce relevant literature, and draw conclusions from presented results. Separate appendices are provided with additional data and supplemental information.

- Chapter 2: *Diagnostic Live Load Tests* describes the diagnostic live load tests performed on two CT girder bridges in Hampden, ME, and observed bridge behavior.
- Chapter 3: *Finite Element Model Development* describes the creation of detailed FE models, calibration, and analysis of the model results. The chapter also describes the creation of simplified models for the use in future parametric studies.
- Chapter 4: *Parametric Study* describes the parameter selection and effect on live load distribution in CT girder bridges by using results of simplified FE models analyzed under AASHTO HL-93 live loading.
- Chapter 5: *Development of Simplified MDF Expressions* describes the development of simplified expressions for moment live load *DF*s based on the parametric study results, makes comparisons to AASHTO *DF* expressions, and provides recommendations for shear live load *DF*s.

The final chapter (Chapter 6) summarizes the completed research, presents the important conclusions from the results, and addresses areas for future work.

1.7 References

AASHTO. 2020. *AASHTO LRFD Bridge Design Specifications*. Washington, DC: AASHTO.

AASHTO. 2018. *AASHTO LRFD Bridge Design Guide Specifications for GFRP-Reinforced Concrete*. Washington, DC: AASHTO.

AASHTO. 2012a. *Guide Specifications for Design of Bonded FRP Systems for Repair and Strengthening of Concrete Bridge Eelements*. Washington, DC: AASHTO.

AASHTO. 2012b. *LRFD Guide Specifications for Design of Concrete-Filled FRP Tubes for Flexural and Axial Members*. Washington, DC: AASHTO.

Barbero, E. J. 2018. *Introduction ot Composite Materials Design (3rd edition).* Boca Raton, FL: CRC Press.

Benmokrane, B., E. El-Salakawy, A. El-Ragaby and T. Lackey. 2006. "Designing and testing of concrete bridge decks reinforced with glass FRP bars." *Journal of Bridge Enginering.* 11 (2): 217-229. https://doi.org/10.1061/(ASCE)1084-0702(2006)11:2(217)

Dagher, H. J., D. Bannon, W. Davids, R. Lopez-Anido, E. Nagy, and K. Goslin. 2012. "Bending behavior of concrete-filled tubular FRP arches for bridge structures." *Construction and Buidling Materials* 37: 432-439. https://doi.org/10.1016/j.conbuildmat.2012.07.067

Davids, W., A. Diba, H. Dagher, D. Guzzi and A. Schanck. 2022a. "Development, assessment and implementation of a novel FRP composite girder bridge." *Construction and Building Materials*. 340: 127818. https://doi.org/10.1016/j.conbuildmat.2022.127818

Davids, W., D. Guzzi and A. Schanck. 2022b. "Development and experimental assessment of friction-type shear connectors for FRP bridge girders with composite concrete decks." *Materials*. 15 (9): 3014. https://doi.org/10.3390/ma15093014

Fam, A., and H. Honickman. 2010. "Built-up hybrid composite box girders fabricated and tested in flexure." *Engineering Structures*. 32 (2010): 1028-1037. https://doi.org/10.1016/j.engstruct.2009.12.029

Gutierrez, E., S. Primi, J. Mires and I. Calvo. 2008. "Structural testing of a vehicular carbon fibre bridge: quasi-static and short-term behaviour." *Journal of Bridge Engineering*. 13 (3): 271-281. https://doi.org/10.1061/(ASCE)1084-0702(2008)13:3(271)

Honickman, H., and A. Fam. 2009. "Investigating a structural form system for concrete girders using commercially available GFRP sheet-pile sections." *Journal of Composites for Construction*. 13 (5): 455-465. https://doi.org/10.1061/(ASCE)CC.1943-5614.0000039

Kim, Y.J., and A. Fam. 2011. "Numerical analysis of pulturded GFRP box girders supporting adhesively-bonded concrete deck in flexure." *Engineering Structures*. 33 (2011): 3527-3536. https://doi.org/10.1016/j.engstruct.2011.07.016

Kumar, S. V., and H. V. S. GangaRao. 1998 "Fatigue response of concrete decks reinforced with FRP rebars." *Journal of Structural Engineering.* 124 (1): 11-16. https://doi.org/10.1061/(ASCE)0733-9445(1998)124:1(11)

Mires, J., I. Calvo, L. Pineda, F. Botello, M. Gomez, S. Primi and J. Bonilla. 2007. "First bridge constructed of carbon fibre reinforced polymers in Spain." in *FRPRCS-8*, Patras, Greece

Schanck, A., W. G. Davids, J. Pinkham and K. Berube. 2023. "Assessment of web shear stresses and shear capacity of FRP composite tub girders for highway bridges." *Structures*. 51: 880-894. https://doi.org/10.1016/j.istruc.2023.03.083

Siwowski, T., and M. Rajchel. 2019. "Structural performance of a hybrid FRP composite-lightweight concrete bridge girder." *Composites Part B Engineering*. 174: 107055. https://doi.org/10.1016/j.compositesb.2019.107055

Siwowski, T., D. Kaleta, and M. Rajchel. 2018. "Structural behaviour of an all-composite road bridge."*Composite Structures.* 192: 555-567. https://doi.org/10.1016/j.compstruct.2018.03.042

U.S. Department of Transportation Federal Highway Administration. 2022. "Bridge Replacement Unit Costs 2020." Accessed 17 July 2023. https://www.fhwa.dot.gov/bridge/nbi/sd2020.cfm

Walton, H. J., W. G. Davids, M. E. Landon and J. D. Clapp. 2016. "Simulation of buried arch bridge response to backfilling and live loading." *Journal of Bridge Engineering.* 21 (9): 04016052. https://doi.org/10.1061/(ASCE)BE.1943-5592.0000893

Ziehl, P., M. Engelhardt, T. Fowler, F. Ulloa, R. Medlock and E. Schell. 2009. "Design and field evaluation of hybrid FRP/reinforced concrete superstructure system." *Journal of Bridge Engineering*. 14 (5): 309-318. https://doi.org/10.1061/(ASCE)BE.1943-5592.0000002

Chapter 2: Diagnostic Live Load Tests

2.1 Introduction

Diagnostic live load testing has often been used as a tool for the determination of bridge live load *DF*s. Zokaie (2000) used live load tests to verify modeling techniques for original development of the AASHTO load and resistance factor design (LRFD) bridge design specifications (AASHTO 2020). Since the introduction of LRFD specifications, many others have conducted research validating analytical models with diagnostic live load test experimental results to develop their own *DF*s for slab on girder bridges. This includes steel and concrete girders (Cross et al. 2009), wide-flange steel girders (Michaelson 2010, Suksawang and Nassif 2007), concrete T-beams (Torres et al. 2019, Ndong et al. 2022), and concrete spread and multicell box girders (Hughs and Idriss 2006, Kong et al. 2020, Choi et al. 2019). However, most diagnostic live load tests have focused exclusively on moment live load distribution, and relatively few studies have considered shear. Cross et al. (2009) monitored shear strains at a girder depth from bearing and used measured strains to validate their FE model. Using the validated FE model, they were able to obtain reactions to be used for determining shear distribution at the bearing. They also found that reactions typically had larger distributions compared to beam shears at a girder depth, suggesting *DFs* determined from reactions would be more conservative in design. Barr and Amin (2006) also determined their shear *DF*s from reactions provided by a validated FE model used in parametric studies.

Four CT girder bridges have been constructed to-date with two located in Hampden, ME, allowing for convenient access for testing. HGMB was first tested in late 2020 after construction had been completed and again in the summer of 2022 with both tests focused on producing maximized moments and flexural strains. In the following summer of 2023 both HGMB and

Twin Bridge were tested with the goal of maximized shear effects produced on the bridges. All four tests provided a database for assessing structural behavior such as live load distribution and for comparison to FE models. It is important to note these tests are not intended to produce any damage and keep the girders in their linear elastic ranges.

2.2 Test Bridges

Photographs of the HGMB and Twin Bridge are shown in Figure 2.1 (a) and (b) respectively. HGMB was completed in late 2020 and is located on US Route 1A over the Souadabscook stream. Twin Bridge opened to traffic in late 2022 and is located on Maine Route 69 over the West Branch Souadabscook stream. HGMB spans 22.9 m, and has a 9.75 m wide travel way, a 508 mm wide curb, and a 2.03 m sidewalk on one side giving a total width of 12.3 m. The 203 mm thick cast-in-place RC deck is supported by five CT girders spaced at 2.46 m, and the bridge has an 82.6 mm asphalt wearing surface as seen in the cross-section in Figure 2.2. The bridge's abutments are skewed at 15° and the structure incorporates both a modest horizontal and sag vertical curve. Twin Bridge spans 16.2 m and consists of an 8.73 m travel way and 0.51 m wide curbs on either side for a total 9.75 m wide bridge. Twin Bridge was erected from three pre-constructed modules consisting of two CT girders each spaced at 1.68 m and a 102 mm thick precast RC deck. The modules each have a total width of 3.25 m resulting in a non-constant girder spacing. An additional 203 mm of RC was cast above the precast deck following placement of all two-girder modules giving a total deck thickness of 305 mm. Like HGMB, Twin Bridge incorporates both a modest horizontal and sag vertical curve with a 15° abutment skew.

(a) (b)

Figure 2.1: (a) HGMB Looking Downstream. (b) Twin Bridge Looking North

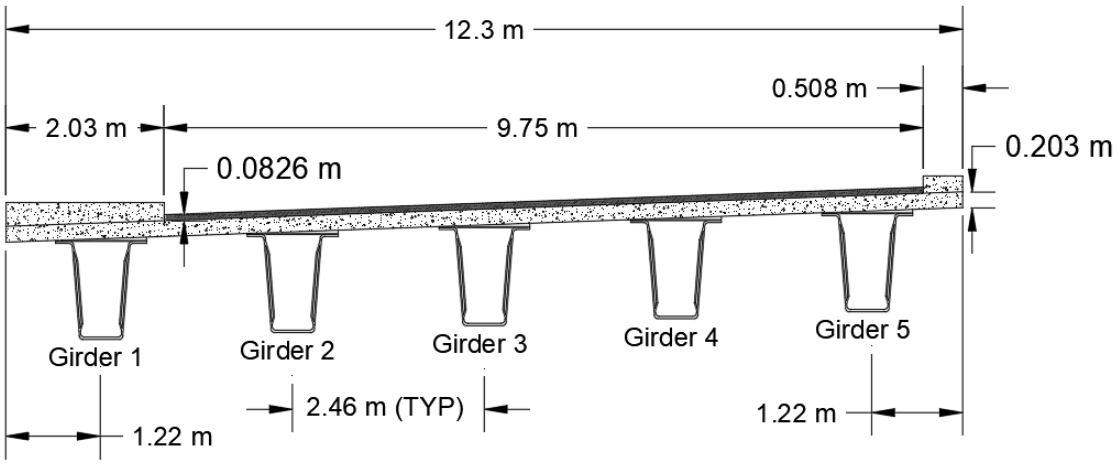

Figure 2.2: HGMB Cross-Section

The CT girders use a hybrid composite layup that has been tailored to efficiently carry moment and shear forces. Typical HGMB and Twin Bridge girder cross-sections are shown in Figures 2.3 and 2.4. The bottom flange consists primarily of stitched unidirectional carbon fabric providing tensile strength and stiffness, which, in conjunction with the compression resisted by the overlying deck, forms the main moment resisting mechanism. Each web has two face sheets containing biaxial E-glass fabric oriented at ±45° relative to the girder span to resist shear stresses as well as a central foam core that increases web shear buckling resistance. The top

flanges consist of E-glass oriented to resist bearing stresses from the shear connectors that extend into the cast-in-place concrete deck and carry bending compressive stress during deck placement. While the two bridges are very similar in appearance, girder architecture and load-carrying mechanism, there are important difference. HGMB has a 203 mm thick RC deck, which is typical in highway bridge construction, compared to Twin Bridge's 305 mm that results from pre-casting the lower 102 mm of deck following by casting the upper 203 mm on site. The span-to-total-depth (girder with deck) ratios also differ, with values of 15.5:1 for HGMB and 20:1 for Twin Bridge. The girder-deck shear connection also varied: HGMB relies on a bearing type connection with A490 bolts spaced at 150 mm in each flange, and Twin Bridge incorporates the newer friction-type connector that relies on deformed top flange upper surfaces and stainless steel bolts spaced at 305 mm on center in each flange (Davids et al. 2022a). To increase design efficiency, throughout the spans of the girders there are slight changes in the FRP girder cross-section in both bridges. Specifically, there are fewer carbon plies in the bottom flange closer to the abutments as moments decrease, and web FRP face sheet thickness is less in the central portion of the span and increases near the supports. These regions of the girders with different layups are referred to as zones. HGMB has two different zones while Twin Bridge has four zones throughout its span.

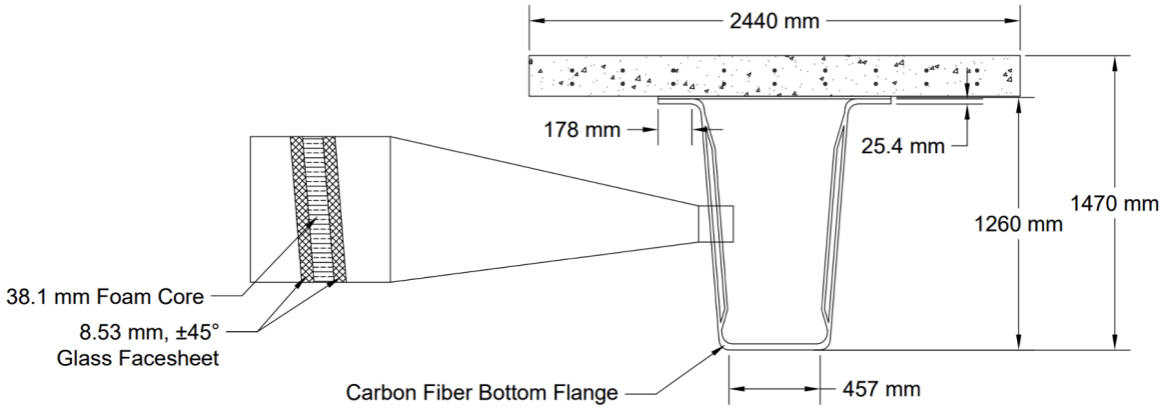

Figure 2.3**:** Typical HGMB Girder Cross-Section

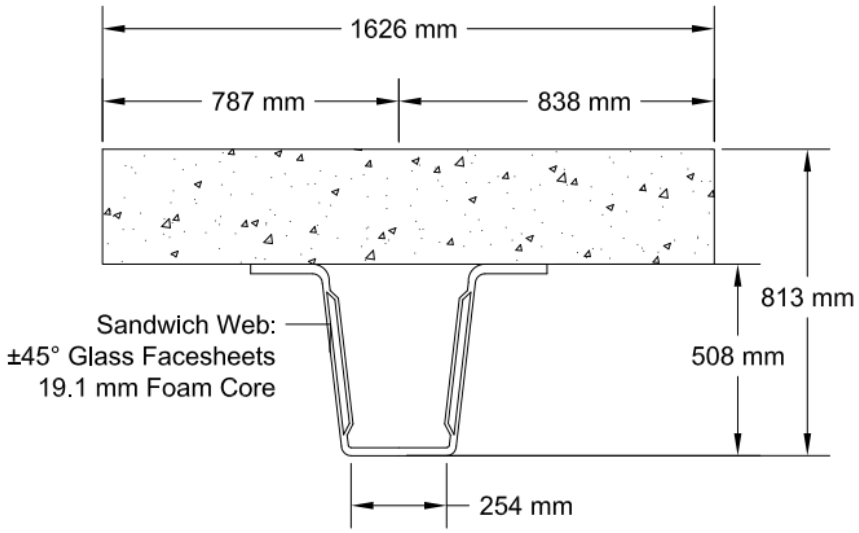

Figure 2.4: Typical Twin Bridge Girder Cross Section

Table 2.1 presents the nominal material properties for the laminae making up the girders, where *E* represents the Young's modulus, *G* is the shear modulus, and ν_{12} is Poisson's ratio as reported by the manufacturer. It should be noted that the 1-direction refers to the fiber direction with the 2-direction being perpendicular to the 1-direction and in the plane of the lamina. Table 2.2 presents the calculated section properties for each girder (as numbered in Figure 2.2) at

midspan with neutral axis height relative to the girder bottom. The moment of inertia, *I*, applies for a transformed section where FRP and steel materials have been transformed to concrete with an elastic modulus of 32.1 GPa, which is based on a compressive strength of 45.3 MPa determined from standard cylinder tests. The higher *I* and neutral axis location for girders 1 and 5 reflect the presence of the integral sidewalk and curb, respectively. Under service loads, the structure responds linearly elastically, and stresses and strains can be computed using conventional strength of materials equations. The girders were designed for the AASHTO Strength I limit state using moment-curvature analysis and incorporating nonlinear compressive response and tensile cracking of the concrete deck as explained by Davids et al. (2022b).

Table 2.1: Nominal Lamina Material Properties

Material	E_1 (GPa)	E_2 (GPa)	G_{12} (GPa)	ν_{12}
Carbon	99.1	4.21	4.00	0.280
E-Glass	36.8	11.2	5.31	0.280

Table 2.2: HGMB Nominal Composite Section Properties

Girder	I (mm^4) X 10^{10}	Neutral Axis Height (m)
1	10.8	1.46
2 - 4	6.58	1.27
5	8.24	1.35

2.3 Flexural Tests

2.3.1 Test Methods and Instrumentation

Diagnostic live load tests can help quantify live load distribution through data acquired under loading that approaches that produced by design service live load. To assess moment effects in the HGMB, girder longitudinal strains were measured under large vehicle loads. The system used to acquire these data was the Wireless Structural Testing System from Bridge

Diagnostics Inc. (Bridge Diagnostics Inc. 2010). This system consists of reusable strain transducers adhered directly to structural members which communicate with a mobile base-station and dedicated laptop computer to record and display strain data in real-time. These data were collected continuously at a sampling rate of 10 Hz. The test protocol was not performed to a specific standard but was informed by guidance from the *Manual for Bridge Evaluation* (AASHTO, 2019).

Longitudinal strain transducers were applied at midspan on the bottom of each girder to measure strains at the extreme tensile fiber, with other sensors placed at mid depth and near the girder top flange as seen in Figure 2.5. The transducers adhered to the bottom flange allowed assessment of maximum longitudinal strains and load distribution, with the other transducers applied to verify linear strain distribution through the section depth and evaluate composite action through inference of the girder neutral axis. Additional transducers were placed one girder depth from the end of most or all girders during each test to identify any unintended rotational restraint. The number of sensors and their placement varied between the two tests. In 2020 a total of 24 sensors were applied with 3 at each girder midspan, while in 2022, 22 sensors were applied with fewer sensors at midspan and more applied to girder ends. This was done to more thoroughly investigate the unintentional end fixity observed in 2020 (Davids and Schanck 2022; Schanck and Davids 2021).

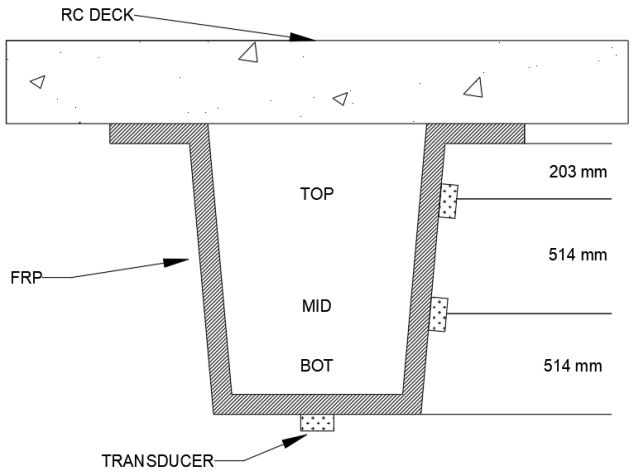

Figure 2.5: HGMB Cross-Sectional Sensor Layout

Loading was provided by four overloaded dump trucks that were measured and weighed prior to testing. Figure 2.6 (a) shows the typical measured axle and wheel dimensions of the trucks as well as wheel load magnitudes applied by each axle. In 2020, the total weight applied from the four trucks was 1170 kN while in 2022, the total was 981 kN. For comparison, the dimensions of a standard, HL-93 truck are given in Figure 2.6 (b). During each test, trucks were positioned on the bridge with their rear tandem axles as close to midspan as possible to produce the largest moment. Eight individual loading cases were used during each test. For the two truck load cases, trucks were positioned back-to-back in one lane and in five transverse positions across the travel way width to mimic a range of one lane loading conditions. For the four truck load cases, two-lane loading was mimicked: two pairs of two trucks were positioned back-to-back with each pair side-by side and in three transverse positions that located them close to the sidewalk, centered in the travelled way, and close to the opposite curb. Load cases were given the naming convention “MXY” where “X” is either 2 or 4 to denote the number of trucks, and “Y” is 1 through 5 to denote the transverse position. For instance, Figure 2.7 shows a plan view of test M42 from 2022 including the positioning of the four trucks in the second, centered 4-

truck position. The 2020 4-truck tests produced a maximum of 92.4% of two lanes of HL-93 live load + impact moment. In 2022, the 2-truck tests produced a maximum of 80.9% of one lane of HL-93 live load + impact moment, and the 4-truck tests produced 76.6% of two lanes of HL-93 live load + impact moment. This loading exceeds the 70% minimum required by AASHTO (2019) for investigation and rating factor analysis.

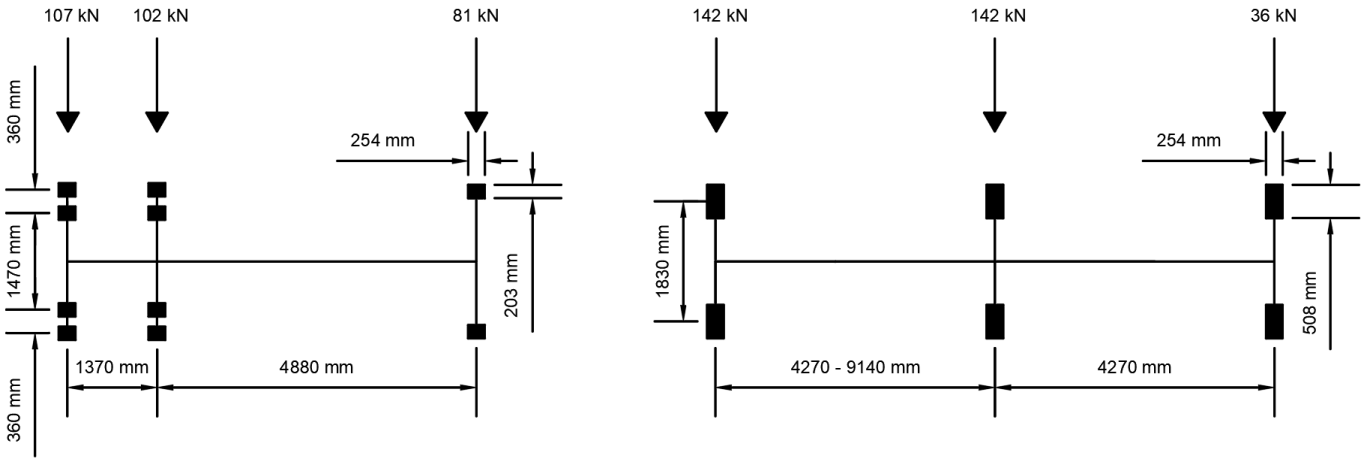

(a) (b)

Figure 2.6: (a) Typical Test Truck Configuration, (b) HL-93 Truck Configuration

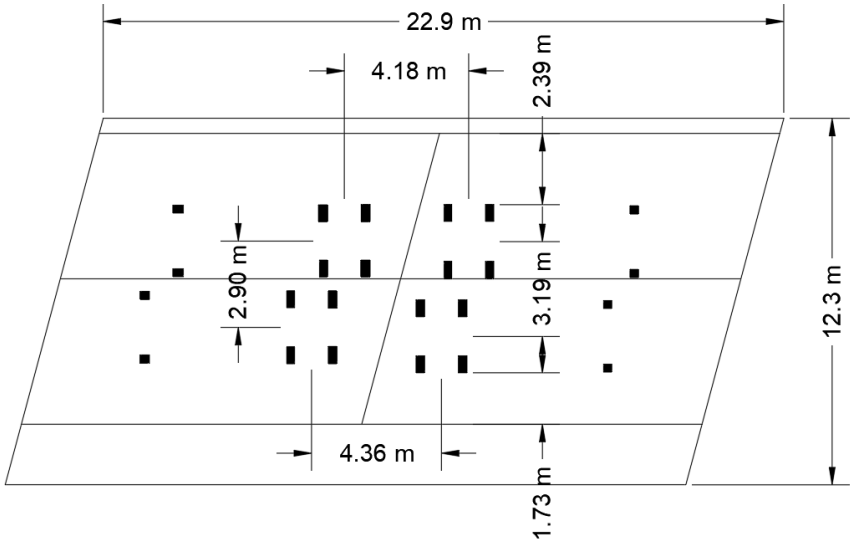

Figure 2.7: HGMB M42 Truck Positioning Diagram

During each load case, traffic across the bridge was stopped to prevent interference from passing vehicles and to allow the bridge to come to rest. Once traffic had been cleared, data collection was initiated, and trucks were backed into their appropriate positions on the span sequentially. When all trucks had been placed, their positions relative to the bridge and relative to each other were measured while strain data were continued to be collected. With all measurements taken, the trucks were then sequentially removed from the bridge.

2.3.2 Results and Analysis

2.3.2.1 Flexural Strains

After the completion of testing, the collected data were analyzed to infer the HGMB's behavior under loading both in December 2020 in its virgin state and in July 2022 after 18 months of service. A typical strain response under loading through the depth of the center girder can be seen in Figure 2.8 for the tests in 2020 (a) and 2022 (b), respectively. In both plots, the point at which a truck drives onto the bridge are evident as an increase in recorded strain followed by a plateau after the truck reaches its intended position and the structure comes to equilibrium. The opposite can be seen as trucks drive off the bridge. Additionally, a linear distribution of strains can be inferred through the section. This is seen more clearly in Figure 2.9 where the strains through the section under the maximum loading M42 are plotted explicitly along with a line of best fit. This shows that the measured strains fell along a straight line (within a small amount of experimental error), confirming the girders behaved as Euler-Bernoulli beams without significant shear deformation. The magnitude of strains recorded were similar accounting for the difference of load between the two tests. This indicates that the bridge's behavior had not significantly changed from 18 months of continuous service and seasonal environmental changes. Based on the linear best fit lines the neutral axis of the section is also

located near the top of the girder section at around 1.27 m from the bottom of the section. This agrees well with the computed value assuming a fully composite deck given in Table 2.2, validating the design assumption of full composite action.

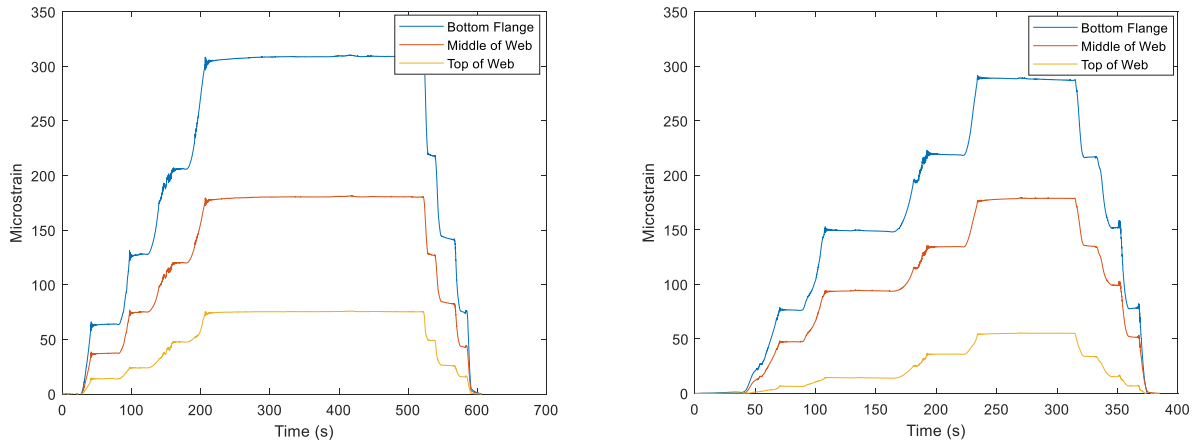

(a) (b)

Figure 2.8: Typical Strain Transducer Output for Girder 3 at Midspan Test M42 (a) 2020 (b) 2022

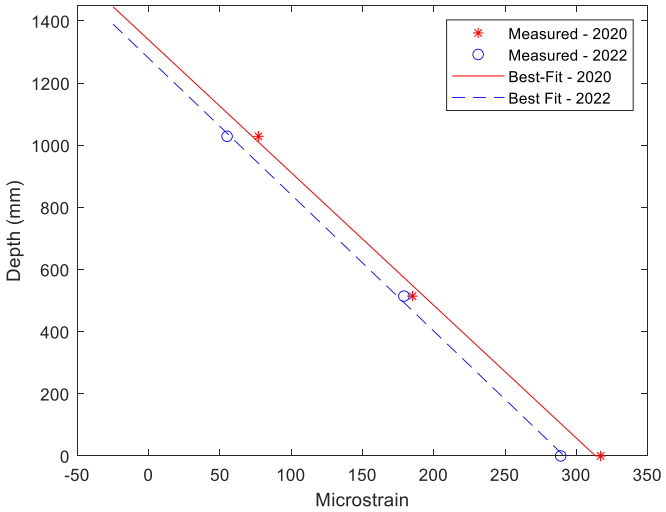

Figure 2.9: Strain Measured Through the Depth of the Center Girder

2.3.2.2 Girder End Restraint

The HGMB was constructed with semi-integral end diaphragms that were doweled to the abutments, and also has approach slabs which bear on ledges and are doweled to the backs of the diaphragms as shown in Figure 2.10. Although not accounted for in design, this detail was expected to impact measured strains, and indeed unintended girder end rotational restraint was indicated by negative longitudinal strains at the bottoms of girders at their ends as shown in Table 2.3 (Girder 1 was not instrumented with end strain gauges during the 2020 test). In Table 2.3 the strains reported in the "End" column are either from one measurement taken at one girder depth from the girder end along the bottom flange or are an average of two measurements taken at both ends of the girders when available. In 2020 Girders 2, 3, and 5 had both ends instrumented with a transducer and therefore report averages while Girder 4 is reporting a measurement on one end, while in 2022 all five girders were instrumented with a transducer at both ends. Somewhat larger negative end strains were measured in 2022 even though the gross weight of trucks placed on the bridge in 2022 was lower than in 2020, which suggests that rotational restraint may have been slightly higher in the summer of 2022 than the winter of 2020. Taken as a whole, the results indicate that specific construction details such as the bridge's approach slabs, end diaphragms, and doweled connection with the abutments are likely providing this rotational restraint.

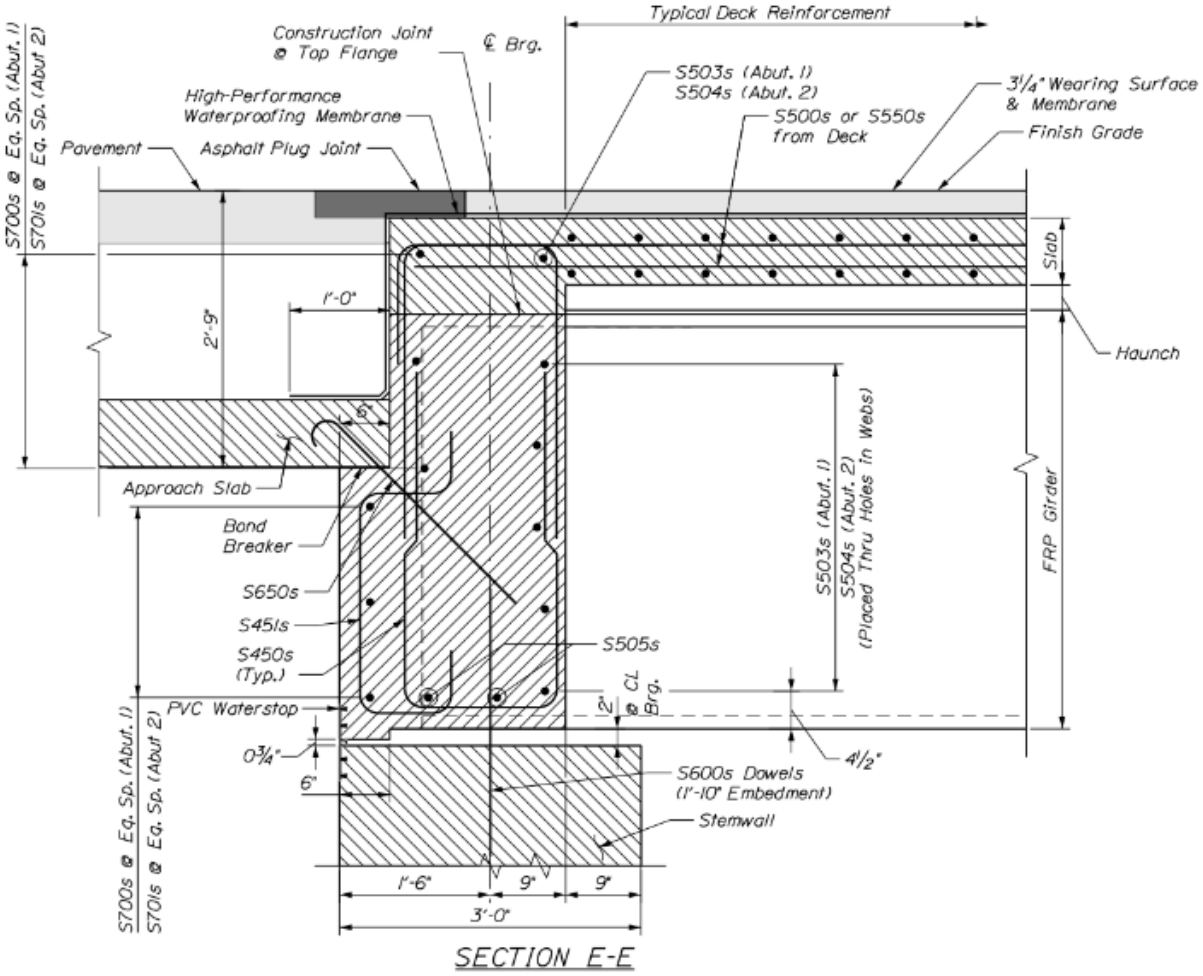

Figure 2.10: As-Designed Girder End Detail

Table 2.3: Measured Midspan and Average End Strain (με)

Year	Test	Girder 1		Girder 2		Girder 3		Girder 4		Girder 5	
		Mid	End	Mid	End	Mid	End	Mid	End	Mid	End
2020	M41	86	–	153	-30	304	-98	280	-110	346	-53
	M42	133	–	201	-64	309	-116	230	-92	202	-18
	M43	206	–	251	-87	303	-109	164	-47	104	10
2022	M41	60	8	104	-27	249	-77	336	-125	305	-68
	M42	131	-4	171	-70	289	-124	260	-108	158	-13
	M43	184	-16	201	-94	273	-134	195	-74	92	6

2.3.2.3 Live Load Distribution

A *DF* is the maximum fraction of a design lane load that is carried by one girder under all possible loading positions. Since it cannot be guaranteed that testing produced the absolute maximum moment effects in all girders, distributions computed from measured strains are referred to as moment girder lane fractions (*MGLFs*), the portion of the moment produced in a test load case that is distributed to a particular girder. For the i^{th}girder, the *GLF* for a specific load case is calculated by Equation 2.1, in which R_i is the ratio of the girder's flexural rigidity *EI* to that of an interior girder (which is greater than one for exterior girders and equal to one for interior girders), ε_i is the measured strain at midspan and N is the number of loaded lanes. The multiple presence factor m, prescribed as 1.2 for one lane loaded and 1.0 for two lanes loaded (AASHTO 2020), is also included to allow direct comparison of *MGLF*s with moment *DF*s (*MDF*) shown in Equation 2.2 where spacing *S* and span *L* are in m and girder depth *d* is in cm.

$$MGLF_i = \frac{R_i \varepsilon_i N m}{\sum_{i=1}^{5} R_i \varepsilon_i} \tag{2.1}$$

$$MDF_{int} = \left(\frac{S}{1.92}\right)^{0.6} \left(\frac{Sd}{100L^2}\right)^{0.125} \tag{2.2}$$

Table 2.4 summarizes the maximum *MGLF*s calculated in the two-lane tests for each girder. These are compared with the two lane *MDF*s calculated using the equations from AASHTO for a type c open concrete box section with a concrete deck (AASHTO 2020) which, as previously noted, are not expected to adequately describe the behavior of CT girders. Most interior girders exhibit a much lower *MGLF* than the corresponding *MDF* predicted by AASHTO. However, the maximum interior *MGLF* for all tests from both years was 0.593, in Girder 4, which is only slightly below the 0.601 predicted by AASHTO. Some of this variation in *MGLF*s produced between 2020 and 2022 for similar test configurations results from differences in individual

truck weights, along with some additional differences in the spacing between trucks. The maximum *MGLF*s produced in Girder 2 in 2020 and 2022 are 0.441 and 0.386 respectively. This difference is likely caused by a tighter transverse truck grouping in 2020, which tended to center more load on Girder 2 than in 2022. Similarly, the maximum *MGLF*s produced on Girder 4 in 2020 and 2022 were 0.441 and 0.593 respectively, again likely caused by a tighter transverse truck spacing in 2022 which pushed more load onto Girder 4.

Table 2.4: Two Lane AASHTO *MDF* vs. Maximum *MGLF* Calculated in Four-Truck Load Cases

Source	Girder 1	Girder 2	Girder 3	Girder 4	Girder 5
AASHTO	0.286	0.601	0.601	0.601	0.609
2020	0.520	0.441	0.533	0.441	0.645
2022	0.506	0.386	0.528	0.593	0.636

AASHTO grossly under-predicts the distribution to Girder 1 in both tests. However, AASHTO's type c open concrete box *MDF* equations are not strictly applicable for Girder 1 due to the presence of the sidewalk, and in this case AASHTO specifies that the lever rule be used. As a result, per AASHTO the wheel loads are positioned a significant distance from Girder 1, and the lever rule predicts an unreasonably low *MDF* compared to the test-based *MGLF*s. The discrepancy between AASHTO and the test results is likely magnified by the fact that the integral sidewalk significantly increases the flexural stiffness of Girder 1, causing it to draw more live load than predicted by AASHTO. However, for Girder 5, which is only stiffened by the integral curb, AASHTO does not utilize the lever rule and instead uses an exterior girder adjustment factor applied to the interior *MDF*, which aligns better with test-inferred *MGLF*.

Overall, the initial comparison of AASHTO *MDF*s and the test computed *MGLF*s indicate that the live load distribution for the interior girders is predicted reasonably well by AASHTO but is not predicted well for the exterior girder supporting the sidewalk. However, it is

important to note that the AASHTO *MDF*s were developed using HL-93 loading, which dictates significantly different truck positions, axle dimensions, and wheel loadings than those employed in the field tests. Further, in some tests wheel loads were placed closer to the curbs than the AASHTO specified 610 mm minimum clearance to curbs and sidewalks, which could explain the larger *MGLF*s on the exterior than AASHTO would predict. These and other aspects of response are explored in more detail via the FE models described in Chapter 3.

2.4 Shear Tests

2.4.1 Test Methods and Instrumentation

The diagnostic live load shear tests were intended to maximize shears in single girders for evaluation of shear load distribution. Loading was applied close to abutments to produce high shear stresses and reactions while transverse positions were varied to monitor their effect on live load shear distribution. Multiple transverse positions also increased the chance that maximized loading was produced in a single girder to better compare test load distributions to the maximum distribution implicit in AASHTO *DF*s.

To assess shear effects produced during diagnostic live load testing, shear strains were continuously measured throughout each test with 0-45-90 rosette foil resistance strain gauges. The rosettes were applied approximately one girder depth from the abutments for both bridges and 102 mm below the top flange for Twin Bridge as shown in Figure 2.11 and 203 mm below the top flange for HGMB to ensure the gauges were located in a region of the web with uniform fiber architecture and a constant thickness.

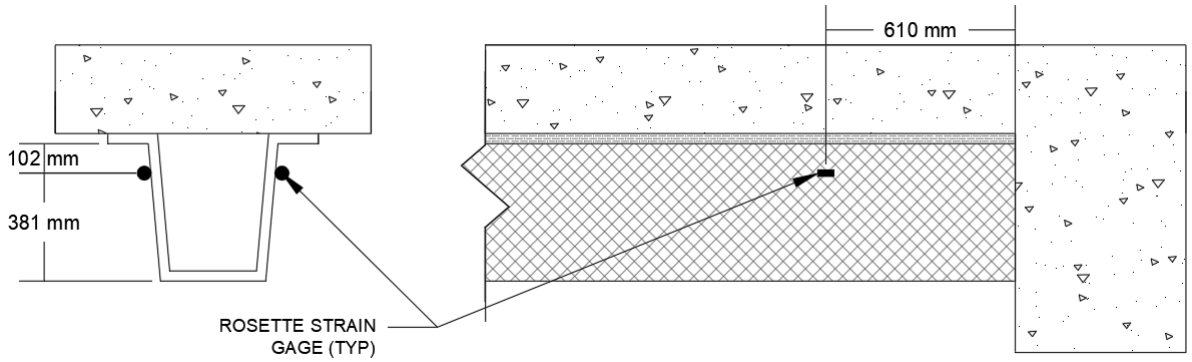

Figure 2.11: Twin Bridge Rosette Location on Girder

Loading was provided by four overloaded dump trucks whose individual wheel weights and dimensions were measured prior to testing. Figure 2.12 shows measured axle and wheel dimensions and wheel loads for a typical truck. The total load applied from the four trucks was 1183 kN om HGMB, while for Twin Bridge, the total was 1095 kN. During a typical test, trucks were positioned with their nearest rear tandem axles within two to three girder depths of the abutment. This positioning produced large web shears and ensured that all wheel loads contributed to shear strains measured at the rosettes located near each support. A relatively constant shear force existed in the girder from the rosettes to the support, ensuring the web shear strains gave an accurate representation of web shear at the end of the girder without directly measuring the reactions during testing. Traffic across the bridge was stopped to prevent interference from passing vehicles during each loading case. Once traffic had been cleared, data collection was initiated, and trucks were backed into their appropriate positions on the span sequentially. Once all trucks had been positioned, their offsets relative to the curbs, bridge center span line, and relative to each other were measured while strain data was continuously collected. After taking all measurements, the trucks were sequentially removed from the bridge.

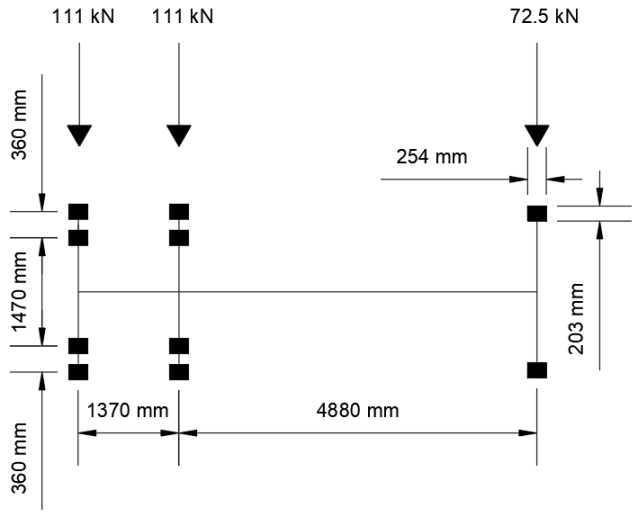

Figure 2.12: Typical Truck Dimensions and Wheel Weights for Shear Tests

Eight individual load cases were applied to each bridge, with each load case using either two or four trucks. For the two-truck load cases, two trucks were positioned back-to-back in five transverse positions across the travel way width to mimic a range of one lane loading conditions. For the four-truck load cases, two pairs of two trucks were positioned back-to-back with each pair side-by-side and in three transverse positions that located them close to one bridge edge, centered in the travel way, and close to the opposite bridge edge. Load cases were given the naming convention "VXY" where X is either 2 or 4 to denote the number of trucks, and Y is 1 through 5 to denote the transverse position. For instance, Figure 2.13 (a) shows a plan view of test V42 from HGMB including the positioning of the four trucks in the second, centered four-truck position. A photo of a four-truck load case in progress with all trucks in their final position is given in Figure 2.13 (b). The HGMB two-truck tests produced a maximum of 72.7% of the shear caused by one lane of HL-93 live load with impact, and four-truck tests produced a shear equal to that due to 70.6% of two lanes of HL-93 live load with impact. For Twin Bridge, the two-truck tests produced a maximum of 73.6% of the shear due to one lane of HL-93 live load

with impact, and the four-truck tests produced 73.2% of the shear due to two lanes of HL-93 live load with impact. This level of load reproduction exceeds the 70% mark set by the AASHTO *Manual for Bridge Evaluation* for test-based rating factor adjustment (AASHTO 2019). The four-truck load cases produced consistently higher shear strains, and therefore the results of the V4Y load cases are the focus of the remainder of this section.

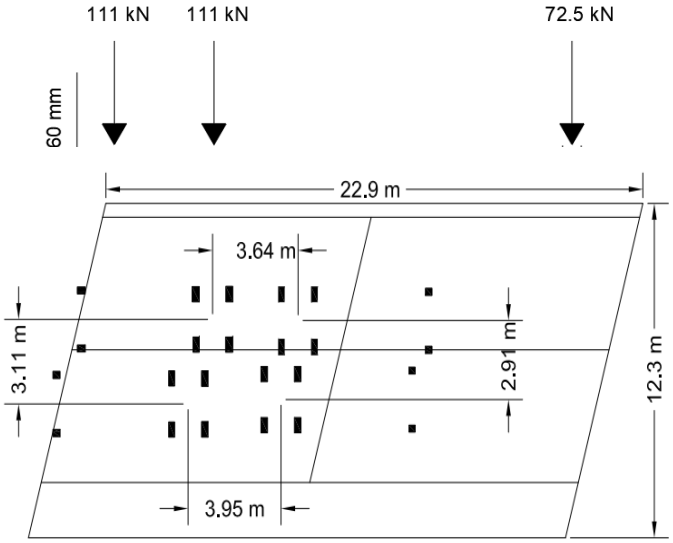

(a)

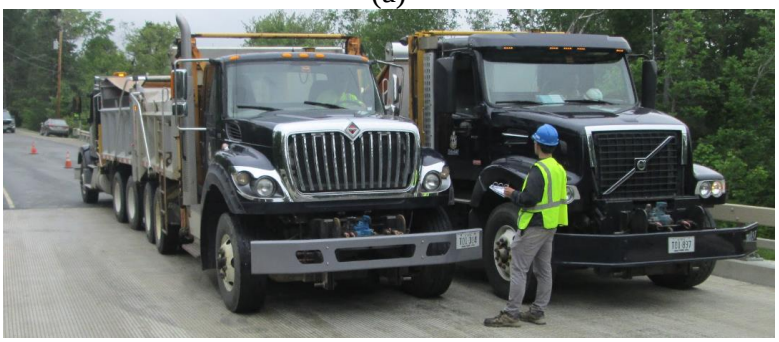

(b)

Figure 2.13: (a) HGMB V42 Truck Positioning Diagram, (b) Four-Truck Two Lane Twin Bridge V41 Test

2.4.2 Results and Analysis

2.4.2.1 Shear Strains

Figure 2.14 shows the shear strains measured from Girder 3 of HGMB during the V42 load case. These data are representative of all four-truck load cases and show the strains measured in both the north and south webs of the same girder. The time at which each truck is backed onto the bridge can be seen through four initial jumps in strains followed by plateaus signifying the system stabilizing and coming to static equilibrium. As seen in Figure 2.14, the peak measured shear strain in the south web was around 1.55 times larger than that in the north web, indicating a significant difference in web shear strains. To better visualize this effect, shear strains measured across the bridge width are plotted alongside the truck positioning for the four-truck load cases applied to HGMB in Figures 2.15-2.17 and Twin Bridge in Figures 2.18-2.20. This effect is typically less pronounced in the most heavily loaded girders but is still apparent and is generally correlated with the truck positions. These and subsequently reported numerical strains are averages over a 20 second period during with all trucks in their final position.

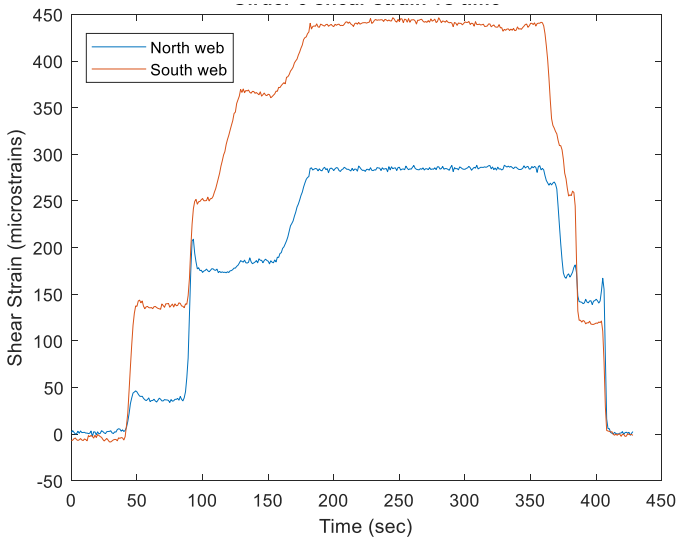

Figure 2.14: Shear Strains HGMB Girder 3 Webs Test V42

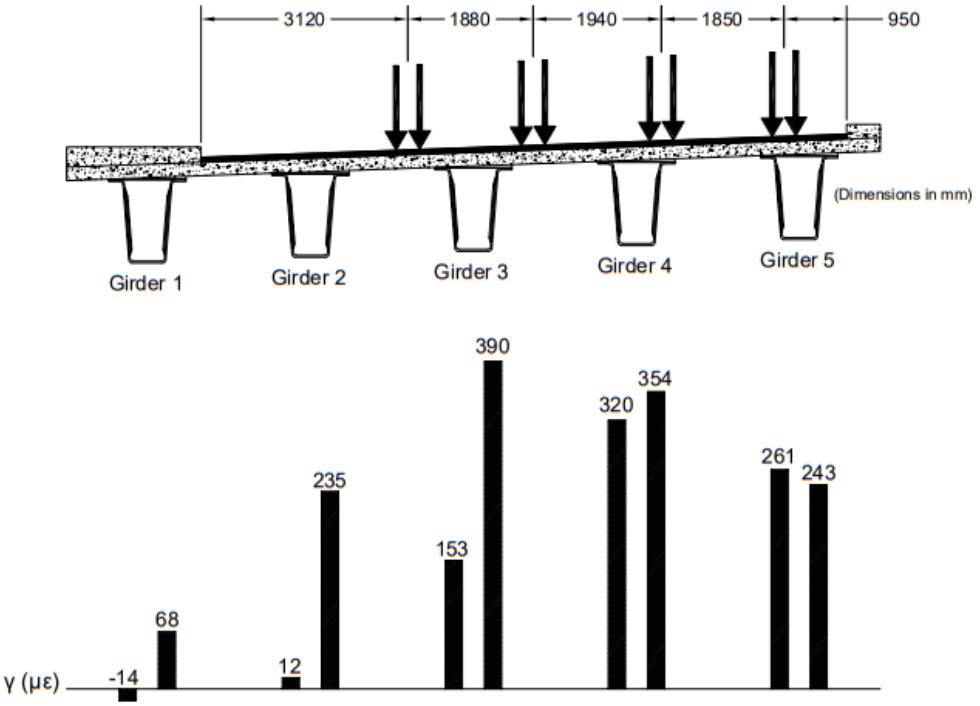

Figure 2.15: HGMB V41 Test Web Shear Strains vs Truck Position

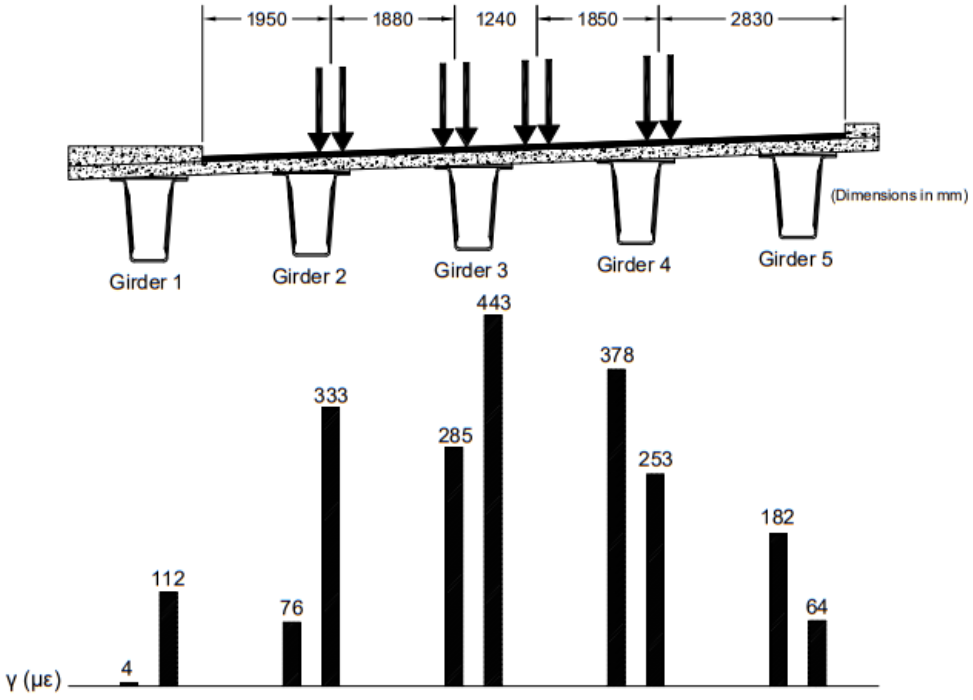

Figure 2.16: HGMB V42 Test Web Shear Strains vs Truck Position

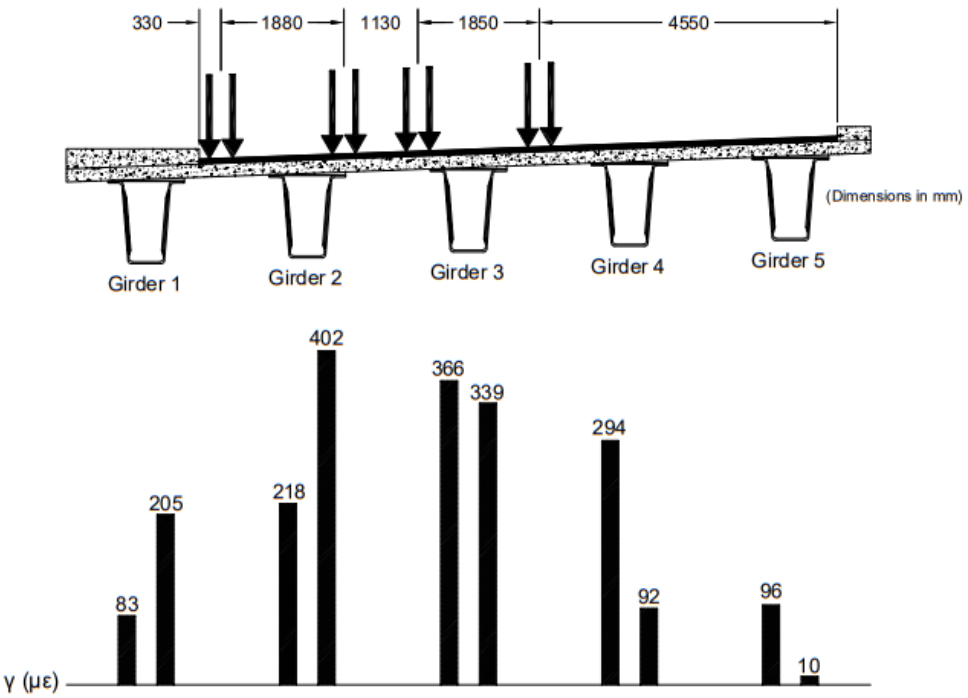

Figure 2.17: HGMB V43 Test Web Shear Strains vs Truck Position

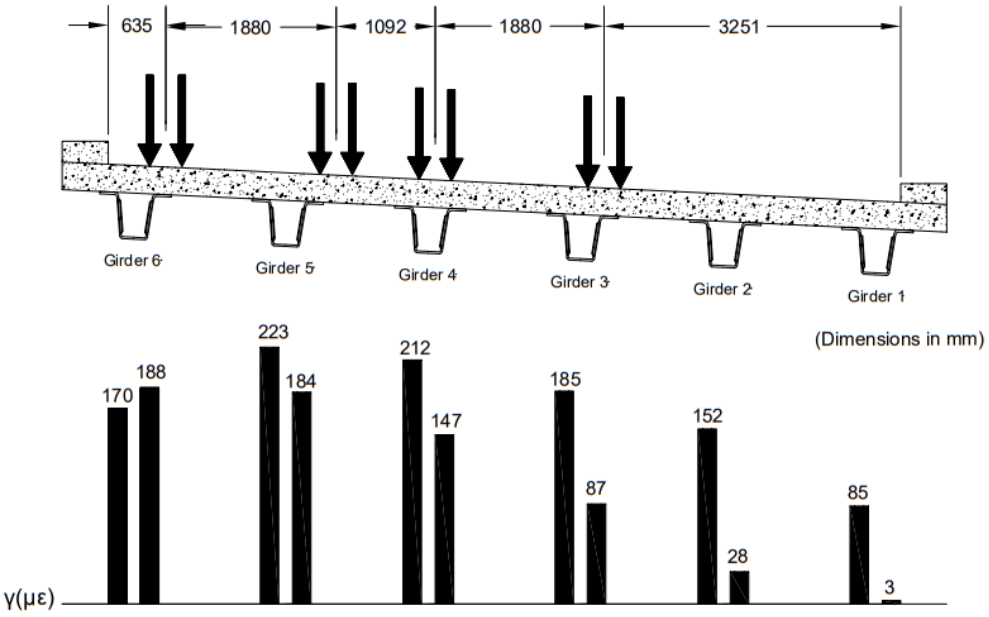

Figure 2.18: Twin Bridge V41 Test Web Shear Strains vs. Truck Position

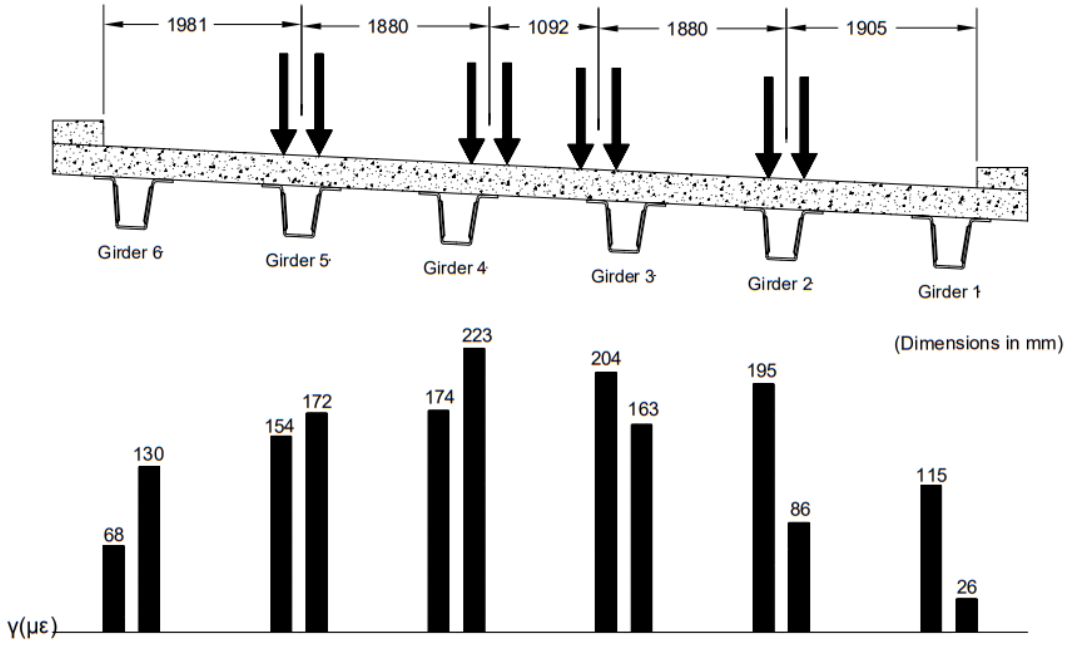

Figure 2.19: Twin Bridge V42 Test Web Shear Strains vs. Truck Position

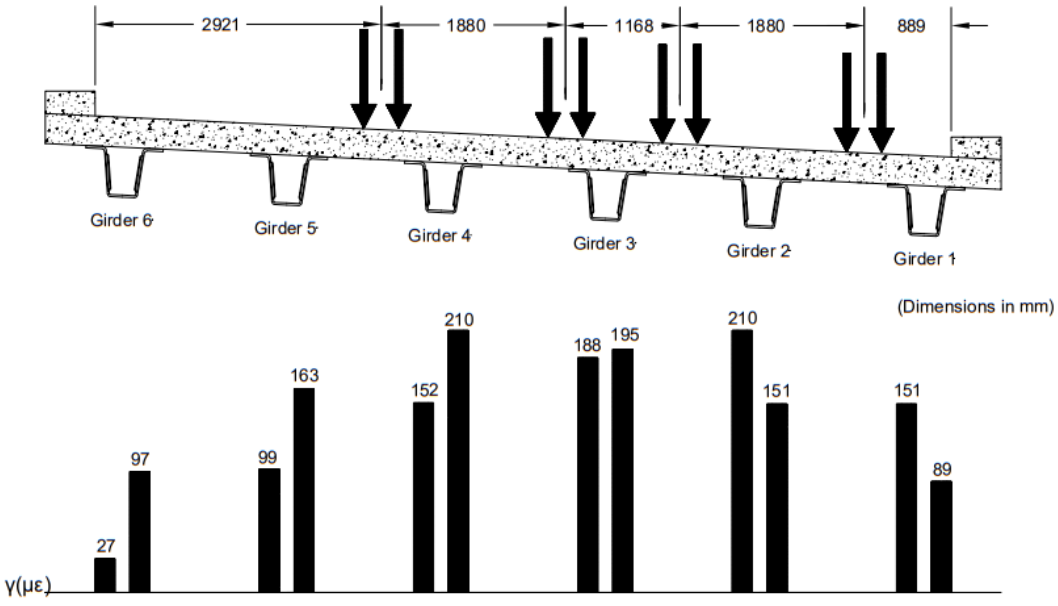

Figure 2.20: Twin Bridge V43 Test Web Shear Strains vs. Truck Position

2.4.2.2 Web Shear Differentiation

As seen in Figure 2.15, the most heavily loaded girders display a more even distribution of shear strains between the webs than more lightly loaded girders when the wheel loads are closer to the center of the girder. However, in Figure 2.16 the most heavily loaded girder 3 shows a significant differential in web shear strains as one axle applies load over the center of the girder with another axle load located closer to one web. The differential web shear strain may be a result of the CT girder's relatively low torsional and transverse bending rigidity compared to a more conventional concrete box girder, reducing its ability to evenly distribute shear between webs. Comparing the results from Twin Bridge (Figures 2.18-2.20) with those from HGMB (Figures 2.15-2.17) indicates shear strains measured at Twin Bridge tend to be lower in magnitude than those measured from HGMB, and that differential web shears are generally lower for Twin Bridge. The lower overall shear strains in Twin Bridge are a result of the fact that it has more girders, and the thicker concrete deck on Twin Bridge will also tend to more evenly distribute load to each girder, reducing differential web shear strain in individual girders.

A typical design assumption for a multi-web girder is even distribution of shear stress to each web. For a two-web girder, this means that each girder web carries half the total shear in the girder. However, the observed differential shear strains clearly do not support this general assumption. This differential is defined by r, the ratio of the maximum web shear strain to the average web shear strain given by Equation 2.3. Here γ_{max} and γ_{min} are the maximum and minimum web shear strains in a single girder for a single load case.

$$r = \frac{2\gamma_{max}}{\gamma_{max} + \gamma_{min}} \tag{2.3}$$

Table 2.5 shows the values of r for the most and second most heavily loaded girders in each four-truck load case from both HGMB and Twin Bridge tests. From Table 2.5, Twin Bridge

had noticeably less differential in shear strains within girders for four truck load cases, with a maximum r of 16% occurring in the second most heavily loaded girder for test V43, whereas the maximum value of r for HGMB was 44% in the second most heavily loaded girder for test V41. It is also clear that the most heavily loaded girders see less differential strain, but the differential can still be significant: 12% in Twin Bridge and 22% in HGMB.

Table 2.5: Ratio of Maximum Single Web Shear Strain to Average Shear Strain, r

HGMB Test	Most Heavily Loaded Girder	Second Most Heavily Loaded Girder
V41	1.05	1.44
V42	1.22	1.20
V43	1.04	1.30
Twin Bridge Test	Most Heavily Loaded Girder	Second Most Heavily Loaded Girder
V41	1.10	1.05
V42	1.12	1.11
V43	1.02	1.16

2.4.2.3 Live Load Shear Distribution Inferred From Measured Srains

The distribution of shear to individual girders for a given loading can be inferred from measured shear strains and nominal section properties. The portion of shear load distributed to each girder from a load case is referred to as a S*GLF* and is calculated using Equation 2.4, where γ_i represents the measured shear strain and I_i and Q_i are second and first moments of inertia for the i^{th} girder section.

$$SGLF_i = \frac{2\frac{\gamma_i I_i t_w}{Q_i}}{\sum_{1=1}^{N_g} \frac{\gamma_i I_i t_w}{Q_i}} \tag{2.4}$$

Calculated values of I_i and Q_i that are representative of the composite girder deck section at the location shear strains were measured can found in Table 2.6. These properties were determined from transformed section analysis after converting all materials to equivalent thicknesses of E-glass face sheets using appropriate modular ratios. For HGMB the longitudinal

elastic moduli of the girder sections were bottom flange 26.2 GPa, web 15.4 GPa, top flange 27.1 GPa and concrete deck 32.1 GPa. For Twin Bridge the longitudinal elastic moduli were bottom flange 59.4 GPa, web 18.6 GPa, top flange 23.7 GPa and concrete deck 35.1 GPa. The higher values of I_i and Q_i for the exterior girders capture the presence of curb and sidewalk features. The steel deck reinforcement was ignored in transformed section analysis.

Table 2.6: Nominal Girder Properties for *SGLF* Inference

HGMB	$\boldsymbol{I}$ (mm^4) X 10^{10}	$\boldsymbol{Q}$ (mm^3) X 10^7
Interior (G2-G4)	6.66	5.40
Exterior Sidewalk (G1)	13.4	6.31
Exterior Curb (G5)	9.29	5.78
Twin Bridge	I (mm^4) X 10^{10}	Q (mm^3) X 10^7
Interior (G2-G5)	1.64	1.71
Exterior (G1 and G6)	2.89	1.86

The *SGLF*s were inferred for all four-truck tests from the HGMB and Twin Bridge tests. The maximum *SGLF*s are reported and compared against the AASHTO shear *DF* (*SDF*) for concrete open box slab-on-girder bridges in Table 2.7. For reference, the AASHTO (2020) *SDF* expression for shear in interior open concrete box girders is given in Equation 2.5, where *S* is girder spacing in m, *d* is girder depth in cm and *L* is span length in m.

$$SDF = \left(\frac{S}{2.26}\right)^{0.8}\left(\frac{d}{100L}\right)^{0.1} \tag{2.5}$$

Table 2.7 shows for HGMB the AASHTO expression over-predicts shear carried by one girder by 38.5% on the interior and 36.8% on exterior Girder 5, except for Girder 1 where AASHTO under-predicts by 24.6%. However, AASHTO specifies the use of the lever rule for Girder 1 due to the presence of the sidewalk, and the AASHTO *DF* is consequently likely inaccurate. The shear distribution inferred from the Twin Bridge test results and Equation 2.4 also proves to be much less conservative than AASHTO, with AASHTO predicting 43.6% more

shear for the interior girders and 27.5% more shear for Girder 1. While Twin Bridge's girder spacing is 8.33% less than the 1.83 m minimum value allowed when using the AASHTO expression of Equation 2.5, the large discrepancy between measured and AASHTO-predicted values is still significant. However, for Twin Bridge AASHTO under-predicts the exterior obtuse corner Girder 6 shear by 15.3%. It must be noted that the test loadings may not have produced the maximum live load shear effect for a girder since only a finite number of transverse load positions could be considered in the test program. This highlights the importance of numerically simulating shear load distribution for a wide range of load positions to find the true maximum load effect. However, even though the *SGLF*s based on measured shear strains and Equation 2.4 may not be the global maxima, these results clearly suggest that AASHTO *SDF* expressions for a concrete box tend to be conservative when applied to CT girders.

Table 2.7: Test Inferred *SGLF*s Compared to AASHTO *SDF*s for Concrete Box Girder

HGMB	Girder 1	Interior Girders	Girder 5
AASHTO	0.319	0.881	0.811
Test Inferred	0.423	0.636	0.593
Twin Bridge	Girder 1	Interior Girders	Girder 6
AASHTO	0.505	0.603	0.505
Test Inferred	0.396	0.420	0.596

2.5 Summary

A total of four live-load diagnostic bridge tests were completed with moments and shears greater than 70% of the HL-93 design live-load with impact. During both moment tests end restraint was observed at the ends of the girders, causing negative strains at girder ends and reducing strains at the girder midspan. The *MGLF*s inferred from test measured flexural strains showed to be slightly below AASHTO predicted *MDF*s for interior girders loaded under two lanes with AASHTO over-predicting the maximum test measured interior *MGLF* by 1.35%. However, on the exterior AASHTO under-predicts the *MGLF*s by as much as 5.58% on the most

heavily loaded exterior girder. During the shear tests significant shear strain differentials were measured with shear strains in one web as much as 22% greater than the average shear strains for the two webs in the most heavily loaded girder. The shear strains were also used to infer *SGLF*s for the two lanes of load cases. AASHTO over-predicts the interior girder shear *SGLF*s by 38.5% and 43.6% for HGMB and Twin Bridge respectively. On the exterior girders AASHTO over-predicts the most heavily loaded HGMB girder by 36.8% but under-predicts the most heavily loaded exterior girder by 15.3% for Twin Bridge. These results suggest that the AASHTO concrete box girder expressions are likely conservative for interior girders but may not be conservative for exterior girders.

2.6 References

AASHTO. 2020. *AASHTO LRFD Bridge Design Specifications*. Washington, DC: AASHTO.

AASHTO. 2019. *The Manual for Bridge Evaluation (3rd edition), with 2019 inerim revisions.* Washington, DC: AASHTO.

Barr, P. J., and M. N. Amin. 2006. "Shear live load distribution factors for I-girder bridges." *J. Bridge Eng*. 11 (2): 197-204. https://doi.org/10.1061/(ASCE)1084-0702(2006)11:2(197)
Bridge Diagnostics Inc. 2010. *Wireless Structrual Testing System STS-WiFi Operations Manual*. Boulder, CO, USA: BDI

Choi, W., I. Mohseni, J. Park and J. Kang. 2019. "Development of live load distribtuion factor equation for concrete multicell box-girder bridges under vehicle loading." *International Journal of Concrete Structures and Materials*. 13 (22). https://doi.org/10.1186/s40069-019-0336-1

Cross, B., B. Vaughn, N. Panahshahi, D. Petermeier, Y. S. Siow, and T. Domagalski. 2009. "Analytical and experimental investigation of bridge girder shear distributions factors." *J. Bridge Eng*. 14 (3): 154-163. https://doi.org/10.1061/(ASCE)1084-0702(2009)14:3(154)

Davids, W., D. Guzzi and A. Schanck. 2022a. "Development and experimental assessment of friction-type shear connectors for FRP bridge girders with composite concrete decks." *Materials*. 15 (9): 3014. https://doi.org/10.3390/ma15093014

Davids, W., A. Diba, H. Dagher, D. Guzzi and A. Schanck. 2022b. "Development, assessment and implementation of a novel FRP composite girder bridge." *Construction and Building Materials*. 340: 127818. https://doi.org/10.1016/j.conbuildmat.2022.127818

Davids, W. G., and A. P. Schanck. 2022. "Field load testing and analysis of a new FRP composite tub girder bridge with a concrete deck." in *Bridge Safety, Maintenance, Management, Life-Cycle, Resilience and Sustainability: Proceedings of the Eleventh International Conference on Bridge Maintenance, Safety, and Management*, Barcelona, Spain

Hughs, E., and R. Idriss. 2006. "Live-load distribution factors for prestressed concrete, spread box-girder bridge." *J. Bridge Eng*. 11 (5): 573-581. https://doi.org/10.1061/(ASCE)1084-0702(2006)11:5(573)

Kong, S., L. Zhuang, M. Tao, and J. Fan. 2020. "Load distribution factor for moment of composite bridges with multi-box girders." *Engineering Structures*. 215: 110716. https://doi.org/10.1016/j.engstruct.2020.110716

Michaelson, G. K.. 2010. "Live load distribution factors for exterior girders in steel I-girder bridges." *West Virginia University Research Repository*. https://doi.org/10.33915/etd.4632

Ndong, A., M. Sherif, B. Kassner, D. Harris and O. Ozbulut. 2022. "Potential Improvement in Rating Factors of Concrete T-Beam Bridges through Refined Analysis: Evaluation of Distribution Factors." *Journal of Bridge Engineering*. 27 (9): 04022081. https://doi.org/10.1061/(ASCE)BE.1943-5592.0001928

Schanck, A. and W. Davids. 2021. "Testing, Monitoring, and Analysis of FRP Girder Bridge with Concrete Deck: Final Report" *TIDC at the University of Maine*, Orono, ME, USA. https://www.tidc-utc.org/kb/project-3-4-testing-monitoring-and-analysis-of-frp-girder-bridge-with-concrete-deck/

Suksawang, N., and H. Nassif. 2007. "Development of live load distribution factor equation for girder bridges." *Journal of the Transportation Research Board*, 9-18. https://doi.org/10.3141/2028-02

Torres, V., N. Zolghadri, M. Maquire, P. Barr and M. Halling. 2019. "Experimental and analytical investigation of live-load distribution factors for double tee bridges." *Journal of Performance of Constructed Facilities*. 33 (1): 04018107. https://doi.org/10.1061/(ASCE)CF.1943-5509.0001259

Zokaie, T.. 2000. "AASHTO-LRFD load distribution Specifications." *Journal of Bridge Engineering*. 5 (2): 131-138. https://doi.org/10.1061/(ASCE)1084-0702(2000)5:2(131)

Chapter 3: Finite Element Modeling

3.1 Introduction

To more thoroughly assess the field test results and distribution of live load shears, FE analyses of both bridges were conducted using the commercial software ABAQUS (Dassault Systèmes 2022). The models described next are high-fidelity discretizations that incorporated all structural and non-structural components that significantly contributed to the structure's response, including the girders, the non-structural FRP top plates spanning between the girder top flanges that supported the wet concrete during the deck pour, deck, wearing surface, concrete backwalls, railings, and curb and sidewalk.

3.2 High-Fidelity Finite Element Models

In the high-fidelity models the concrete and asphalt components (deck, sidewalk, curb, backwalls, and wearing surface) were discretized with C3D20R three-dimensional, quadratic, 20-node, reduced integration brick elements. These elements were assigned isotropic, linearly elastic constitutive behavior corresponding to standard concrete and asphalt mixes specified by the MaineDOT. The FRP components (girder and top plates) were modeled with S8R three-dimensional, quadratic, 8-noded shell elements while the steel railings were modeled with S4R three-dimensional, linear, 4-noded shell elements. FRP elements were assigned a simulated composite layup consisting of sub-layers of orthotropic, linear elastic constitutive properties corresponding to the non-prismatic layup of the girder and manufacturer-specified material properties. This modeling approach allows ABAQUS to perform the required laminate analysis and assign the elements with equivalent constitutive behavior in global coordinates. This laminate analysis could also be done by hand using a procedure such as that suggested by Barbero (2018) with the resulting laminate moduli being assigned to the elements directly. The

steel shell elements used to model the railings were assigned isotropic, linear elastic constitutive behavior with E = 200 GPa. The steel rebar was explicitly modeled using B31 linear elastic, isotropic, linear beam elements with E = 200 GPa. The required level of discretization was assessed through a convergence study on individual components based on the maximum girder displacement. A typical high-fidelity model has 150,000 elements and 1.4 to 2.4 x 10^6 DOFs for HGMB and Twin Bridge respectively. Model convergence was demonstrated in an earlier report by Schanck (2021). Twin Bridge has more DOFs due to its inclusion of six girders.

During testing, the truck wheel positions on the deck were measured, and loads were placed on patches of the model wearing surface that directly corresponded with the measured tire locations. Each partitioned wheel patch was assigned a uniform pressure corresponding to the applied wheel loading measured in the field. The girders were simply supported with the vertical and longitudinal displacements of each girder restrained on one end. The other end has vertical displacements of each girder restrained with one transverse displacement restrained to prevent rigid body translation. The deformed model and mesh are shown in Figure 3.1 for the M42 four truck loading in 2022 with a deformation scale factor of 30.

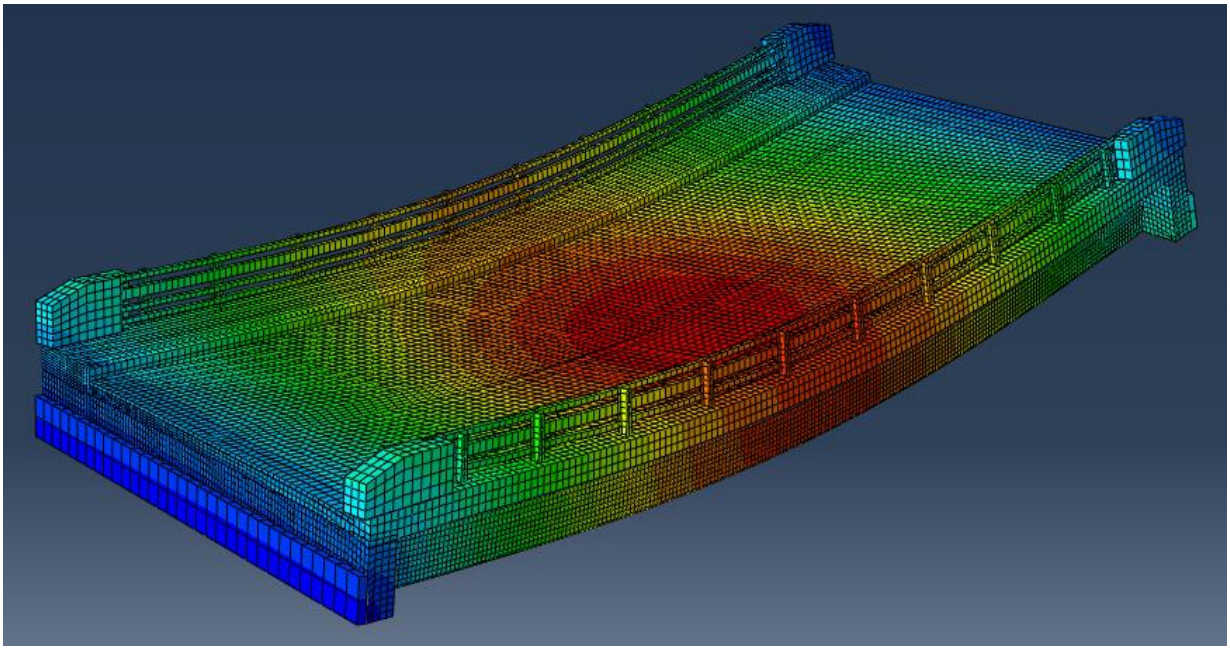

Figure 3.1: Nominal Deformed Model with Load Applied from Four Trucks Centered on the Bridge

3.3 Flexural Test Modeling

3.3.1 HGMB Nominal Model

3.3.1.1 Nominal Girder End Behavior

Table 3.1 shows the resulting midspan and end strains predicted by the nominal model analyses. It was observed from the test results that most end strains were negative, however the nominal model does not predict this, with all strains being positive and larger in magnitude than the measured negative strains. The positive end strains are consistent with the assumed simply supported boundary conditions, but do not reflect the rotational restraint observed in the field. Comparing Tables 2.3 and 3.1, the model in its base form also over-predicts strains at midspan by as much as 192%. Much of this is likely due to its lack of consideration of rotational end restraint, although the carbon in the bottom flange may also be stiffer than the nominal value reported by the manufacturer which would contribute to the model's over-estimation of strains.

The improvement of midspan and end strain predictions via model calibration process that considers both rotational constraint and girder stiffness is addressed later in this section.

Table 3.1: Nominal Model-Predicted Midspan and Average End Strains (με)

Year	Test	Girder 1		Girder 2		Girder 3		Girder 4		Girder 5	
		Mid	End	Mid	End	Mid	End	Mid	End	Mid	End
2020	M41	207	–	291	164	422	109	497	38	506	67
	M42	298	–	385	139	461	91	441	69	348	134
	M43	315	–	397	127	454	84	409	72	294	148
2022	M41	175	207	245	152	349	88	308	61	420	76
	M42	226	184	296	110	367	64	365	80	305	143
	M43	296	150	343	70	358	58	299	114	210	190

3.3.1.2 Nominal Live Load Distribution

*MGLF*s were calculated for all girders for all load cases in the 2020 and 2022 tests and compared with equivalent *MGLF*s developed from the corresponding FE analyses with the nominal model. An example of this comparison can be seen in Figure 3.2 where the *MGLF*s for test run M42 of 2020 and M42 of 2022 are compared (the calibrated model results shown in Figure 3.2 are discussed and referred to later in section 3.3.2.). As shown in Figure 3.2 (a) and 3.2 (b), the nominal model predicts a more even distribution of live load to each girder than what was inferred from testing. The nominal model under-predicts the *MGLF* in the most heavily loaded girder while slightly overpredicting the *MGLF*s of less heavily loaded girders. This inaccurate prediction of live load distribution provides additional justification for conducting model calibration. One possible explanation for this phenomenon is that the girders are significantly less stiff than the concrete deck, which allows the deck to more evenly distribute live load across its width. This can be addressed by adjusting the stiffness of the girders and deck to better reflect the actual condition of the bridge.

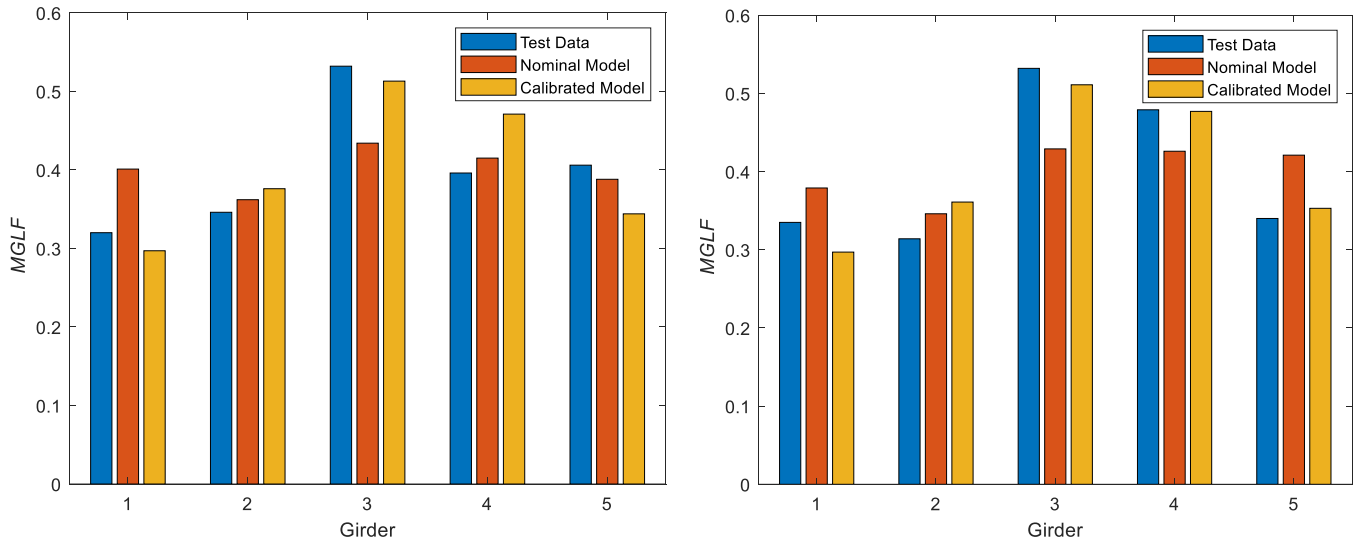

Figure 3.2: *MGLF* M42 Calibrated and Nominal Model Prediction vs. Test *MGLF* (a) 2020 (b) 2022

3.3.2 HGMB Model Calibration

3.3.2.1 Calibration Parameters

A key difference between the nominal model and the test results was the negative bottom flange strains near the support observed during testing. This is a clear indication that the abutment provided rotational restraint that the simply supported boundary conditions of the model cannot capture. Abutment details similar to that of the HGMB have been investigated by Dicleli and Erhan (2009) who captured this effect by adding linear translational spring elements to the back of the abutments to represent the effect of the backfill soil loading on the structure. A similar approach is taken here, where linear translational spring elements were added with stiffness in the bridge's longitudinal direction at the top of the deck and bottom of the girder at each girder centerline and at both abutments to represent the soil, abutment, and girder interaction as seen in Figure 3.3. The paired springs induce a moment couple as the girder ends rotate to provide the required rotational restraint and can also capture any small curvature-induced overall shortening of the bridge. The stiffness of these spring elements is one variable

that is used throughout the calibration process to help best fit the model to the test data. Each spring is assumed to have the same stiffness and does not vary from girder to girder.

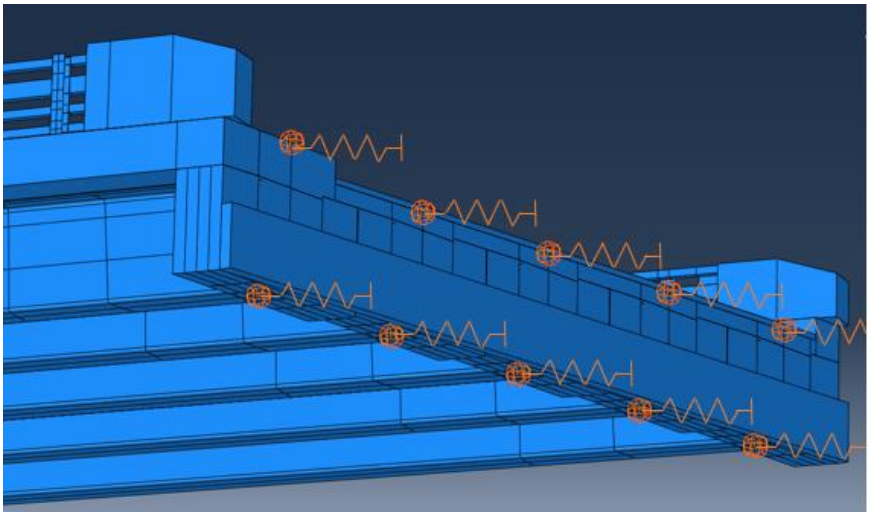

Figure 3.3: Side Angle View of Paired Springs at One End

It is common for RC bridge decks to experience transverse and longitudinal cracking, especially early in their service lives due to restrained concrete shrinkage and live loading (Wiss, Janney, Elstner Associates 2017). Even though deck cracking is a common phenomenon in bridges it was not considered in the development of the AASHTO *DF*s. Sotelino et. al (2004) found that simulating longitudinal deck cracking led to calculated *DF*s up to 17% higher than those reported by AASHTO while transverse cracks were found to have no significant effect on load distribution. To implement a cracked deck in the model, the concrete elements were redefined with an orthotropic constitutive model with a reduced transverse elastic modulus (E_2). The calculated, cracked elastic modulus, E_{cr} is found by Equation 3.1, where E_{nom} is the nominal elastic modulus, I_{nom} is the nominal section moment of inertia, and I_{cr} the cracked section moment of inertia. The original nominal model assumed an isotropic concrete deck with the elastic moduli in all directions of 32.1 GPa. Using a cracked deck, E_2 is reduced to 5.08 GPa while the moduli orthogonal to that direction remained unchanged. To account for the added

thickness of the curb and sidewalk on the cracked sections, the modulus corresponding to a cracked deck was calculated to be 2.15 GPa for the width of deck on the exterior where curbs and sidewalks were present.

$$E_{cr} = \frac{E_{nom} I_{cr}}{I_{nom}} \tag{3.1}$$

The final calibration parameter considered is the longitudinal elastic modulus of the carbon fiber bottom flange. The vacuum infusion process used to manufacture CT girders is similar to Vacuum-Assisted Resin Transfer Molding, which has been used to produce carbon lamina with elastic moduli in the longitudinal direction that are significantly higher than the 99.1 GPa assumed for the carbon laminae in the HGMB model. For example, Pirvu et al. (2004) reported a carbon composite E_1 = 134 GPa, Tan and Nieu (1996) reported E_1 = 122 GPa, Figiolini (2011) reported E_1 = 113-127 GPa and Jose-Trujillo et al. (2019) reported E_1 =129 GPa. The average of these values is 125 GPa, 26.3% higher than the nominal 99.1 GPa used for girder design and the initial analyses with the nominal model, which justifies increasing the carbon E_1 while calibrating the FE models to match test data.

3.3.2.2 Calibration Process

The nominal model was calibrated by minimizing the error, ϕ, defined in Equation 3.2 that captures the difference between the i^{th} predicted strains, ε_{model_i}, and the i^{th} strains measured during testing, $\varepsilon_{\exp\_i}$. The two calibration parameters that varied were the carbon modulus and the abutment spring stiffness. The two tests selected for calibration were M42 from 2020 and 2022 since they represented a heavy load case with four trucks centered along the bridge in both the longitudinal and transverse direction that produced large strains in the interior girders. Readings from each sensor (n equals 24 sensors and 22 sensors from 2020 and 2022,

respectively) from each of the two tests were used for calibration, and each sensor was given equal weight in Equation 3.2.

$$\phi = \sqrt{\sum_{i=1}^{n} (\varepsilon_{model\_i} - \varepsilon_{\exp\_i})^2} \tag{3.2}$$

Figure 3.4 shows the results of calibration against the (a) 2020 and (b) 2022 tests, respectively. In both cases increasing the longitudinal carbon modulus toward the upper end of the range of reasonable values tended to improve the quality of predicted strains for the entire range of moduli tested. Increasing the abutment spring stiffness tended to improve prediction up to a stiffness of 8.76x10^7 $\frac{N}{m}$ after which the predictions worsened. The model appears to better predict strains from the 2022 test than the 2020 test. However, it should be noted that during the 2020 test, the deck formwork that had not yet been removed from the structure was not included in the simulations, which could have affected measured strains. Overall, it is clear that calibration leads to significant improvement in model-predicted strains.

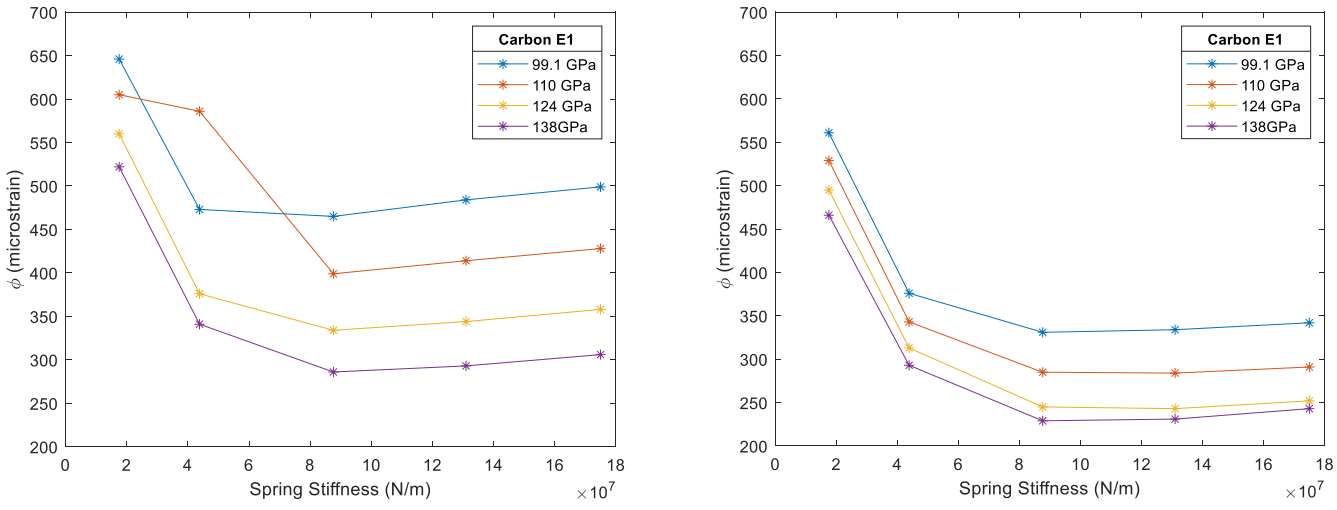

Figure 3.4: Calibration of Test M42 (a) 2020 (b) 2022

The final values selected for the two calibration variables of abutment spring stiffness and carbon longitudinal elastic modulus were 8.76 x10^7 $\frac{N}{m}$ and 124 GPa respectively. These were used to simulate tests from both 2020 and 2022. Even though the models with a carbon E_1 = 138 GPa gave the lowest error in predicted strains, a carbon E_1 = 124 GPa was selected as it is close to the average of the values reported in the literature cited earlier. The chosen spring stiffness minimizes error for both sets of tests. Table 3.2 compares the midspan strains measured from the four truck load cases in 2020 and 2022 with those predicted from the nominal and calibrated models. The average absolute value of error given for reference in Table 3.2 was calculated as the average of the absolute values between calibrated and nominal models and the measured strains across all girders in each test. The results show the calibration process significantly improved the agreement between midspan strains predicted by the model and those measured in the field. Predictions are best for the 2022 test, which is consistent with the lower least-squares error for 2022 predicted by Equation 3.2.

Table 3.2: Comparison of Measured and Model-Predicted Strains at Bottom of Girders at Midspan (με)

Year/ Test	Measured or Model	Girder 1	Girder 2	Girder 3	Girder 4	Girder 5	Average Absolute Error
2020 M41	Measured	86	153	304	280	346	-
	Nominal Model	207	291	422	497	506	121
	Calibrated Model	80	172	320	380	348	6
2022 M41	Measured	60	104	249	336	305	-
	Nominal Model	175	245	349	308	420	115
	Calibrated Model	68	143	261	319	284	8
2020 M42	Measured	133	201	309	230	202	-
	Nominal Model	298	385	461	441	348	165
	Calibrated Model	148	261	356	327	206	15
2022 M42	Measured	131	171	289	260	158	-
	Nominal Model	226	296	367	365	305	95
	Calibrated Model	120	203	287	268	170	11
2020 M43	Measured	206	251	303	164	104	-
	Nominal Model	315	397	454	409	294	109
	Calibrated Model	168	282	362	303	162	38
2022 M43	Measured	184	201	273	195	92	-
	Nominal Model	296	343	358	299	210	112
	Calibrated Model	187	251	266	192	94	3

3.3.2.3 Calibrated Girder End Behavior

In addition to improving the prediction of midspan strains, the paired springs were added to the calibrated model to help simulate the rotational restraint observed from the test data. Table 3.3 compares the resulting average end strains from the calibrated models to those measured during the four-truck tests. The average absolute value of error was calculated as the average across all girders of the absolute values between calibrated and nominal models and the measured strains in each test. The results in Table 3.3 suggest the springs reasonably simulate the effect of end restraint acting on the bridge structure as can be seen by the improved prediction of girder end strains. With few exceptions, the predicted strains match the measured strains well, with an average difference of 20.2 με.

Table 3.3: Average End Strains Measured during Tests and Predicted by Models (με)

Year/ Test	Measured or Model	Girder 1	Girder 2	Girder 3	Girder 4	Girder 5	Average Absolute Error
2020 M41	Measured	–	-30	-98	-110	-53	-
	Nominal Model	–	164	109	38	67	167
	Calibrated Model	–	-19	-127	-96	-122	31
2020 M42	Measured	–	-64	-116	-92	-18	-
	Nominal	–	139	91	69	134	181
	Calibrated	–	-81	-159	-75	-19	20
2020 M43	Measured	–	-87	-109	-47	10	-
	Nominal	–	127	84	72	148	166
	Calibrated	–	-98	-169	-71	10	24
2022 M41	Measured	8	-27	-77	-125	-68	-
	Nominal	207	152	37	82	113	176
	Calibrated	41	-16	-107	-142	-96	24
2022 M42	Measured	-4	-70	-124	-108	-13	-
	Nominal	184	110	88	61	76	168
	Calibrated	24	-63	-133	-112	-16	10
2022 M43	Measured	-16	-94	-134	-74	6	-
	Nominal	150	70	64	80	143	164
	Calibrated	-5	-101	-128	-60	30	12

3.3.3 HGMB Simplified Moment Model

3.3.2.1 Model Description

To assess live load distribution in slab-on-girder bridges, including CT girder bridges, the effect of parameters such as girder spacing, span length, and girder depth must be considered. FE-based parametric studies are vital to fully assessing live load distribution and the subsequent development of live load distribution factors, as demonstrated in prior studies of bridges made with conventional RC and steel girders (Choi et al. 2019; Barr and Amin 2006; Razzaq et al. 2021). However, such FE-based parametric studies can require thousands or tens of thousands of analyses to cover the full range of parameters and load cases. Due to the high-fidelity model's significant computational expense, using it for such a parametric study would require excessive time. Thus, investigators typically use simpler FE models that pair a shell element discretization of the concrete deck with beam elements for individual girders (Suksawang and Nassif 2007;

Barr and Amin 2006). Toward this end, a simplified FE model with the CT girders discretized as beam elements and the deck as shell elements is developed here, and the results of a parametric study are presented to assess the impact of important parameters on live load distribution.

The simplified three-dimensional model uses a geometrically linear analysis that includes only the girders and deck as opposed to the high-fidelity model that explicitly incorporates the wearing surface, curbs, railings and concrete reinforcement. The concrete deck is discretized using S8R quadratic, reduced integration shell elements with 8 nodes and 6 degrees of freedom per node. The shells were assigned a uniform thickness of 203 mm, neglecting the added thickness of the sidewalks and curbs. The shells were assigned an elastic orthotropic lamina material with cracked concrete properties based on the analysis presented previously. The girders are represented by offset B32 quadratic beam elements with 3 nodes and 6 degrees of freedom per node which are kinematically constrained to the overlying deck shell elements to ensure full composite action between the girders and deck. The B32 element is a Timoshenko shear deformable beam element with shear deformation controlled by the user-specified cross sectional area and shear modulus. Displacement boundary conditions are applied to the ends nodes of the girders to enforce simple supports, with sufficient additional boundary conditions applied to eliminate rigid body motion and rotation of the structure as a whole. Mesh convergence was achieved with deck and beam elements 635 mm in length for a span length of 22.9 m. Figure 3.5 shows the simplified model loaded to simulate the M42 load case during the 2022 test as well as the applied boundary conditions. The model has a total of 100,000 DOFs as opposed to the 1.4 million DOFs in the high-fidelity model employed previously, and the solution time is approximately 5% that required for the high-fidelity model.

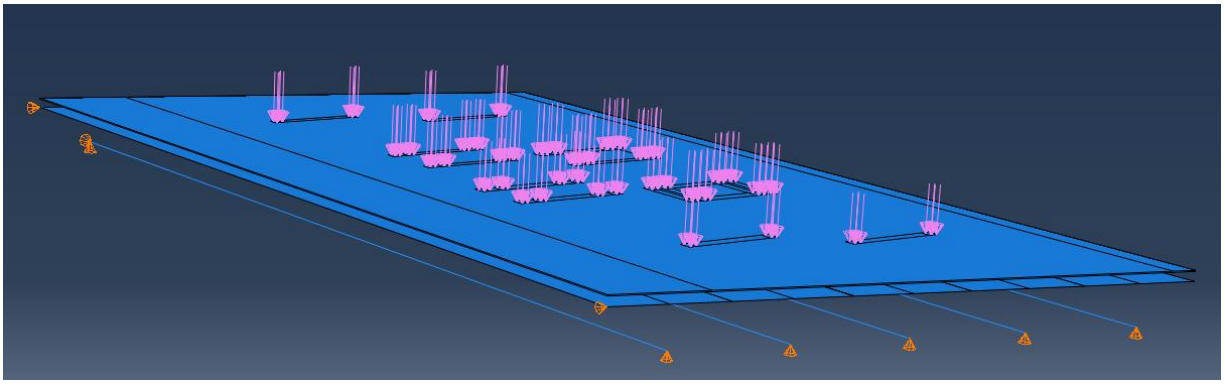

Figure 3.5: Simplified Model HGMB M42 2022

3.3.2.2 Results Comparison

The maximum strains from all girders were taken as output values and used in Equation 2.1 for calculating the *MGLF* of each girder from the simplified model during a load case. Table 3.4 compares the maximum interior and exterior *MGLF*s predicted by the simplified model with maximum *MGLF*s determined from the field data based on all one lane and two lanes of load cases. For most load conditions, the simplified model predicts maximum interior *MGLF*s well. For the 2020 test cases, the simplified model over predicts the interior maximum *MGLF* by nearly 1.8% whereas in 2022 the maximum interior *MGLF* is under-predicted by 5.7% by the simplified model. In exterior girders the simplified model did a relatively poor job predicting *MGLF*s for two lanes of loading with a maximum under-prediction of 45% in 2020 and 18.7% in 2022. These under-predictions are most likely due to the simplified model's neglect of secondary features such as railings, curbs, and sidewalks which draw load to exterior girders. The under-prediction in Girder 5 is also consistent between the two years with 18.1% in 2020 and 18.7% in 2022 suggesting an adjustment factor to simplified model results might be applicable for exterior girders that do not support a sidewalk. The simplified model's *MGLF* predictions are significantly worse for Girder 1, as the large sidewalk has a larger effect on distribution than the curb. For one lane loading the simplified model also predicts both interior and exterior Girder 5

*MGLF*s well with a nearly 8% over-prediction on the most heavily loaded interior girder and less than 4% under-prediction for Girder 5.

Table 3.4: Comparison of Maximum *MGLF*s Derived from all Field Tests with the Simplified Model

Year and # Lanes Loaded	GLF Calculation Data Set	Interior Girders	Girder 1	Girder 5
2020 Two Lanes	Field Measured	0.538	0.510	0.640
	Simplified Model	0.548	0.281	0.524
	% Change	1.80%	-45.0%	-18.1%
2022 Two Lanes	Field Measured	0.597	0.496	0.630
	Simplified Model	0.563	0.376	0.512
	% Change	-5.70%	-24.2%	-18.7%
2022 One Lane	Field Measured	0.390	0.484	0.491
	Simplified Model	0.421	0.317	0.474
	% Change	7.95%	-34.4%	-3.46%

Figure 3.6 gives a visual comparison of all *MGLF*s computed from the test data, calibrated detailed model, and simplified model for load case M42 in 2020 (a) and 2022 (b). There is good agreement of all three *MGLF*s for the three most heavily loaded girders in 2022. However, the simplified model gives less accurate predictions for exterior and less heavily loaded girders, which again can be attributed to its exclusion of secondary features that increase stiffness on the exterior girders.

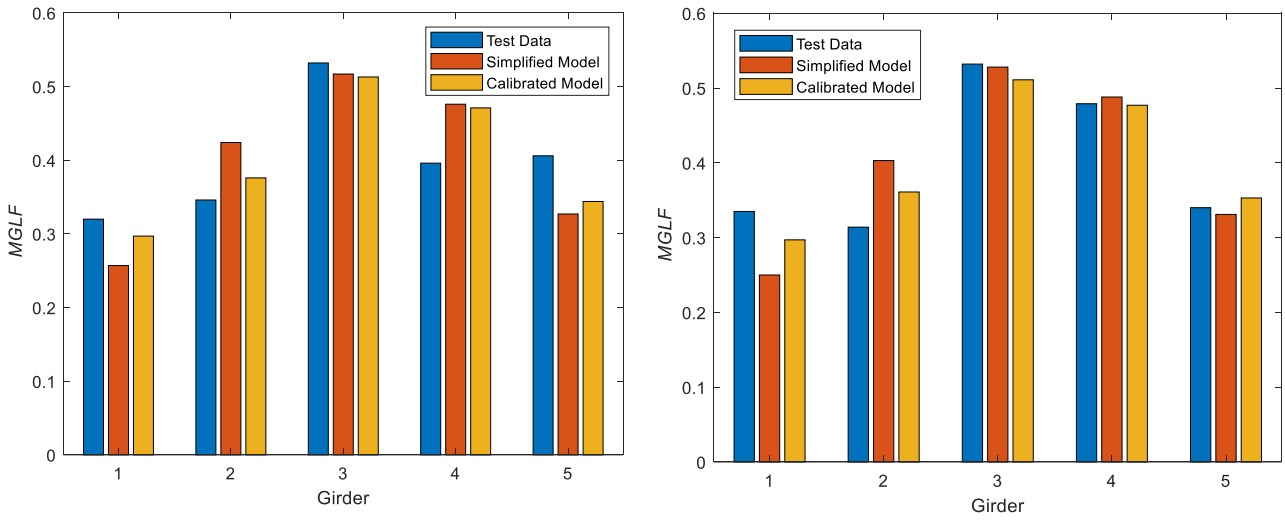

(a) (b)

Figure 3.6: Comparison of M42 *MGLF* Results Test Data, Simplified Model, and Calibrated Model (a) 2020 (b) 2022

3.4 Shear Test Modeling

3.4.1 Baseline HGMB Model

As described in section 3.3.2 the HGMB high-fidelity model was calibrated to the results of the moment live-load diagnostic tests. This included linear springs at the girder ends, decreased transverse concrete modulus to simulate a cracked deck, and increased carbon longitudinal elastic modulus. These parameters were used as the starting point for using the high-fidelity model to predict the results of the shear live-load diagnostic test. This is referred to as the baseline model. Figure 3.7 shows the average shear strains predicted by the baseline high-fidelity model compared to those measured during field testing for HGMB test V42. The most heavily loaded girders are the most important for the model to accurately predict. As seen in Figure 3.7 the baseline model over-predicts the average shear strains for all girders except exterior Girder 1. The over-prediction is also greatest in the most heavily girders which signifies the baseline model predicts a higher percentage of load distributed to the interior girders than the test

measured data suggests. This would suggest some inherent conservatism for shear live load distribution by the baseline model.

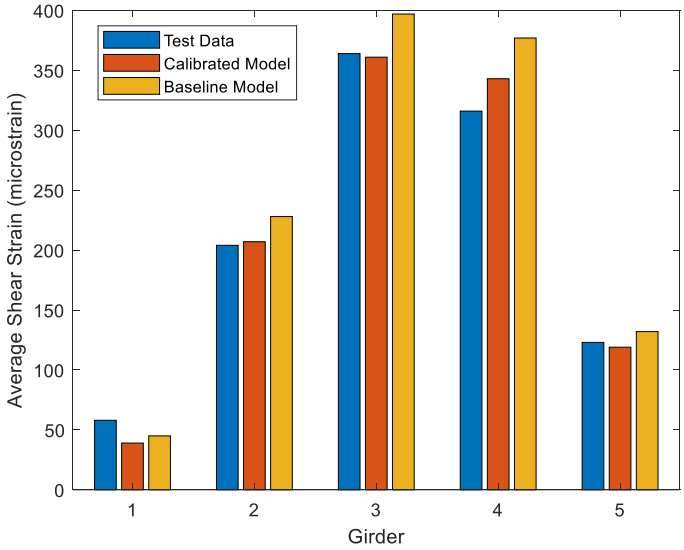

Figure 3.7: HGMB V42 Average Shear Strains

3.4.2 HGMB Baseline Model Calibration

3.4.2.1 Calibration Parameter

The baseline model for HGMB proved to predict live load distribution well with slight over-predictions in the magnitude of average shear strains compared to test results. These higher model-predicted shear strains suggest that the web shear modulus of the as-built girders might be greater than the nominal value used to develop the baseline model. This is supported by the results of picture frame shear tests of girder web samples detailed in Schanck et al. (2023) that indicate that the E-glass web shear modulus is slightly higher than the nominal manufacturer-reported value. To simulate this higher web shear modulus, the longitudinal elastic modulus of the uniaxial GFRP used in the web biaxial fabric was increased to minimize the least squares error between measured and predicted web shear strains. In the error minimization process, all 10 rosette shear strain measurements (two for each girder) were considered for the V42 load cases

and weighted equally. The calibration shows that a modest increase in the longitudinal elastic modulus of the glass from the nominal 36.8 GPa to 41.4 GPa minimizes the least squares error, reducing it by approximately 30%. The better alignment of predicted and measured strains is visually apparent from the results of the calibrated models shown in Figure 3.7.

3.4.2.2 Calibration Results

The comparison between the baseline high-fidelity models, calibrated high-fidelity models and shear test results for the HGMB are summarized in Table 3.5 for all four-truck tests. Average shear strains (Avg.) and the ratio of maximum to average web shear strain per girder (r) are reported for each girder.

Table 3.5: Measured and Model-Predicted Shear Strains, γ (με) for HGMB

Test V41										
(με)	Girder 1		Girder 2		Girder 3		Girder 4		Girder 5	
	Avg.	*r*	Avg.	*r*	Avg.	*r*	Avg.	*r*	Avg.	*r*
Test	27.4	2.49	124	1.90	272	1.44	337	1.05	252	1.04
Baseline	2.04	24.5	130	1.76	305	1.27	394	1.04	293	1.21
Calibrated	0.96	49.2	117	1.79	277	1.28	358	1.04	266	1.22
Test V42										
(με)	Girder 1		Girder 2		Girder 3		Girder 4		Girder 5	
	Avg.	*r*	Avg.	*r*	Avg.	*r*	Avg.	*r*	Avg.	*r*
Test	58.2	1.93	204	1.63	364	1.22	316	1.20	123	1.48
Baseline	44.8	2.48	228	1.47	397	1.11	377	1.14	132	1.82
Calibrated	39.2	2.63	207	1.49	361	1.11	343	1.15	119	1.86
Test V43										
(με)	Girder 1		Girder 2		Girder 3		Girder 4		Girder 5	
	Avg.	*r*	Avg.	*r*	Avg.	*r*	Avg.	*r*	Avg.	*r*
Test	144	1.42	310	1.30	352	1.04	193	1.52	52.6	1.82
Baseline	144	1.52	344	1.21	411	1.06	260	1.33	34.9	3.11
Calibrated	129	1.55	313	1.21	374	1.06	235	1.34	31.0	3.21

The calibration of the HGMB model helped reduce strains and better align the average of the two web shear strains within a girder with test measurements. The calibrated model acknowledges there is differential web shear, however it typically predicts a lower ratio than measured in the field for interior girders. For the exterior girders, where strains are typically less, the models significantly over-predict the ratio of maximum shear strain to average. However, this is an artifact of the very small shear strains in the exterior girders: for example, for test V41 in Girder 1, the calibrated model predicts $r = 49.2$, but this is largely due to the average strain being around 1 με due to a small negative strain predicted in one web of the girder.

3.4.3 Twin Bridge Baseline Model

The Twin Bridge girders were manufactured with the same biaxial GFRP web material as HGMB, and the baseline Twin Bridge model employed the same 41.4 GPa web longitudinal glass elastic modulus determined from calibration of the HGMB model. All other material constitutive properties were assigned based on nominal values provided by manufacturer data sheets or design drawing specifications as with the HGMB model. The concrete material was assumed isotropic with 25.1 GPa elastic modulus.

Figure 3.8 shows the average shear strains predicted for test V42 by the baseline high-fidelity Twin Bridge model compared to the test measured data. The baseline model consistently under-predicted the average shear strains within each girder with less under-prediction on the most heavily loaded interior girders. The exterior Girder 6 has the largest disparity with a 38.8% under-prediction, although the under-prediction is much less for the most heavily loaded girders – only 6.57% for Girder 4 in test V42. This level of under-prediction is consistent across all tests. The higher degree of under-prediction in the exterior girders likely results in a higher model-predicted distribution of shear to the interior girders.

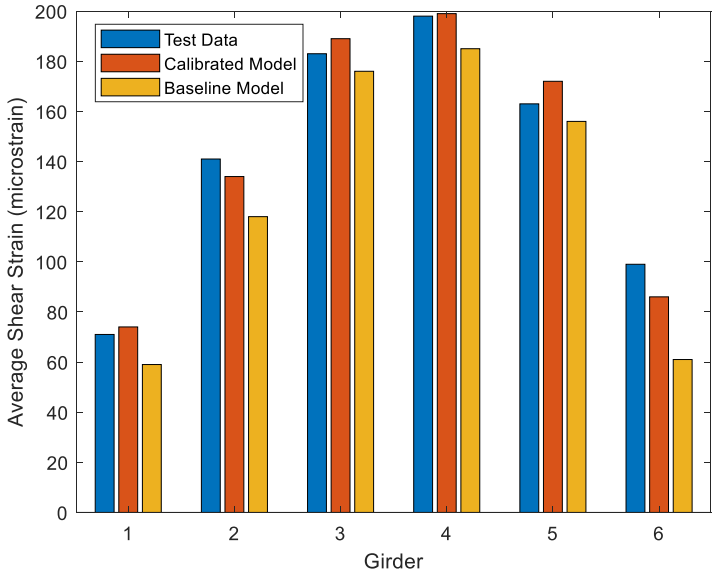

Figure 3.8: Twin Bridge Average Shear Strains Test V42

3.4.4 Twin Bridge Baseline Model Calibration

3.4.4.1 Calibration Parameter

A possible source of the consistently larger under-prediction of shear strains in the exterior girders of the Twin Bridge could be due to the model's lack of incorporation of abutment rotational restraint. As detailed in section 3.3.2, the inclusion of the paired abutment springs (see Figure 3.3) that simulate this rotational restraint observed in flexural load tests improved the model's ability to predict moment live load distributions across all girders. Given that the Twin Bridge's abutments were constructed similarly to those of the HGMB, it is reasonable to assume that the Twin Bridge also experiences abutment rotational restraint. To simulate this, paired abutment longitudinal springs were included in the Twin Bridge model and treated as a calibration parameter when minimizing the least squares error between model-predicted and measured shear strains using data from test V42. This test was used for calibration as it caused high shears and the trucks were close to centered on the bridge, which will minimize

the stiffening effects of features such as curbs and railings. Similar to HGMB calibration, both shear strain measurements from each girder were weighted equally in the calibration process for a total 12 measurements across the six girders in Twin Bridge. The model-predicted values were compared to the measured strains using a least squares error, and the spring stiffness applied to the model that created the minimum least square errors was determined. For the Twin Bridge model, the calibrated spring stiffness was $1.75 \times 10^7 \frac{N}{m}$, roughly 20% of the spring stiffness for HGMB. The calibration improved the least squares error by an average 36.4% relative to the baseline model across the three four-truck tests for Twin Bridge. As shown by the calibrated model results in Figure 3.8, the inclusion of the abutment springs increased shear strains in all girders with a larger increase occurring on the exterior girders resulting in improved distribution.

3.4.4.2 Calibration Results

As with HGMB, the calibrated model resulted in improved shear strain predictions for Twin Bridge. For example, for test V41, where loads were shifted to heavily load Girder 6, the baseline model predicts an average 123 με in the webs of Girder 6 vs. a measured averaged strains 179 με, whereas the calibrated model improves predictions to 154 με. The calibrated model improved the average shear strain prediction for test V42 in HGMB and under-predicted the most heavily loaded Girder 3's average shear strains by a mere 0.82% compared to the baseline model's previous 9.07% over-prediction for Girder 3. In the Twin Bridge V42 test simulation the baseline model under-predicted the average shear strains in the most heavily loaded Girder 4 by 6.57% while the calibrated model over-predicted by 0.51%.

While the calibration process for HGMB did not significantly improve the prediction of differential strain ratio *r*, the results in Table 3.6 show that calibration did generally improve the prediction of differential strain for the Twin Bridge in most girders. Unlike HGMB, Twin Bridge

was calibrated by including the optimal spring coefficient to simulate end rotational restraint, and this effect was already included before calibration for HGMB. This suggests that the differential web shears are affected by the rotational end restraint resulting from semi-integral abutments. Figure 3.8 also shows how the inclusion of the paired springs in the Twin Bridge model increased the shear strains in the exterior girder more than in the interior girders, implying that the rotational springs created more even shear distribution across girders than predicted by the baseline model where more shear was drawn to the interior girders.

Table 3.6: Measured and Model-Predicted Shear Strains, γ (με) for Twin Bridge

Test V41												
(με)	Girder 1		Girder 2		Girder 3		Girder 4		Girder 5		Girder 6	
	Avg.	*r*	Avg.	*r*	Avg.	*r*	Avg.	*r*	Avg.	*r*	Avg.	*r*
Test	43.8	1.93	90.2	1.69	136	1.36	179	1.18	204	1.10	179	1.05
Baseline	40.2	2.94	75.2	2.44	129	1.57	176	1.45	183	1.01	123	1.10
Calibrated	49.1	2.37	87.2	2.06	139	1.44	190	1.34	200	1.04	154	1.01
Test V42												
(με)	Girder 1		Girder 2		Girder 3		Girder 4		Girder 5		Girder 6	
	Avg.	*r*	Avg.	*r*	Avg.	*r*	Avg.	*r*	Avg.	*r*	Avg.	*r*
Test	70.5	1.63	141	1.39	183	1.11	198	1.12	163	1.05	99.1	1.31
Baseline	59.1	2.19	118	1.75	176	1.16	185	1.10	156	1.23	60.6	1.43
Calibrated	73.7	1.82	134	1.55	189	1.11	199	1.04	172	1.24	86.3	1.39
Test V43												
(με)	Girder 1		Girder 2		Girder 3		Girder 4		Girder 5		Girder 6	
	Avg.	*r*	Avg.	*r*	Avg.	*r*	Avg.	*r*	Avg.	*r*	Avg.	*r*
Test	120	1.26	180	1.16	192	1.02	181	1.16	131	1.25	61.9	1.57
Baseline	91.9	1.54	149	1.42	185	1.07	165	1.10	117	1.49	30.9	2.42
Calibrated	112	1.36	168	1.29	198	1.10	178	1.15	131	1.46	52.9	1.92

3.4.5 HGMB Simplified Shear Model

The overarching goal of the FE modeling and diagnostic live load testing detailed here is to quantify live load shear distribution in CT girder bridges and provide a basis for the development of CT girder-specific shear *DF*s. However, while the calibrated high-fidelity

models can predict girder shear strains very accurately, those models are specific to the individual bridges and include many secondary structural features such as curbs, railings, sidewalks, and details of steel reinforcement that are not considered in design. Further, not all bridges will exhibit end rotational restraint, which distributes shear loads more evenly across girders and therefore should not be considered in development of shear live load *DF*s. Further, the high-fidelity models are time-consuming to create and computationally expensive due to their high level of refinement. Developing a simplified FE modeling approach without secondary structural features that can accurately predict the shear distribution in CT girder bridges for a wide range of nominal bridge configurations is therefore essential to determine shear *DF*s.

3.4.5.1 Model Description

Section 3.3.3 described a simplified model developed to predict the flexural behavior of the HGMB where the girders were discretized with beam line elements and the deck was discretized with shell elements. This model was able to predict live-load moment distribution well and was very computationally efficient due to the use of beam elements for each girder. However, such a model cannot predict differential web shear, which the tests and analyses reported here have both shown to be an important phenomenon displayed by CT girders. Therefore, the simplified model detailed here must capture the girder geometry with shell elements. Further, due to their effect on girder behavior at the abutments where shear is the highest, the reinforced concrete end diaphragms were also maintained. Not only are secondary features like the sidewalk not included in the simplified model, but the girders are modeled with prismatic girder sections with smeared orthotropic properties, whereas the high-fidelity models captured the true non-prismatic girders with composite lamina layup assignments. This not only decreases model run time and model complexity but is reasonable since not all CT girder bridges

are designed with non-prismatic sections. Ultimately, the simplified model represents the girders with S8R, 8-noded shell elements with 6 DOFs per node and reduced integration, and the concrete deck and abutments are simulated with solid C3D20R 20-noded quadrilateral brick elements with three DOFs per node and reduced integration. Figure 3.9 shows the simplified model for the HGMB. A typical simplified model was discretized with 75000 elements and 1.3 x 10^6 DOFs and resulted in a roughly 50% reduction in analysis time compared to the high-fidelity model. This discretization relied on the same seeding and element sizing as used for the high-fidelity model.

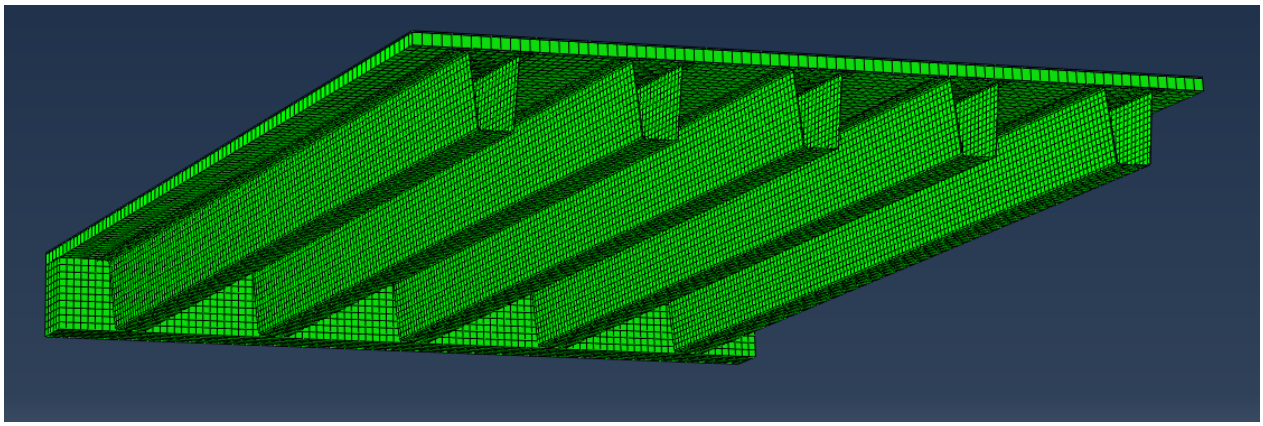

Figure 3.9: Fully Meshed Cross-Section Cut of Simplified HGMB FE Model

3.4.5.2 Results Comparison

To assess the efficacy of the simplified modeling approach, model predictions of the HGMB diagnostic live load test configurations are compared here with an explicit focus on the shear force carried by each girder, which is typically quantified by the live load support reaction (Cross et al. 2009, Barr and Amin 2006). Further, *SGLF*s that describe the portion of the total reaction carried by each girder (R_j) as a fraction of the total load produced by a given live loading can be computed using Equation 3.3, where N_L represents the number of loaded lanes.

$$SGLF_j = \frac{R_j N_L}{\sum_{i=1}^{N} R_i} \quad (3.3)$$

*SGLF*s predicted by the simplified and high-fidelity models for the V42 test configuration are chosen for comparison and summarized in Figure 3.10. Girders 3 and 4 had the highest shear based on the recorded shear strains and proved to have relatively equal shear distribution based on model-predicted end reactions as shown in Figure 3.10. The calibrated model also predicts Girder 5 will have a very similar reaction to that of interior Girders 3 and 4. However, the average shear strains reported in Figure 3.7 suggest that Girder 5 carries much less shear when compared to Girders 3 and 4. This phenomenon of increased reactions in the obtuse corner is consistent with AASHTO guidelines which have an adjustment factor to increase obtuse corner reactions in skewed bridges (AASHTO 2020, Huo et al. 2005). However, the simplified model does not predict the same level of shear distributed to the obtuse corner, but under-predicts the *SGLF* compared to the calibrated model. The simplified model also under-predicts the shear distribution to the acute corner at Girder 1. This is likely due to the exclusion of the sidewalk in the simplified model, which reduces the stiffness of Girder 1, causing it to attract less load resulting in higher shears in the interior girders. The lack of abutment springs in the simplified model also tends to result in less uniform distribution of shear to each girder. Taken together, these also help explain the simplified model's over-prediction of shear in the most heavily loaded Girders 3 and 4.

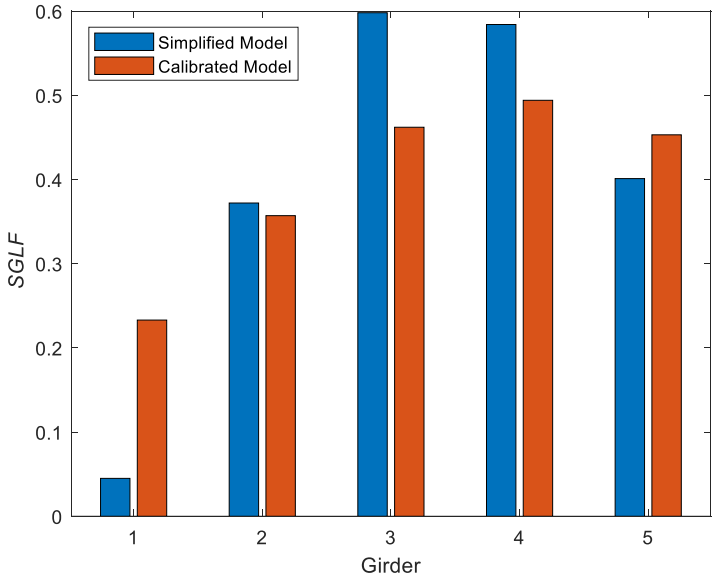

Figure 3.10: HGMB V42 *SGLF* Inferred from Model Reactions

Table 3.7 compares the *SDF*s determined from AASHTO's expression for concrete box girders and the model-predicted *SGLF*s for the HGMB. Since the *SDF*s from AASHTO are governed by two lanes of loading the model-predicted *SGLF*s are the maximums from the three 4 truck tests. The Girder 1 SDF is based on the lever rule since the AASHTO expression is not applicable. The results show that the baseline high-fidelity model *SGLF*s are all below AASHTO SDFs except for Girder 1 where the lever rule is used. The over-prediction by AASHTO is a maximum of 54.6% in the interior girders and 5.19% in the exterior Girder 5 relative to the calibrated model. However, when compared to the simplified model AASHTO over-predicted interior girder shear by 28.4% and under-predicted shear for Girders 1 and 5 by 15.8% and 7.00%. Overall, these results indicate that AASHTO over-predicts shear distribution to the interior beams of CT girder bridges but is reasonably accurate for exterior girders. The interior girder over-prediction is consistent with the *SGLF*s inferred from strains in Table 2.7. The simplified also predicts higher *SGLF*s using reactions compared to Table 2.7 *SGLF*s inferred from girder shear strains, which is consistent with the observation of Cross et al. (2009) that

reactions create higher *SDF*s than girder shears a girder depth from bearing. To explore this further and provide a more comprehensive assessment of AASHTO *SDF*s, a parametric study is performed next using the simplified model subjected to a wider spectrum of AASHTO live loads.

Table 3.7: HGMB Maximum Model Predicted Two Lane *SGLF*s vs. AASHTO *SDF*s

	Girder 1 (sidewalk)	Interior Girders	Girder 5 (obtuse corner)
AASHTO	0.319	0.881	0.811
Calibrated Model *SGLF*	0.441	0.570	0.771
Simplified Model *SGLF*	0.379	0.686	0.872

3.5 Summary

The high-fidelity models can predict test measured strains very well following calibration, where the calibration parameters of abutment rotational spring stiffness and web shear modulus are justifiable based on observed bridge response and previous laboratory tests. Both bridges have end rotational restraint due to their semi-integral abutment detailing that causes slightly more even live-load distribution. The simplified model typically predicts the interior girder *DF* well for moment compared to the field test results. For moment the simplified model does not predict the exterior girder *DF* well with upwards of 18% under-predictions compared to the field test results, which likely reflects the simplified model's neglect to integral curbs and/or sidewalk. For shear the simplified model shows more conservative *DF*s for the most heavily loaded interior and exterior girders. These results indicate that the simplified models are appropriate for parametric studies on interior girders for both shear and moment, although their prediction of exterior girder live load moments may not be as accurate.

3.6 References

AASHTO. 2020. *AASHTO LRFD Bridge Design Specifications*. Washington, DC: AASHTO.

Barbero, E. J. 2018. *Introduction ot Composite Materials Design (3rd edition).* Boca Raton, FL: CRC Press.

Barr, P. J., and M. N. Amin. 2006. "Shear live load distribution factors for I-girder bridges." *J. Bridge Eng*. 11 (2): 197-204. https://doi.org/10.1061/(ASCE)1084-0702(2006)11:2(197)

Choi, W., I. Mohseni, J. Park and J. Kang. 2019. "Development of live load distribtuion factor equation for concrete multicell box-girder bridges under vehicle loading." *International Journal of Concrete Structures and Materials*. 13 (22). https://doi.org/10.1186/s40069-019-0336-1

Cross, B., B. Vaughn, N. Panahshahi, D. Petermeier, Y. S. Siow, and T. Domagalski. 2009. "Analytical and experimental investigation of bridge girder shear distributions factors." *J. Bridge Eng*. 14 (3): 154-163. https://doi.org/10.1061/(ASCE)1084-0702(2009)14:3(154)

Dassault Systèmes. 2022. *ABAQUS/CAE 2022.* Velizy-Villacoubly, France

Dicleli, M., and S. Erhan. 2009. "Live load distribution formulas for single-span prestressed concrete integral abutment bridge girders." *Journal of Bridge Engineering*. 14 (6): 472-486. https://doi.org/10.1061/(ASCE)BE.1943-5592.0000007

Figiolini, A. M. 2011. "Degradation of Mechanical Properties of Vinylester and Carbon Fiber/Vinylester Composites Due to Environmental Exposure: Masters Thesis." Florida Atlantic University , Boca Raton, FL, USA. http://purl.flvc.org/FAU/3332182

Huo, X. S., E. P. Wasserman, and R. A. Iqbal. 2005. "Simplified method for calculating lateral distribution factors for live load shear." *J. Bridge Eng*. 10 (5). https://doi.org/10.1061/(ASCE)1084-0702(2005)10:5(544)

Jose-Trujillo, E., C. Rubio-Gonzalez and J. A. Rodriguez-Gonzalez. 2019. "Seawater ageing effect on the mechanical properties of composites with different fiber and matrix types." *Journal of Composite Materials*. 53 (23): 3229-3241. https://doi.org/10.1177/0021998318811514

Pirvu, A., D. J. Gardner and R. Lopez-Anido. 2004. "Carbon fiber-vinyl ester composite reinforcement of wood using the VARTM/SCRIMP fabrication process." *Composites: Part A*. 35 (11): 1257-1265. https://doi.org/10.1016/j.compositesa.2004.04.003

Razzaq, M. K., K. Sennah and F. Ghrib. 2021. "Live load distribution factors for simply-supported composite steel I-girder bridges." *Journal of Constructional Steel Research*. 181: 106612. https://doi.org/10.1016/j.jcsr.2021.106612

Sotelino, E. D., J. Liu, W. Chung and K. Phuvoravan. 2004. "Simplified load distribution factor for use in LRFD design." *Indiana DOT*, West Lafayette, IN, USA. Accessed 16 May 2023. https://docs.lib.purdue.edu/cgi/viewcontent.cgi?article=1662&context=jtrp

Schanck, A.. 2021. "Determination of Bridge Behavior Through Live-Load Testing and Advanced Numerical Analysis." Electronic Theses and Dissertations. 3535. https://digitalcommons.library.umaine.edu/etd/3535

Schanck, A., W. G. Davids, J. Pinkham and K. Berube. 2023. "Assessment of web shear stresses and shear capacity of FRP composite tub girders for highway bridges." *Structures*. 51: 880-894. https://doi.org/10.1016/j.istruc.2023.03.083

Suksawang, N., and H. Nassif. 2007. "Development of live load distribution factor equation for girder bridges." *Journal of the Transportation Research Board*, 9-18. https://doi.org/10.3141/2028-02

Tan, T. T. M., and N. H. Nieu. 1996. "Hybrid carbon-glass fiber vinyl ester resin composites." *Macro-molecular Materials and Engineering*. 234: 53-58. https://doi.org/10.1002/apmc.1996.052340106

Wiss, Janney, Elstner Associates, Inc.. 2017. "Montana Department of Transportation (MDT) Investigation of Bridge Decks." *WJE* , Northbrook, IL, USA. Accessed 16 May 2023. https://www.mdt.mt.gov/publications/docs/brochures/Forensic-Deck-Analysis-Report-2017-04-21.pdf

Chapter 4: Parametric Study

4.1 Introduction

The simplified models for moment and shear have been shown to predict test live load distributions well, especially for interior girders. However, these do not capture the full set of likely bridge geometries. The simplified models were designed to facilitate generalization so that the model geometries can be adjusted automatically for a given set of geometric parameters. This allows critical parameters to be changed programmatically to generate a model of a complete bridge and perform live load analysis under AASHTO HL-93 loading (AASHTO 2020). This produces a wider array of results for many bridges with varying parameters to develop live load *DF* expressions for CT girders comparable to AASHTO expressions. For clarity, the distribution factors for moment will be referred to as *MDF* and shear *SDF*.

4.2 Assumptions

Previous attempts at *DF* expression determination with parametric studies have used databases of constructed bridges to provide reasonable bridge and girder geometries and properties to generate structural models (Cross et al. 2009, Ndong et al. 2022). Due to the novelty of the CT girder, there are only four bridges constructed to date which do not provide a sufficiently large sample size of typical bridge and girder designs to use in the models for a parametric study. Therefore, some assumptions were made on the material properties and geometries of the bridge and girders to develop adequate designs for each set of parameters. These assumptions were based on communication with Advanced Infrastructure Technologies (the designer and manufacturer of all CT bridge girders to-date), and girder designs from the four existing bridges. Only two-lane bridges were considered, and the AASHTO definition of number of lanes as the total travel width divided by 3.66 m rounded down to the nearest whole number

was enforced. As a results, travel width ranged from 7.32 m to 11.0 m. It was assumed that a typical bridge would have 508 mm wide curbs on each side, bringing the range of overall bridge widths to between 8.33 m and 12.0 m. It should be noted that although the curb width was considered to define overall bridge deck width, the curbs were not explicitly modeled and therefore their contribution to stiffness was neglected.

4.2.1 Girder Design

The CFRP and GFRP material properties from the HGMB design, previously listed in Table 2.1, were applied to the girders designed for the parametric study. The elastic moduli of the bottom flange and web were found by classical lamination theory as described in Barbero (2018). The dimensions of the top flanges were kept to a constant 25.4 mm thick by 165 mm wide with a longitudinal elastic modulus 27.1 GPa, which matches typical CT girder construction. The splay angle of the web was assumed to be 5°, also a typical value used for CT girders. The bottom flange width was kept as 305 mm for spans under 18.3 m, and 610 mm for spans from 18.3 m to 24.4 m unless otherwise noted.

For each set of parameters, an iterative design process was performed such that candidate girders met the AASHTO Strength I limit state for shear and moment with applicable capacity and environmental reduction factors as detailed in Davids et al. (2022). The design was automated using software consisting of a series of functions that took input parameters for bridge geometry, performed capacity calculations, and determined ultimate factored dead and live load moment and shear per AASHTO requirements. To comply with current design methodology, the AASHTO concrete box girder *DF*s were used to determine the number of lanes of live load carried by each girder. The girders were also designed to meet the AASHTO recommended live load (truck plus impact) deflection limit of $L/1000$. Deflection was the first check as it often

controls flexural design based on previous experience. When needed, sufficient stiffness to meet the deflection limit was achieved by adding carbon plies to thicken the bottom flange which is current design practice. Following the deflection check, the number of glass plies in the web were determined to ensure sufficient shear capacity assuming a 68.9 MPa characteristic failure stress. This is the current characteristic failure stress used in design, which testing by Schanck et al. (2023) showed is likely conservative. This value was further reduced by an environmental reduction factor of 0.65, a statistical reliability factor of 0.85, and a resistance factor of 0.75 (AASHTO 2012, Davids et al. 2022). Web shear buckling capacity was then checked using a 0.35 resistance factor based on the results of the buckling analyses performed in Schanck et al. (2023). Finally, the moment capacity was checked using moment-curvature analysis and all appropriate reduction factors as explained by Davids et al. (2022) for both the composite section under Strength I loading and the non-composite section under the dead load during the deck construction phase. The concrete material in the deck was assumed to have a compressive strength of 27.6 MPa and the deck reinforcement was neglected, a conservative assumption which slightly reduces predicted flexural capacity and stiffness.

4.2.2 Moment Model Implementation

Once a girder had been designed for a given set of parameters, the simplified FE model to predict *MDF*, previously described in section 3.3.3, was created. For the beam elements, the properties were given for the non-composite girder section from the transformed section analysis performed in the girder design process. Modular ratios were used to transform all materials to concrete with an elastic modulus (E) of 25.1 GPa. Along with E, the beam is defined in the model using its moments of inertia (I) about the 11 and 22 axes seen in Figure 4.1. Additional geometric and constitutive properties included the polar moment of inertia (J), cross sectional

area (*A*), and shear modulus (*G*). The shear modulus was assumed constant with a value of 10.7 GPa, the value of the ±45° oriented GFRP face sheets in the webs. The polar moment of inertia was calculated assuming a closed thin wall rectangle with a height equal to the girder depth and width of the bottom flange and thickness of the 2 face sheets per web. This notional section is depicted in Figure 4.2. A separate sensitivity study was performed to verify the effect of varying *J* from 0.5*J* to 2*J*, which resulted in minimal change in the model output. This indicates that, although crude, this approximation was adequate for the analyses performed here.

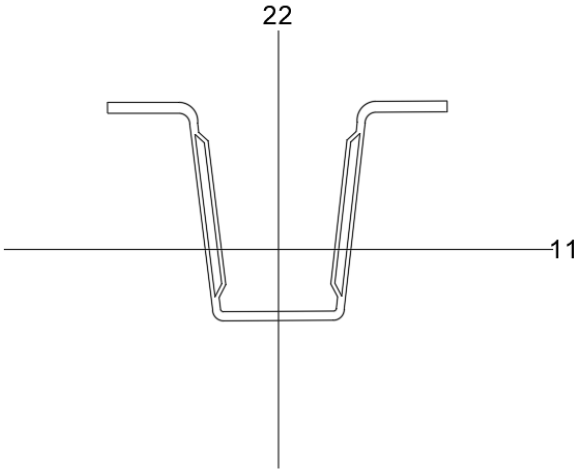

Figure 4.1: Girder Axes

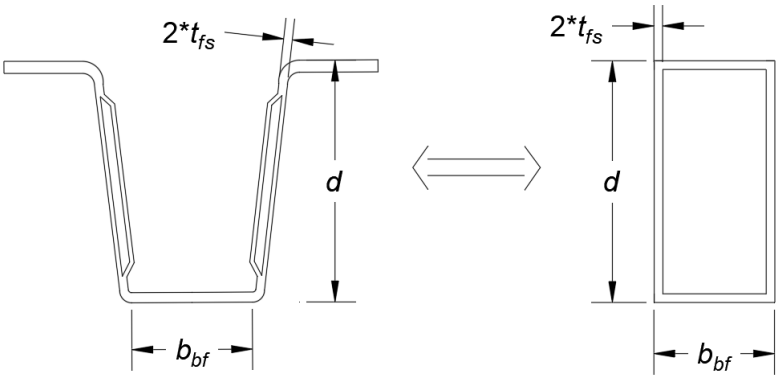

Figure 4.2: Polar Moment of Inertia Simplified Thin-Wall Cross Section

Each beam was also discretized with 10 equal length elements evenly spaced along inner 30% of the span as shown in Figure 4.3. The ends of the elements were constant nodes that helped locate maximum strains which may not occur directly at midspan, especially in bridges with skewed abutments. When calculating the moment in a single girder it was determined from the maximum strain of the 11 discrete nodes near midspan of the girder. The maximum strain was converted to a moment through the section modulus, which was determined by a simple tributary width (determined from girder spacing) transformed section analysis of the girder deck cross section. Using individual girder moments, the format of Equation 2.1 with a ratio of girder moment to total moment was implemented for model output *MDF*s and includes multiple presence and number of lanes loaded. Finally, the deck was assigned as S8R shell elements with orthotropic properties to represent a cracked deck as described previously. The transverse elastic modulus was different for each deck thickness put into the model and listed in Table 4.1.

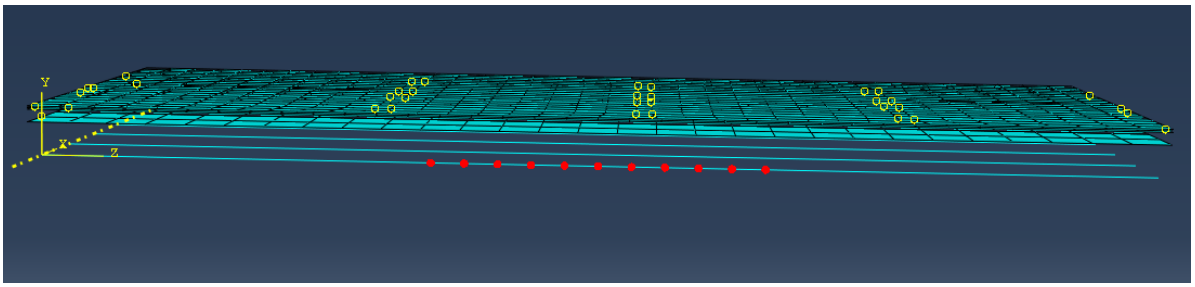

Figure 4.3: Girder Center Span Nodes Highlighted in Red for Girder 1

Table 4.1: Transverse Elastic Modulus of Concrete for Certain Deck Thickness

Deck Thickness (mm)	Transverse Elastic Modulus (GPa)
178	5.32
203	5.12
229	4.90

4.2.3 Shear Model Implementation

As described in section 3.4.5, the simplified model used for shear parametric studies models the true CT girder cross sectional geometry with shell elements. These shells were

modeled with prismatic girder sections having smeared orthotropic properties obtained from the girder design described in section 4.2.1. The thickness of the web foam core was considered in the design process and assignment of properties for the web. The bottom flange was partitioned at the end to provide seven nodes (shown in Figure 4.4) for the application of boundary conditions and lower the discontinuities and stress concentrations in the model. The reaction at a single girder end was the sum of the reactions output at these seven nodes. The model output *SDF* was determined as the ratio of single girder reaction to the sum of all girders under the same loading with multiple presence and number of lanes applied to directly compare to AASHTO predictions.

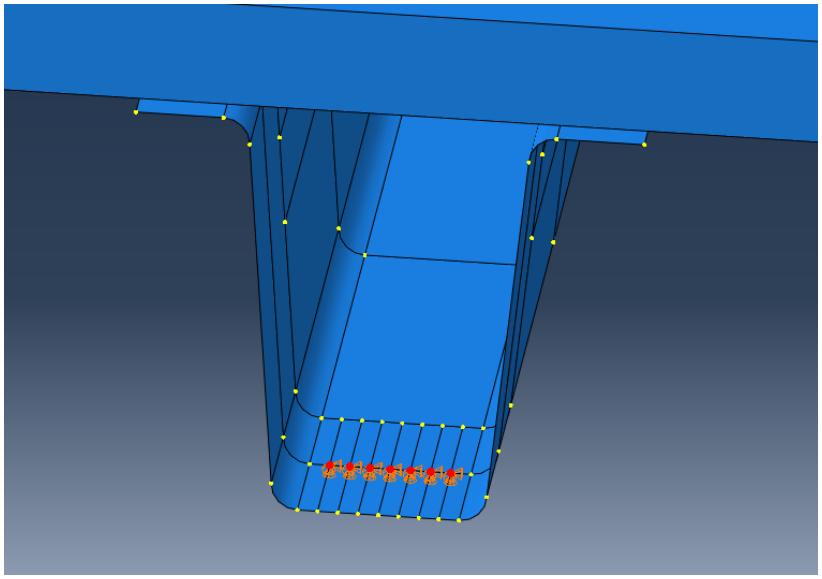

Figure 4.4: Shear Model Girder End Partitions and Nodes for Boundary Conditions

4.2.4 Load Application

AASHTO HL-93 loading is defined in section 3.6 of the *AASHTO LRFD Bridge Design Specifications* (AASHTO 2020). There are rules the application of load must follow including 3.66 m wide design lanes, with 3.05 m wide uniform lane loads and multiple truck axle configurations. The truck and lane loads must be positioned to maximize load effects. The truck load also must be increased by a 33% impact factor, which does not apply to the 3.06 kPa

uniform lane load. The loads were applied on shell surfaces that were given minimal mechanical properties that effectively added zero strength and stiffness to the structure but provided consistent surfaces to use for offsets and creating a generalized and easily edited surface for load application.

Two truck configurations were considered, the HL-93 truck shown in Figure 2.6 (b) and the tandem axles with two 111 kN axles spaced longitudinally by 1.22 m. With either truck configuration, a wheel centerline cannot be applied any closer than 610 mm to the edge of a lane. Since these loads must be moved transversely and longitudinally to maximize load effects, the precise positions of the truck and lane load that will cause a maximum load effect is not known, especially for bridges with complex geometry. However, performing a very large number of analyses to completely examine all possible load positions is not tractable, and therefore some assumptions were made to limit the number of analyses.

First, it was assumed that applying the load center of gravities as close to the girder of interest as possible transversely within the guidelines of AASHTO would produce the maximized live load distribution effects for shear and moment. This meant that for exterior girders, the first lane started at the inside of the assumed 508 mm curb and the second lane started an additional 3.66 m after. Within each lane, the uniform 3.05 m width was applied on the side closest to the girder in question. The nearest truck wheels were placed 610 mm from the start of the lane. This exterior girder load application can be seen in Figure 4.5 (a). To maximize load distributed to the interior girders the two-lane loads were grouped together with one uniform load applied to the right edge of the lane with the truck 610 mm from that right edge and in the second lane the uniform lane load shifted all the way to the left edge and the truck 610 mm from

that edge as seen in Figure 4.5 (b). The longitudinal positioning of loads is described after mesh refinement.

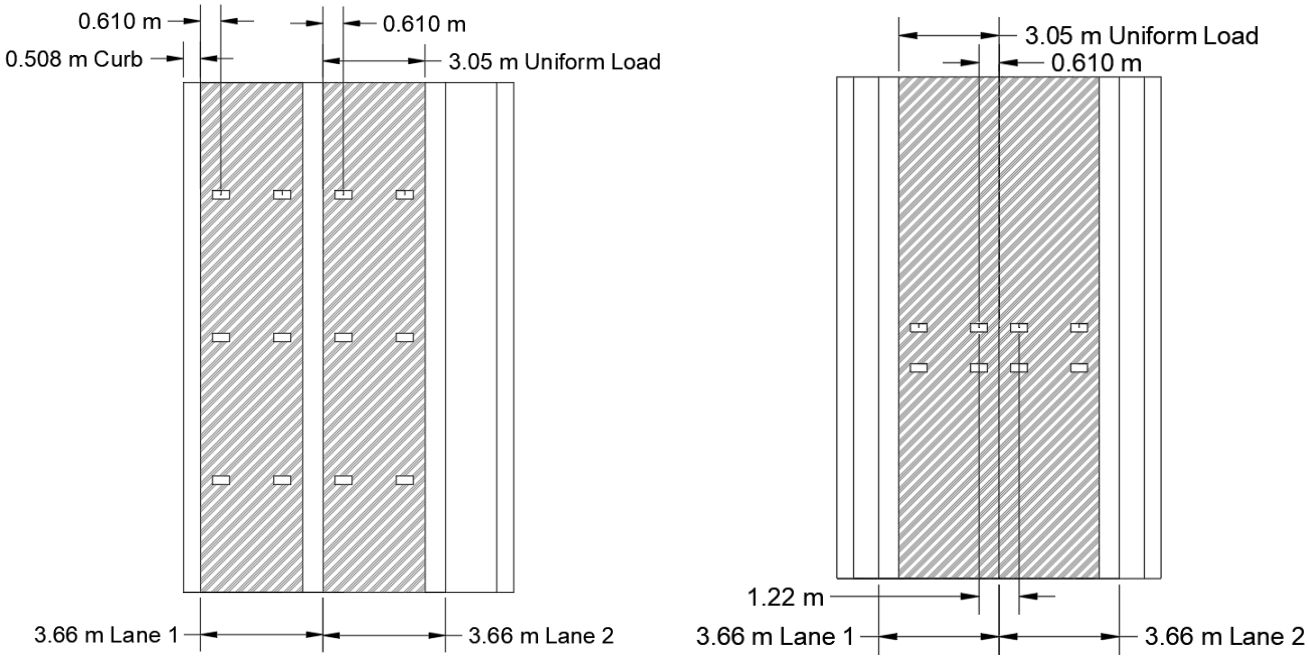

Figure 4.5: AASHTO HL-93 Load Applications to Model (a) Optimized on Exterior with Truck Axles (b) Interior Optimized Positioning with Tandem Axles

4.3 Convergence Studies

4.3.1 Moment Parametric Model Convergences

4.3.1.1 Mesh Convergence

Element size was examined for the moment simplified model to produce converged *MDF* and strain results. The load surface was fixed at a maximum element side length of 50.8 cm while the deck and girder element sizes were varied. Figure 4.6 shows the results of varying the mesh density for the deck and girders on output interior *MDF* for multiple span lengths. Mesh densities greater than 0.0157 elements per cm results in essentially constant *MDF* values for most span lengths and was selected as the element size for the girder and deck moving forward. This translates to element dimensions of approximately 63.5 cm.

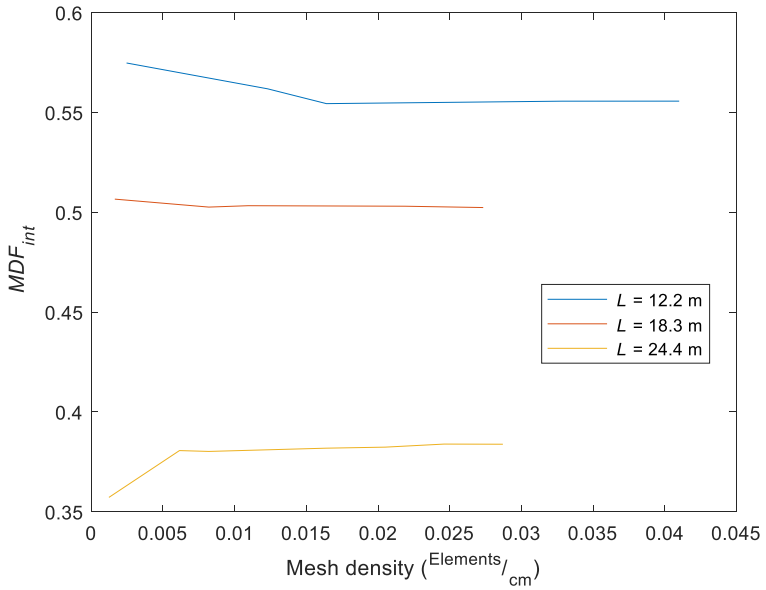

Figure 4.6: Simplified Moment Model Mesh Convergence

4.3.1.2 Longitudinal Positioning Convergence

Once an adequate discretization was defined, the longitudinal placement that produced the maximum moment could be determined. This position becomes less trivial for skewed bridges as two-way bending effects start to reduce the moment in the longitudinal direction. For non-skewed bridges, the truck load was applied nearly centered on the span to produce a maximum moment with the assumed simply supported boundary conditions. The uniform lane load was applied over the full length of bridge to produce maximum moment. The longitudinal position was measured relative to the rear axle and moved the entire truck in 610 mm increments, tracking the total moment produced in the model at each truck positioning. Skewed and non-skewed bridges were examined for maximum moment positions for both the truck and tandem axle configurations.

An example is shown in Figure 4.7 for a truck axle with varying bridge skews at spans of 18.3 m and 24.4 m. At higher skews a lower percentage of the design moment is achieved when

summing the moments in each girder converted from the maximum strains. The axle locations that produced the three highest total moments in the model at each skew were selected and used in the parametric study. Table 4.2 summarizes the positions used in the study for each skew and load configuration as an offset of the rear axle from the support. For instance, a non-skewed 18.3 m span bridge loaded under the truck axle configuration would have three longitudinal positions assessed with the rear axle starting at 4.88 m, 5.49 m, and 6.10 m from the support.

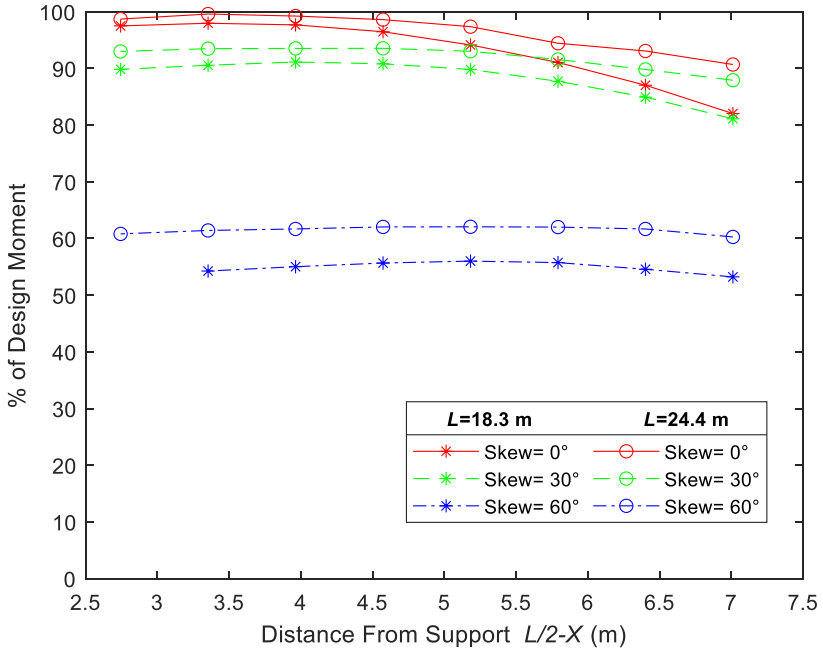

Figure 4.7: Percent (%) Live Load Moment Achieved for Rear Axle Position from Support

Table 4.2: Longitudinal Position from Support to Rear Axle

Skew Range	Truck	Skew Range	Tandem
$0° \leq \theta \leq 20°$	$\frac{L}{2} - 4.27\ m$ to $\frac{L}{2} - 3.05\ m$	$0° \leq \theta \leq 15°$	$\frac{L}{2} - 1.52\ m$ to $\frac{L}{2} - 0.305\ m$
$20° < \theta \leq 45°$	$\frac{L}{2} - 4.88\ m$ to $\frac{L}{2} - 3.66\ m$	$15° < \theta \leq 45°$	$\frac{L}{2} - 2.13\ m$ to $\frac{L}{2} - 0.914\ m$
$45° < \theta$	$\frac{L}{2} - 5.79\ m$ to $\frac{L}{2} - 4.57\ m$	$45° < \theta$	$\frac{L}{2} - 2.74\ m$ to $\frac{L}{2} - 1.52\ m$

4.3.1.3 Transverse Positioning Convergence

With the model mesh defined and the longitudinal positions established, the transverse positions required to maximize *MDF* were determined. The loading was positioned at the minimum allowed offset from the curb and then centered in the travel width. The distance between these two positions was divided into equal step sizes based on the number of total load positions desired. The number of positions was varied until convergence to a maximum interior *MDF* was achieved. The exterior maximum *MDF* was typically achieved with the load applied with the minimum allowed offset to the curb line. For skewed bridges the load was placed by varying its position across the entire travel width but for the non-skewed bridges the load is only varied to the point where loading was centered in the travel width taking advantage of symmetry of the bridge transversely. The results of the transverse load study for a typical bridge with HL-93 truck loading are shown in Figure 4.8 for (a) one lane and (b) two lanes. From the results of this examination, seven transverse positions were selected for one lane loading and five positions were selected for two lane loading. The total number of analyses for a bridge was 42 and 30 for one and two lanes of load respectively.

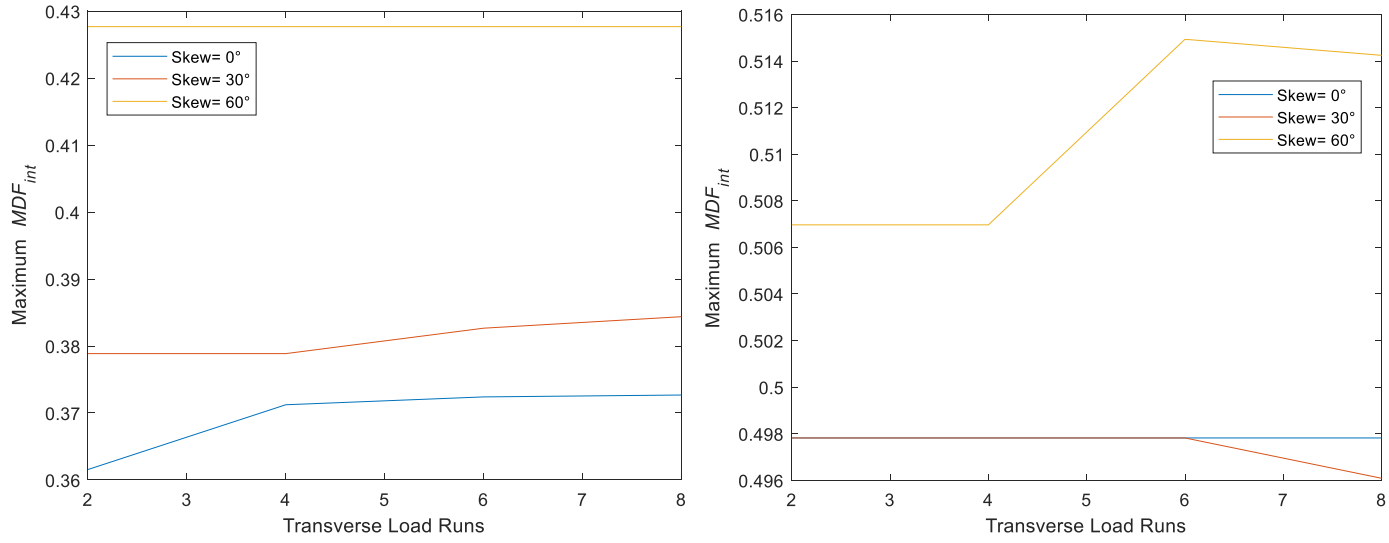

(a) (b)

Figure 4.8: Number of Transverse Load Runs Convergence (a) One Lane (b) Two Lanes

4.3.2 Shear Parametric Model Convergences

4.3.2.1 Mesh Convergence

A different model was required for modeling shear live load distribution due to the tub shape of the girders with two webs as highlighted in Chapter 3. The shear parametric model required a different discretization compared to the moment model as it has multiple components including the deck, diaphragm, girders, and load surfaces. The diaphragms were meshed with an element size of 152 mm to create 3 elements through their thickness. The girder and deck seed sizes were varied to find a mesh that gave convergent distribution factors and reactions at the girder ends. First, the girder mesh was varied from two to six elements through the girder depth shown in Figure 4.9 for a 12.2 m span bridge and a 24.4 m span bridge. During this study the deck and load surface were meshed with 508 mm elements. Following the girder discretization study, a mesh of four elements through the depth was selected. The deck mesh was studied, varying the number of elements in the span from forty to eighty. The results of this study found minimal effect on the number of elements in the span of the deck and forty elements in the span was selected moving forward. The mesh of the load surface was found to have little effect and the seeding was kept at 508 mm.

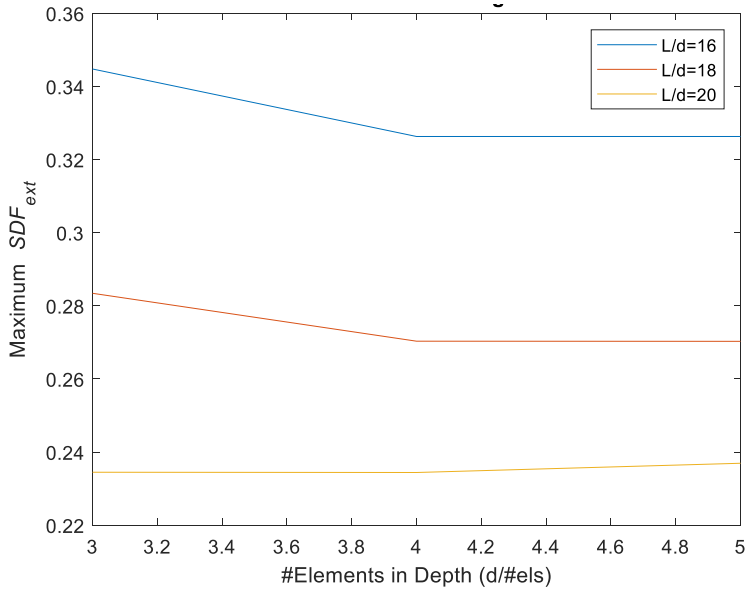

(a)

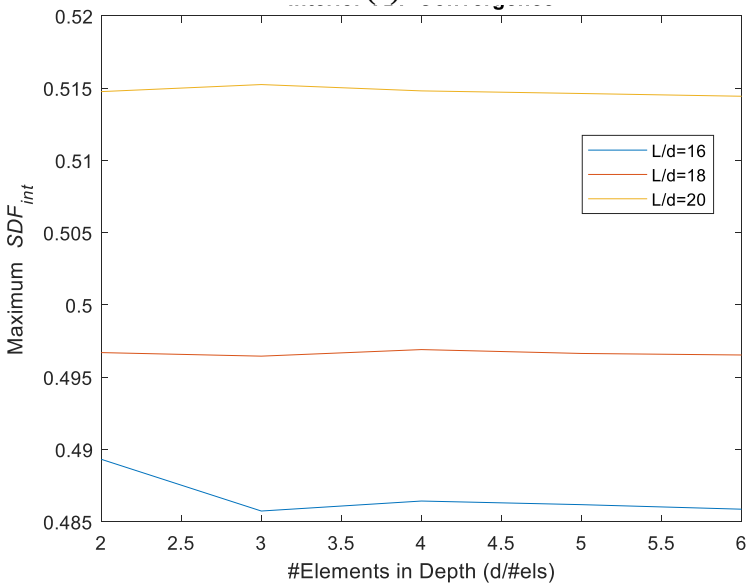

(b)

Figure 4.9: Shear Parametric Model Girder Mesh Convergence (a) 12.2 m Span Exterior *SDF* (b) 24.4 m Span Interior *SDF*

4.3.2.2 Longitudinal Positioning Convergence

Following the convergence study a study of longitudinal position producing maximum shear and shear distribution was performed. Intuitively, loads placed directly over the bearing produces the highest reactions at girders. However, this may not produce maximum shear distributions. The model was analyzed with the load positioned in the exterior optimized position

and centered transversely on the bridge to produce large shears in an exterior girder and an interior girder at each longitudinal position. The longitudinal position was varied from 230 mm from centerline bearing to twice the depth of the girder. It was found that the longitudinal position minimally affected the shear *DF* on the interior and exterior, however as trucks were placed further from centerline bearing the overall reactions were reduced. Therefore, the trucks were placed one girder depth from centerline bearing longitudinally.

4.3.2.3 Transverse Positioning Convergence

One extreme for transverse load positioning is with live loads towards the exterior of the lanes to maximum shear in an exterior girder as shown in Figure 4.5 (a), and the second extreme transverse load position is with loads centered in the bridge travel width as shown in Figure 4.5 (b). Intermediate evenly spaced positions between those two extremes were also considered. Ultimately it was determined five different transverse positions were sufficient to determine the maximum *SDF*s in most cases. This resulted a total of ten live load cases for an individual bridge to determine the *SDFs* corresponding to the five transverse positions for both the HL-93 truck and tandem load configurations.

4.4 Moment Parametric Study

Typical AASHTO (2020) design procedure is to determine the interior girder *MDF* using the expressions for one lane and two or more lanes and use the larger of the two. After finding the interior girder *MDF* a skew reduction factor is applied as well as an eccentricity for the exterior girder *MDF*. Within the AASHTO expression (seen in Equations 4.1-2) for interior girders, spacing (*S*), girder depth (*d*), and span length (*L*) are the three parameters included with *S* being the most influential as indicated by its larger exponent. For the expressions *S* and *L* are in m and *d* in cm. These three parameters were assessed, along with deck thickness and number of

girders, for their effect on interior girder *MDF*. The *d* and *L* terms are also related in the expression as the inverse of the span-to-depth ratio which was also assessed. For the skew reduction factor, the skew angle itself has the greatest effect, and so the effect of skew angle was studied. Finally, the eccentricity factor relies on d_e, a term which relates the distance from the inside of the curb to the centerline of the exterior web at the intersection with the top flange.

One Lane Interior Moment

$$MDF_{int} = \left(\frac{S}{0.914}\right)^{0.35} \left(\frac{Sd}{100L^2}\right)^{0.25} \quad (4.1)$$

Two Lanes Interior Moment

$$MDF_{int} = \left(\frac{S}{1.92}\right)^{0.6} \left(\frac{Sd}{100L^2}\right)^{0.125} \quad (4.2)$$

4.4.1 Effect of Spacing

Girder spacing *S* is the most influential parameter for interior *MDF*s according to AASHTO and was assessed first. Five non-skewed girder bridges were examined with span-to-total-depth ratio fixed at 18:1, deck thickness fixed at 203 mm, and overhang fixed at 0.914 m. *S* was varied from 1.83 m to 2.44 m for spans of 12.2 m, 18.3 m, and 24.4 m. The results of the *S* parameter study are shown in Figure 4.10 for (a) one lane and (b) two lanes of load. As seen in Figure 4.10 the two lanes *MDF*s are greater than those for one lane. For the two lanes *MDF* AASHTO over-predicts MDF compared to the model. However, AASHTO under-predicts for one lane *MDF*. For both one and two lanes, the model and AASHTO predict very similar variation in *MDF* with *S*.

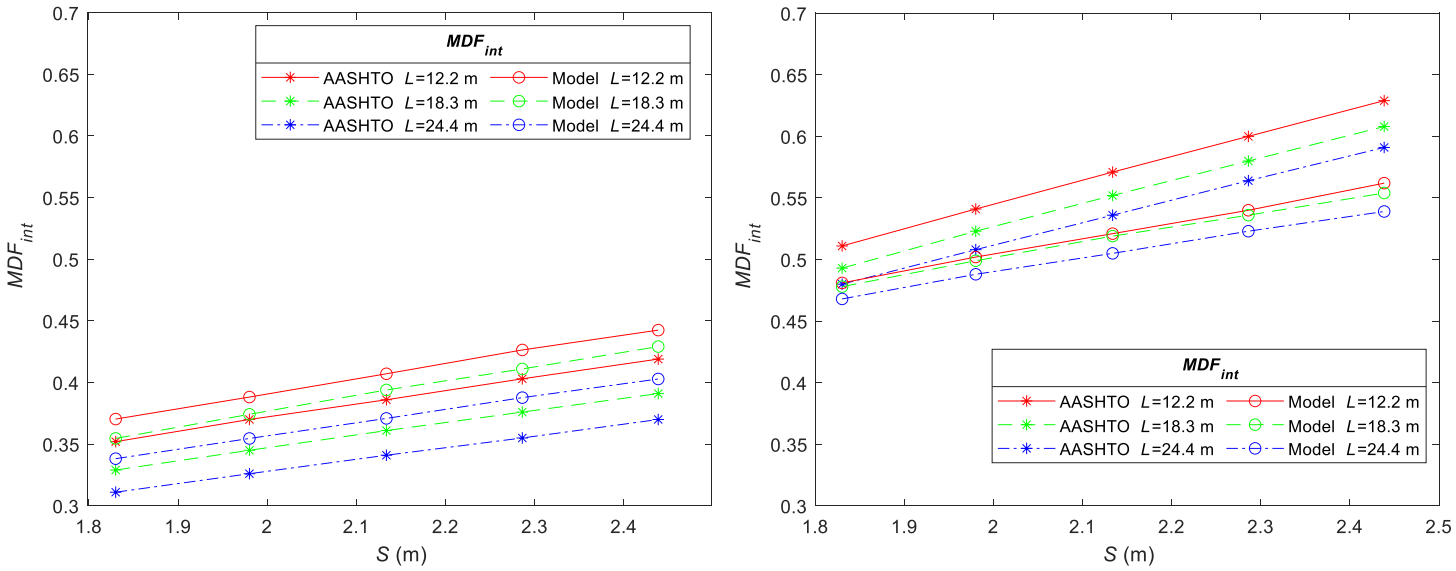

(a) (b)

Figure 4.10: Interior *MDF* with Varying *S* (a) One Lane (b) Two Lanes

4.4.2 Effect of Span Length

In the study of *S*, it was noticed that at lower span length for the same spacing the *MDF* tended to be lower which agrees with AASHTO's treatment of *L*. To further investigate the effect of *L* on interior *MDF* five values of *L* from 12.2 m to 24.4 m were assessed for three separate girder spacings (*S*=1.83 m, 2.13 m, and 2.44 m). The same constant values were applied as in section 4.4.1. The results are shown in Figure 4.11 for (a) one lane and (b) two lanes respectively. Again, the two lanes of load applied to the bridge resulted in higher interior *MDF*s. Also, AASHTO under-predicts the model-predicted one lane *MDF* and over-predicts the two lanes *MDF* from the models. The results show that as *L* increases the interior *MDF* decreases at a similar rate to AASHTO's expression predicts.

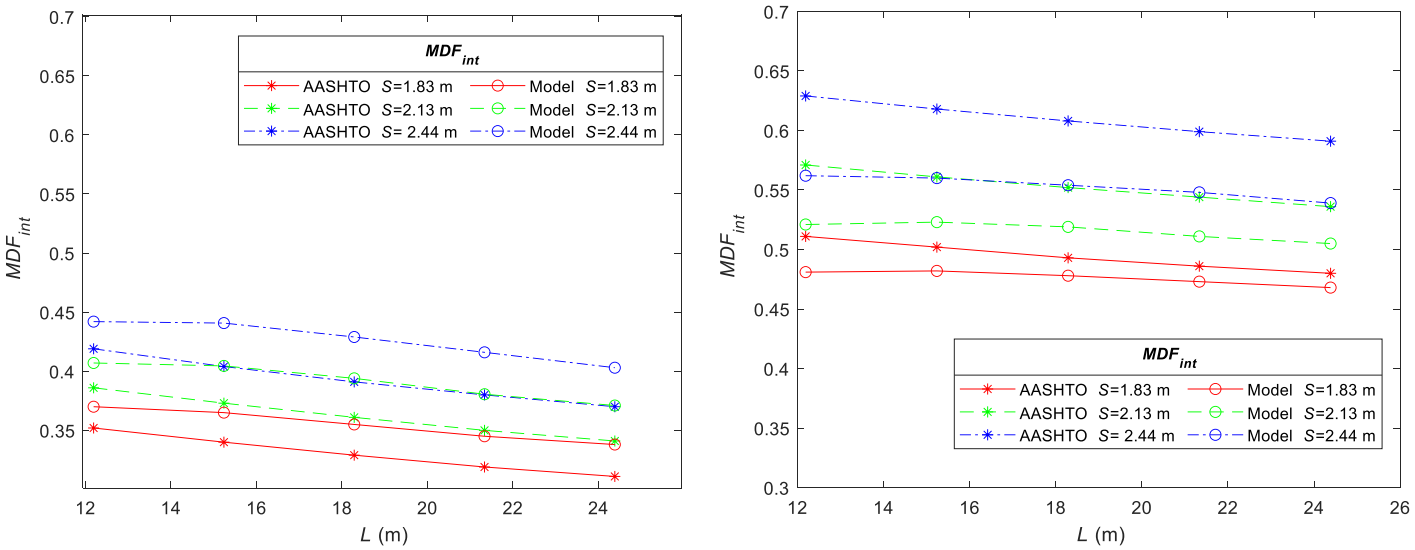

Figure 4.11: Interior *MDF* with Varying *L* (a) One Lane (b) Two Lanes

4.4.3 Effect of Span-to-Depth Ratio

The span-to-total-depth ratio was varied for non-skewed five girder bridges with S = 1.83 m and other constants consistent with section 4.4.1. The ratios assessed range from 16:1 to 20:1 which is typical for current CT girder bridges built to date. The results of this variation are shown in Figure 4.12 for (a) one lane and (b) two lanes interior *MDF*s. The model predicts a minimal effect on the ratio to the interior *MDF* which is contrary to AASHTO. This is expected due to the nature of the parametric study. Each girder was designed through the same process and typically governed by the deflection requirement. The deflection requirement is met through achieving a certain stiffness (*EI*) for that span length regardless of span-to-total-depth ratio. Since the stiffness is the same regardless of the girder depth there is no change in relative stiffness and the distribution within the bridge does not vary as shown by Figure 4.12. These results suggest that any future *MDF* expression for interior girders may not need to include the span-to-total-depth ratio or girder depth to predict the *MDF*.

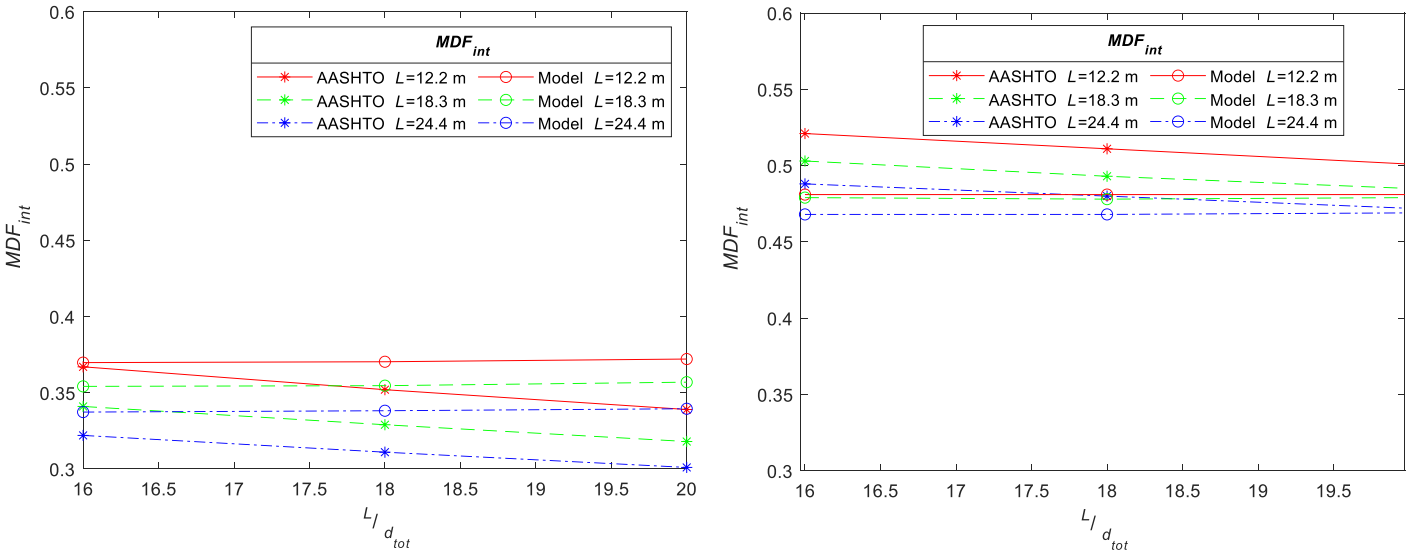

(a) (b)

Figure 4.12: Interior *MDF* with Varying Span-to-Total-Depth (a) One Lane (b) Two Lanes

4.4.4 Effect of Deck Thickness

Although span-to-total depth was shown to have minimal effect on the model-predicted interior *MDF* the concrete deck thickness was fixed in that study. Intuitively, as the deck thickness increases the deck should carry more of the load due to its increased stiffness and girders' stiffness is less important to meet the required section strength limits. Therefore, the load distribution was expected to be more evenly spread to each girder in thicker decks. This was examined for non-skewed, five girder bridges with S = 1.83 m and 18:1 span-to-total-depth ratio. The deck thickness was varied from the minimum thickness allowed by AASHTO (2020) of 178 mm to a maximum of 229 mm. The results of varying deck thickness (t) are shown in Figure 4.13 for (a) one lane and (b) two lanes interior *MDF*. Again, the one lane *MDF* is under-predicted by AASHTO yet smaller in magnitude compared to the two lanes *MDF*. AASHTO still over-predicts the two lanes *MDF* and does not anticipate the effect of t, whereas the model does show that as t increases the interior *MDF* decreases.

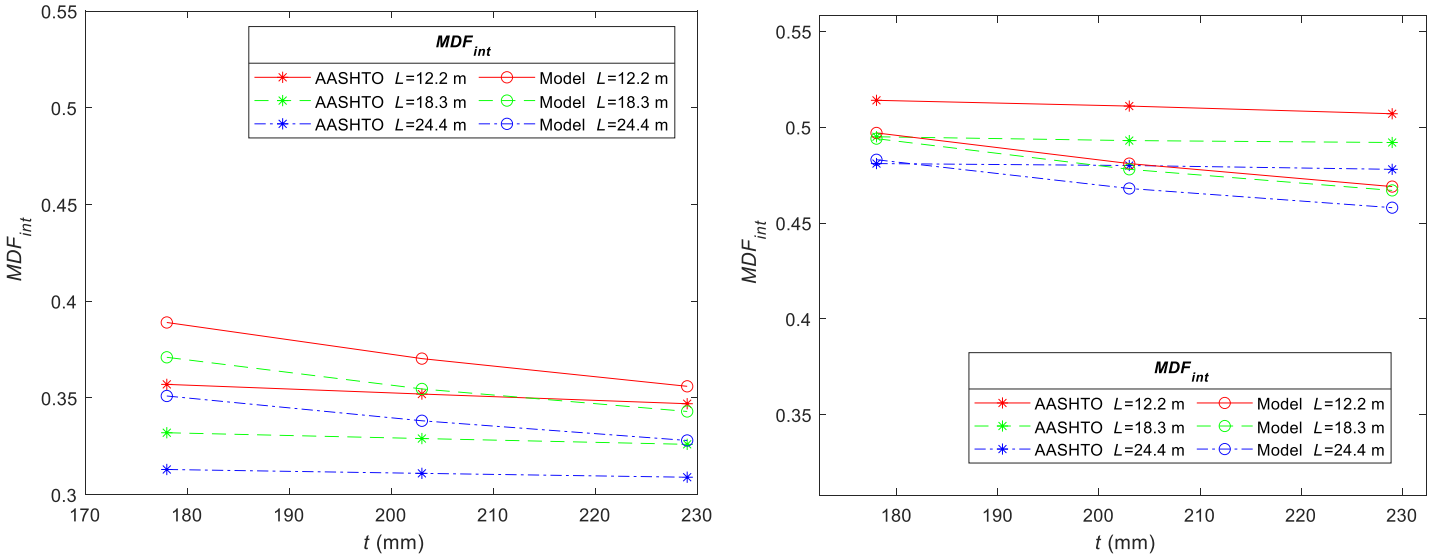

(a) (b)

Figure 4.13: Interior *MDF* with Varying Deck Thickness *t* (a) One Lane (b) Two Lanes

4.4.5 Effect of Number of Girders

In each of the previous analyses, all the bridges assessed used five girders. To maintain total bridge widths for two-lane bridges and spacings between 1.52 m and 2.44 m bridges built to-date have used five and six girders. It was expected that five girder bridges would have higher *MDF*s than six girder bridges. A few bridges were analyzed with both five and six girders for non-skewed bridges with S = 1.83 m and t = 203 mm. The span-to-total-depth was fixed at 18:1. The results are shown in Table 4.3 for one lane and two lanes of load. As expected, the increase in the number of girders leads to decreases in the interior *MDF*. Therefore, basing *MDF* expressions on model predictions from five girder bridges, the lowest number of girders used to-date for two lanes CT girder bridges, will lead to the higher *MDF*.

Table 4.3: Interior *MDF* for Varying Girder Numbers

Span Length L (m)	Interior *MDF* Determination	One Lane		Two Lanes	
		5 Girders	6 Girders	5 Girders	6 Girders
L = 12.2	AASHTO Expression	0.352		0.511	
	Model Predicted	0.375	0.364	0.486	0.433
L = 18.3	AASHTO Expression	0.329		0.493	
	Model Predicted	0.357	0.342	0.481	0.423
L = 24.4	AASHTO Expression	0.311		0.480	
	Model Predicted	0.338	0.322	0.469	0.413

4.4.6 Effect of Deck Overhang on Exterior Girder *MDF*

In previous analyses, the overhang was fixed at 0.914 m which was no more than half of the girder spacing. According to AASHTO, the overhang treated as d_e, as seen in Equation 4.3, is the parameter that affects the edge correction factor. The value d_e is in m and represents the distance from the web centerline to the inside of the curb on the exterior girder. The overhang was varied from the initial 0.914 m to half the spacing, which is the maximum in typical designs for girder spacings of 1.98 m, 2.13 m, and 2.29 m. The span was also varied however showed minimal effect on the results. The exterior correction factor *e* is the ratio of the exterior *MDF* to the interior *MDF*, meaning a value greater than 1 signifies exterior girders have a higher distribution than the interior. The bridges assessed were all non-skewed, five girder bridges with 203 mm thick decks and 18:1 span-to-total-depth ratio. Figure 4.14 shows the results for the 18.3 m span bridges for (a) one lane and (b) two lanes of live load. The results show the exterior girders for the one lane case had a much higher correction factor than the two lanes loaded girders. The results also show that under two lanes of load, the correction factor was typically less than AASHTO predicts and less than 1.0, meaning the exterior girder had a lower *MDF* than the interior. The one lane plot was not compared to AASHTO as AASHTO requires the use of the lever rule in this situation. For both one and two lanes the factor goes at a consistent slope at all spacings and shows minimal difference in magnitude at each spacing. The results suggest that

the overhang is the parameter that effects the exterior correction factor like AASHTO predicts and is not affected by spacing and span length. Regardless of the one lane having a higher correction factor the two lanes interior *MDF* is still much larger and results in the two lane exterior *MDF* still governing the one lane exterior *MDF*.

$$MDF_{ext} = e\,(MDF_{int})\,;\ where\ \ e = 0.97 + \frac{d_e}{8.69} \tag{4.3}$$

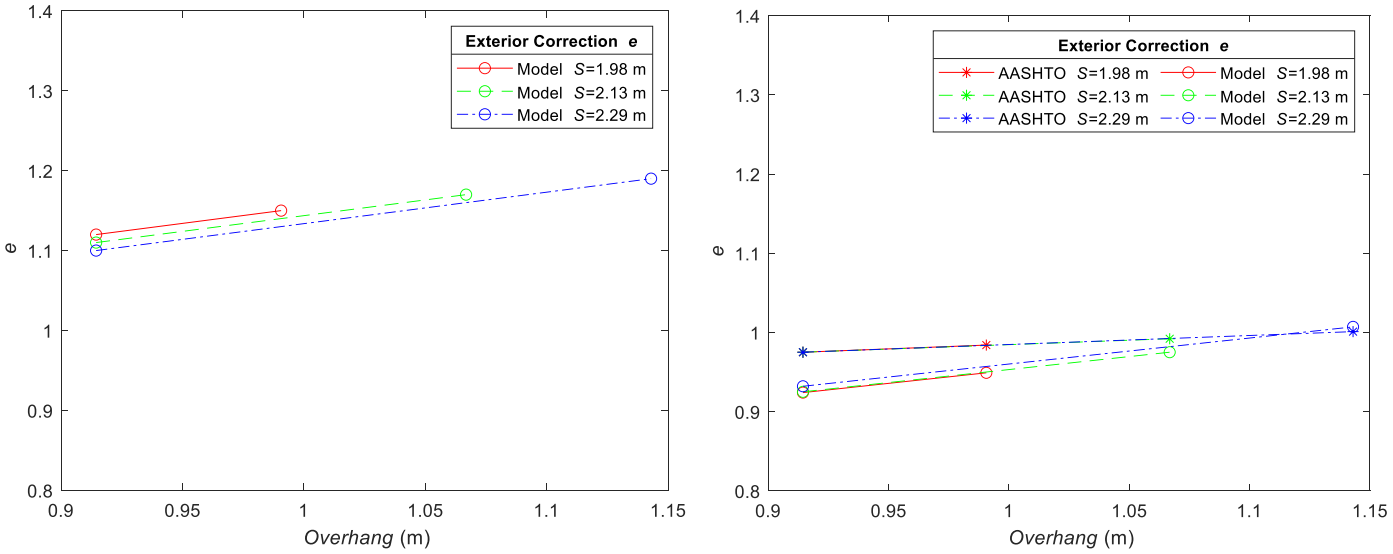

(a) (b)

Figure 4.14: Moment Exterior Correction Factor *e* with Varying Overhang (a) One Lane (b) Two Lanes

4.4.7 Effect of Skew Angle

The bridges so far have all been non-skewed. However, skew is very common to meet roadway geometry requirements as bridges are not usually perfectly perpendicular with the obstructions over which they pass. AASHTO refers to the adjustment for skew as a skew reduction factor, which implies that skew decreases the *MDF*. This was tested with the moment simplified model by analyzing skews up to 60°. The bridges had five girders, a 203 mm deck, span-to-total-depth ratio of 18:1 and 2.13 m girder spacing. The model-predicted skew correction

factor C_θ is the ratio of maximum flexural strain from a skewed bridge divided by the maximum flexural strain for the same non-skewed bridge. The results of varying skew are shown in Figure 4.15 for (a) one lane and (b) two lanes of live loading for interior girders. The model predicts that at shorter spans the reduction in *MDF* due to skew is greater than for longer spans. This makes intuitive sense as for shorter spans, the length and width become closer in size, creating larger two-way bending effects. The model also predicts less of a skew reduction than AASHTO in most cases meaning AASHTO would under-predict the *MDF* in a skewed CT girder bridge. The first 0-15° range shows very minimal change in the moment distribution.

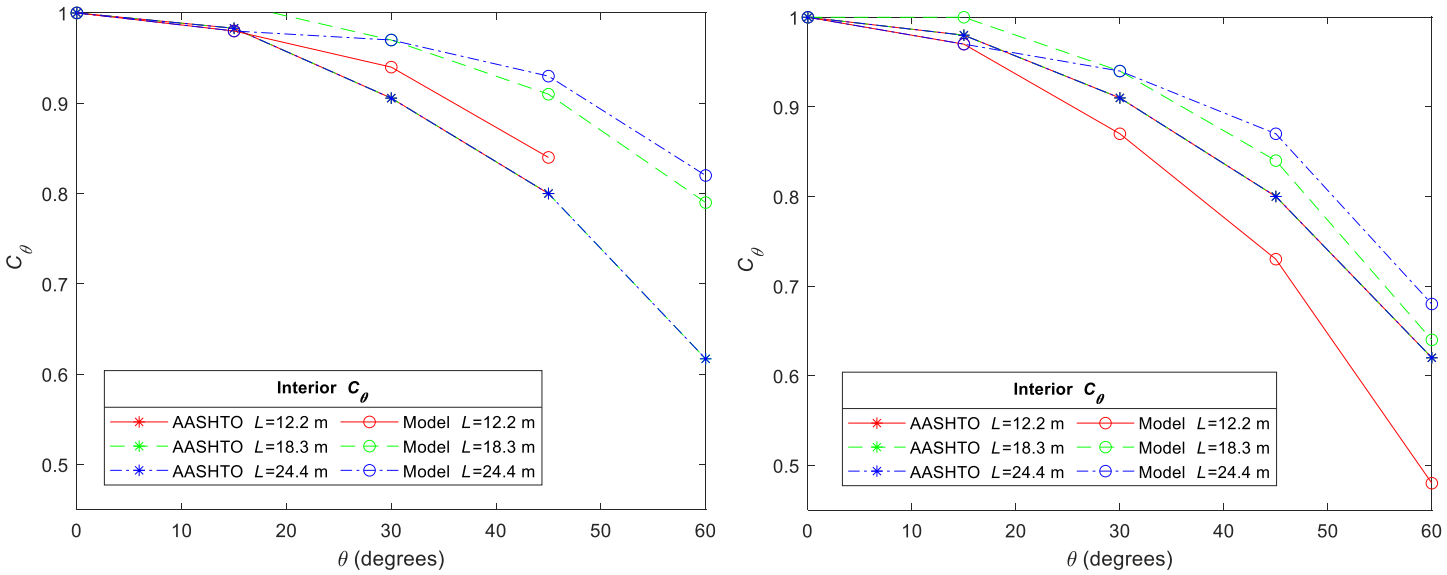

(a) (b)

Figure 4.15: Interior Skew Correction Factor (a) One Lane (b) Two Lanes

4.5 Shear Parametric Study

Spacing (*S*), girder depth (*d*), and span length (*L*) are the three parameters included in the AASHTO expression for concrete box girder bridges with *S* being the most influential (AASHTO 2020). In this parametric study, *S* and *L* were varied for typical non-skewed, two-lane CT girder bridges with five girders to assess the impact of these critical parameters. Two lanes of

live load were only applied and no one lane loadings were assessed. Overall roadway width was varied from 9.14 m to 11.6 m and girder spacing was varied from 1.83 m to 2.44 m. Other parameters including the deck thickness of 203 mm and exterior girder deck overhang of 914 mm were held constant. To-date, bridges have been designed with span-to-total-depth ratios of 15.5:1 to 20:1, and for this parametric study the span-to-total-depth ratio was maintained at an intermediate value of approximately 18:1. In addition to the other constant parameters, the bottom flange width was fixed at 457 mm, the average of the typical bottom flange widths for the span lengths considered here.

4.5.1 Effect of Spacing

The results of the spacing study are shown in Figure 4.16 where model -predicted *SDF*s and AASHTO *SDFs* are compared for interior girders. In Figure 4.16 there is good agreement between the AASHTO and model-predicted *SDF*s for the shortest span assessed (12.2 m) with AASHTO showing a slightly higher SDF. The model-predicted *SDF*s suggest that spacing is an influential parameter and follows a similar pattern to the AASHTO expression, but as span length increases the degree of conservatism in the AASHTO SDF increases dramatically. This suggests that the term including *S* in the AASHTO expression could be utilized in any future CT girder-specific expression, but that the coefficients should be altered to adjust the levels of conservatism.

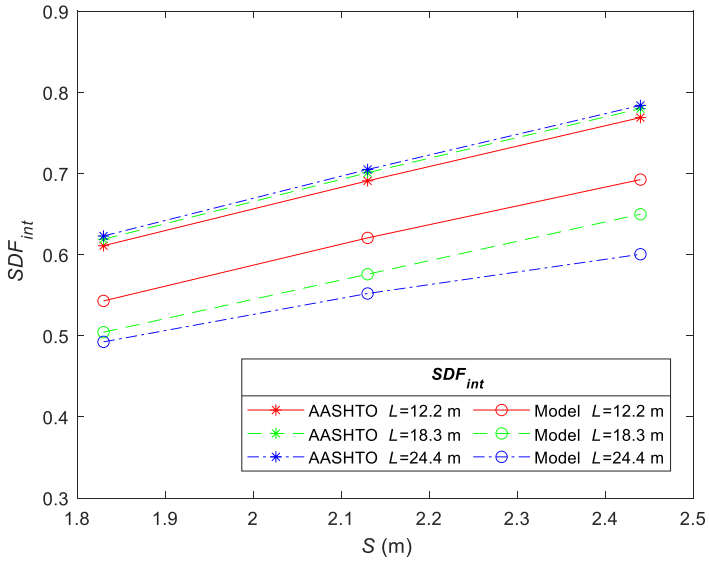

Figure 4.16: Effect of Girder Spacing S on Interior SDF

4.5.2 Effect of Span Length

Figure 4.17 indicates that AASHTO shows a small increase in *SDF* as the span length increases, whereas the models show a consistent and more marked decrease in *SDF*s as *L* increases. However, AASHTO still over-predicts the S*DF*s compared to the model as seen in Figure 4.17. This suggests that the $\frac{d}{100L}$ term in the AASHTO expression, seen in Equation 2.4, may not accurately capture shear live load distribution for CT girders. However, the *L* in the denominator of Equation 2.4 indicates that as *L* increases, the *SDF* should decrease. Figures 4.16 and 4.17 show that the model predicts this as well. This suggests that the treatment of girder depth *d* in Equation 2.4 may need to be adjusted for use with CT girders.

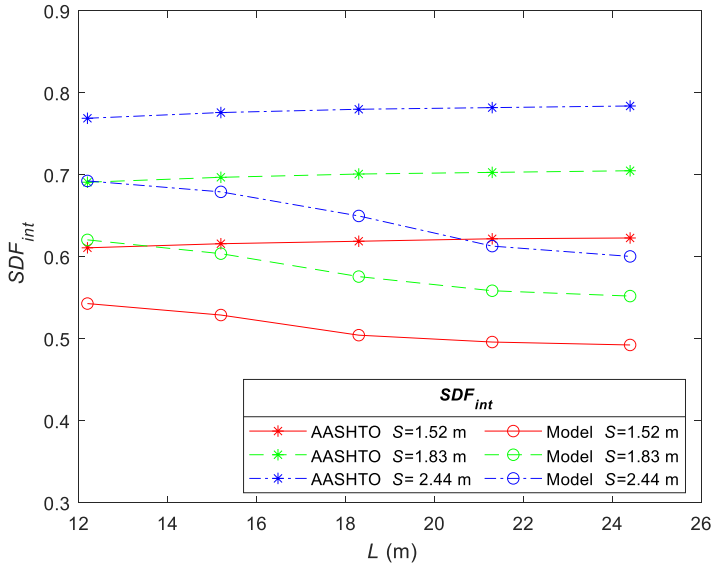

Figure 4.17: Effect of Span Length L on Interior SDF

4.5.3 Effect of Bottom Flange Width

Typical CT girder designs increase bottom flange width (b_{bf}) as span length increases to provide adequate area to for CFRP bottom flange material for required flexural strength and stiffness. The result is that for wider girders, the effective spacing between adjacent webs decreases as span length increases, resulting in more uniform load distribution. The prior results of the parameter study kept a constant bottom flange width. To test the effect of bottom flange width on live load shear distribution, S was varied for an 18.3 m bridge with three separate values for b_{bf} of 305, 457, and 610 mm, and results are reported in Figure 4.18. As expected, as b_{bf} is increased the model predicts more even load distribution and lower *SDF*s. The *SDF* decrease is considerable, which suggests any future CT girder *SDF* expressions should consider girder b_{bf} or total width of the girder. Further, as girder depth increases so does the girder width and therefore relative spacing between the webs in adjacent girders decreases. Following the same logic, for bottom flange width, increased girder depth for a given b_{bf} should result in lower

*SDF*s. This supports the earlier conclusion that the inclusion of *d* in the AASHTO expression may need to be changed to accurately capture shear live load distribution in CT girders.

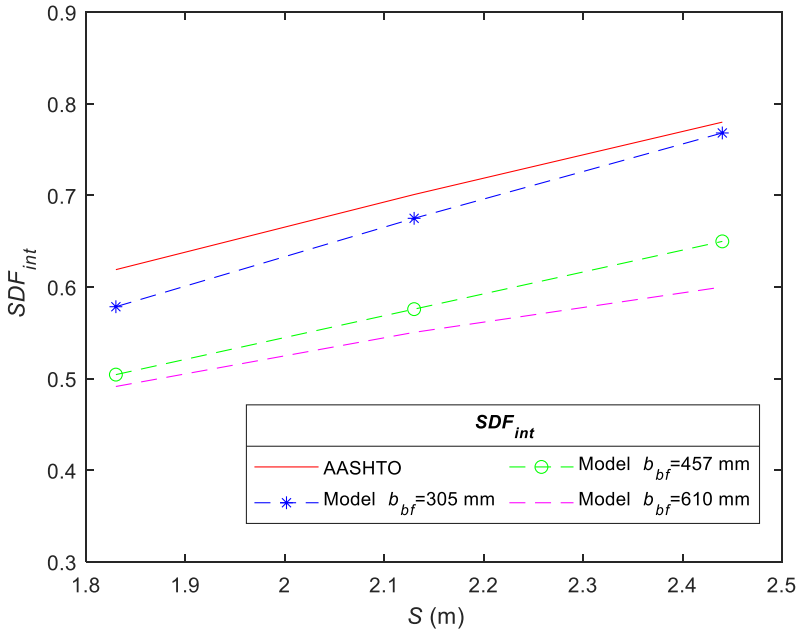

Figure 4.18: Effect of Bottom Flange Width b_{bf} on Interior SDF

4.6 Summary

The parametric study on *MDF*s showed that spacing and span length are the most influential parameters for the interior M*DF*, which is consistent with the AASHTO *MDF* expressions. The results of the model also show that two lanes of live load result in a larger M*DF* as compared to one lane of live load. The model predicts higher one lane *MDF*s than AASHTO, but AASHTO over-predicts the larger two lanes M*DF*s which generally control girder strength design. Higher skews reduce longitudinal flexural strains, especially for skew angles greater than 15°, although for two lanes of loading the model-predicted skew reduction is significantly greater than that given by AASHTO. For two lanes of live load the model predicts exterior *MDF*s are typically less than the interior *MDF* for overhangs that are less than half the girder spacing. The models predict higher exterior *MDF*s compared to interior for one lane of load for most bridges.

As expected, increasing the deck thickness and the number of girders decreased the *MDF*, and therefore if *MDF* expressions are developed for the lower limit of those two parameters they should be conservative for larger deck thicknesses and two-lane bridges with more than five girders.

For shear live load distribution, girder spacing is the key driver of the *SDF*. Span length also plays a role and causes decreases in the shear distribution at longer spans. There are also geometric effects from bottom flange width and depth that highlight the importance of analyzing bridges with girder geometries typical for their spans and spacings when examining *SDF*s. It is also important to note that, although AASHTO typically over-predicts the interior *SDF*s compared to the model, there has not been any adjustment considered for the differential web shears observed in the field live load tests and consistently predicted by the finite-element models. Any future *SDF* expression development will need to consider this effect. Further, the simplified finite-element models over-predict *SDF*s compared to high-fidelity model calibrated to test results, and further investigation may be required to balance the conservatism inherent in the simplified model with the effect of differential web shears.

4.7 References

AASHTO. 2020. *AASHTO LRFD Bridge Design Specifications*. Washington, DC: AASHTO.

AASHTO. 2012b. *LRFD Guide Specifications for Design of Concrete-Filled FRP Tubes for Flexural and Axial Members*. Washington, DC: AASHTO.

Barbero, E. J. 2018. *Introduction ot Composite Materials Design (3rd edition).* Boca Raton, FL: CRC Press.

Cross, B., B. Vaughn, N. Panahshahi, D. Petermeier, Y. S. Siow, and T. Domagalski. 2009. "Analytical and experimental investigation of bridge girder shear distributions factors." *J. Bridge Eng*. 14 (3): 154-163. https://doi.org/10.1061/(ASCE)1084-0702(2009)14:3(154)

Davids, W., A. Diba, H. Dagher, D. Guzzi and A. Schanck. 2022. "Development, assessment and implementation of a novel FRP composite girder bridge." *Construction and Building Materials*. 340: 127818. https://doi.org/10.1016/j.conbuildmat.2022.127818

Ndong, A., M. Sherif, B. Kassner, D. Harris and O. Ozbulut. 2022. "Potential Improvement in Rating Factors of Concrete T-Beam Bridges through Refined Analysis: Evaluation of Distribution Factors." *Journal of Bridge Engineering*. 27 (9): 04022081. https://doi.org/10.1061/(ASCE)BE.1943-5592.0001928

Schanck, A., W. G. Davids, J. Pinkham and K. Berube. 2023. "Assessment of web shear stresses and shear capacity of FRP composite tub girders for highway bridges." *Structures*. 51: 880-894. https://doi.org/10.1016/j.istruc.2023.03.083

Chapter 5: Development of *MDF* Expressions

5.1 Introduction

The results of the previous parametric study show that spacing, span, and deck thickness influence interior girder *MDF*. The results also show that the AASHTO concrete box girder *MDF* expressions currently used in CT girder design have varying levels of conservatism. This justifies the development of new *MDF* expressions that will better predict *MDF*s for CT girder bridges and improve design efficiency. In this chapter all units for expression are SI with S, L, and d_{cl} in m and d and t_d in cm.

5.2 Regression Analysis

Chapter 4 showed AASHTO was typically conservative for two lanes of live load, but un-conservative for one lane loaded interior *MDF*s. Despite this conservatism, the AASHTO expressions likely provide a reasonable format for new *MDF* expressions given that the parametric studies generally showed that AASHTO followed similar patterns to the model predictions. To illustrate, regression plots were generated which compare model-predicted *MDF*s to the AASHTO concrete box girder values.

Figure 5.1 shows the linear regression plots for interior moment for (a) one lane and (b) two lanes of live loading comparing AASHTO and the model predictions. In the plots a formula for a regression line is shown, as well as the coefficient of determination (R^2) to show the goodness of fit for the data. A perfect 1:1 correlation line is also plotted with any data over the line signifying conservatism by AASHTO and any data points under the line signifying AASHTO is not conservative. Figure 5.1 (a) shows the results of simplified FE models of 280 non-skewed bridges subject to one lane of live load with AASHTO being un-conservative for most sets of parameters. Figure 5.1 (b) shows the FE model results for 304 non-skewed bridges

under two lanes of live load with AASHTO giving conservative predictions for most sets of parameters. For both the correlation is reasonably high with slightly better correlation in the two lanes *MDF* expression. This suggests the AASHTO *MDF* equations could be used with different values for the constants in the expressions to minimize the error between the model and expression while keeping generally good correlation.

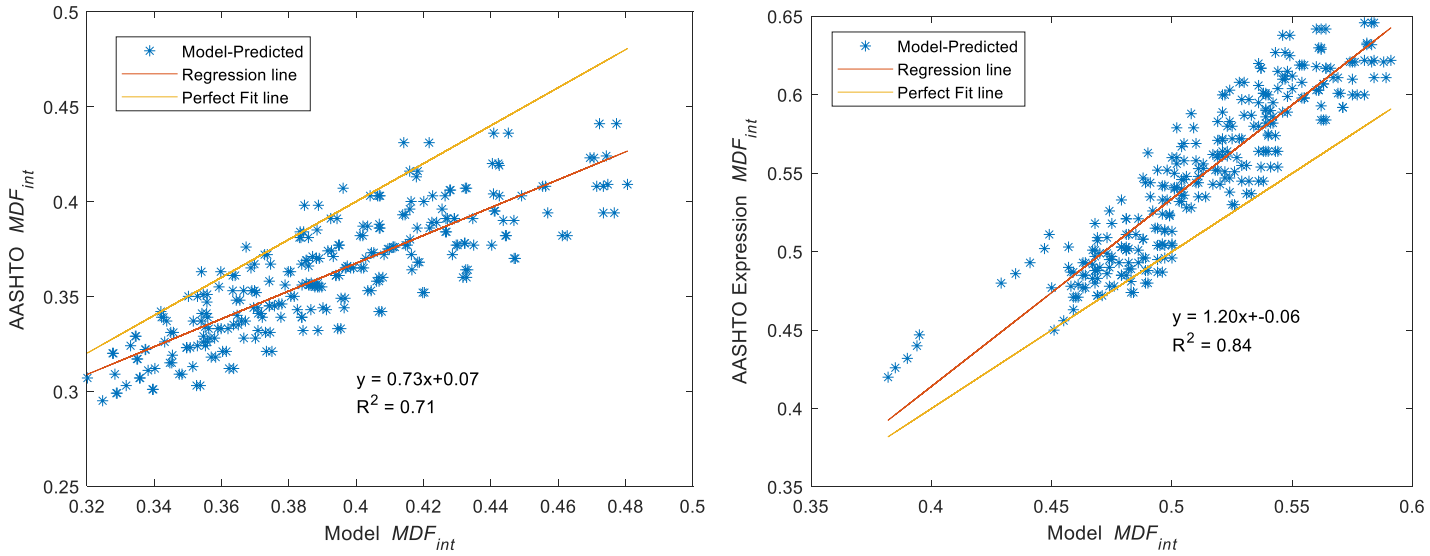

(a) (b)

Figure 5.1: AASHTO vs. Model Interior *MDF* Regression Analysis (a) One Lane (b) Two Lanes

Exterior girder *MDF*s are also of importance and are handled by AASHTO with the eccentricity correction factor (*e*) which is applied to the interior *MDF*. The parametric study in section 4.4.6 showed that overhang influences the value of *e*. AASHTO advises the use of the lever rule for one lane loading but does have an expression for *e* in two lane loadings. Figure 5.2 shows the regression plot for AASHTO *e* vs the model prediction *e* value. The results show AASHTO to be conservative in its prediction of *e*, but the R^2 value of 0.66 is lower than the values for the interior girders. The low correlation suggests the form of the AASHTO equation for *e* may not be appropriate for CT girder bridges.

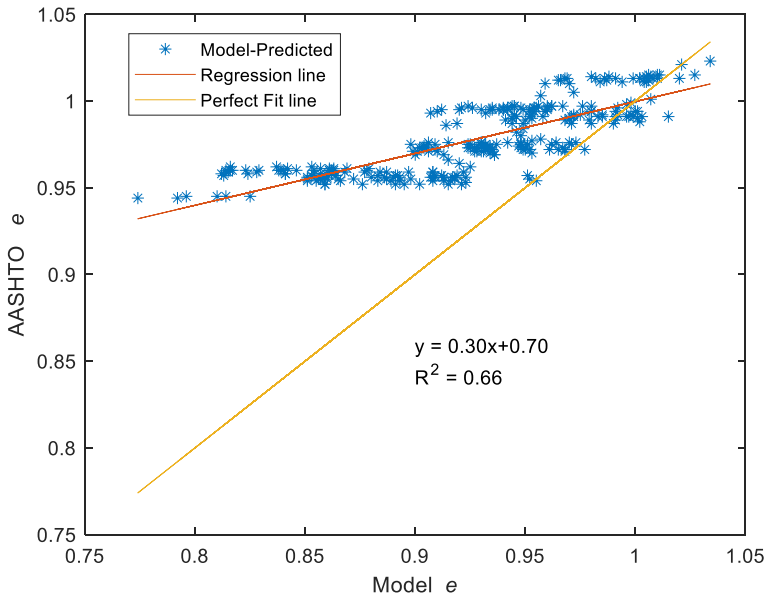

Figure 5.2: AASHTO vs. Model *e* Regression Analysis Two Lanes

5.3 Proposed Equations

5.3.1 Interior *MDF*

The regression analysis showed that for both one and two lanes of loading AASHTO provided good correlation with the results and shows promise for its format in the use of new CT girder specific interior moment *DF* expressions. The equations to be proposed for the interior *MDF* used the trial functions shown in Equation 5.1. The expressions include spacing (*S*), span (*L*), and girder depth (*d*). While the studies in Chapter 4 found the number of girders and deck thickness to impact the interior *MDF*, fewer girders and less deck thickness result in higher *MDF*s. Therefore, expressions fit to the results of models with a minimum deck thickness and number of girders will be conservatively applicable to bridges with more girders and thicker decks, and the results for bridges with 178 mm decks and five girders were used as the data set for optimizing the new expression function. This corresponds to 79 and 81 different bridge geometries for one and two lanes of live load, respectively.

$$MDF_{exp} = \left(\frac{S}{X_1}\right)^{X_2} \left(\frac{Sd}{100L^2}\right)^{X_3} \quad (5.1)$$

The MATLAB non-linear least square's function *lsqnonlin* (Mathworks 2022) was used to determine the optimal parameters $X_1, X_2, X_3$with the trust-region-reflective algorithm (Coleman and Li 1996) that minimizes nonlinear objective functions with accuracy and proven previously to run in seconds by Schanck (2021). The optimization code varies X_1, X_2, X_3 until the gradient of the sum of square errors (SSE) drops below a tolerance of 1 x 10^{-6}. The expression for *SSE* is given in Equation 5.2 where MDF_{exp} is the *MDF* predicted by the trial function (initially Equation 5.1), MDF_{model} is the model-predicted *MDF* and *N* is the total number of bridges assessed.

$$SSE = \sum_{i=1}^{N} (MDF_{exp} - MDF_{model})^2 \quad (5.2)$$

Prior to optimization the initial *SSE* values of 0.213 and 0.058 for one and two lanes, respectively, given initial guesses of $X = [0.914 \;\; 0.35 \;\; 0.25]$ for one lane and $X = [1.92 \;\; 0.6 \;\; 0.125]$ for two lanes. The optimized one lane expression (Equation 5.3) was achieved in four iterations and reduced the *SSE* to 0.009, a 95.8% decrease. The two lanes expression (Equation 5.4) was achieved in sixteen iterations and reduced the SSE to 0.002, a 96.6% decrease.

One Lane

$$MDF_{int} = \left(\frac{S}{3.02}\right)^{0.59}\left(\frac{Sd}{100L^2}\right)^{0.13} \quad (5.3)$$

Two Lanes

$$MDF_{int} = \left(\frac{S}{4.74}\right)^{0.5}\left(\frac{Sd}{100L^2}\right)^{0.04} \quad (5.4)$$

The proposed moment expressions showed to reduce the *SSE* value. However, this does not illustrate how well the expressions correlate with the model *MDF*s and level of conservatism. A new linear regression plot is shown in Figure 5.3 to illustrate the expressions' ability to match the model predictions over a wide range of bridges. For the one lane expression (Equation 5.3) the correlation is slightly improved from $R^2 = 0.71$ (Figure 5.1 (a)) to $R^2 = 0.74$ (Figure 5.3 (a)). For the two lanes expression (Equation 5.4) the correlation is worse decreasing from $R^2 = 0.84$ (Figure 5.1 (b)) to $R^2 = 0.72$ (Figure 5.3 (b)). There is also more conservatism in the proposed expressions compared to the initial AASHTO expressions. Although conservatism means designing for higher moments which increases factor of safety there comes a point certain levels of conservatism is inefficient. With correlation values in the 0.7 range and high conservatism especially for the two lanes expression there calls for a new format that can improve correlation and have a more efficient level of conservatism.

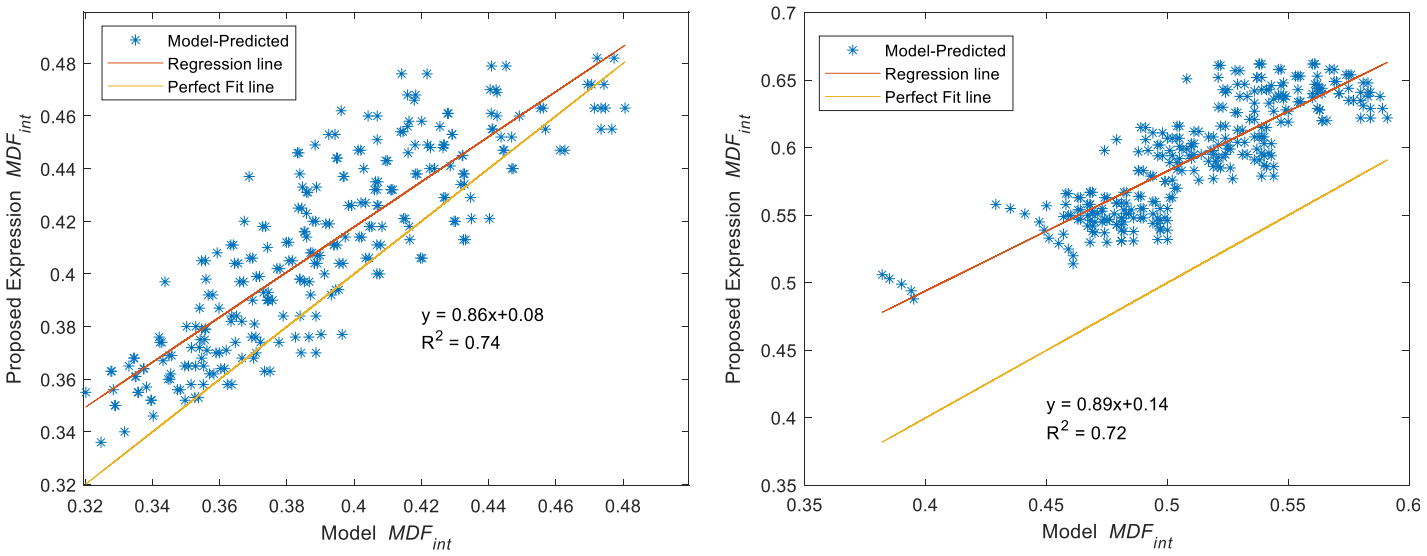

Figure 5.3: Proposed Equation vs. Model Interior *MDF* Regression Analysis (a) Equation 5.3 (b) Equation 5.4

Equations 5.3 and 5.4 do not consider the deck thickness (t_d) which does cause significant decrease in *MDF* for increased t_d. A second trial function was therefore assessed to include t and within which girder depth was removed due to its minimal effect. Since all values of t were included the entire data set of bridges could be used to minimize the objective function which was 280 and 304 bridges for one and two lanes respectively. The new trial functions are shown in Equations 5.5 and 5.6 for one and two lanes of live loading. The initial parameters for one lane of loading were chosen to be $X = [0.35 \;\; 0.1 \;\; 0.125]$, and for two lanes of loading were set as $X = [0.6 \;\; 0.1 \;\; 0.125]$. For the one lane expression four iterations improved *SSE* to 0.009 from the initial guess *SSE* of 25.1. The second version one lane interior moment *MDF* expression is shown in Equation 5.7. For the two lanes expression three iterations found a local minimum and reduced the *SSE* to 0.023 from the initial value of 0.373. The second version two lanes interior moment DF expression is shown in Equation 5.8.

One Lane $$MDF_{exp} = \left(\frac{S}{0.914}\right)^{X_1}\left(\frac{1}{L}\right)^{X_2}\left(\frac{1}{t_d}\right)^{X_3} \quad (5.5)$$

Two Lanes $$MDF_{exp} = \left(\frac{S}{1.92}\right)^{X_1}\left(\frac{1}{L}\right)^{X_2}\left(\frac{1}{t_d}\right)^{X_3} \quad (5.6)$$

One Lane $$MDF_{int} = \left(\frac{S}{0.914}\right)^{0.648}\left(\frac{1}{L}\right)^{0.129}\left(\frac{1}{t_d}\right)^{0.369} \quad (5.7)$$

Two Lanes $$MDF_{int} = \left(\frac{S}{1.92}\right)^{0.554}\left(\frac{1}{L}\right)^{0.042}\left(\frac{1}{t_d}\right)^{0.199} \quad (5.8)$$

The regression plots for the Equations 5.7 and 5.8 versus the model-predicted values are shown in Figure 5.4 (a) and (b) respectively. The correlations are substantially improved with this new format (Equations 5.7 and 5.8) with $R^2 = 0.98$ and $R^2 = 0.95$ compared to the initially proposed expressions (Equations 5.3 and 5.4) $R^2 = 0.74$ and $R^2 = 0.72$. Although the correlation has improved, the level of conservatism is slightly less with more bridge parameters having expression predictions less than the model-predicted *MDF*s. Currently 48.9% of the Equation 5.7 *MDF* predictions and 37.8% of the Equation 5.8 *MDF* predictions are greater than the model-predicted values for the bridge parameters analyzed. The development of the current AASHTO equations relied on the average ratio of expression-predicted *DF*s to analysis-predicted *DF*s be greater than 1 to ensure conservatism (Zokaie 1991). This level of conservatism is adjustable with a constant that can be applied to the expressions to shift the values slightly higher. As the CT girder is a novel technology, this level of conservatism would ideally be quantified rather than simply being assumed. For this reason, the adjustment was varied by 0.001 until more than 90% of expression-predicted *MDF*s exceeded those predicted by the model. It should be noted that this 90% factor is not rigorously based in statistics. The result was an adjustment of 0.007 and 0.008 being applied to Equations 5.7 and 5.8 respectively as shown in Equations 5.9 and 5.10. Figure 5.5 shows updated regression plots using expression predictions from Equations 5.9 and 5.10. The adjustment maintains the high level of correlation

and then achieves the desired 90% of data points being conservatively predicted by the expressions with 91.1% and 91.1% of the parameters assessed being conservative for Equations 5.9 and 5.10 respectively.

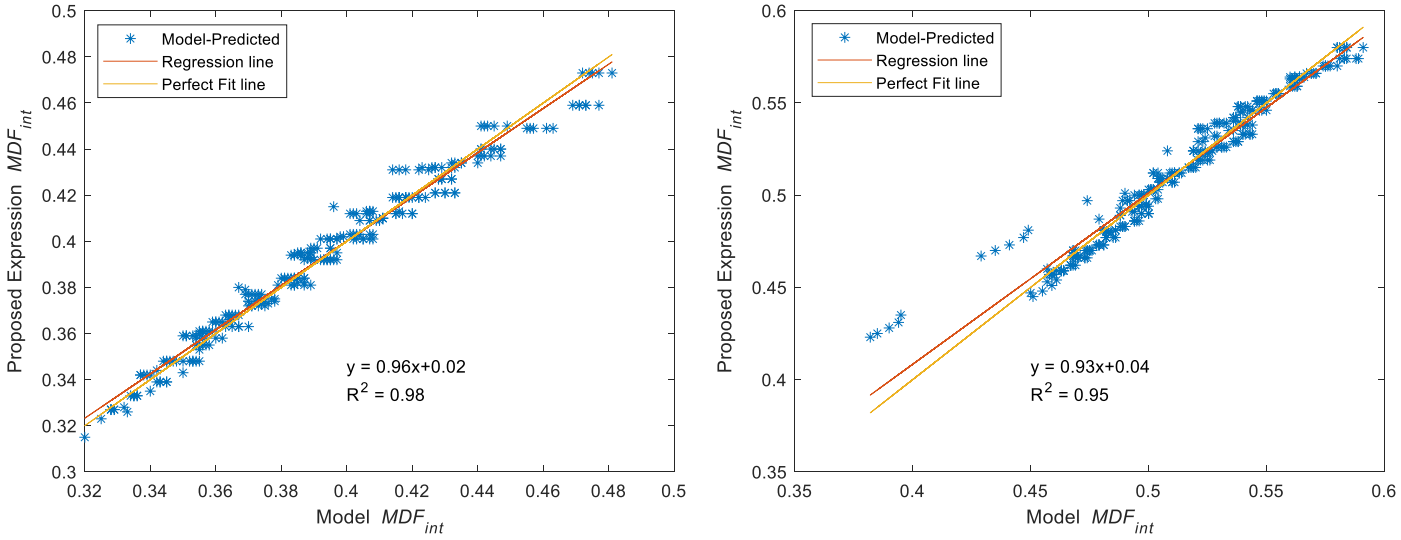

(a) (b)

Figure 5.4: Proposed Equation vs. Model Interior *MDF* Regression Analysis (a) Equation 5.7 (b) Equation 5.8

One Lane $$MDF_{int} = 0.007 + \left(\frac{S}{0.914}\right)^{0.611}\left(\frac{1}{L}\right)^{0.175}\left(\frac{1}{t_d}\right)^{0.463} \quad (5.9)$$

Two Lanes $$MDF_{int} = 0.013 + \left(\frac{S}{1.92}\right)^{0.602}\left(\frac{1}{L}\right)^{0.075}\left(\frac{1}{t_d}\right)^{0.285} \quad (5.10)$$

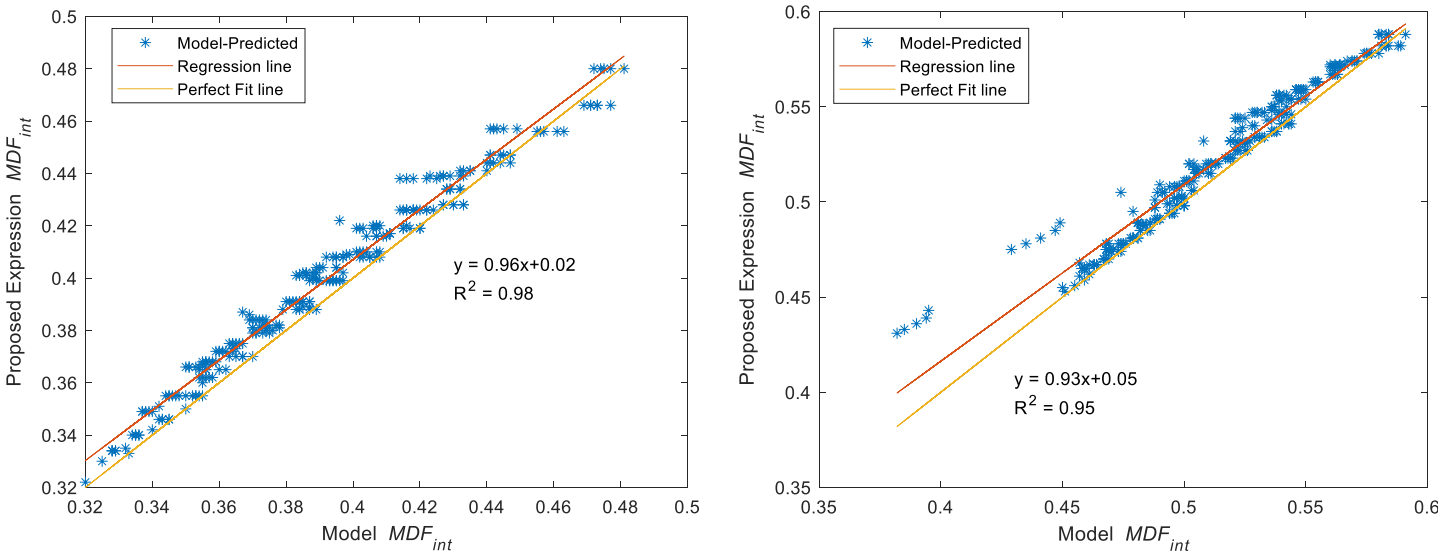

Figure 5.5: Proposed Equation vs. Model Interior *MDF* Regression Analysis (a) Equation 5.9 (b) Equation 5.10

Table 5.1 summarizes the proposed expressions and the original AASHTO expression with the total sum of square errors, correlation, and percentage of the total bridges predicted conservatively reported for each. The expressions for the interior *MDF* proposed in Equations 5.9 and 5.10 show to provide a format that provides a much higher correlation to the model-predicted *MDF*s compared to the expressions proposed originally in Equations 5.3 and 5.4. Equations 5.3 and 5.4 had *SSE* values of 0.202 and 2.16 while Equations 5.9 and 5.10 had *SSE* values 0.024 and 0.043 respectively showing lower magnitudes or errors and therefore lower magnitudes of over-predictions and conservatism. Therefore Equations 5.9 and 5.10 have high correlation and ensure >90% of data is conservative but at a lower magnitude to keep efficiency in design and not designing for moments much larger than model predicted. This can be seen in Figure 5.6 where the AASHTO prediction is compared to the proposed Equation 5.10 where AASHTO is predicted higher interior *MDF* values with most data falling above the perfect fit line. The Equations 5.7 and 5.8 prove to have the lowest *SSE* however the conservatism built in is lower than a desirable amount and are therefore not recommended without the adjustment to

increase conservatism. The original AASHTO expression proved to be inconsistent with lower correlation values and larger *SSE* values compared to the proposed Equations 5.9 and 5.10.

Table 5.1: Interior MDF Expressions Comparison

Lanes Loaded	Equation #	*SSE*	R^2	% Data Conservative	Number of Bridges
One Lane	AASHTO (4.1)	0.363	0.71	3.21	280
	5.3	0.202	0.74	84.3	
	5.7	0.009	0.98	48.9	
	5.9	0.024	0.98	91.1	
Two Lanes	AASHTO (4.2)	0.549	0.84	96.1	304
	5.4	2.16	0.72	100	
	5.8	0.023	0.95	37.8	
	5.10	0.043	0.95	91.1	

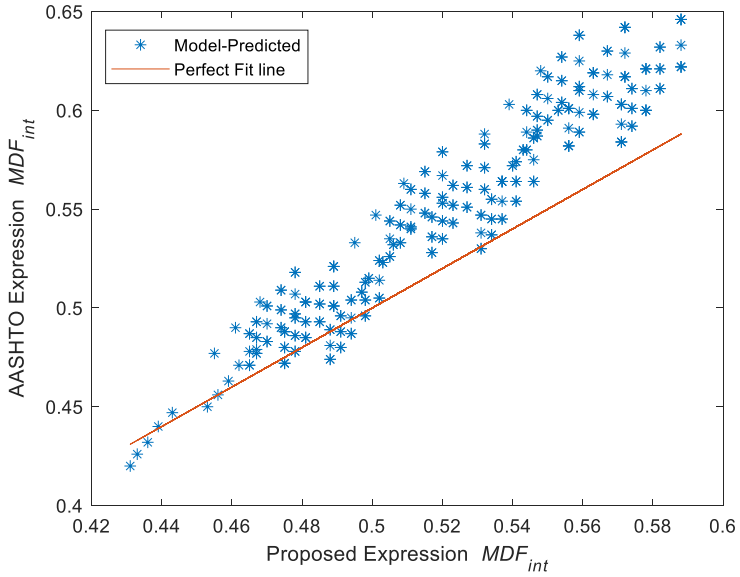

Figure 5.6: AASHTO vs. Proposed Equation 5.10 Interior *MDF*

5.3.2 Exterior *MDF*

The current AASHTO correction factor *e* for the exterior girder relies on the d_e value which determines the cantilever distance from the centerline of the web at the top flange intersection to the inside of the curb (AASHTO 2020). This value can be difficult to calculate and potentially change throughout the design process if girder dimensions change. To simplify the exterior girder correction factor, the centerline girder to bridge exterior overhang distance was used in the expression and referred to as d_{cl} (in meters) the full cantilever overhang from the girder centerline. The trial function used in the minimization of the *SSE* value is shown in Equation 5.11 with the initial parameters set as $X = [0.97 \quad 8.69]$.

Trial Function Exterior Correction

$$e = X_1 + \frac{d_{cl}}{X_2} \tag{5.11}$$

The parametric results in Chapter 4 showed the exterior correction factor was different for the one and two lanes of load cases and therefore each was assessed independently. The resulting expressions are shown in Equations 5.12 and 5.13. For one lane of loading, the optimum *X* was found in 14 iterations and decreased the *SSE* from 0.081 to 0.004. For two lanes of loading, 13 iterations were required to determine the optimum *X* and *SSE* decreased from 0.29 to 0.0029.

One Lane

$$e = 0.794 + \frac{d_{cl}}{2.80} \tag{5.12}$$

Two Lanes

$$e = 0.63 + \frac{d_{cl}}{2.99} \tag{5.13}$$

The correction factors proposed in Equations 5.12 and 5.13 were applied to the proposed expressions for the interior *MDF* (Equations 5.9 and 5.10) to obtain the exterior *MDF*. These results are represented in Figure 5.7 where (a) is the one lane exterior *MDF* and (b) is two lanes.

The correlation is high with $R^2 = 0.97$ and $R^2 = 0.96$ for the one and two lanes respectively. For all bridges assessed (280 for one lane loading and 304 for two lanes loading) the percent with higher exterior *MDF*s predicted by the expression compared to the model is 89.6% and 67.4% for the one and two lanes respectively. To continue with the goal of achieving a percentage over 90% new scalars were determined for the correction factor *e* expressions leading to new expressions seen in Equations 5.14 and 5.15. With the scaling in Equations 5.14 and 5.15 the exterior *MDF* is predicted conservatively by the expression compared to the model 90.0% and 90.1% for the one and two lanes of load respectively while maintaining correlations similar to those in Figure 5.7.

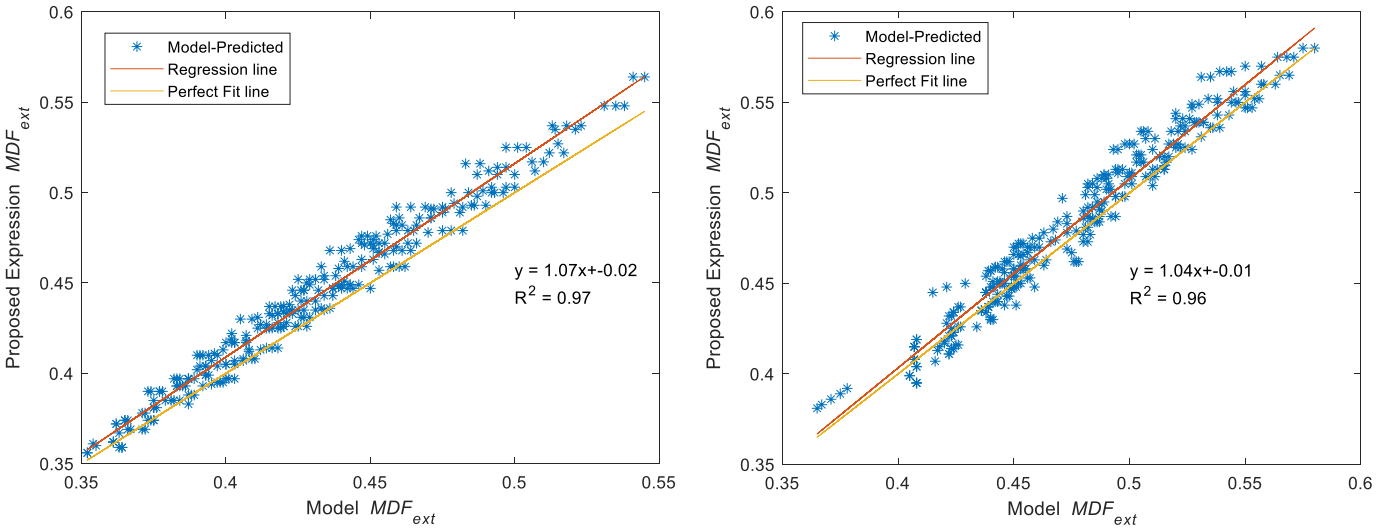

(a) (b)

Figure 5.7: Proposed Equation vs. Model Exterior *MDF* Regression Analysis (a) Equation 5.12 (b) Equation 5.13

One Lane $$e = 0.795 + \frac{d_{cl}}{2.80} \quad (5.14)$$

Two Lanes $$e = 0.641 + \frac{d_{cl}}{2.99} \quad (5.15)$$

Figure 5.8 compares the AASHTO exterior *MDF* prediction to the results of the proposed correction factor (Equation 5.15) applied to the interior *MDF* (Equation 5.10). AASHTO shows it is predicting higher values meaning it is more conservative. We already adjusted the proposed the equations to ensure >90% of *MDF*s predictions to exceed the model prediction, any further conservatism becomes inefficient. The proposed expressions are resulting in improved correlation to the model data compared to AASHTO with less conservatism leading to efficient designs and an improvement in live load *MDF* predictions.

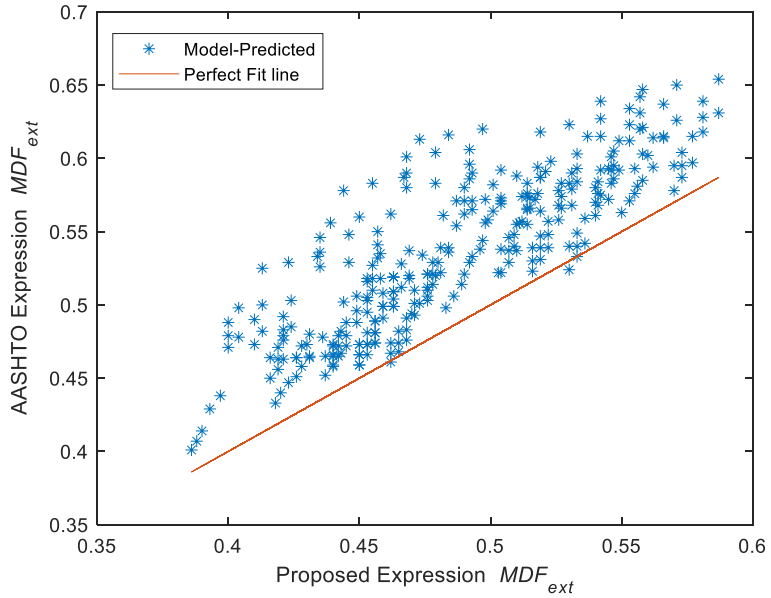

Figure 5.8: AASHTO vs. Proposed Equation 5.15 Exterior *MDF*

5.3.3 Skew *MDF*

In Chapter 4 the effect of skew showed with higher skew angles there was a decrease in the *MDF* on the interior. AASHTO also predicts a decrease with increasing skew however AASHTO predicts a larger decrease than model-predicted therefore the AASHTO expression for skew adjustment is not applicable to the CT girder. The span length also appeared to effect the skew effect as at linger spans the decrease was less. Three different span bridges were assessed at increasing skews to provide for a fifteen-bridge sample size to develop a skew adjustment. The format of the AASHTO expression was used with an addition of slight increase for span increases as a trial function shown in Equation 5.16. The skew angle θ is in degrees, span L in meters and the initial parameters were $X = [1.05 \;\; 0.25 \; 0.01\;]$ provided from AASHTO (2020) and an educated guess on the constant applied to L. The exterior showed to have less of a decrease due to skew than on the interior and therefore resulted in separate equations. For both one and two lanes of load 1 iteration was required to determine the optimum X. The *SSE* for the one lane was 0.006 and 0.007 for interior and exterior, respectively. The *SSE* for two lanes was 0.028 and 0.026 for interior and exterior, respectively. The resulting corrections are shown in Equations 5.17 and 5.18 for the interior and Equations 5.19 and 5.20 for the exterior.

Trial Function Skew Correction	$C_\theta = X_1 - X_2 \tan(\theta) + X_3 L$	(5.16)
Interior One Lane	$C_\theta = 0.971 - 0.12 \tan(\theta) + 0.0023L \leq 1.0$	(5.17)
Interior Two Lanes	$C_\theta = 0.909 - 0.24 \tan(\theta) + 0.0069L \leq 1.0$	(5.18)
Exterior One Lane	$C_\theta = 0.984 - 0.06 \tan(\theta) + 0.002L \leq 1.0$	(5.19)
Exterior Two Lanes	$C_\theta = 0.929 - 0.15 \tan(\theta) + 0.006\, L \leq 1.0$	(5.20)

Figures 5.9 and 5.10 show the regression analysis comparing the model predicted skewed bridge MDFs to the final expression predicted MDFs once all correction factors are applied. For the interior girder the MDF is the MDF_{int} from Equations 5.9 and 5.10, for a non-skewed bridge, with the proper C_θ multiplied to it derived from Equations 5.17 and 5.18. On the exterior it is the same MDF_{int} from a non-skewed bridge with the proper e applied from Equations 5.14 and 5.15 and then lastly apply the correct C_θ value for the exterior from Equations 5.19 and 5.20. For the one lane of load expressions shown in Figure 5.9 the interior *MDF* is predicted with an $R^2 = 0.92$ and exterior with $R^2 = 0.85$ both with ample conservatism. Figure 5.10 shows the two lanes of load expressions also correlate well with $R^2 = 0.94$ on the interior and $R^2 = 0.89$ on the exterior again with conservative predictions for both. Consider this is a small sample size and does not truly verify these are applicable to a large set of bridges, but it shows promise.

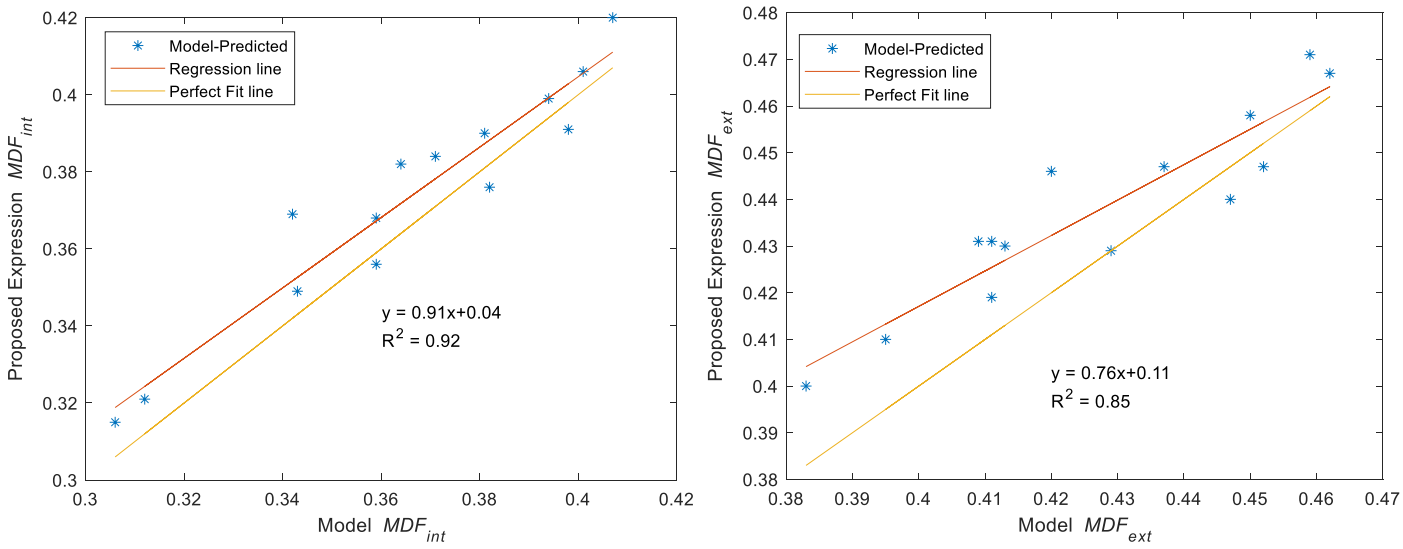

(a) (b)

Figure 5.9: Proposed Equation vs. Model Skewed *MDF* Regression Analysis (a) Equation 5.17 (b) Equation 5.19

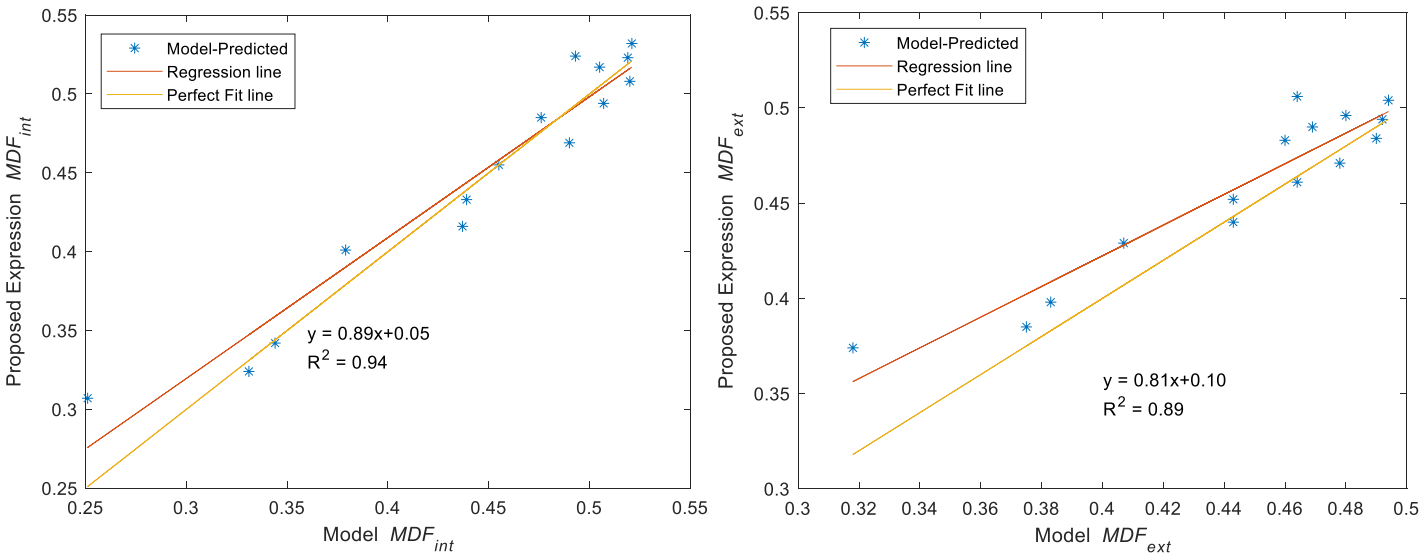

(a) (b)

Figure 5.10: Proposed Equation vs. Model Skewed *MDF* Regression Analysis (a) Equation 5.18 (b) Equation 5.20

5.4 Summary

The AASHTO *MDF* equations for concrete box girders capture several important parameters governing live load distribution for CT girders, but do not accurately predict live load distribution. The AASHTO expressions were used as a baseline for development of new *MDF* expressions for CT girders. The proposed expressions more accurately predict the interior and exterior *MDF* compared to the AASHTO *MDF* expressions for concrete box girders that are currently used.

Initially, a new CT girder-specific *MDF* expression that mimics the AASHTO expression for concrete boxes was developed based on model-predicted data for only 178 mm thick decks. These new expressions (Equations 5.3 and 5.4) lowered the *SSE* value for the 178 mm thick deck bridges, but ultimately increased the *SSE* value for all 304 bridges under two lanes of loading due to significantly more conservatism for CT girder bridges with thicker decks. The correlation

was also worse in the two lanes of loading expression (Equation 5.4) compared to AASHTO signifying there was minimal, if any, improvement.

To decrease this conservatism and improve prediction for a wider range of CT girder structures, a second CT girder specific *MDF* formula was proposed that explicitly includes deck thickness and was fit to the results for all non-skewed bridges assessed in the parametric study (280 bridges for one lane of live load and 304 bridges for two lanes of live load). These expressions (Equations 5.7 and 5.8) showed much better correlation with less conservatism as low as 47% of *MDF*s predicted conservatively compared to model-predictions. To increase the conservatism a scalar adjustment was added to the equations to shift the predictions higher and increase conservatism to reach 90% of *MDF*s over predicting the model on the interior. These final expressions for the interior *MDF* are shown in Equations 5.9 and 5.10 and are recommended for CT girder bridges as they show good correlation to the model and are generally conservative. An exterior girder correction factor was also fit to 18 bridges with different varying deck overhangs on the exterior girder. The initial exterior correction factors when applied to the interior *MDF* expressions showed good correlation to the model predicted exterior *MDF*s, but below 90% of exterior *MDF*s predicted higher than the model. Therefore, just as with the interior an adjustment was made to the correction factor expressions to obtain above 90% conservatism in the total number of bridges assessed leading to final exterior correction factors expressions proposed seen in Equations 5.14 and 5.15. Skew correction factors were also investigated on 15 bridges and four individual equations were created for various cases of application. Tables 5.2 and 5.3 summarizes the proposed *MDF* expressions in S.I. and U.S. Customary units with ranges of applicability. The notation mg is used to denote the distribution

factors to emphasize that the multiple presence factor m is incorporated to be consistent with AASHTO.

Table 5.2: Proposed CT Girder Live Load Moment Distribution Factors (S.I. Units)

Condition	Expression	Range of Applicability
Interior One Lane	$mg_{int} = 0.007 + \left(\frac{S}{0.914}\right)^{0.648}\left(\frac{1}{L}\right)^{0.129}\left(\frac{1}{t_d}\right)^{0.369}$	$1.68\ m \le S \le 2.44\ m$ $12.2\ m \le L \le 24.4\ m$ $38.1\ cm \le d \le 135\ cm$ $N_g \ge 5$ $t_d \ge 17.8\ cm$
Interior Two Lanes	$mg_{int} = 0.008 + \left(\frac{S}{1.92}\right)^{0.554}\left(\frac{1}{L}\right)^{0.042}\left(\frac{1}{t_d}\right)^{0.199}$	$1.68\ m \le S \le 2.44\ m$ $12.2\ m \le L \le 24.4\ m$ $38.1\ cm \le d \le 135\ cm$ $N_g \ge 5$ $t_d \ge 17.8\ cm$
Exterior One Lane	$mg_{ext} = e \times mg_{int}$ $Where\ e = 0.795 + \frac{d_{cl}}{2.80}$	$0.84\ m \le d_{cl} \le 1.1\ m$
Exterior Two Lanes	$mg_{ext} = e \times mg_{int}$ $Where\ e = 0.641 + \frac{d_{cl}}{2.99}$	$0.84\ m \le d_{cl} \le 1.1\ m$
Skew Correction One Lane	Interior: $C_\theta\ mg_{int}$ where $C_\theta = 0.971 - 0.12\tan(\theta) + 0.0023L \le 1.0$ Exterior: $C_\theta\ mg_{ext}$ where $C_\theta = 0.984 - 0.06\tan(\theta) + 0.002L \le 1.0$	$0° \le \theta \le 60°$ $12.2\ m \le L \le 24.4\ m$
Skew Correction Two Lanes	Interior: $C_\theta\ mg_{int}$ where $C_\theta = 0.909 - 0.24\tan(\theta) + 0.0069L \le 1.0$ Exterior: $C_\theta\ mg_{ext}$ where $C_\theta = C_\theta = 0.929 - 0.15\tan(\theta) + 0.006\ L \le 1.0$	$0° \le \theta \le 60°$ $12.2\ m \le L \le 24.4\ m$

Table 5.3: Proposed CT Girder Live Load Moment Distribution Factors (U.S. Units)

Condition	Expression	Range of Applicability
Interior One Lane	$mg_{int} = 0.007 + \left(\frac{S}{3}\right)^{0.648}\left(\frac{3.281}{L}\right)^{0.129}\left(\frac{1}{2.54t_d}\right)^{0.369}$	$5.5\ ft \le S \le 8\ ft$ $40\ ft \le L \le 80\ ft$ $15\ in \le d \le 53\ in$ $N_g \ge 5$ $t_d \ge 7\ in$
Interior Two Lanes	$mg_{int} = 0.008 + \left(\frac{S}{6.3}\right)^{0.554}\left(\frac{3.281}{L}\right)^{0.042}\left(\frac{1}{2.54t_d}\right)^{0.199}$	$5.5\ ft \le S \le 8\ ft$ $40\ ft \le L \le 80\ ft$ $15\ in \le d \le 53\ in$ $N_g \ge 5$ $t_d \ge 7\ in$
Exterior One Lane	$mg_{ext} = e \times mg_{int}$ $Where\ e = 0.795 + \frac{d_{cl}}{9.2}$	$2.75\ ft \le d_{cl} \le 3.50\ ft$
Exterior Two Lanes	$mg_{ext} = e \times mg_{int}$ $Where\ e = 0.641 + \frac{d_{cl}}{9.80}$	$2.75\ ft \le d_{cl} \le 3.50\ ft$
Skew Correction One Lane	Interior: $C_\theta\ mg_{int}$ where $C_\theta = 0.971 - 0.12\tan(\theta) + 0.0007L \le 1.0$ Exterior: $C_\theta\ mg_{ext}$ where $C_\theta = 0.984 - 0.06\tan(\theta) + 0.0006L \le 1.0$	$0° \le \theta \le 60°$ $40\ ft \le L \le 80\ ft$
Skew Correction Two Lanes	Interior: $C_\theta\ mg_{int}$ where $C_\theta = 0.909 - 0.24\tan(\theta) + 0.0021L \le 1.0$ Exterior: $C_\theta\ mg_{ext}$ where $C_\theta = C_\theta = 0.929 - 0.15\tan(\theta) + 0.0018\ L \le 1.0$	$0° \le \theta \le 60°$ $40\ ft \le L \le 80\ ft$

5.5 References

AASHTO. 2020. *AASHTO LRFD Bridge Design Specifications*. Washington, DC: AASHTO.

Coleman, T.F. and Y. Li. 1996. "An interior trust region approach for nonlinear minimization subject to bounds." *S.I.A.M. Journal of Optimization*. 6(2) 418-445. https://doi.org/10.1137/0806023

MathWorks Inc. 2022. *MATLAB version 9.11.0 (R2021b)* [Computer Software]. Natick, Massachusetts. https://www.mathworks.com

Schanck, A.. 2021. "Determination of Bridge Behavior Through Live-Load Testing and Advanced Numerical Analysis." Electronic Theses and Dissertations. 3535. https://digitalcommons.library.umaine.edu/etd/3535

Zokaie, T., T. Osterkamp and R. Imbsen. 1991. "Distribution of wheel loads on highway bridges." *National Cooperative Highway Research Program 12-26.* Accessed May 16, 2023. https://onlinepubs.trb.org/onlinepubs/nchrp/docs/NCHRP12-26_FR.pdf

Chapter 6: Summary and Conclusions

6.1 Summary

Bridges are critical components in the national transportation system, and understanding their behavior and live load response is essential for efficient and safe design. This study aimed to assess live load distribution in the novel CT girder highway bridges through a combination of field load testing and FE analysis. Moment was assessed first through two diagnostic live load tests conducted on the first CT girder bridge placed in service (the HGMB) in two separate years, during which flexural strains were recorded under maximum moment loadings. The test results were used to calibrate a high-fidelity FE model to more closely examine live load distribution in the HGMB. The results were then compared to a simplified FE model that is more readily generalized to a wide range of geometries and feasible for use in parametric studies. Using the simplified FE model, a parametric study was conducted to assess the effect of spacing, span length, depth, deck thickness, and number of girders on the distribution of live load moment to interior girders. Exterior overhang distance was assessed for its effect on exterior girder moment distribution. A small subset of skewed bridges was also analyzed to determine the effect of abutment skew on moment distribution.

To assess shear live load distribution, both the HGMB and the Hampden Twin bridge were tested under truck loads producing over 70% of girder shear forces due AASHTO HL-93 live load plus impact. Shear strains were recorded with rosette strain gages during testing and used to calibrate high-fidelity FE models that were subsequently used to more closely analyze the test results. The FE models were then simplified to reflect typical design assumptions and reduce computational effort. Model-predicted reactions were used to calculate shear the shear carried by each girder, and results of the calibrated and simplified models were assessed relative

to the field data and each other. The simplified model was also used to isolate the effects of critical parameters on shear live load distribution factor (*DF*s) under AASHTO HL-93 live load plus impact.

6.2 Conclusions

From the results of this work the following conclusions can be drawn.

6.2.1 Conclusion 1: Finite Element Analysis Accurately Predict Live Load Distribution in CT Girder Bridges

The results of diagnostic live load tests were compared to different discretization levels of finite element (FE) models and showed good agreement. The high-fidelity FE models incorporated many bridge components believed to affect bridge behavior. Calibrating these models using rational and defensible changes to a small number of parameters showed that shear and bending strains measured in the tests correlate well with model predictions. The high-fidelity models were also able to predict measured phenomena such as girder end restraint and differential web shears with reasonable accuracy. Therefore, the high-fidelity models are shown to be a viable option in predicting CT girder bridge behavior.

Simplified FE models containing only the structural components typically considered in design were created for both moment distribution and shear distribution. The predictions of the simplified models compared well with the test measured results, generally providing some conservatism for the interior girders and under-predictions on the exterior girders. However, the simplified models to not capture secondary structural features like the curbs, railings, and sidewalk which increase the stiffness of the exterior girders and draw more load to the exterior girders. Further, this additional load carried by the exterior girders is offset by the tendency of the secondary features to increase girder strength. Ultimately, due to their reduced complexity,

the simplified models give very reasonable results while requiring fewer computational resources, and are therefore ideal tools for parametric studies that capture a large CT girder design space.

6.2.2 Conclusion 2: Current Design Practices Tend to Over-Predict Moment Live Load Distribution to Interior Girders and Warrants Newly Developed *MDF* Expressions

Current design practice assumes that AASHTO concrete box girder *DF*s are applicable to CT girder bridges. The results presented in this thesis from two diagnostic live load tests and extensive FE analysis show the AASHTO expressions consistently over-predict the *DF* for interior girders for moment under two lanes of load. The interior girders also proved to have much higher *DF*s under two lanes of load than one lane of load, and therefore two lane *DF*s typically govern strength design. Therefore, while the use of current AASHTO concrete box girder *DF*s can continue to be used for future designs, more efficient design requires the development of CT girder-specific *DF*s.

Toward this end, moment distribution was quantified via FE models of 319 non-skewed bridges (280 loaded under one lane of load all 304 under two lanes of load) possessing a wide range of geometric parameters, and CT girder-specific moment *DF*s were proposed for non-skewed bridges. These new moment *DF*s correlate much better with model predictions than the current AASHTO moment *DF* expression and with less conservatism. The proposed moment *DF*s were also developed to be conservative relative to FE model predictions for >90% of the total bridges assessed. A correction factor was also developed for the exterior girder moment *DF* which also ensured >90% of predictions were conservative for the assessed bridges.

6.2.3 Conclusion 3: Live Load Shear Distribution in CT Girders is Conservatively Predicted by AASHTO but Requires Additional Investigation

The parametric study showed that AASHTO concrete box girder shear *DF*s are generally conservative when applied to CT girders. Girder spacing is the most influential parameter for shear *DF*s in CT girder bridges, which is consistent with the AASHTO *DF*s for concrete box girders. Further, overall girder width and bottom flange width also play a significant role in the distribution of live load shears, and the existing AASHTO expression for live load shear *DF*s in concrete box girders does not capture these effects.

Additionally, significant differential web live load shears occur within CT girders, which is likely a consequence of their low transverse bending stiffness and torsional effects. This effect is smallest in the most heavily loaded girders, but the even most heavily loaded webs saw as much as 22% more strain than the average web shear strain under two lanes of live load and 26% more shear strain than the average web shear strain for one lane of live load. These differential web shears are not accounted for by the AASHTO *DF*s. More investigation is warranted to fully assess if accounting for the increased web shear is necessary and if current AASHTO concrete box girder shear *DF*s are conservative after differential web shear is accounted for.

6.3 Future Work and Recommendations

The research presented here represents a first step toward quantifying live load distribution in CT girder bridges. Only 15 skewed bridges were analyzed and showed AASHTO's expression over predicts the skew reduction factor in many cases and is therefore un-conservative when applied to CT girders. While new skew correction factor expressions were developed, these must be regarded as preliminary, and it is recommended that in the future a larger number of skewed bridges be assessed to provide a broad data set for determining skew

correction factors. It is also recommended there be an investigation into whether one skew correction factor can be determined that is applicable for both interior and exterior *MDF*s.

Further shear parametric studies are required to fully assess the shear live load distribution in CT girder bridges over a wider range of bridge geometries that encompass a range of realistic span-to-depth ratios, bottom flange widths and overall girder widths before developing CT girder-specific shear *DF* expressions. It is recommended that differential web shears in the most heavily loaded girders be assessed to determine the effects of girder spacing, span, and other parameters on differential web shear. Further studies should also determine if a correction is necessary to account for the increased shear in a single web.

All simplified models discussed assumed prismatic girder sections, however some CT girders in current bridges are non-prismatic. While this assumption is assumed to not have a large effect on girder response, future studies assessing the effect of a non-prismatic girder section on live load distribution would be beneficial.

Appendix A: Test Data

A.1 HGMB 2022

A.1.1 Instrumentation

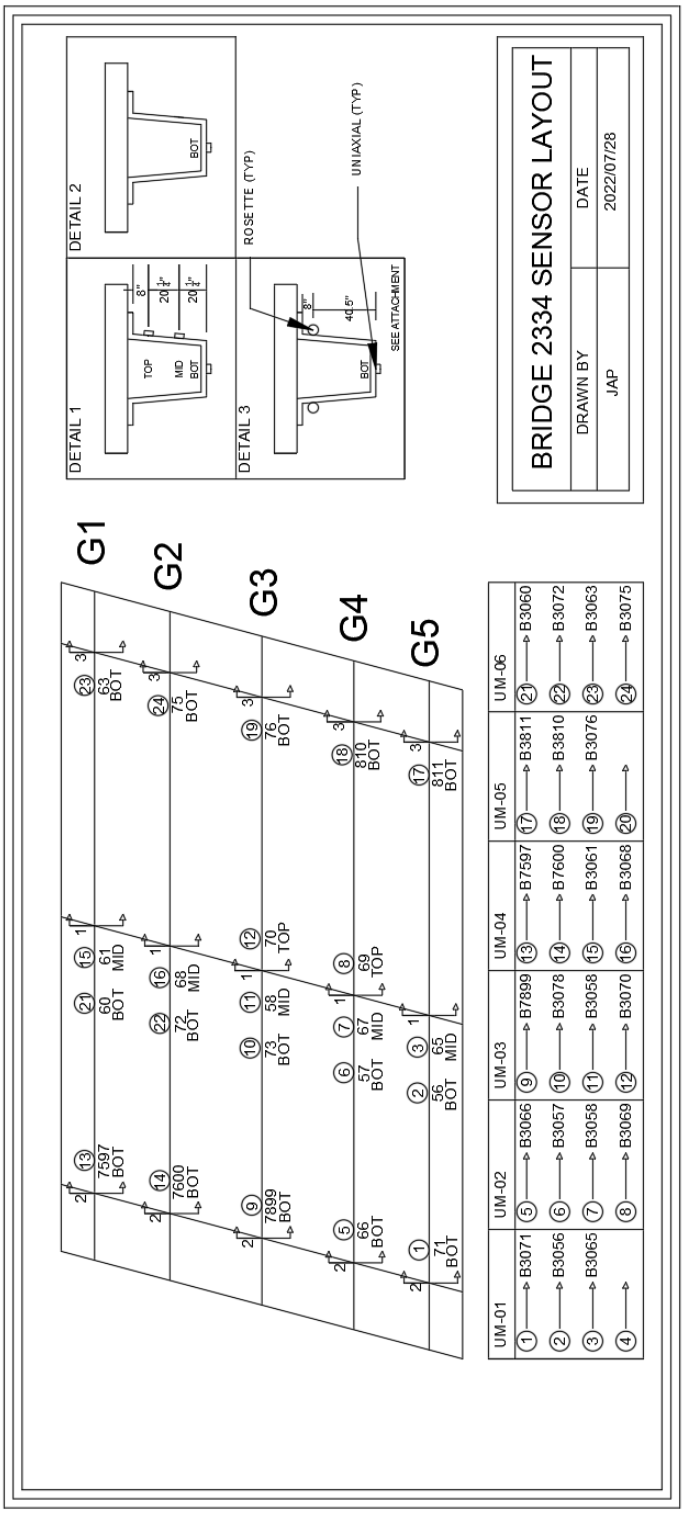

A.1.2 Loading

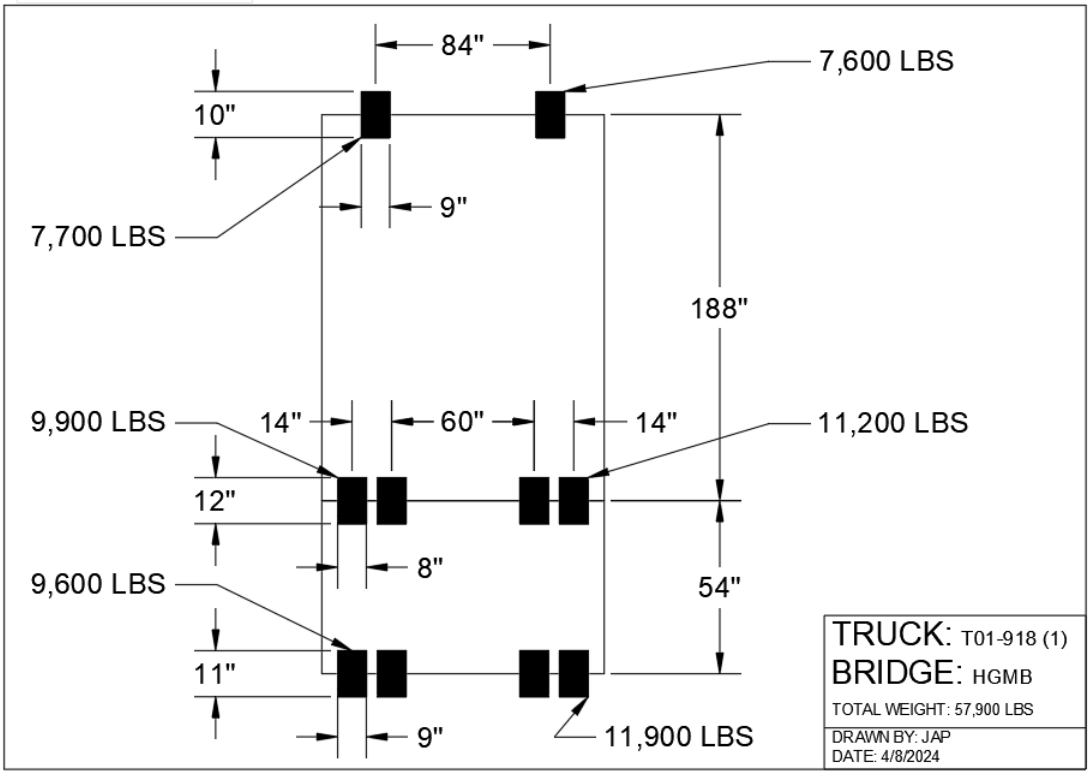
84"
7,600 LBS
10"
9"
7,700 LBS
188"
9,900 LBS
14"
60"
14"
11,200 LBS
12"
8"
9,600 LBS
54"
11"
9"
11,900 LBS
TRUCK: T01-918 (1)
BRIDGE: HGMB
TOTAL WEIGHT: 57,900 LBS
DRAWN BY: JAP
DATE: 4/8/2024

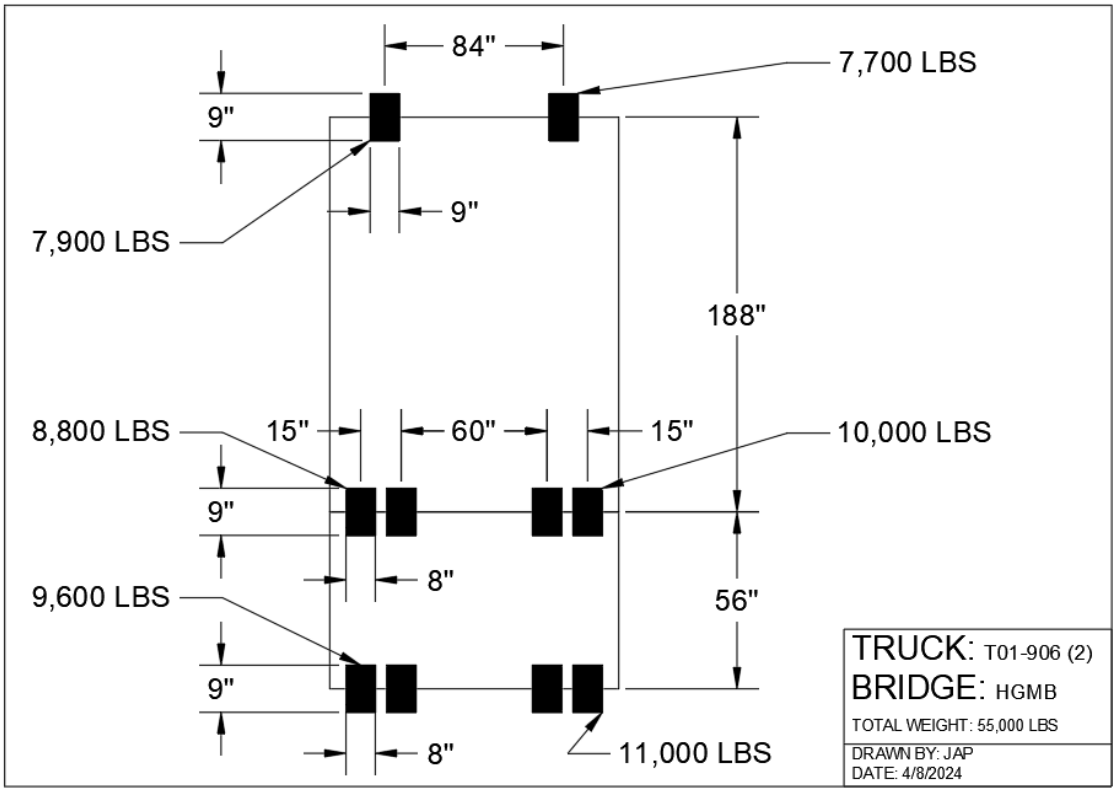
84"
7,700 LBS
9"
9"
7,900 LBS
188"
8,800 LBS
15"
60"
15"
10,000 LBS
9"
8"
9,600 LBS
56"
9"
8"
11,000 LBS
TRUCK: T01-906 (2)
BRIDGE: HGMB
TOTAL WEIGHT: 55,000 LBS
DRAWN BY: JAP
DATE: 4/8/2024

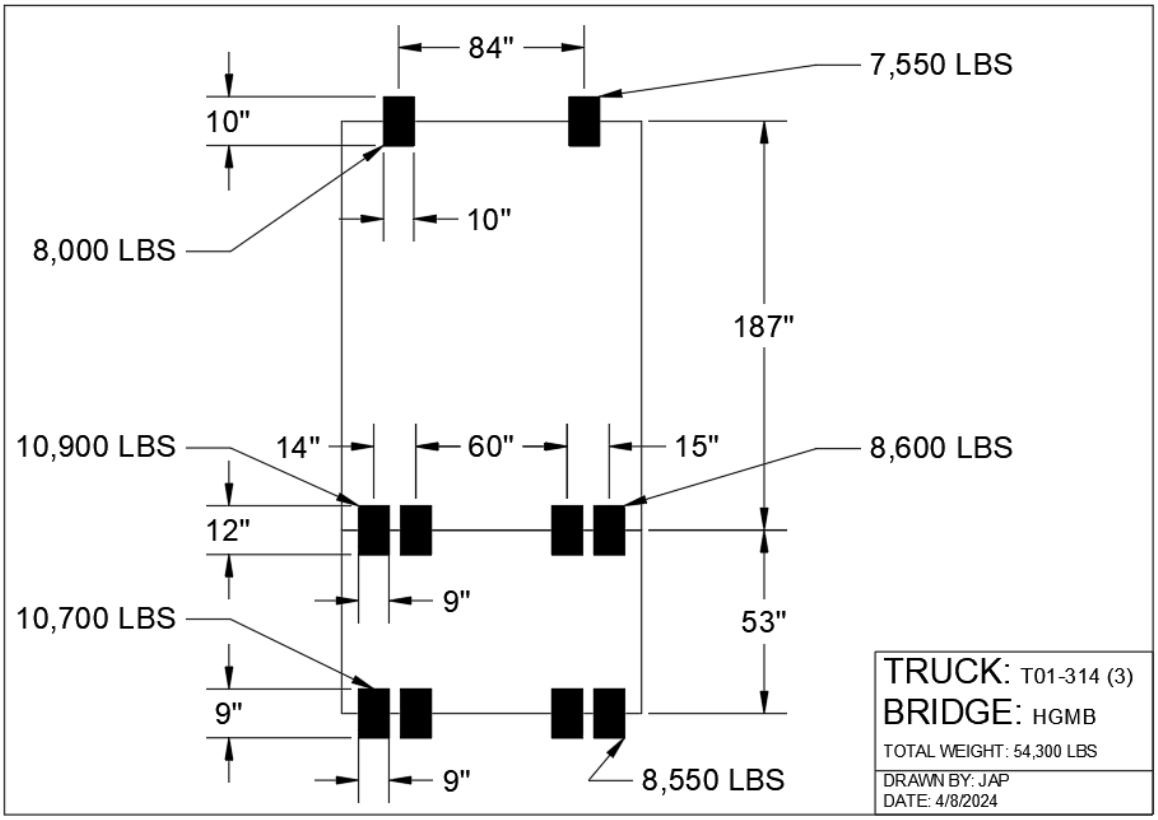
84"
7,550 LBS
10"
10"
8,000 LBS
187"
10,900 LBS
14"
60"
15"
8,600 LBS
12"
9"
10,700 LBS
53"
9"
9"
8,550 LBS
TRUCK: T01-314 (3)
BRIDGE: HGMB
TOTAL WEIGHT: 54,300 LBS
DRAWN BY: JAP
DATE: 4/8/2024

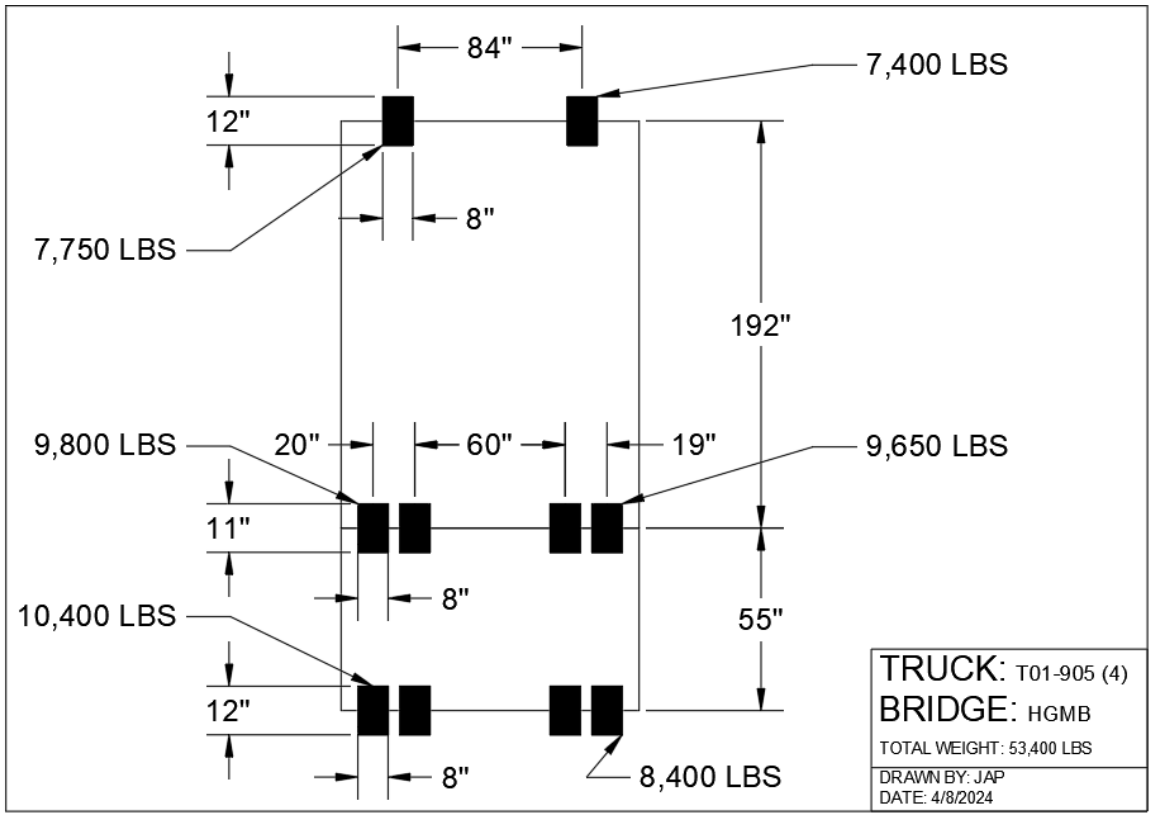
84"
7,400 LBS
12"
8"
7,750 LBS
192"
9,800 LBS
20"
60"
19"
9,650 LBS
11"
8"
10,400 LBS
55"
12"
8"
8,400 LBS
TRUCK: T01-905 (4)
BRIDGE: HGMB
TOTAL WEIGHT: 53,400 LBS
DRAWN BY: JAP
DATE: 4/8/2024

A.1.3 Representative Data Plots

A.1.3.1 M41 Test

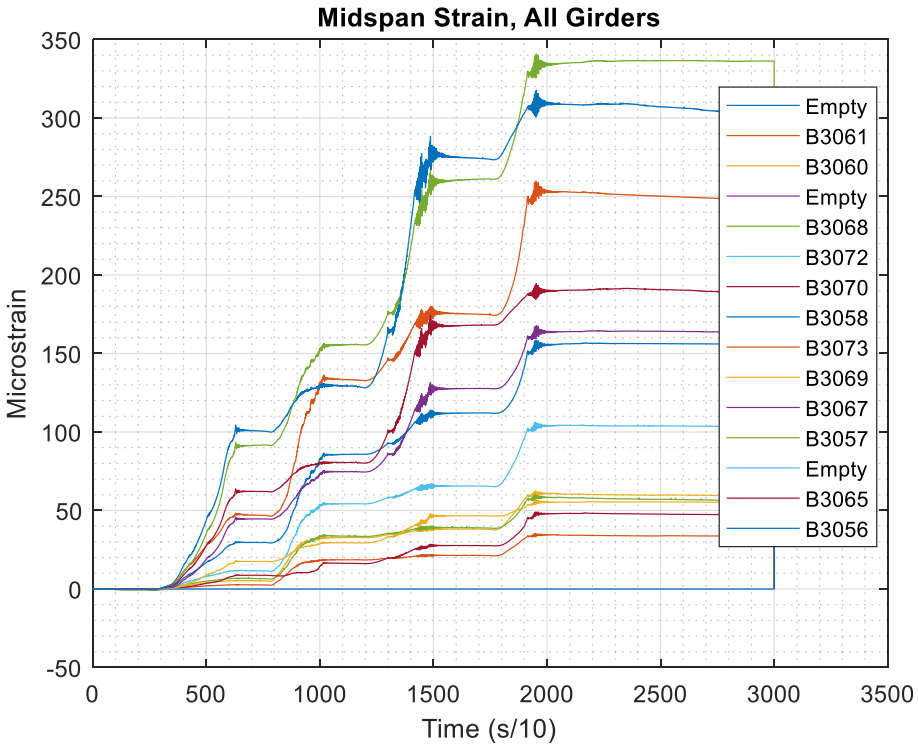

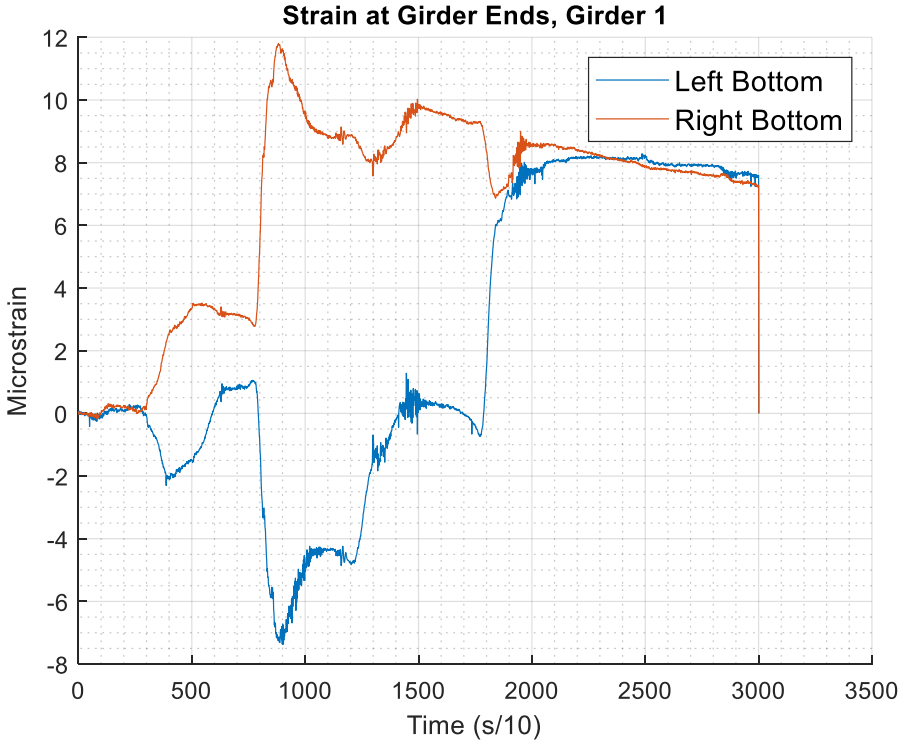

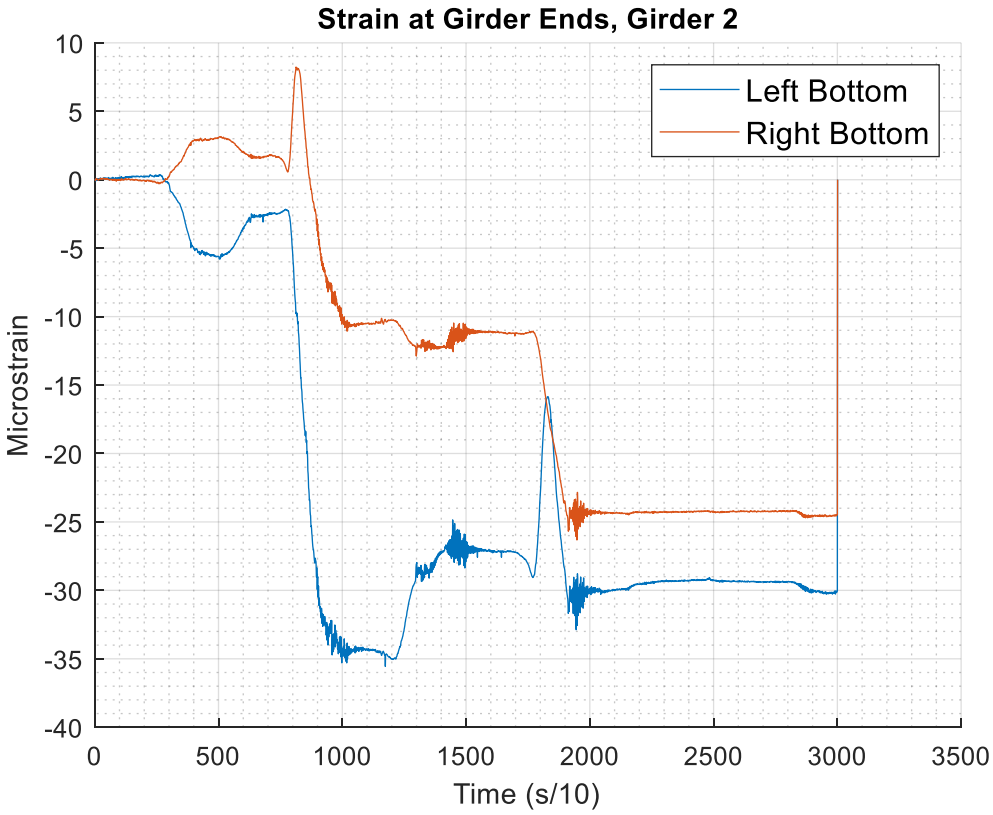
Strain at Girder Ends, Girder 2
Left Bottom
Right Bottom
Microstrain
Time (s/10)
10
5
0
-5
-10
-15
-20
-25
-30
-35
-40
0
500
1000
1500
2000
2500
3000
3500

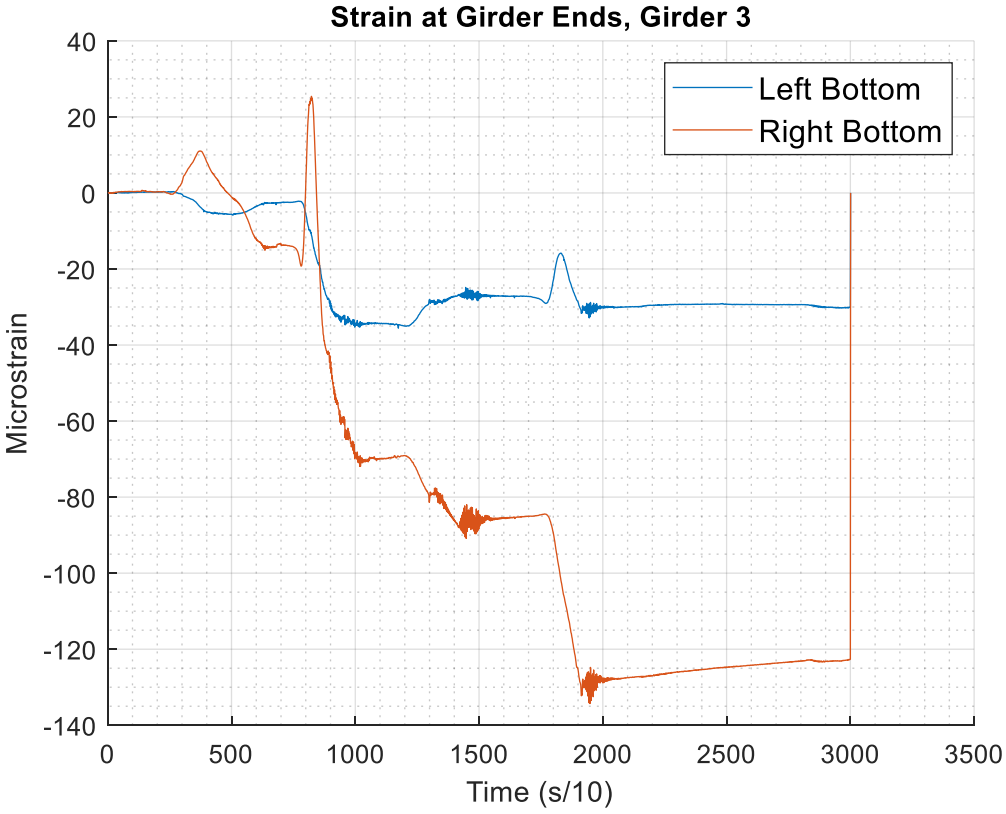
Strain at Girder Ends, Girder 3
Left Bottom
Right Bottom
Microstrain
Time (s/10)
40
20
0
-20
-40
-60
-80
-100
-120
-140
0
500
1000
1500
2000
2500
3000
3500

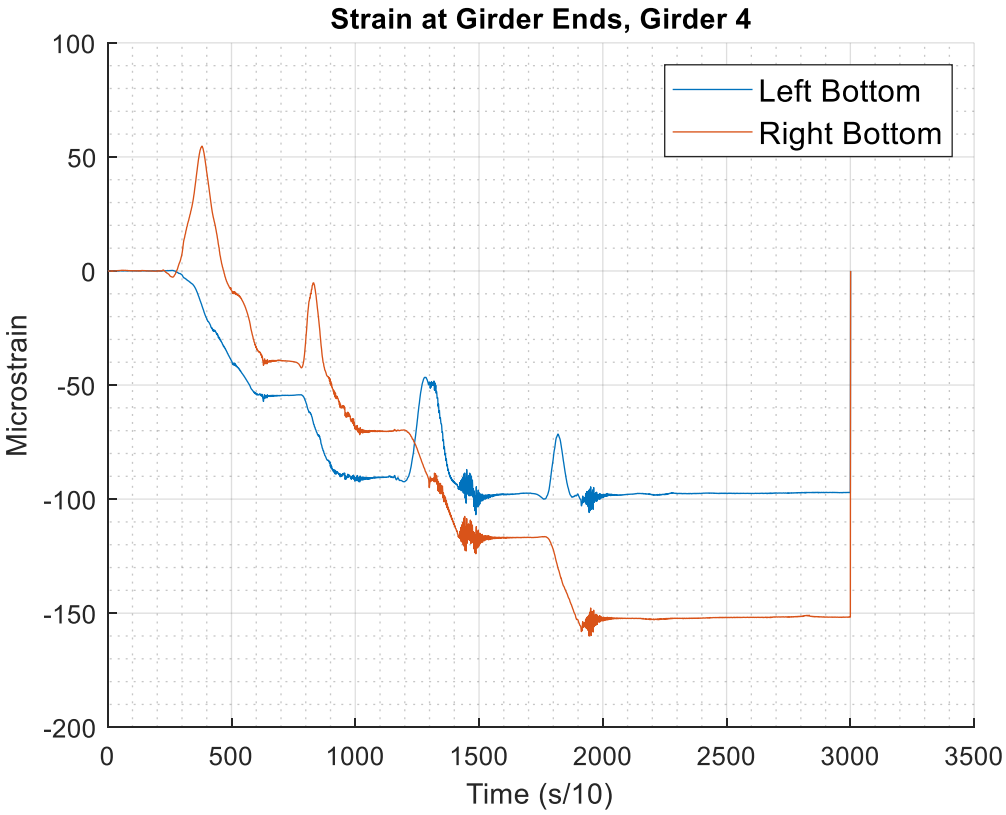
Strain at Girder Ends, Girder 4
Left Bottom
Right Bottom
Microstrain
Time (s/10)
100
50
0
-50
-100
-150
-200
0
500
1000
1500
2000
2500
3000
3500

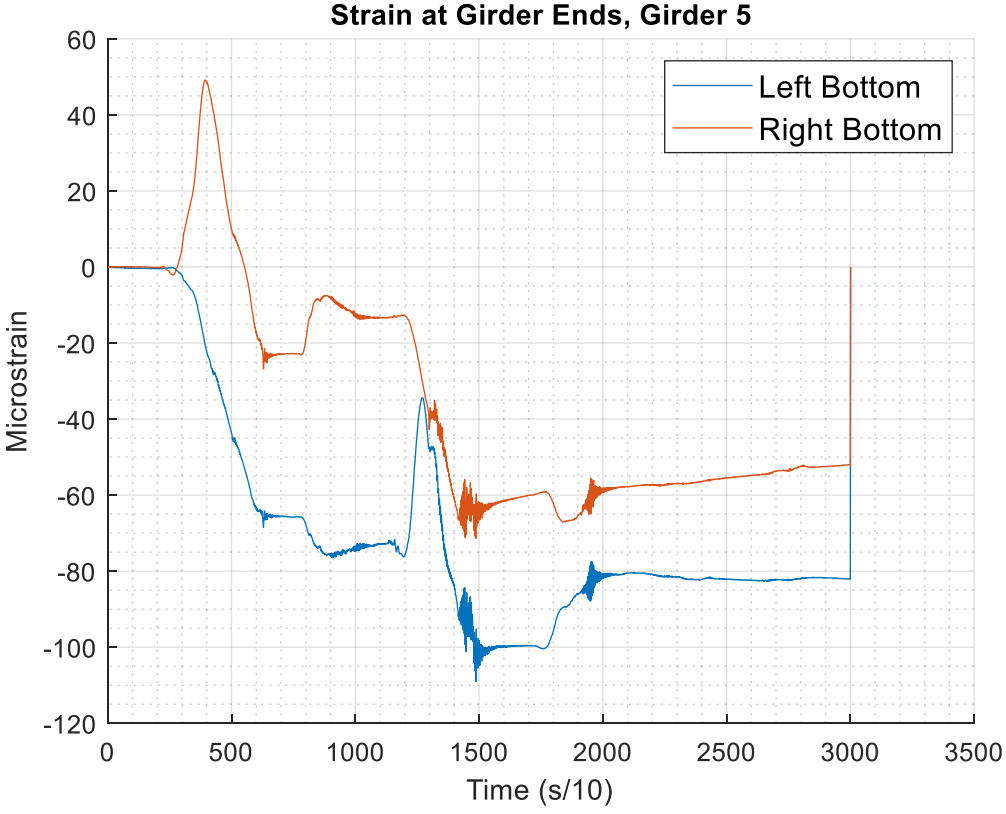
Strain at Girder Ends, Girder 5
Left Bottom
Right Bottom
Microstrain
Time (s/10)
60
40
20
0
-20
-40
-60
-80
-100
-120
0
500
1000
1500
2000
2500
3000
3500

A.1.3.2 M42 Test

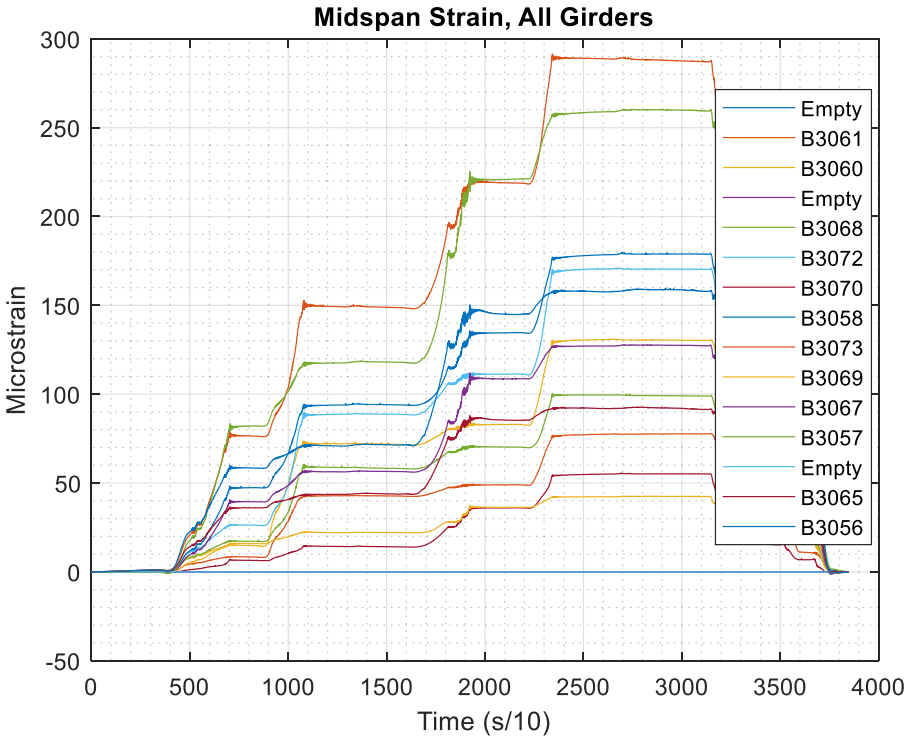

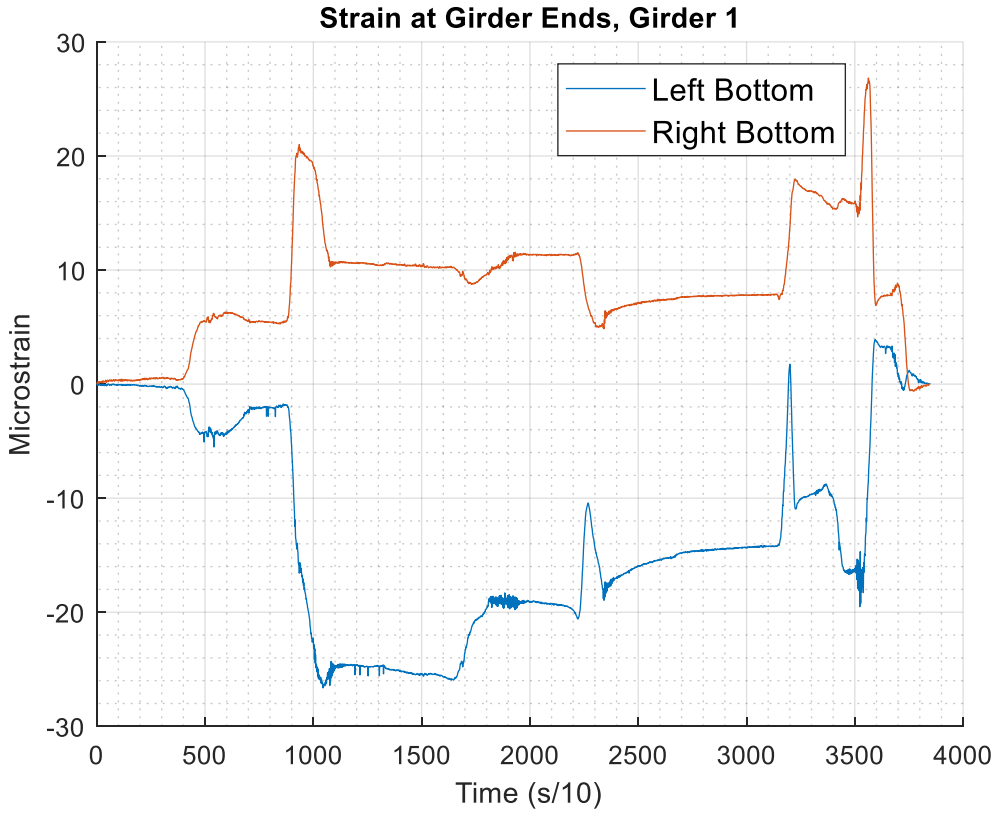

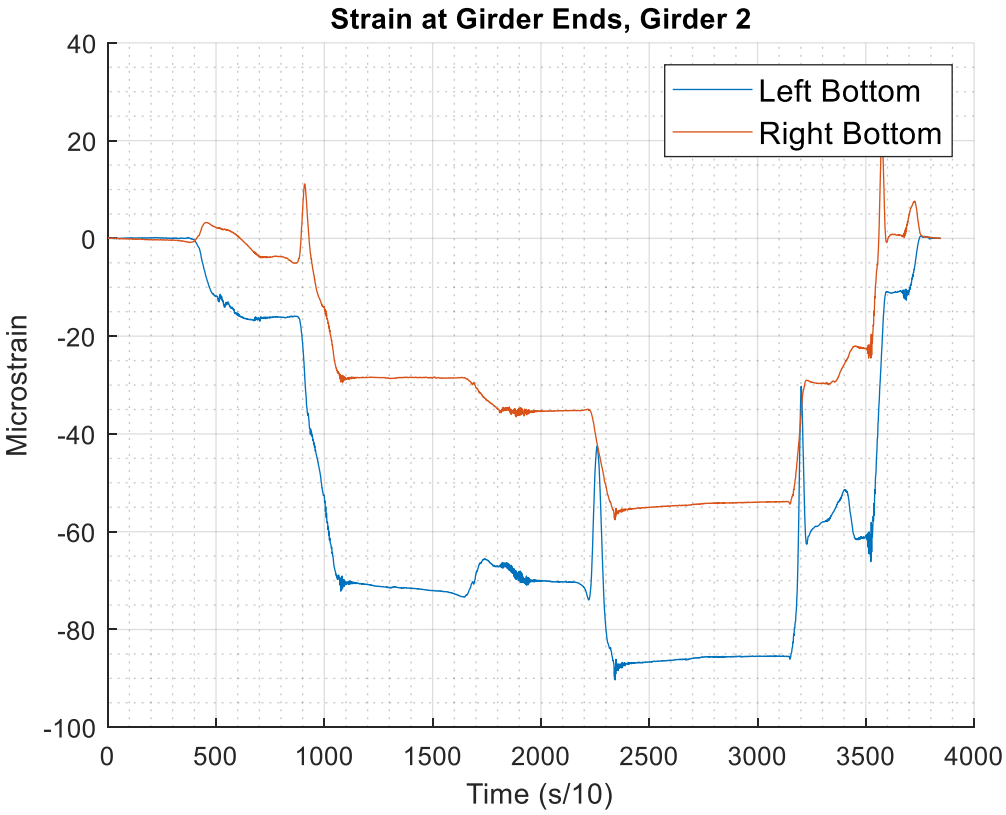
Strain at Girder Ends, Girder 2
Left Bottom
Right Bottom
Microstrain
Time (s/10)
40
20
0
-20
-40
-60
-80
-100
0
500
1000
1500
2000
2500
3000
3500
4000

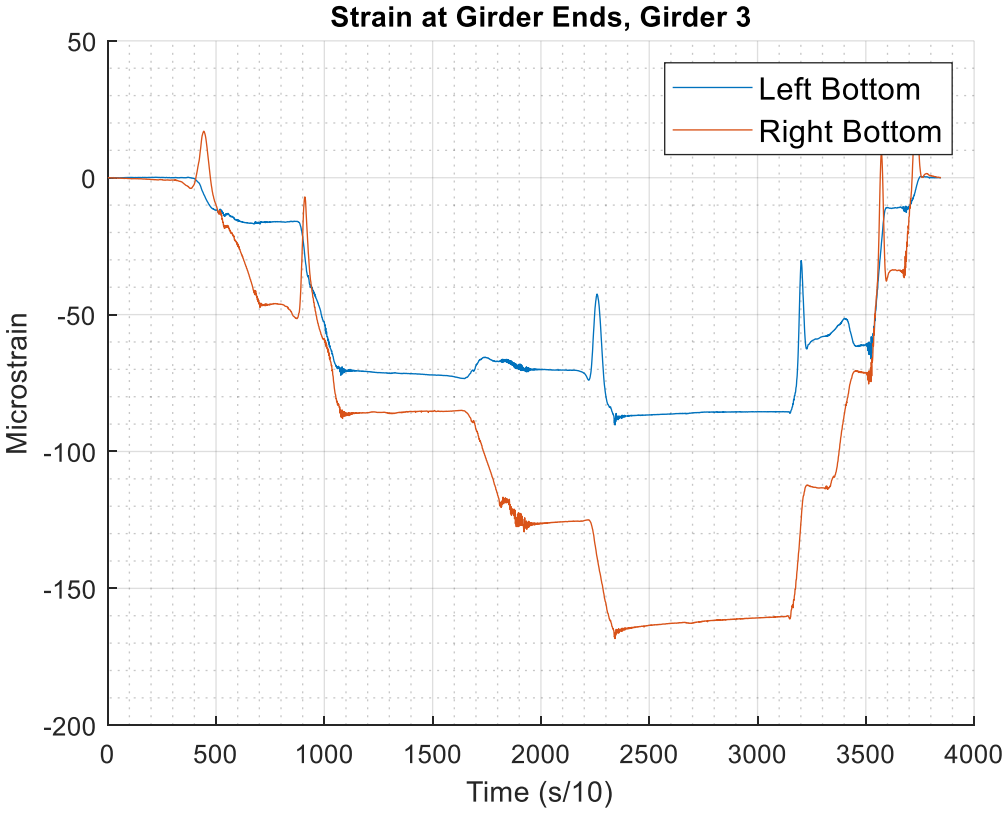
Strain at Girder Ends, Girder 3
Left Bottom
Right Bottom
Microstrain
Time (s/10)
50
0
-50
-100
-150
-200
0
500
1000
1500
2000
2500
3000
3500
4000

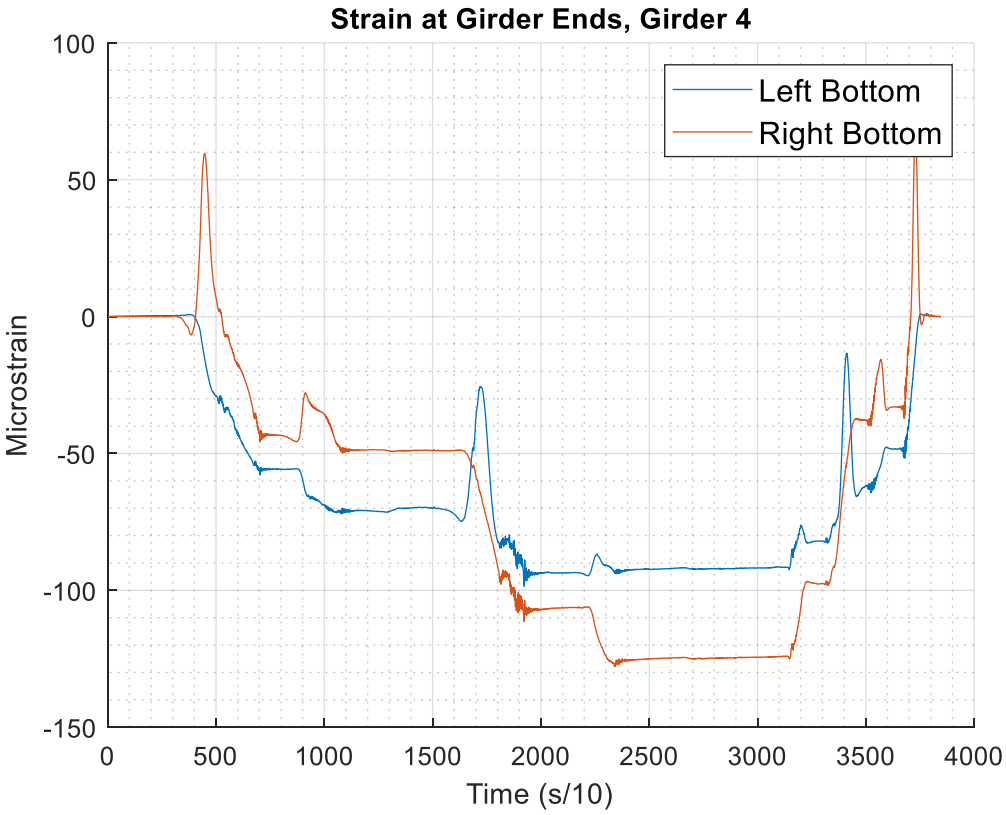
Strain at Girder Ends, Girder 4
Left Bottom
Right Bottom
Microstrain
Time (s/10)
100
50
0
-50
-100
-150
0
500
1000
1500
2000
2500
3000
3500
4000

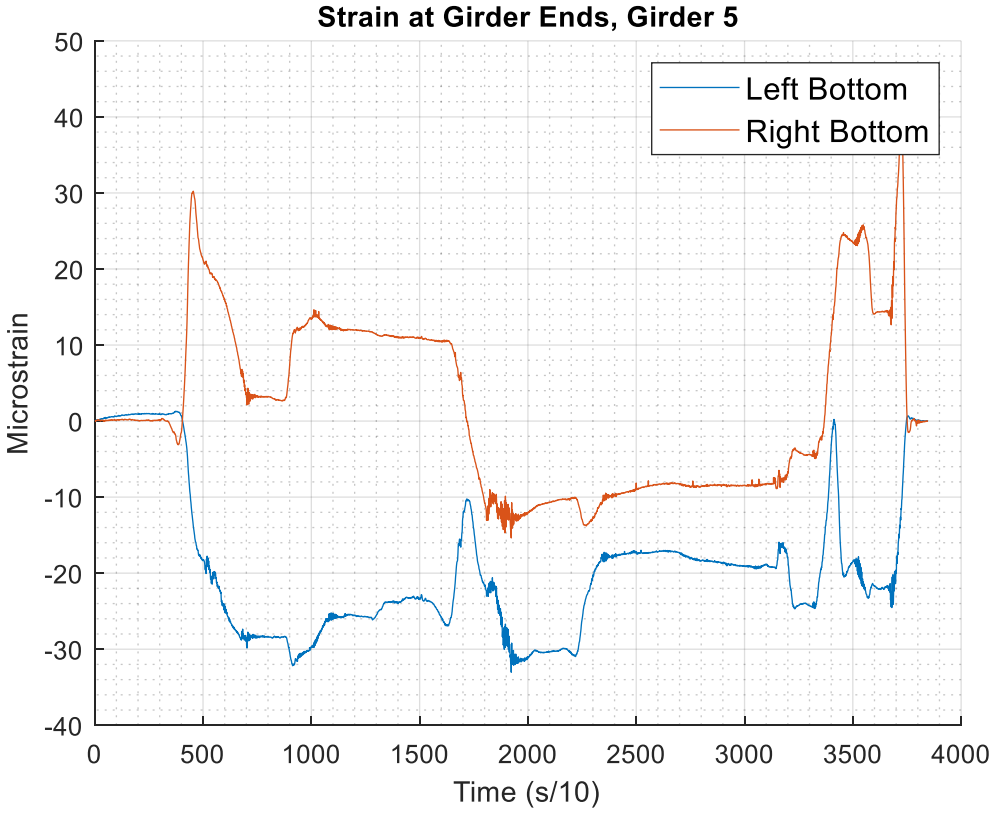
Strain at Girder Ends, Girder 5
Left Bottom
Right Bottom
Microstrain
Time (s/10)
50
40
30
20
10
0
-10
-20
-30
-40
0
500
1000
1500
2000
2500
3000
3500
4000

A.1.3.3 M43 Test

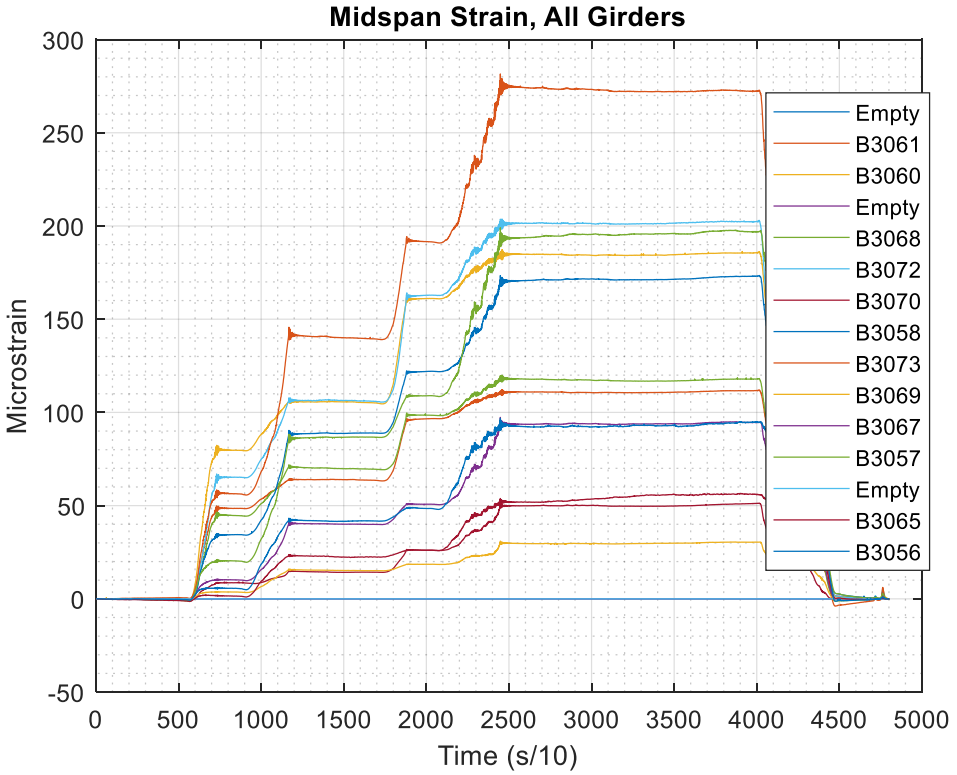

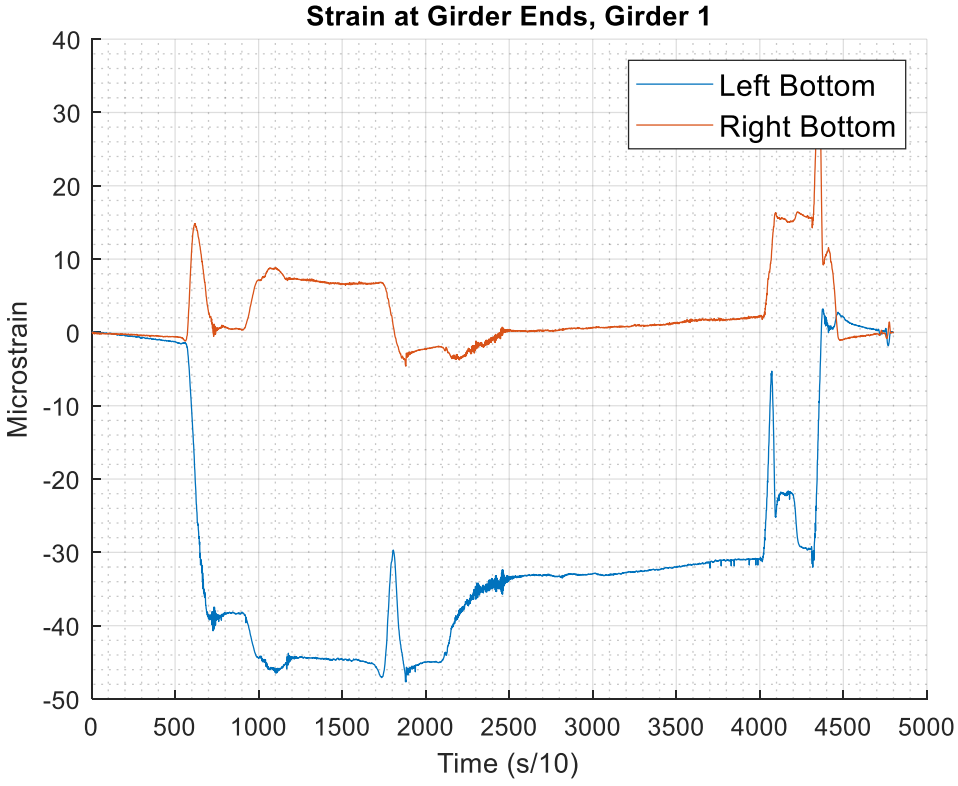

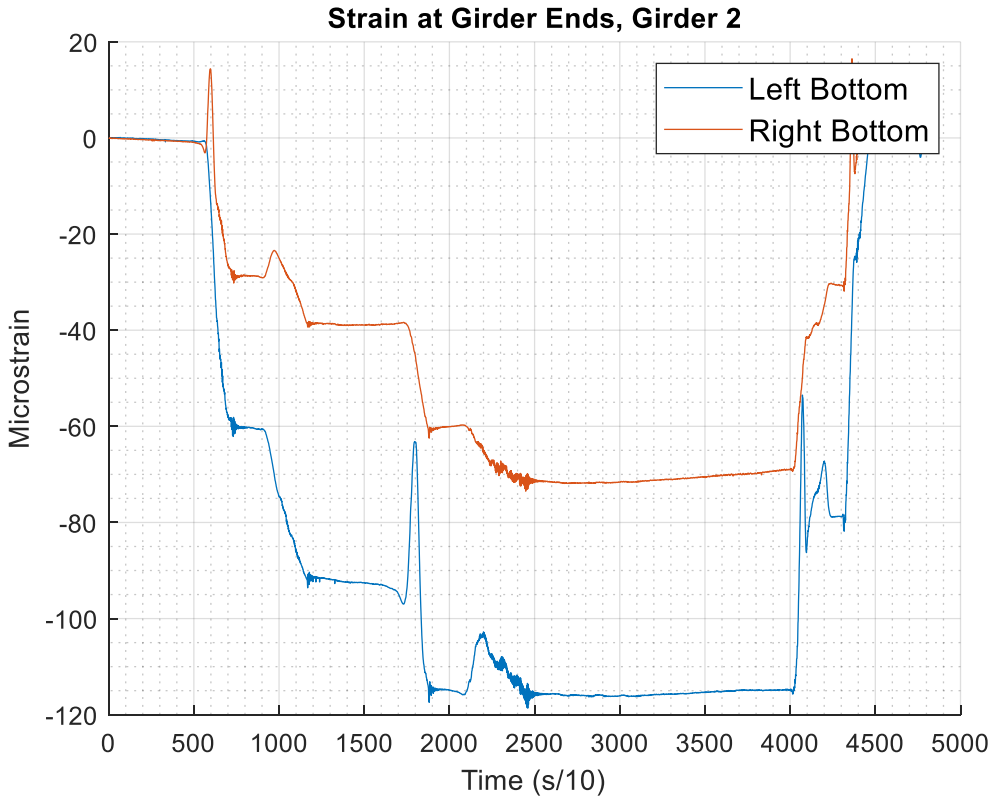
Strain at Girder Ends, Girder 2
Left Bottom
Right Bottom
Microstrain
Time (s/10)
20
0
-20
-40
-60
-80
-100
-120
0
500
1000
1500
2000
2500
3000
3500
4000
4500
5000

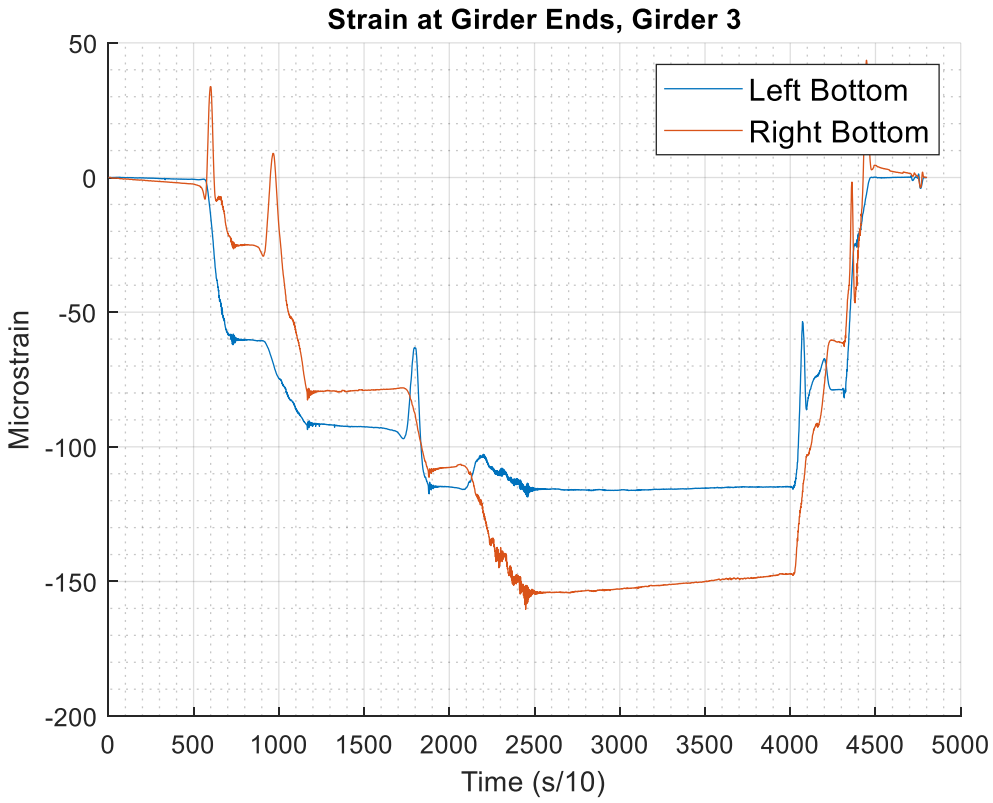
Strain at Girder Ends, Girder 3
Left Bottom
Right Bottom
Microstrain
Time (s/10)
50
0
-50
-100
-150
-200
0
500
1000
1500
2000
2500
3000
3500
4000
4500
5000

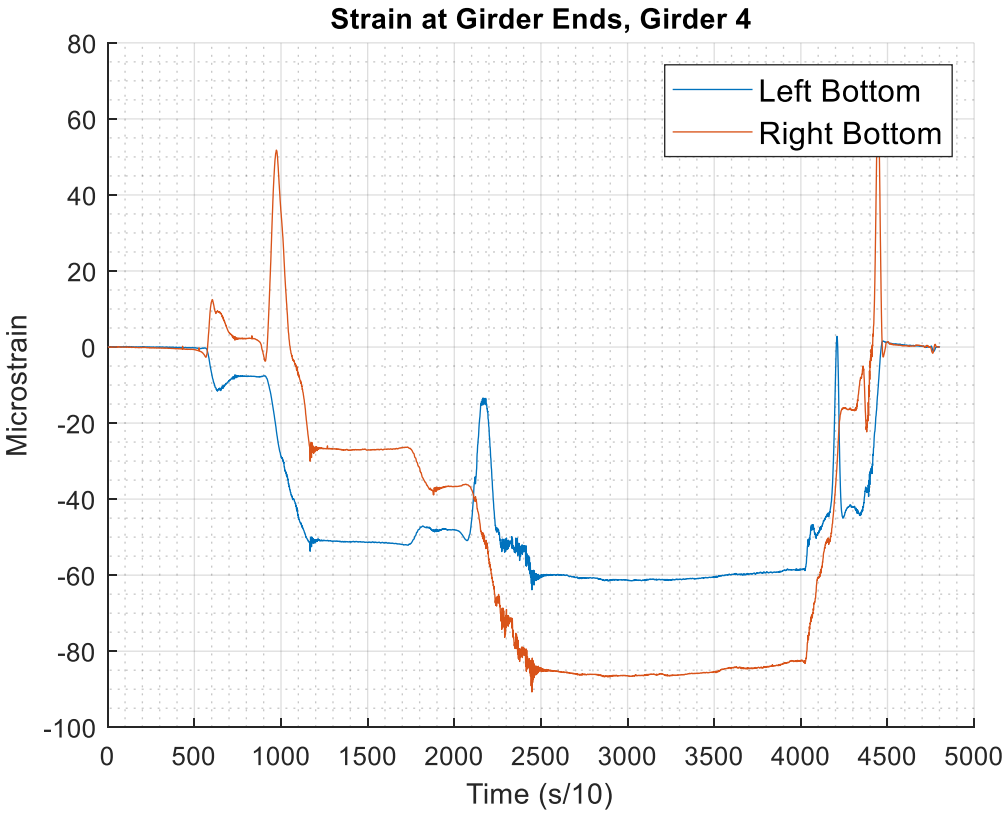
Strain at Girder Ends, Girder 4
Left Bottom
Right Bottom
Microstrain
Time (s/10)
80
60
40
20
0
-20
-40
-60
-80
-100
0
500
1000
1500
2000
2500
3000
3500
4000
4500
5000

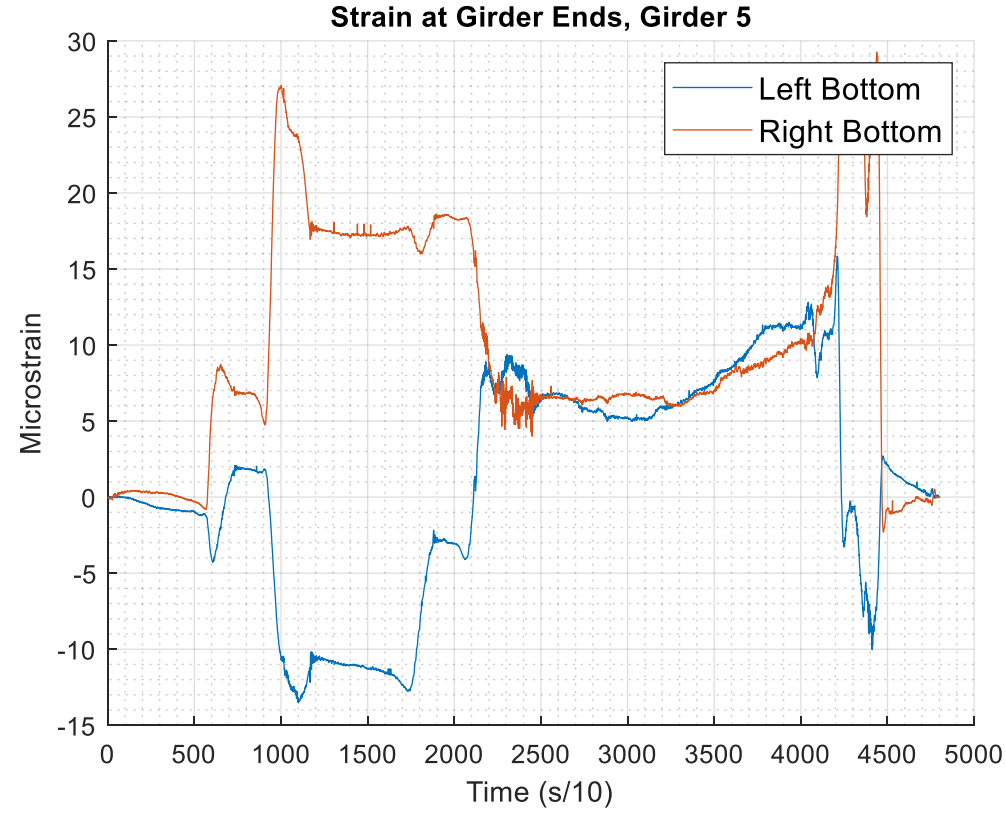
Strain at Girder Ends, Girder 5
Left Bottom
Right Bottom
Microstrain
Time (s/10)
30
25
20
15
10
5
0
-5
-10
-15
0
500
1000
1500
2000
2500
3000
3500
4000
4500
5000

A.1.3.4 M21 Test

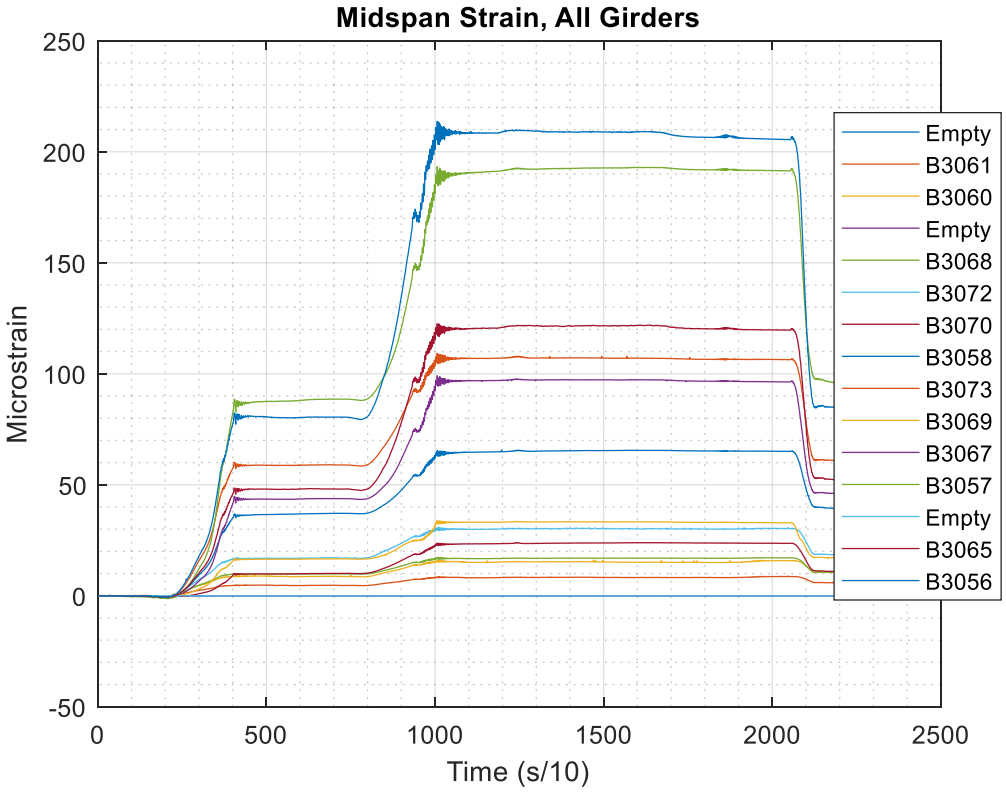

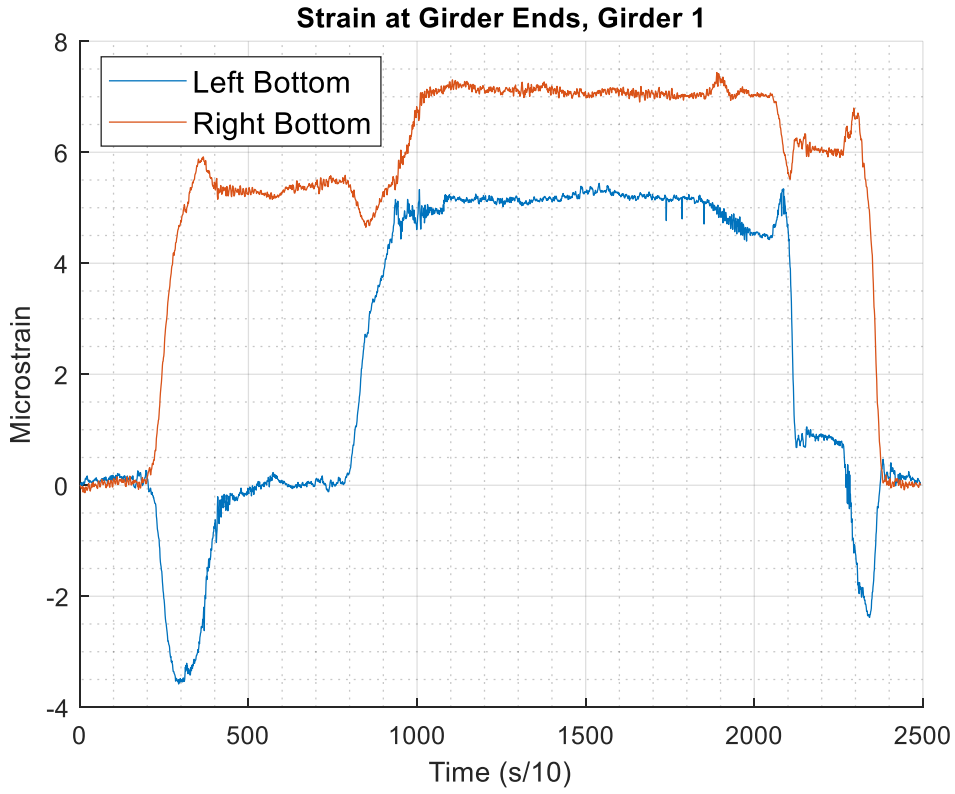

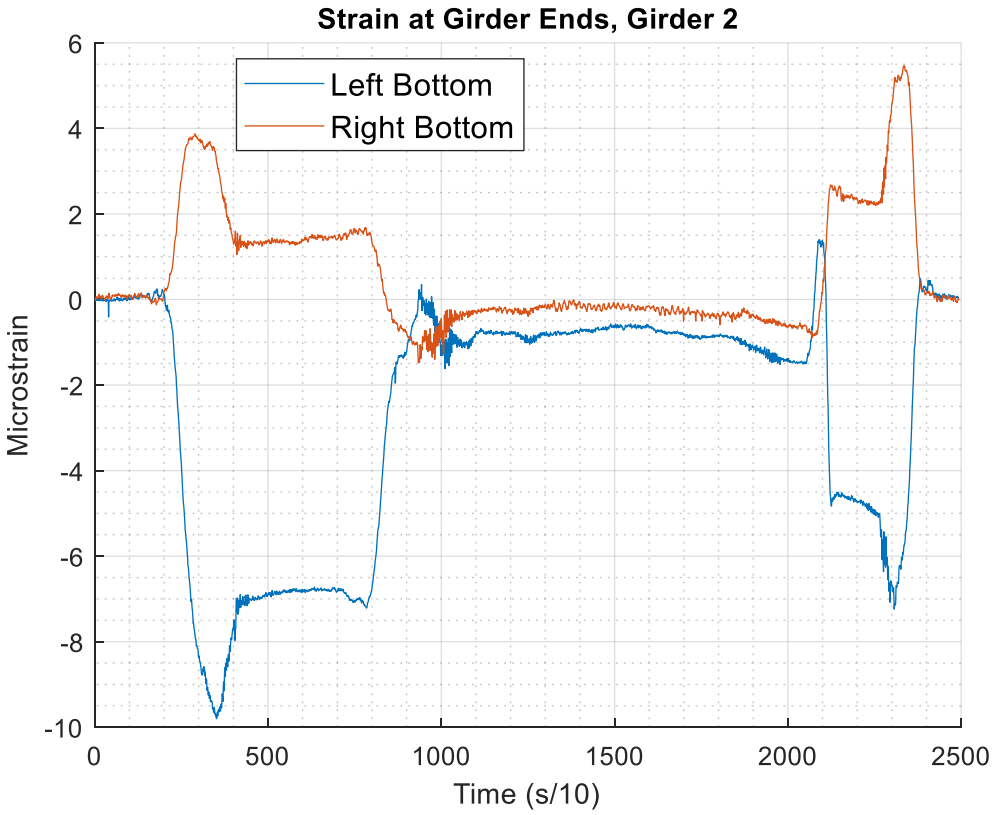
Strain at Girder Ends, Girder 2
Left Bottom
Right Bottom
Microstrain
Time (s/10)
6
4
2
0
-2
-4
-6
-8
-10
0
500
1000
1500
2000
2500

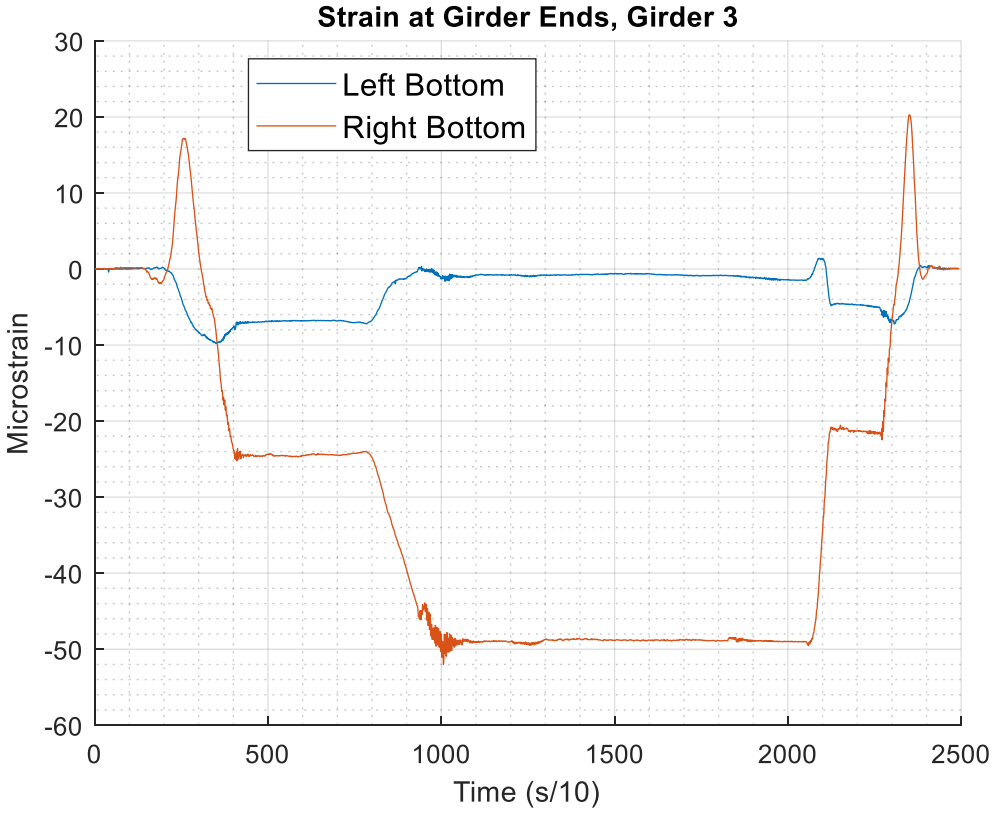
Strain at Girder Ends, Girder 3
Left Bottom
Right Bottom
Microstrain
Time (s/10)
30
20
10
0
-10
-20
-30
-40
-50
-60
0
500
1000
1500
2000
2500

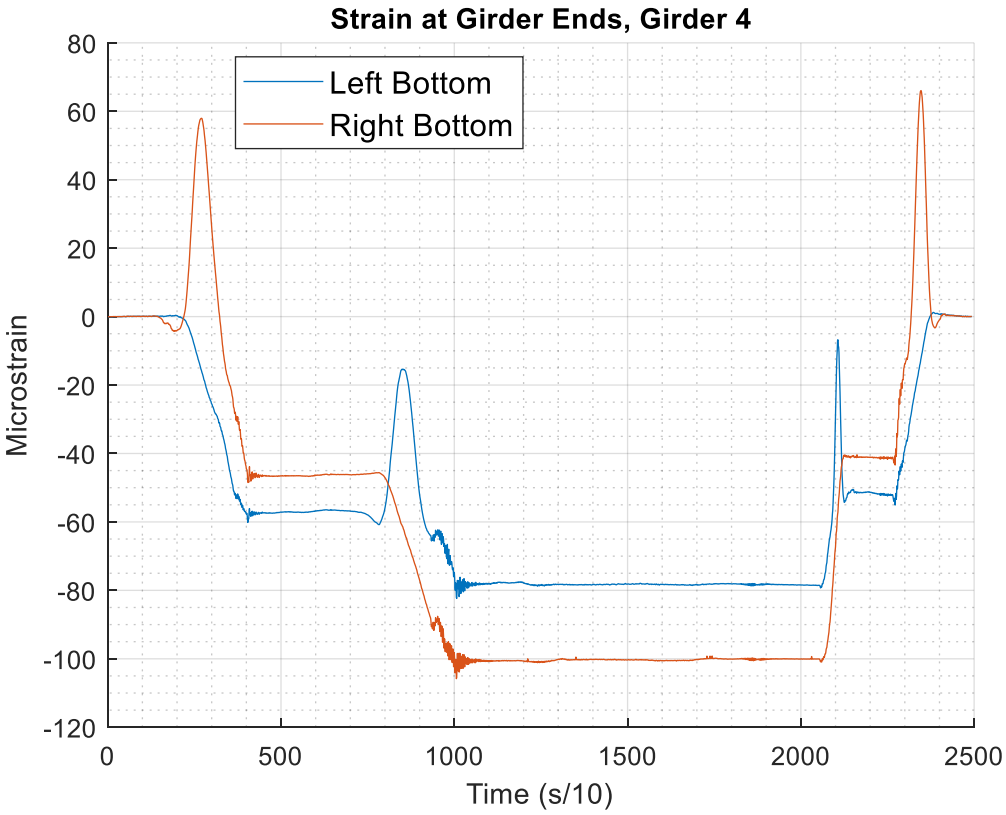
Strain at Girder Ends, Girder 4
Left Bottom
Right Bottom
Microstrain
Time (s/10)
80
60
40
20
0
-20
-40
-60
-80
-100
-120
0
500
1000
1500
2000
2500

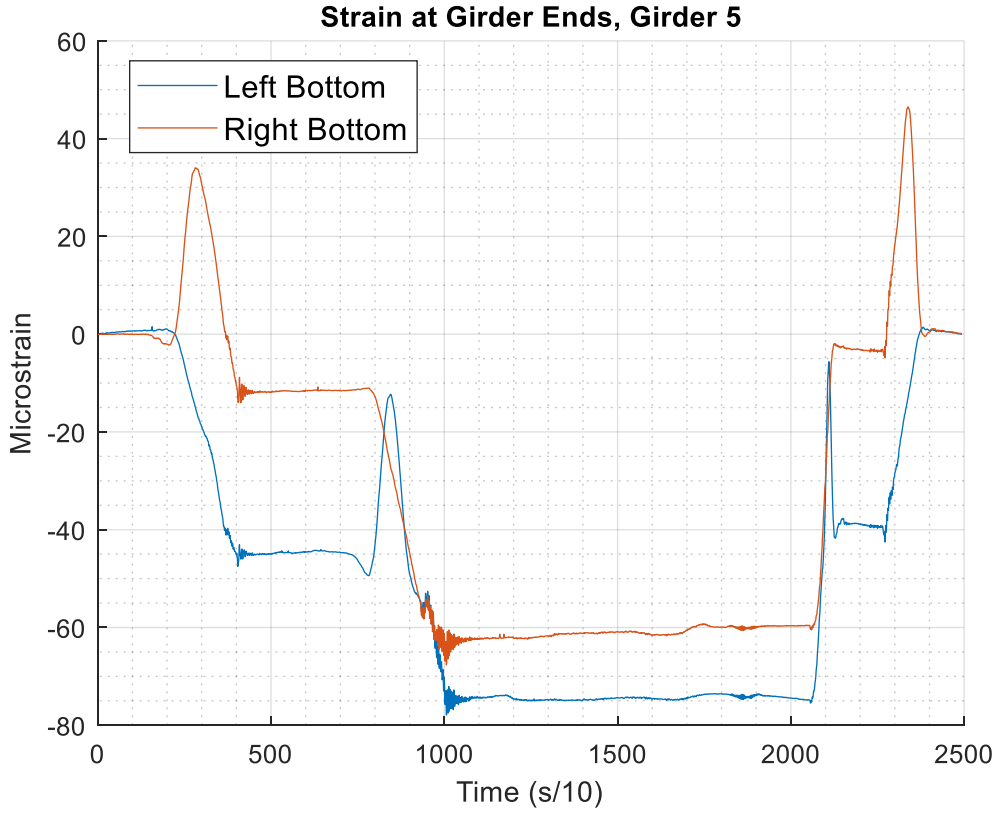
Strain at Girder Ends, Girder 5
Left Bottom
Right Bottom
Microstrain
Time (s/10)
60
40
20
0
-20
-40
-60
-80
0
500
1000
1500
2000
2500

A.1.3.5 M22 Test

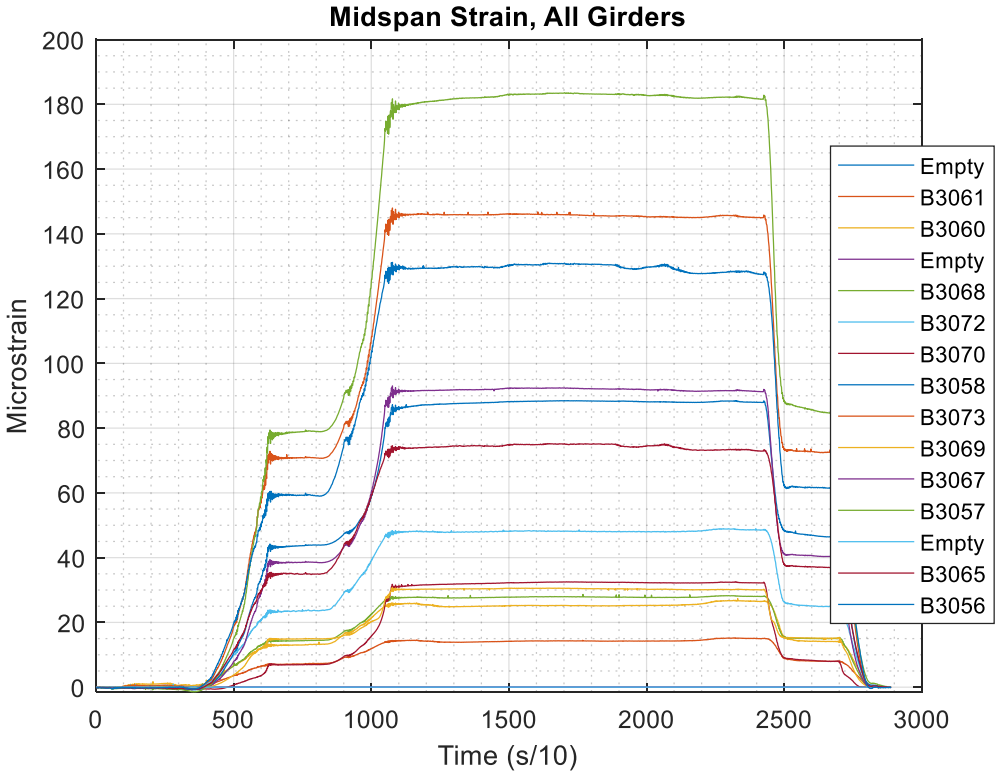

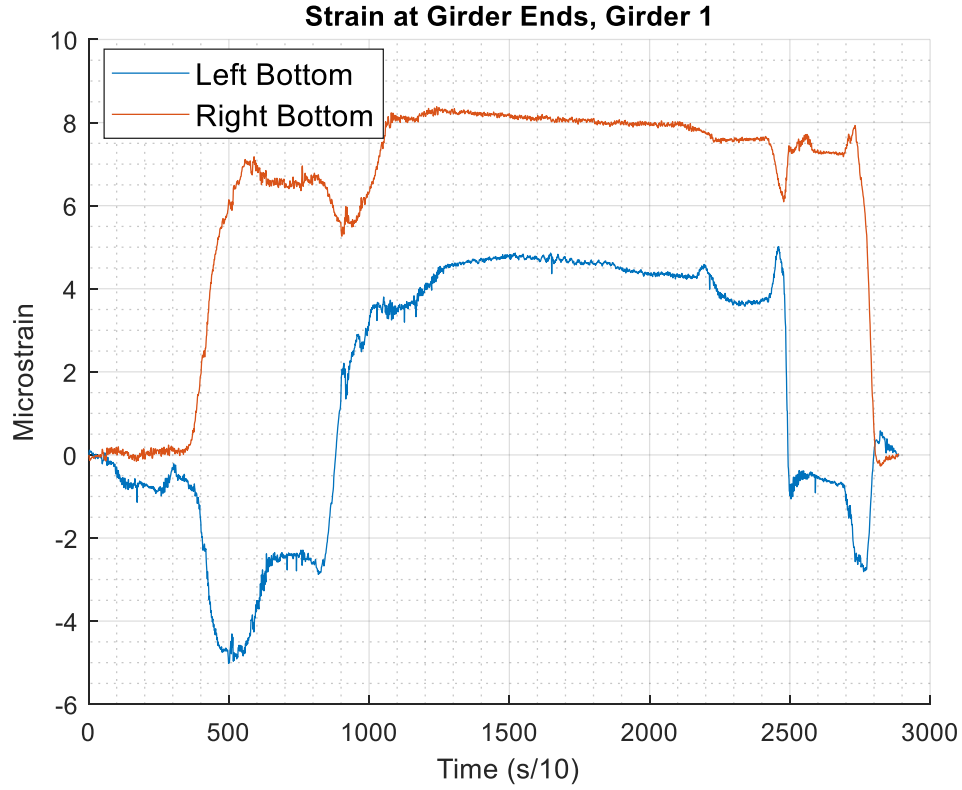

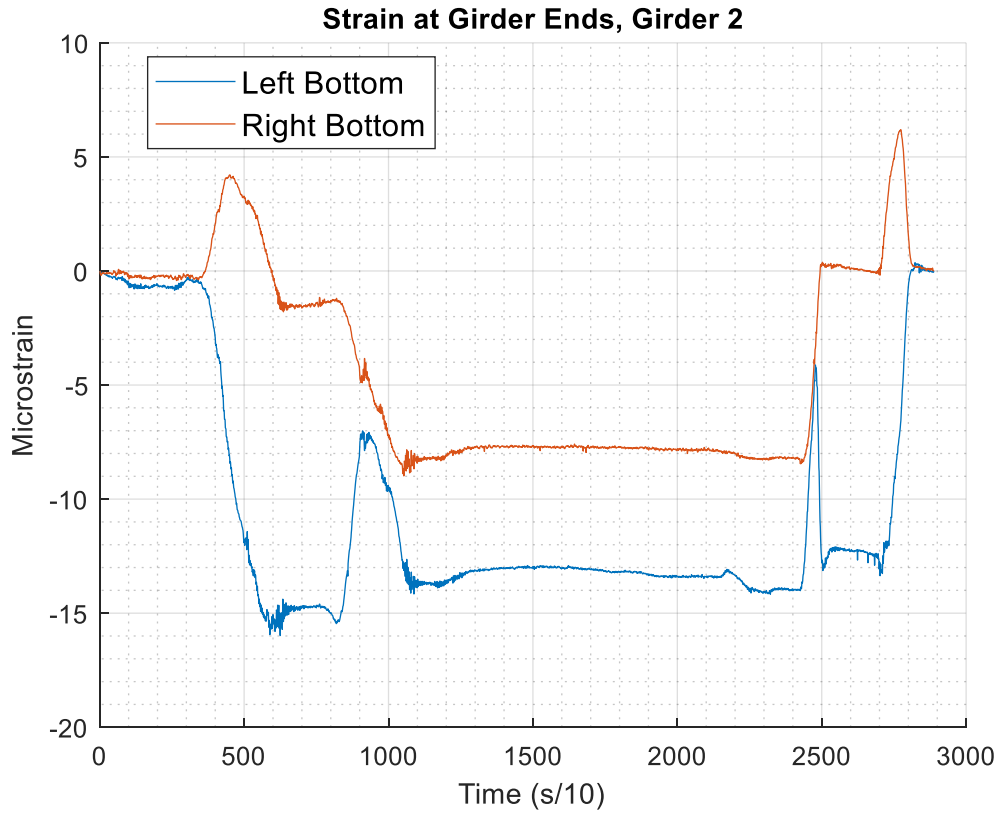
Strain at Girder Ends, Girder 2
Left Bottom
Right Bottom
Microstrain
Time (s/10)
10
5
0
-5
-10
-15
-20
0
500
1000
1500
2000
2500
3000


Strain at Girder Ends, Girder 3
Left Bottom
Right Bottom
Microstrain
Time (s/10)
40
20
0
-20
-40
-60
-80
-100
0
500
1000
1500
2000
2500
3000

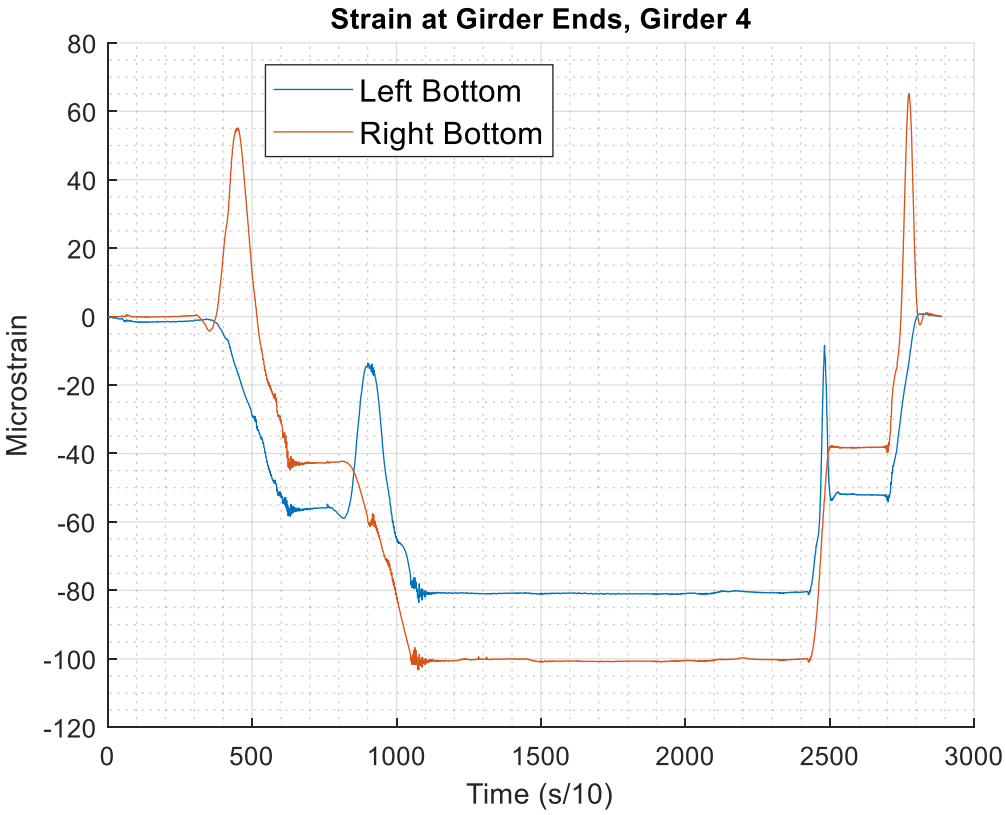
Strain at Girder Ends, Girder 4
Left Bottom
Right Bottom
Microstrain
Time (s/10)
80
60
40
20
0
-20
-40
-60
-80
-100
-120
0
500
1000
1500
2000
2500
3000


Strain at Girder Ends, Girder 5
Left Bottom
Right Bottom
Microstrain
Time (s/10)
40
30
20
10
0
-10
-20
-30
-40
0
500
1000
1500
2000
2500
3000

A.1.3.6 M23 Test

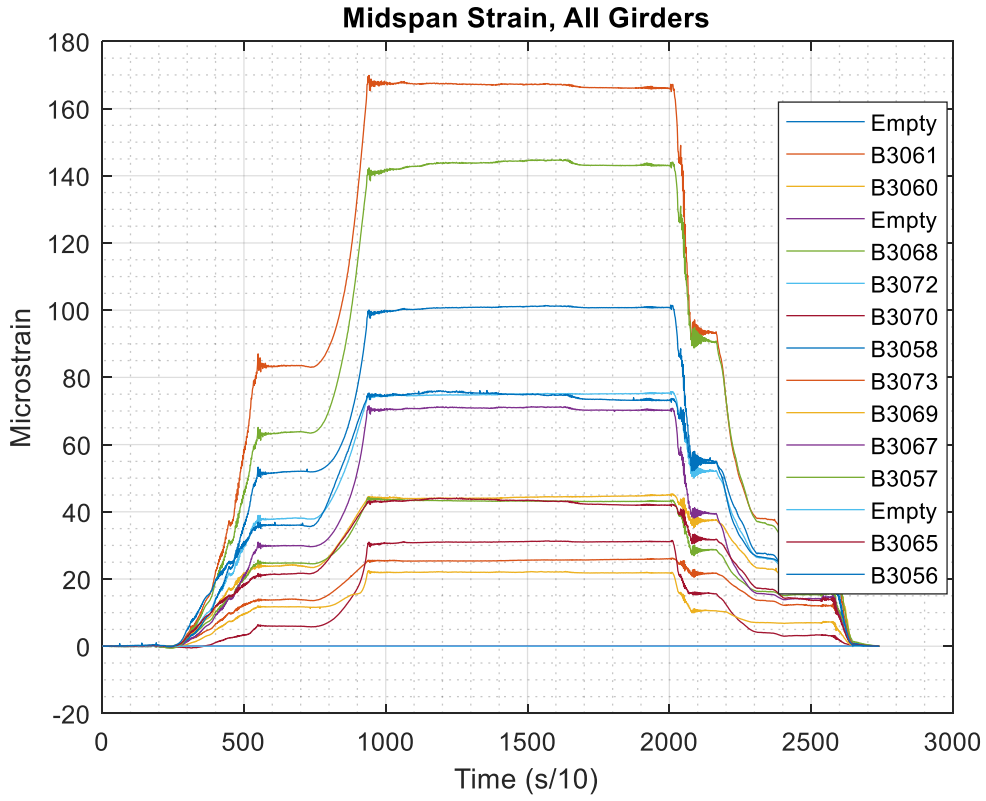

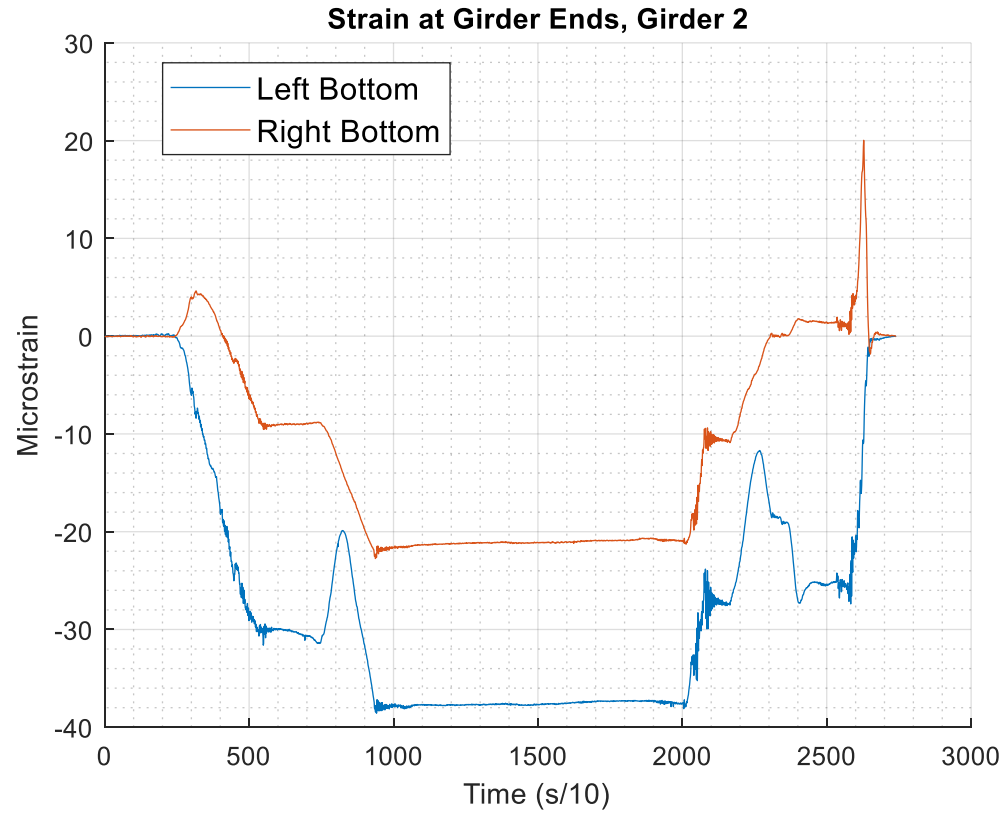
Strain at Girder Ends, Girder 2
Left Bottom
Right Bottom
Microstrain
Time (s/10)
30
20
10
0
-10
-20
-30
-40
0
500
1000
1500
2000
2500
3000


Strain at Girder Ends, Girder 3
Left Bottom
Right Bottom
Microstrain
Time (s/10)
60
40
20
0
-20
-40
-60
-80
-100
-120
0
500
1000
1500
2000
2500
3000

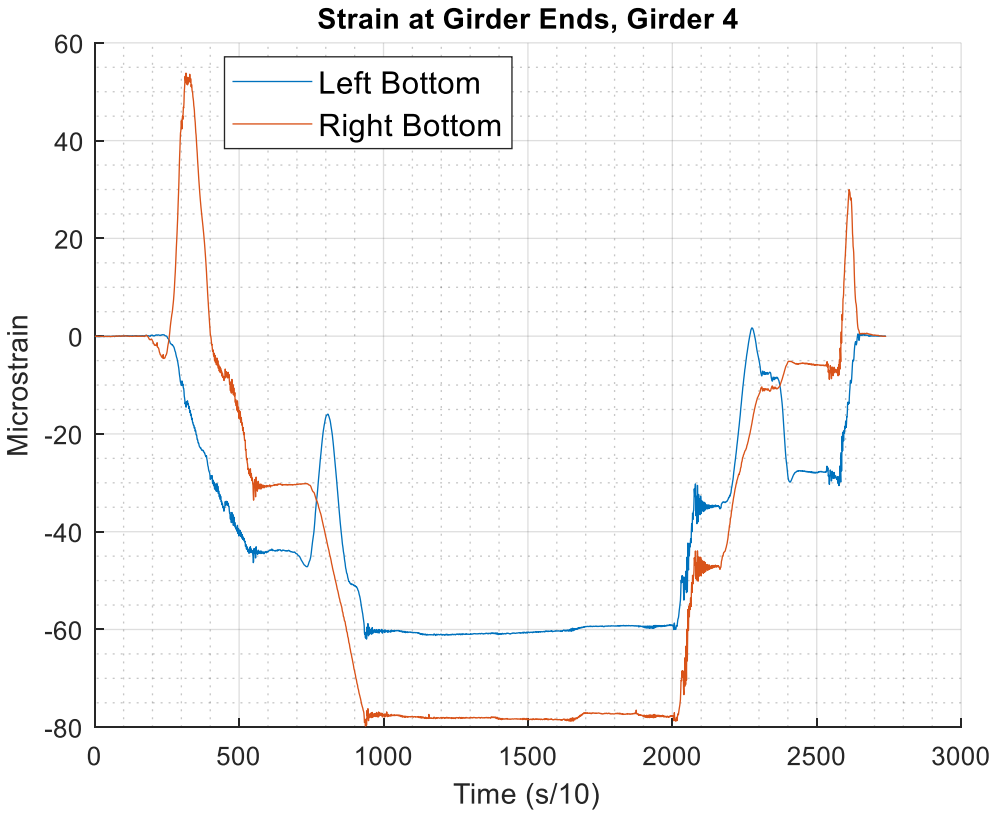
Strain at Girder Ends, Girder 4
Left Bottom
Right Bottom
Microstrain
Time (s/10)
60
40
20
0
-20
-40
-60
-80
0
500
1000
1500
2000
2500
3000

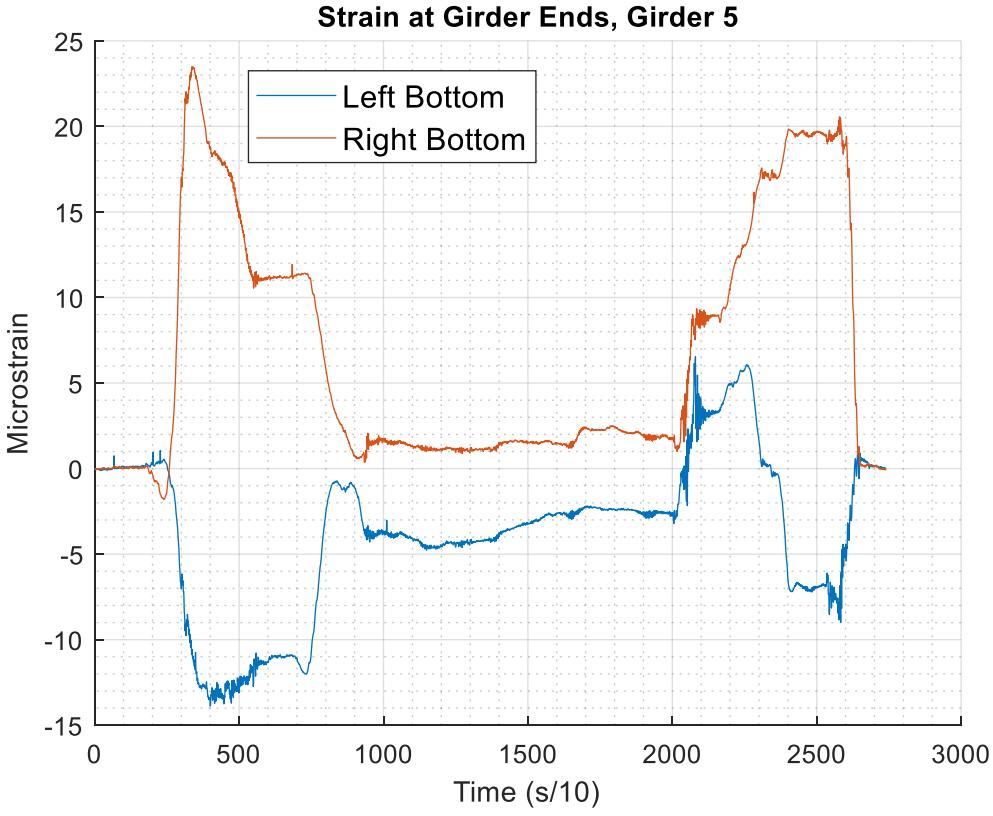
Strain at Girder Ends, Girder 5
Left Bottom
Right Bottom
Microstrain
Time (s/10)
25
20
15
10
5
0
-5
-10
-15
0
500
1000
1500
2000
2500
3000

A.1.3.7 M24 Test

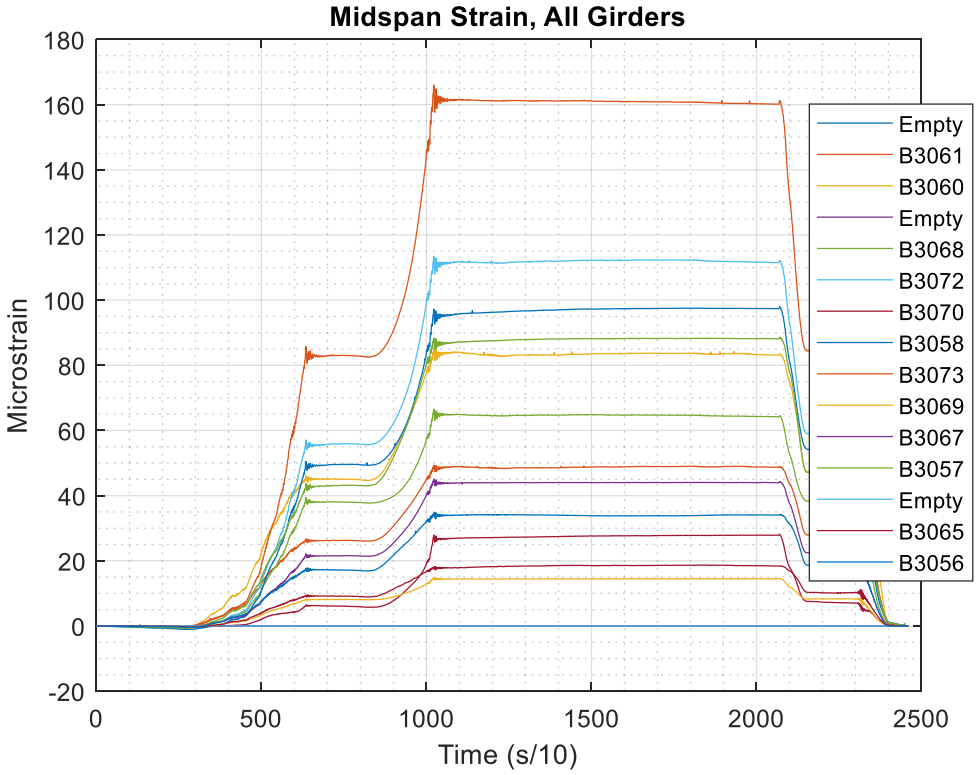

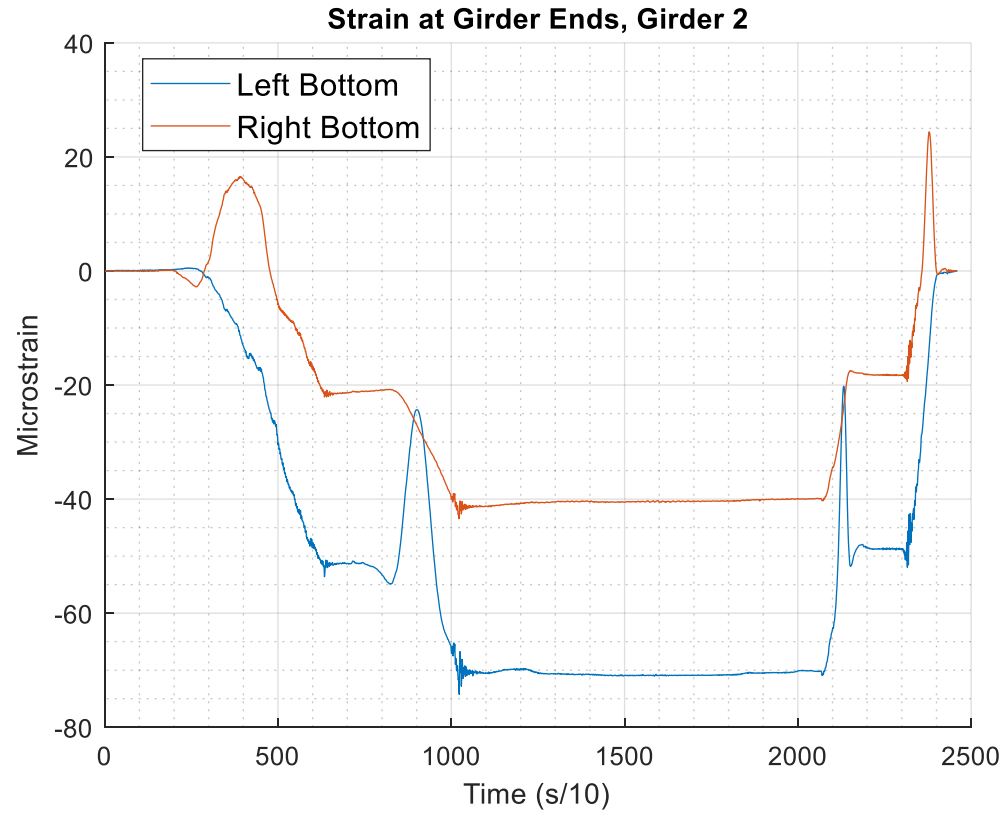
Strain at Girder Ends, Girder 2
Left Bottom
Right Bottom
Microstrain
Time (s/10)
40
20
0
-20
-40
-60
-80
0
500
1000
1500
2000
2500

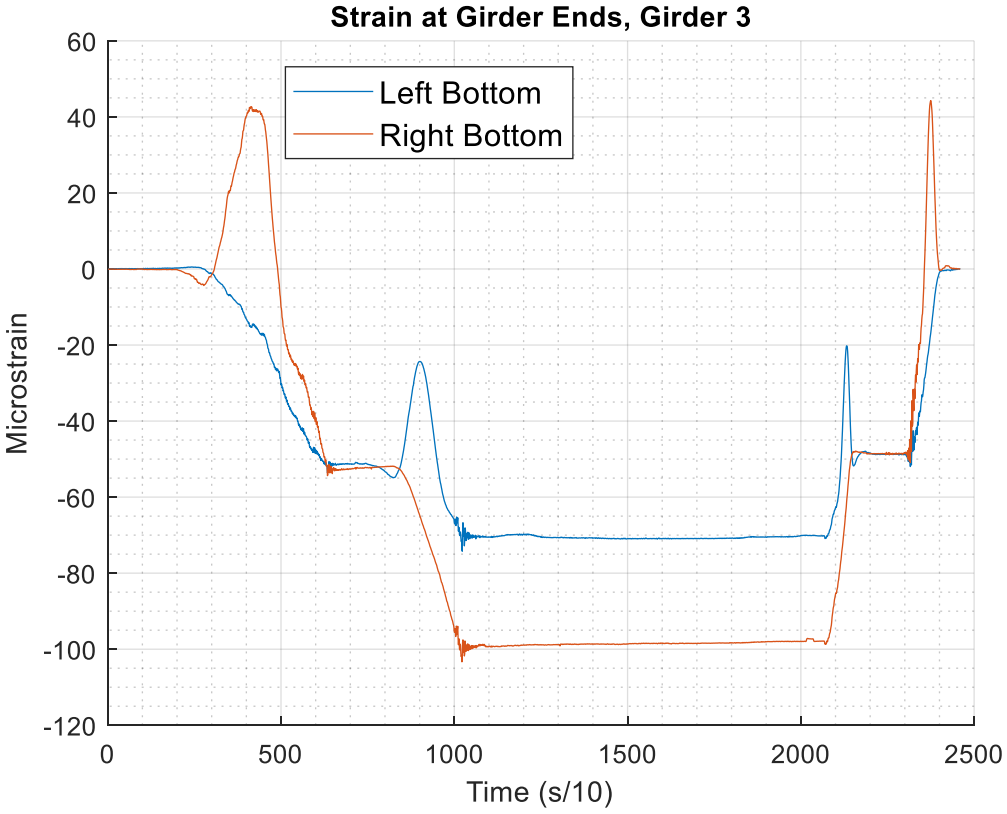
Strain at Girder Ends, Girder 3
Left Bottom
Right Bottom
Microstrain
Time (s/10)
60
40
20
0
-20
-40
-60
-80
-100
-120
0
500
1000
1500
2000
2500

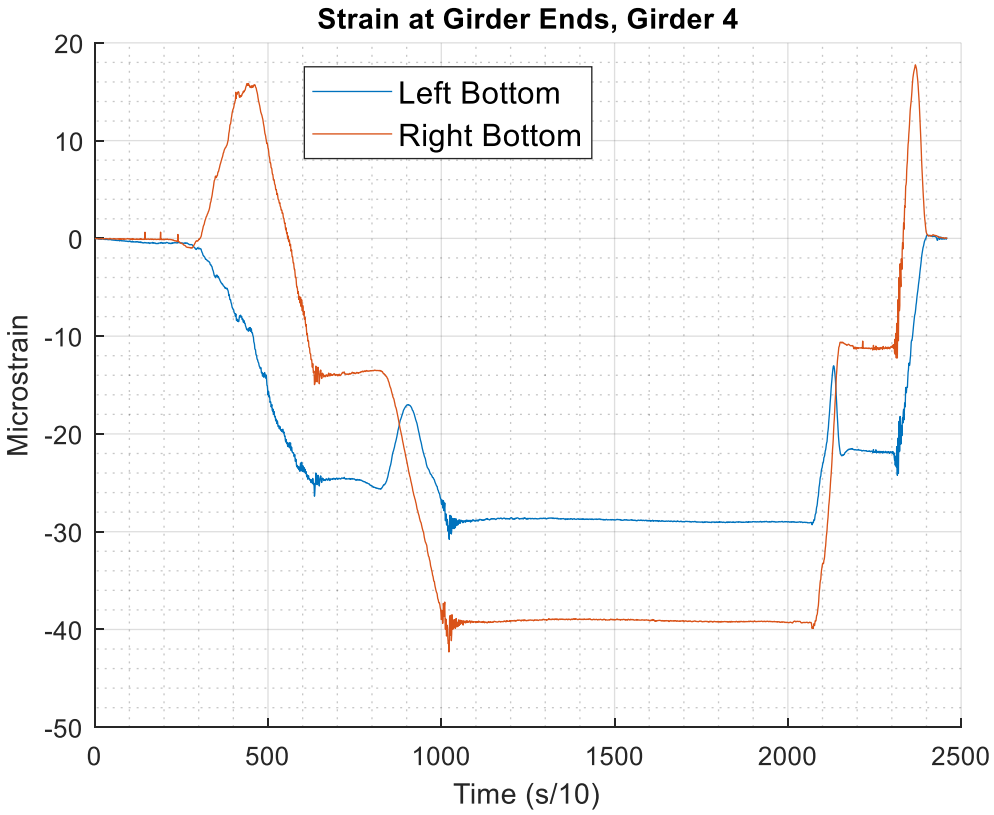
Strain at Girder Ends, Girder 4
Left Bottom
Right Bottom
Microstrain
Time (s/10)
20
10
0
-10
-20
-30
-40
-50
0
500
1000
1500
2000
2500

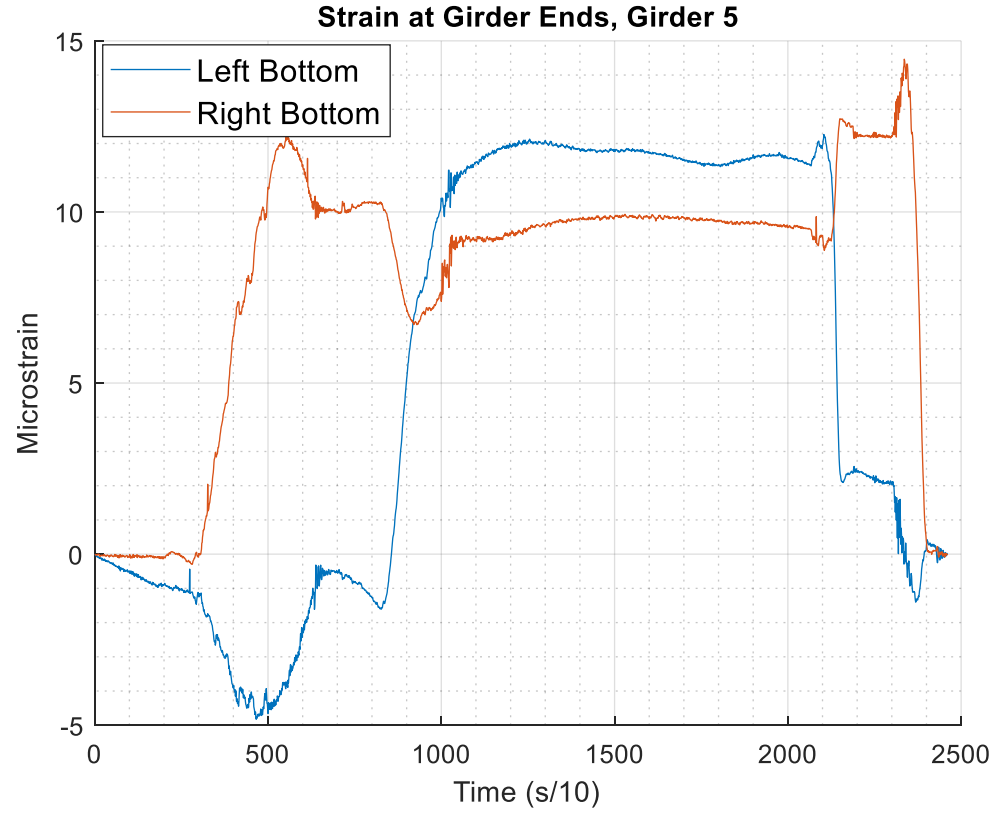
Strain at Girder Ends, Girder 5
Left Bottom
Right Bottom
Microstrain
Time (s/10)
15
10
5
0
-5
0
500
1000
1500
2000
2500

A.1.3.8 M25 Test

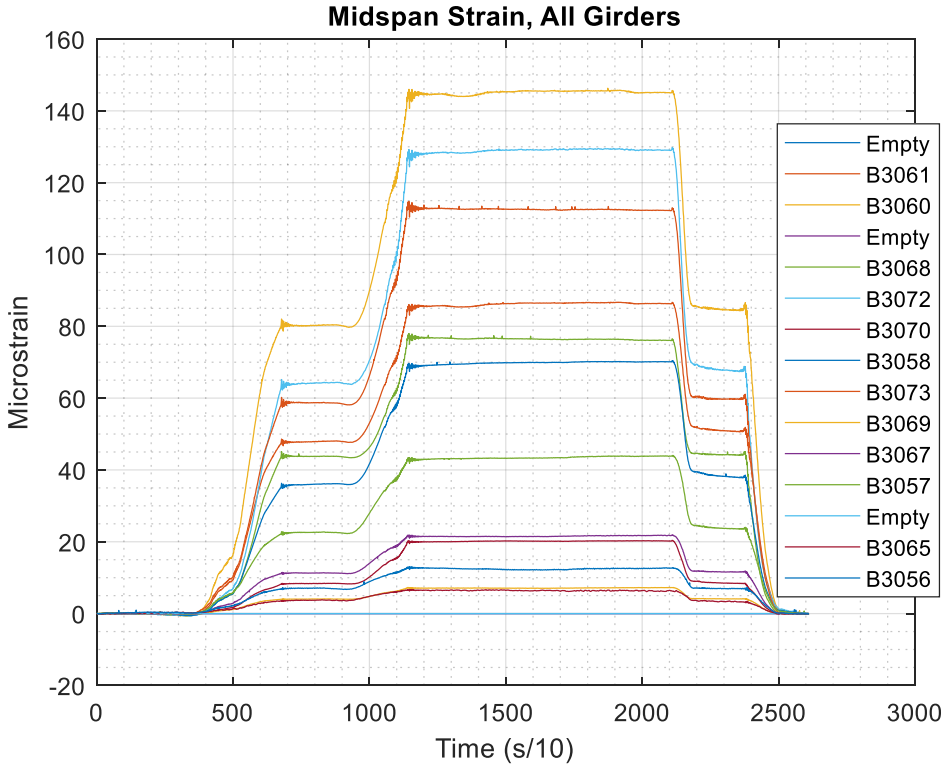


Strain at Girder Ends, Girder 2
Left Bottom
Right Bottom
Microstrain
Time (s/10)
40
20
0
-20
-40
-60
-80
-100
0
500
1000
1500
2000
2500
3000

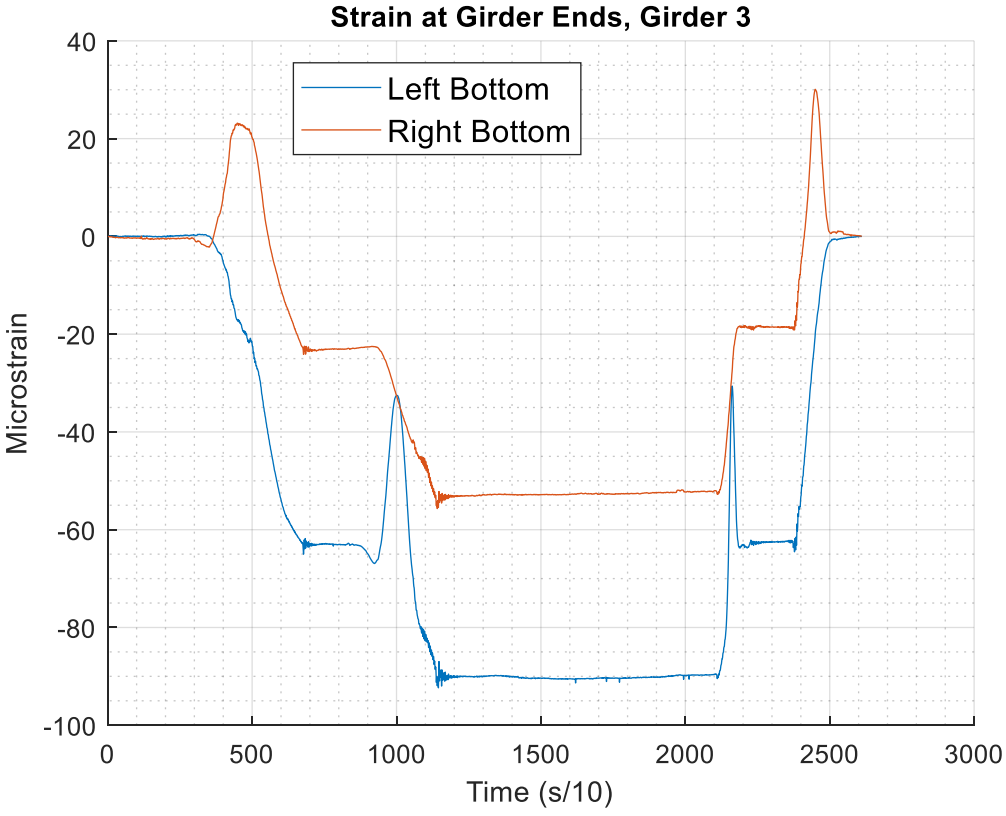
Strain at Girder Ends, Girder 3
Left Bottom
Right Bottom
Microstrain
Time (s/10)
40
20
0
-20
-40
-60
-80
-100
0
500
1000
1500
2000
2500
3000

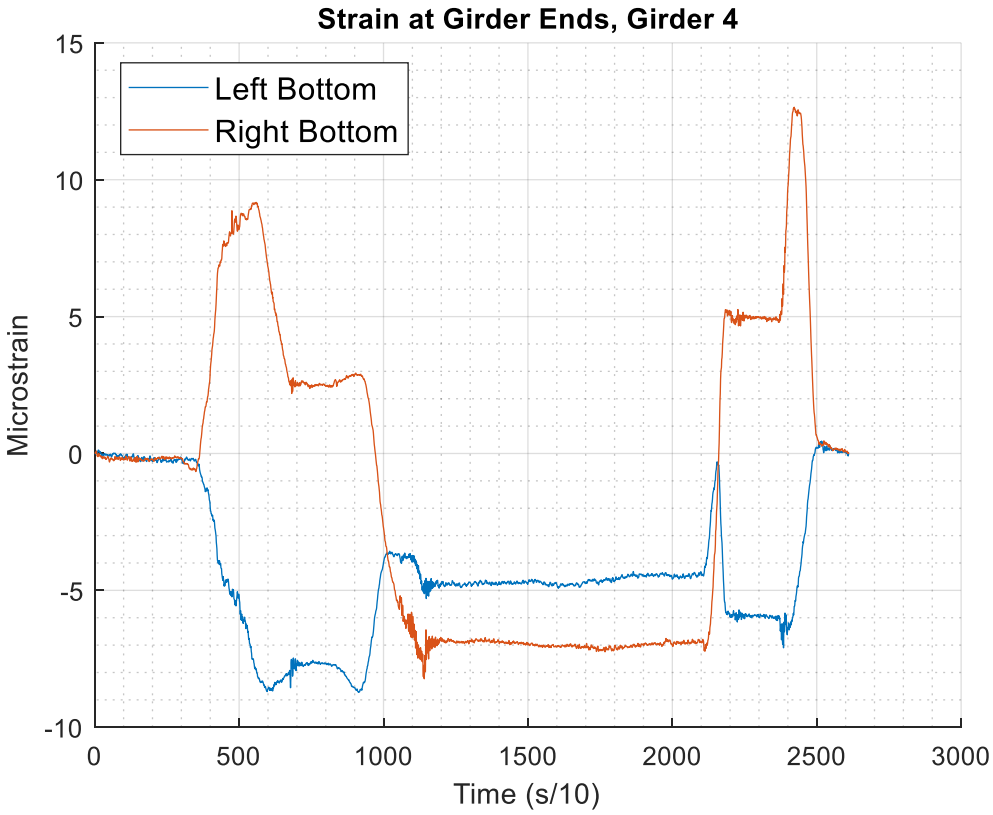
Strain at Girder Ends, Girder 4
Left Bottom
Right Bottom
Microstrain
Time (s/10)
15
10
5
0
-5
-10
0
500
1000
1500
2000
2500
3000


Strain at Girder Ends, Girder 5
Left Bottom
Right Bottom
Microstrain
Time (s/10)
16
14
12
10
8
6
4
2
0
-2
-4
0
500
1000
1500
2000
2500
3000

A.2 HGMB 2023

A.2.1 Instrumentation

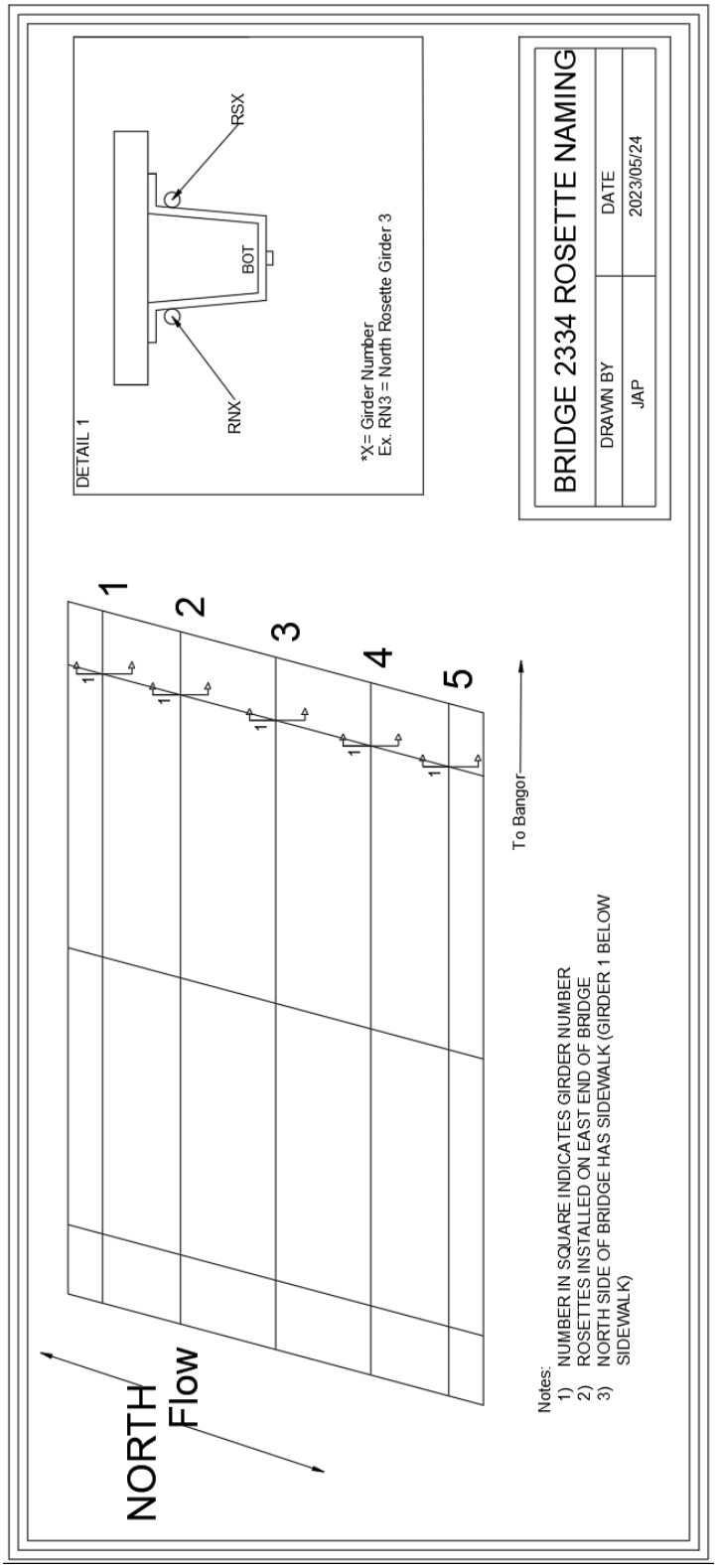

A.2.2 Loading

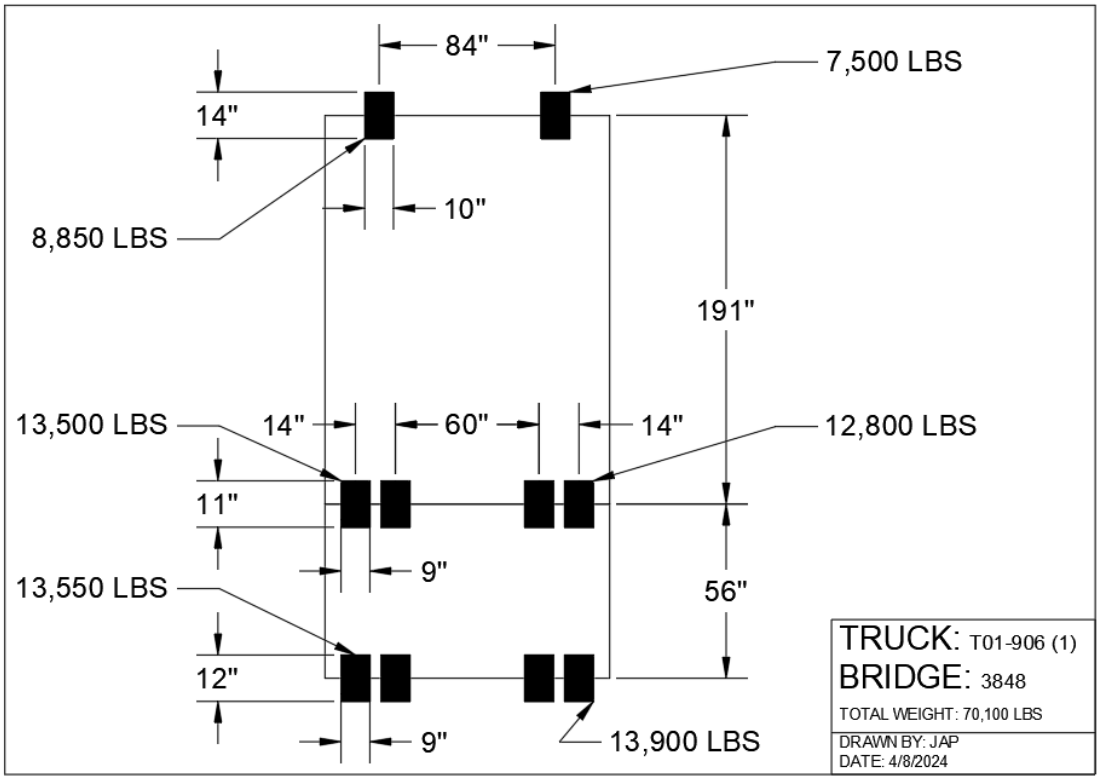
84"
7,500 LBS
14"
10"
8,850 LBS
191"
13,500 LBS
14"
60"
14"
12,800 LBS
11"
9"
13,550 LBS
56"
12"
9"
13,900 LBS
TRUCK: T01-906 (1)
BRIDGE: 3848
TOTAL WEIGHT: 70,100 LBS
DRAWN BY: JAP
DATE: 4/8/2024

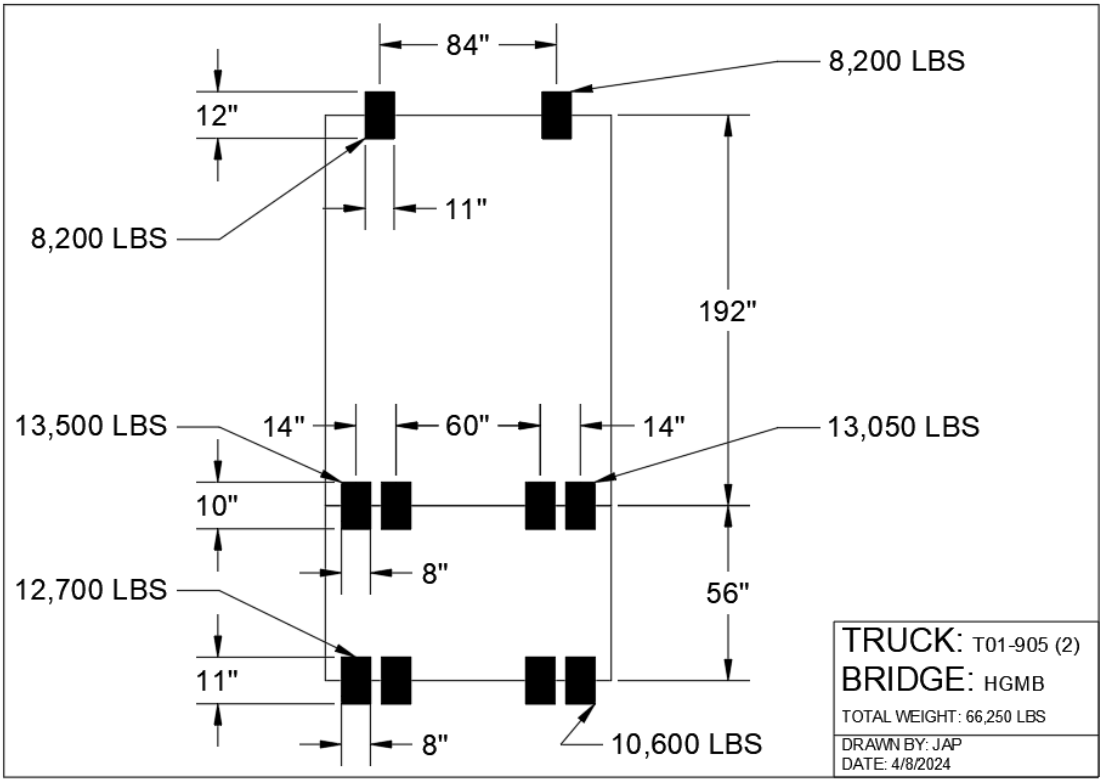
84"
8,200 LBS
12"
11"
8,200 LBS
192"
13,500 LBS
14"
60"
14"
13,050 LBS
10"
8"
12,700 LBS
56"
11"
8"
10,600 LBS
TRUCK: T01-905 (2)
BRIDGE: HGMB
TOTAL WEIGHT: 66,250 LBS
DRAWN BY: JAP
DATE: 4/8/2024

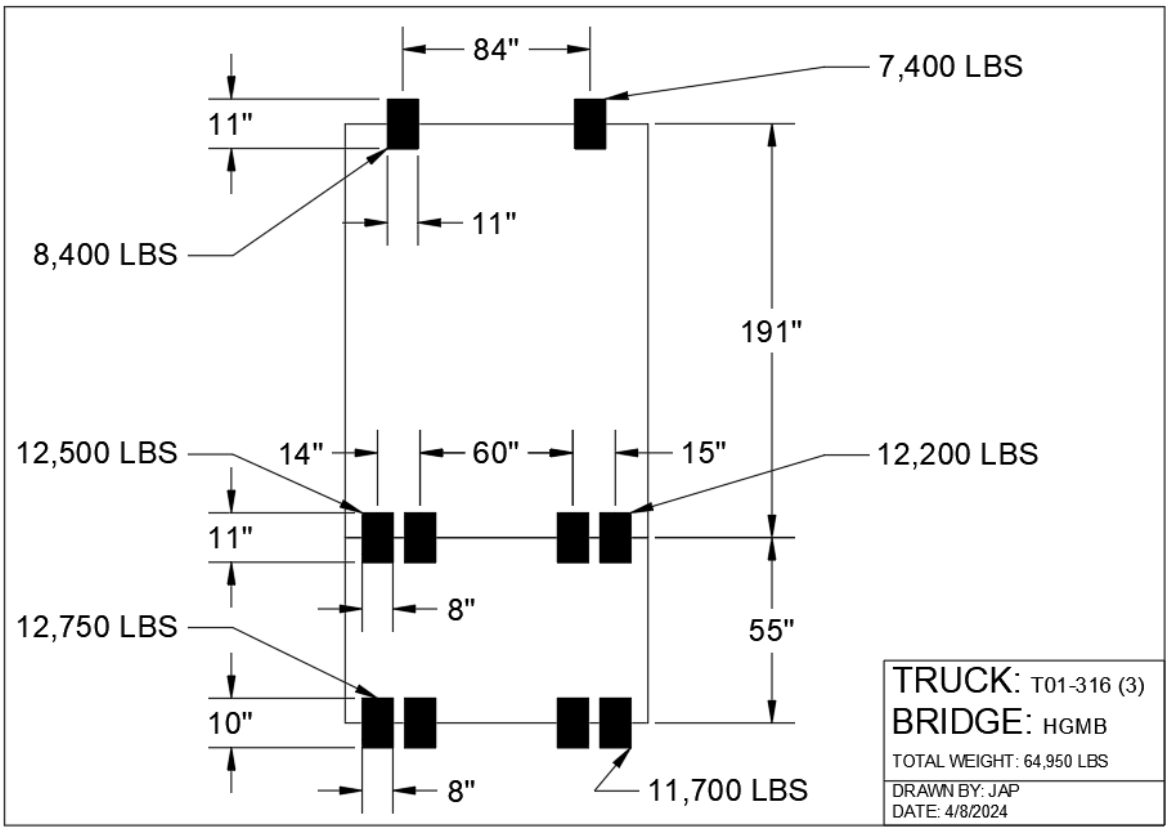
84"
7,400 LBS
11"
11"
8,400 LBS
191"
12,500 LBS
14"
60"
15"
12,200 LBS
11"
8"
12,750 LBS
55"
10"
8"
11,700 LBS
TRUCK: T01-316 (3)
BRIDGE: HGMB
TOTAL WEIGHT: 64,950 LBS
DRAWN BY: JAP
DATE: 4/8/2024

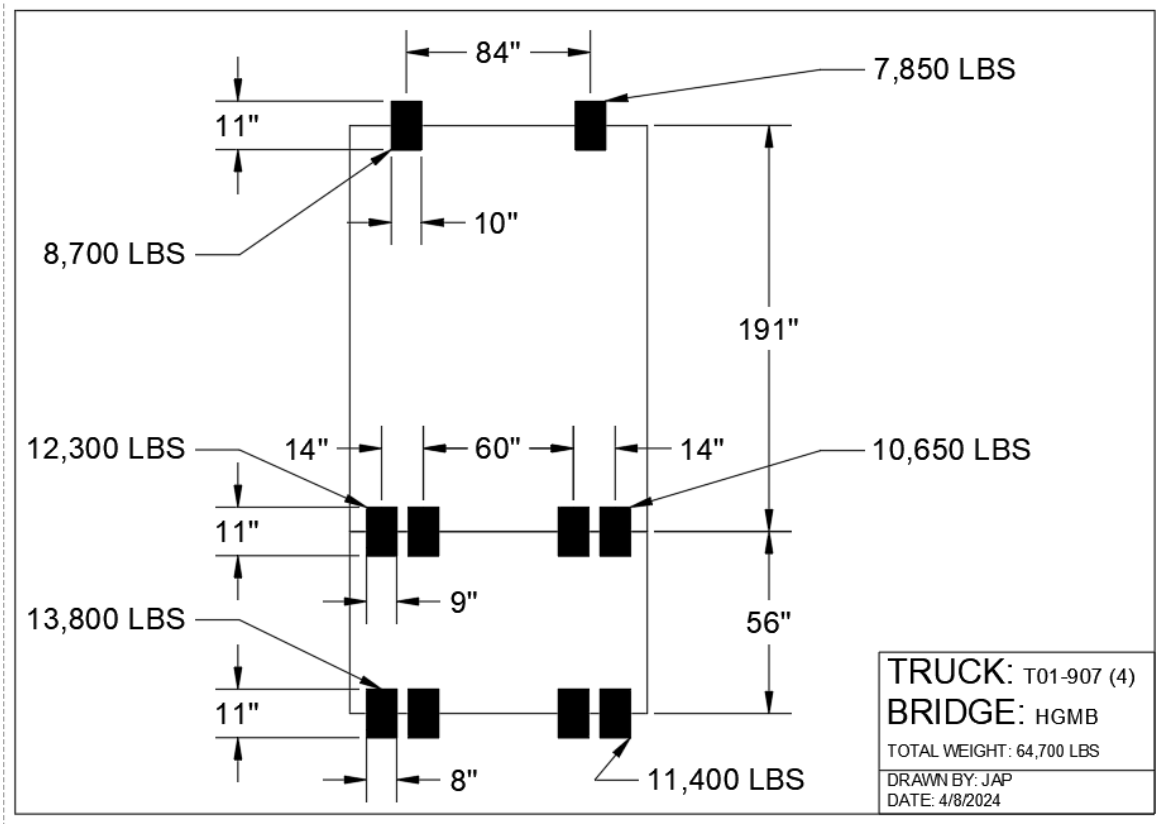
84"
7,850 LBS
11"
10"
8,700 LBS
191"
12,300 LBS
14"
60"
14"
10,650 LBS
11"
9"
13,800 LBS
56"
11"
8"
11,400 LBS
TRUCK: T01-907 (4)
BRIDGE: HGMB
TOTAL WEIGHT: 64,700 LBS
DRAWN BY: JAP
DATE: 4/8/2024

A.2.3 Representative Data Plots

A.2.3.1 V41 Test

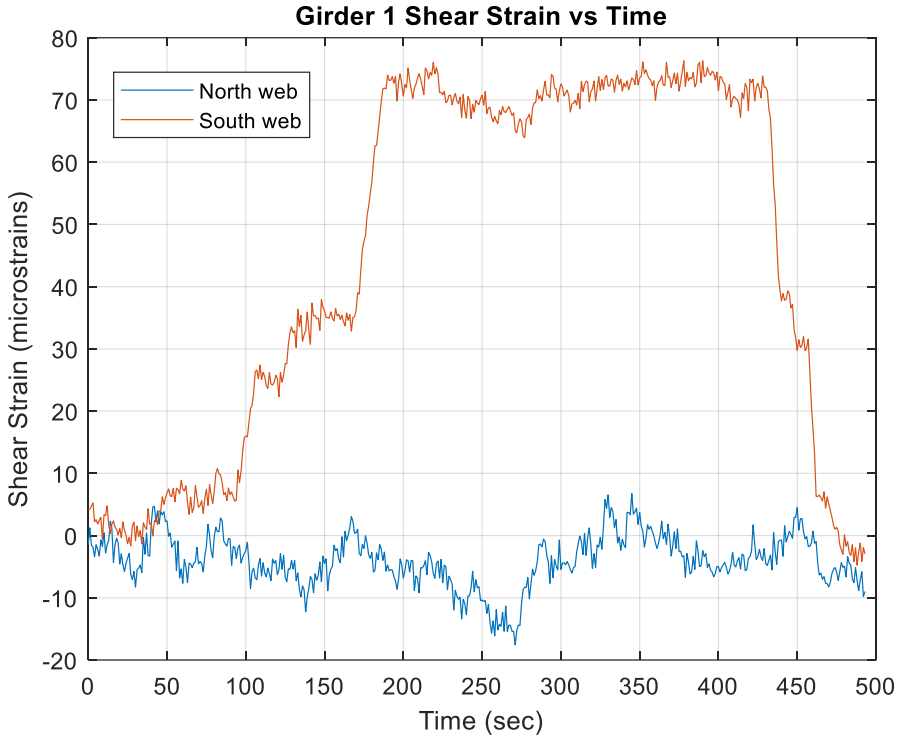

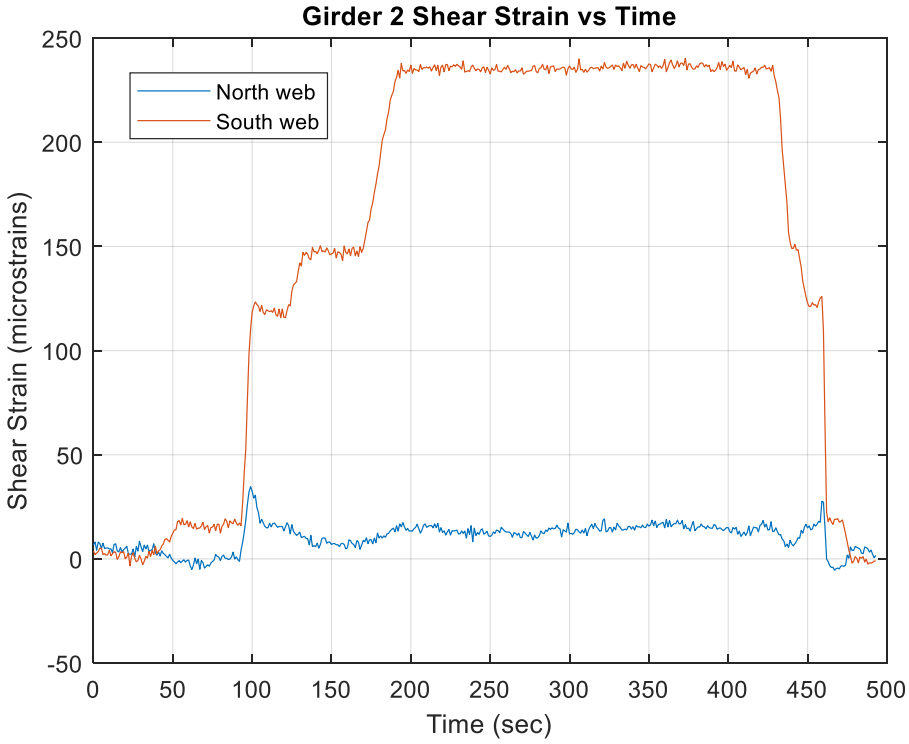

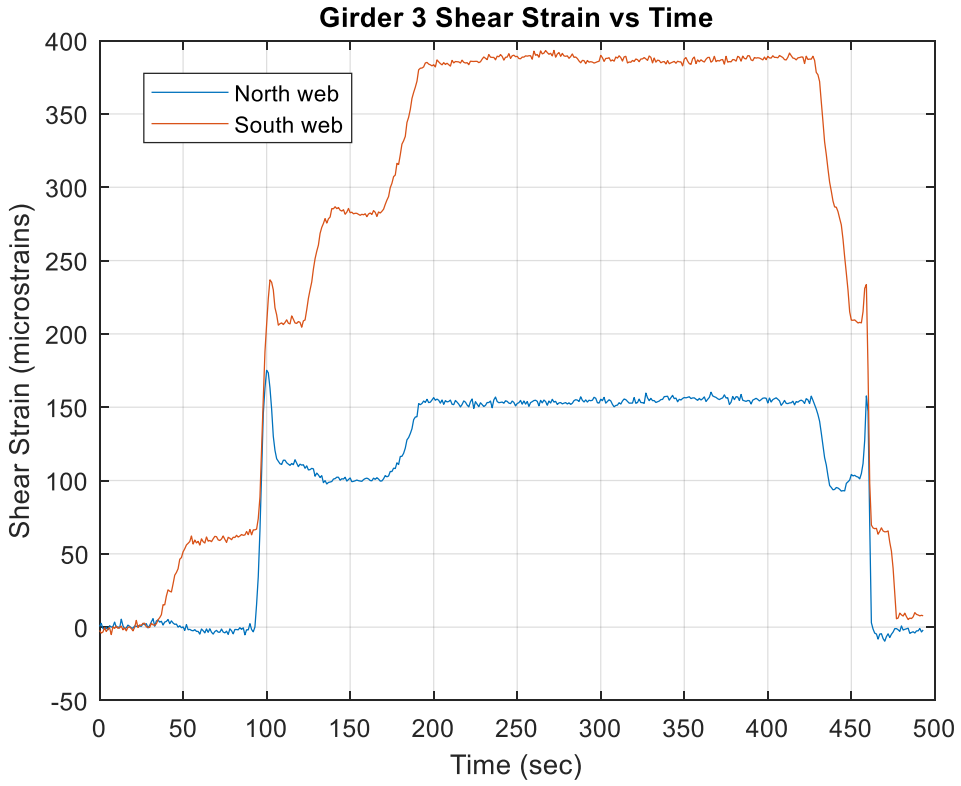
Girder 3 Shear Strain vs Time
North web
South web
Shear Strain (microstrains)
Time (sec)
400
350
300
250
200
150
100
50
0
-50
0
50
100
150
200
250
300
350
400
450
500

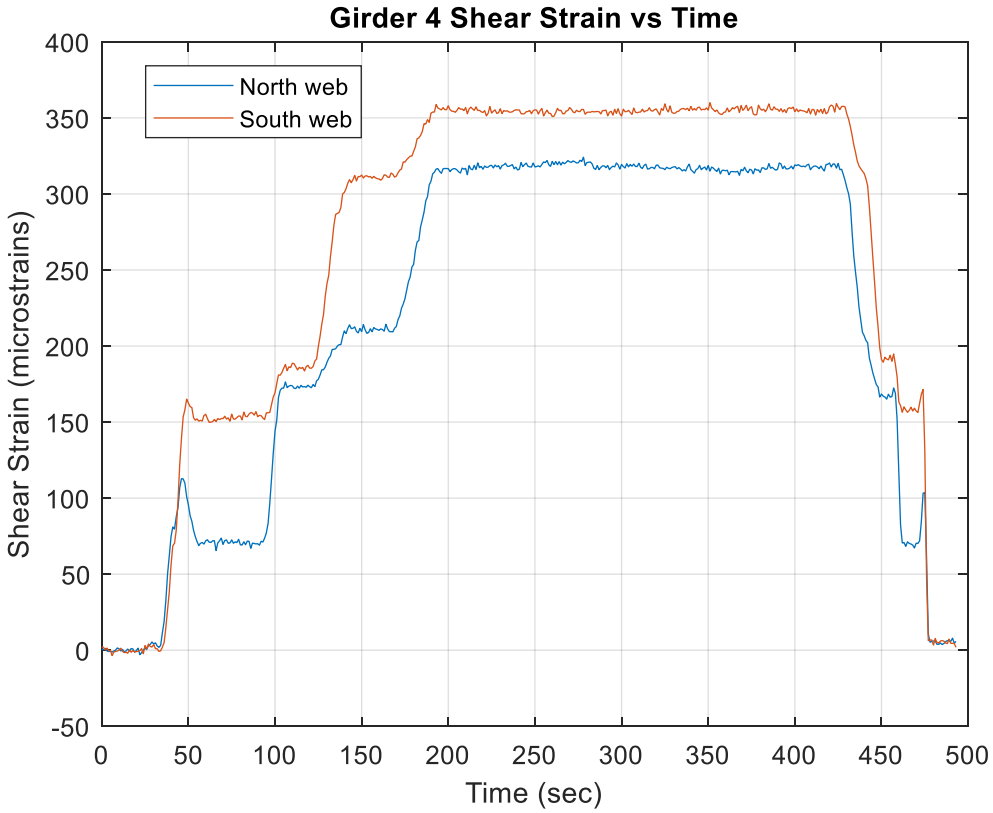
Girder 4 Shear Strain vs Time
North web
South web
Shear Strain (microstrains)
Time (sec)
400
350
300
250
200
150
100
50
0
-50
0
50
100
150
200
250
300
350
400
450
500

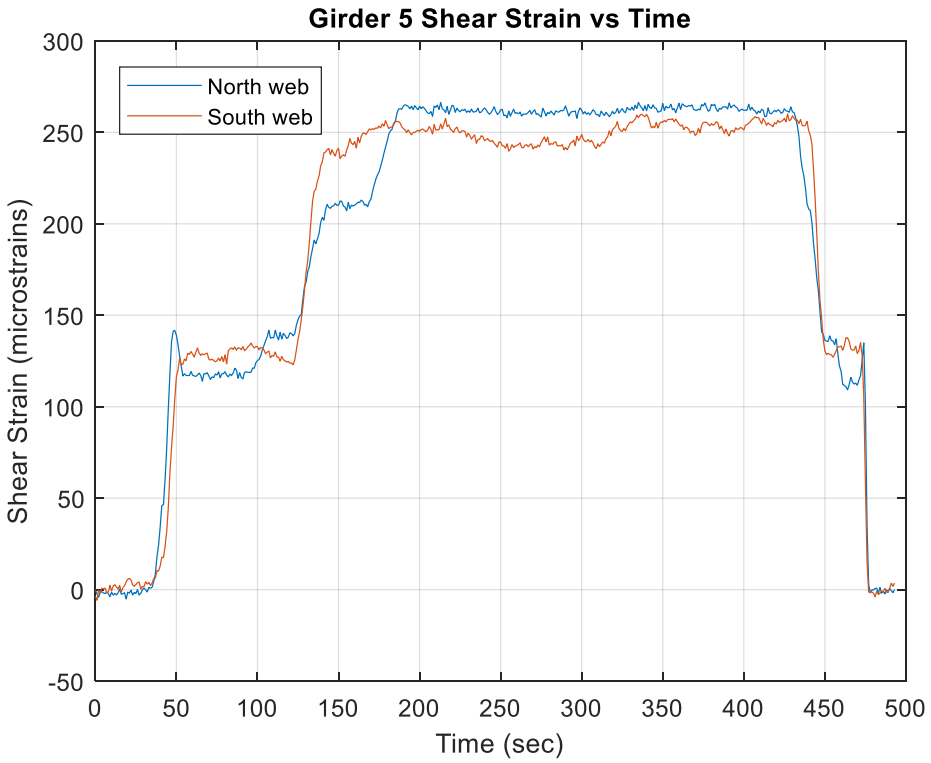

A.2.3.2 V42 Test

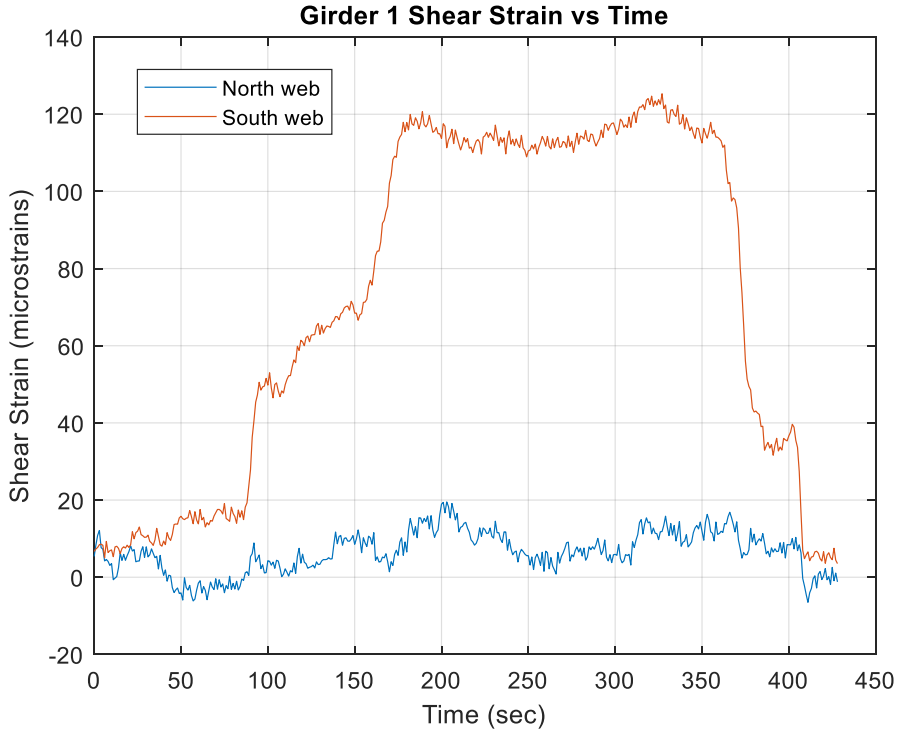

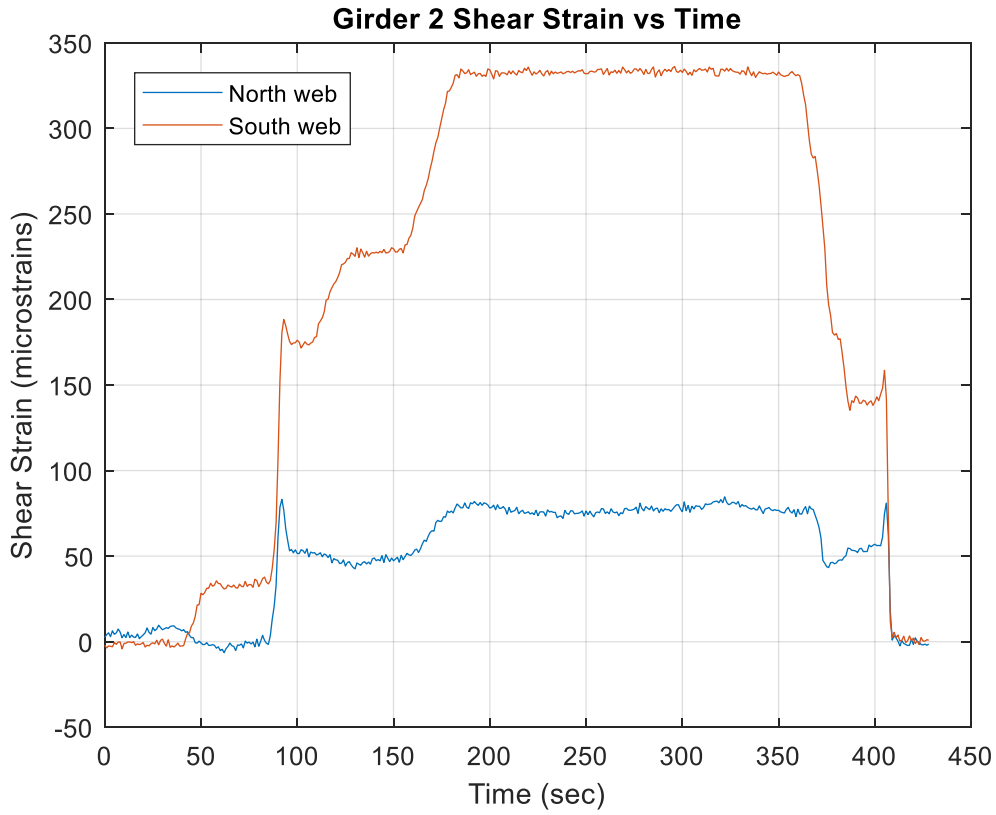
Girder 2 Shear Strain vs Time
North web
South web
Shear Strain (microstrains)
Time (sec)
350
300
250
200
150
100
50
0
-50
0
50
100
150
200
250
300
350
400
450

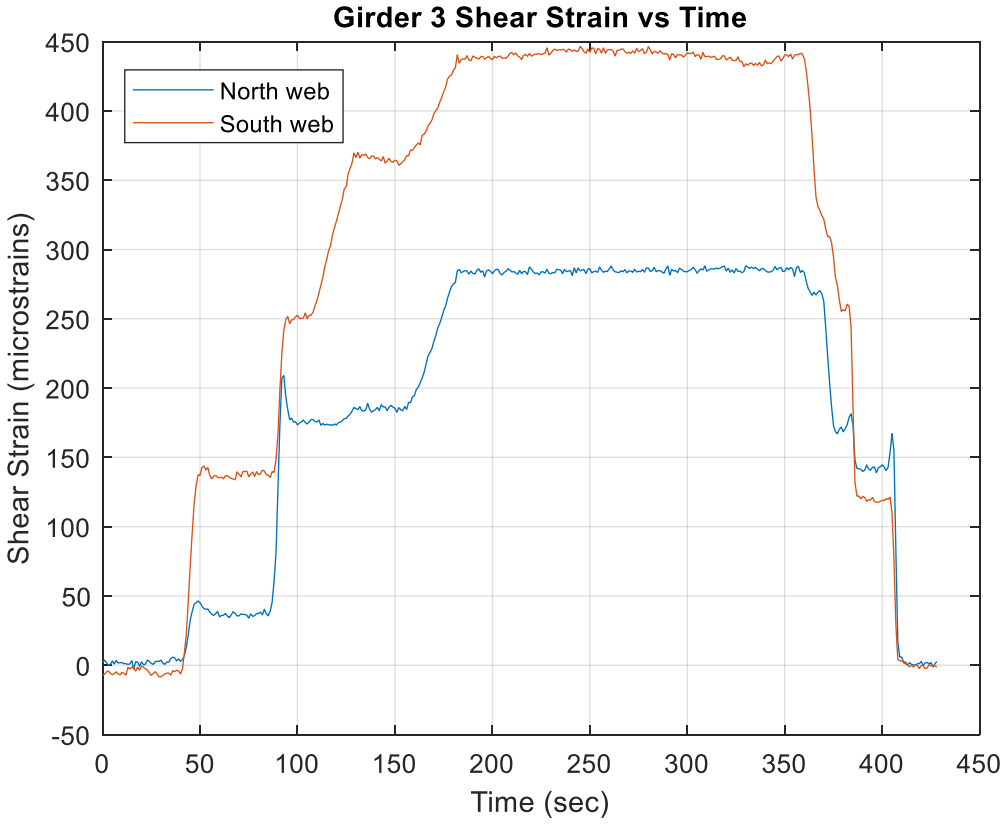
Girder 3 Shear Strain vs Time
North web
South web
Shear Strain (microstrains)
Time (sec)
450
400
350
300
250
200
150
100
50
0
-50
0
50
100
150
200
250
300
350
400
450

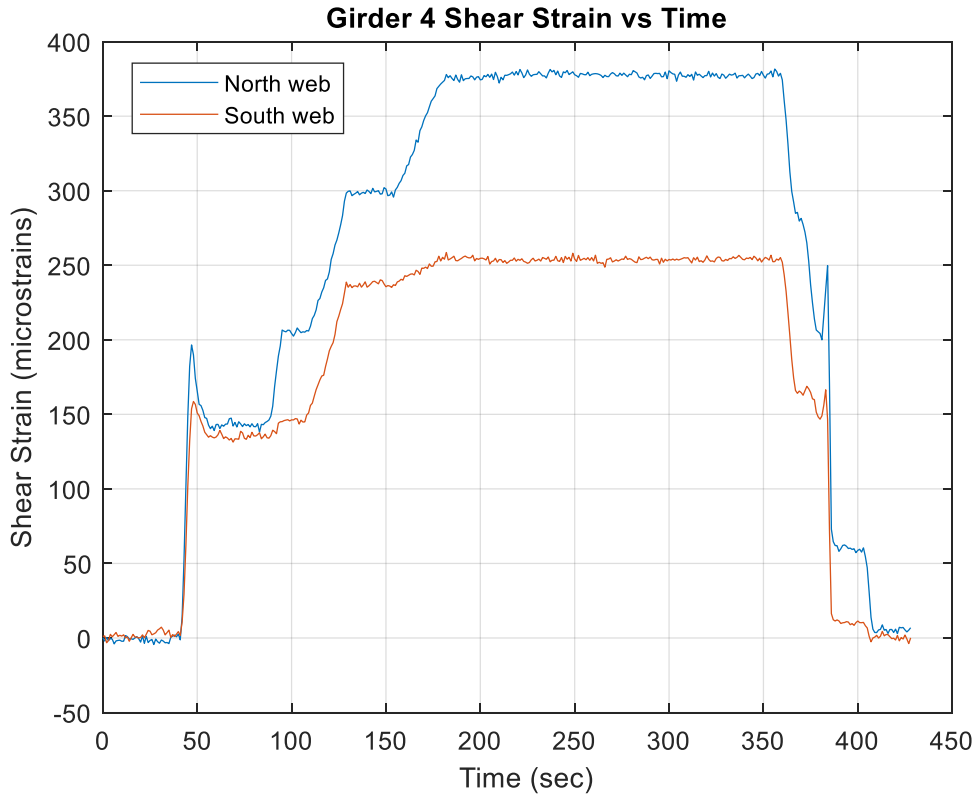
Girder 4 Shear Strain vs Time
North web
South web
Shear Strain (microstrains)
Time (sec)
400
350
300
250
200
150
100
50
0
-50
0
50
100
150
200
250
300
350
400
450

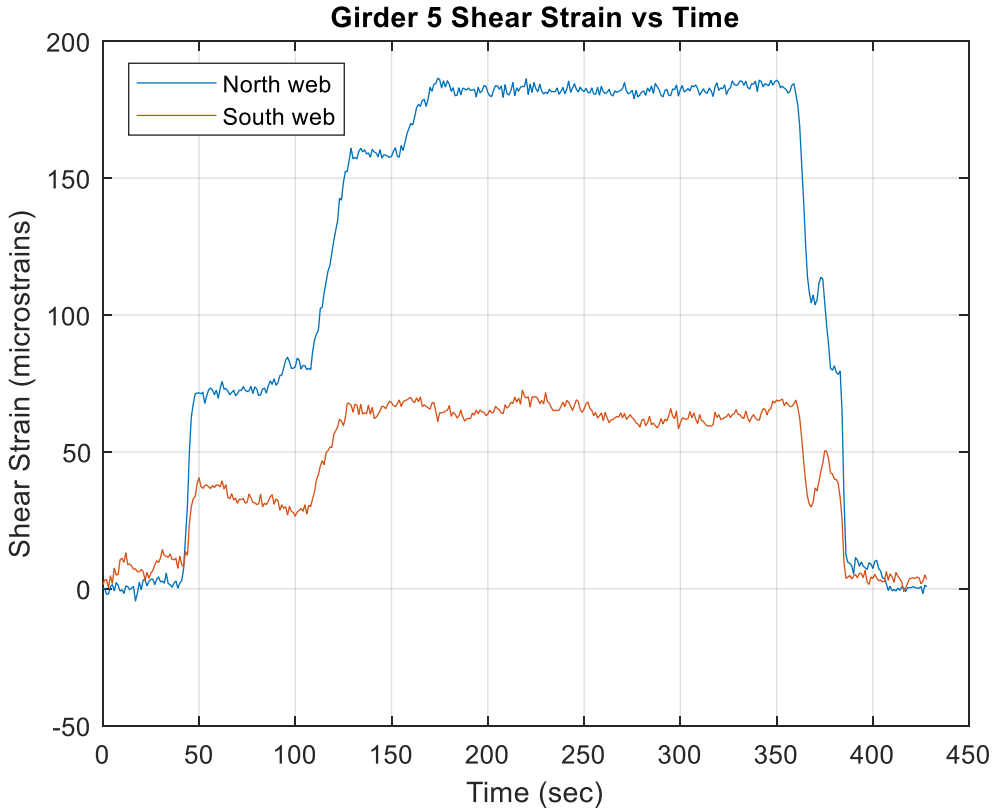
Girder 5 Shear Strain vs Time
North web
South web
Shear Strain (microstrains)
Time (sec)
200
150
100
50
0
-50
0
50
100
150
200
250
300
350
400
450

A.2.3.3 V43 Test

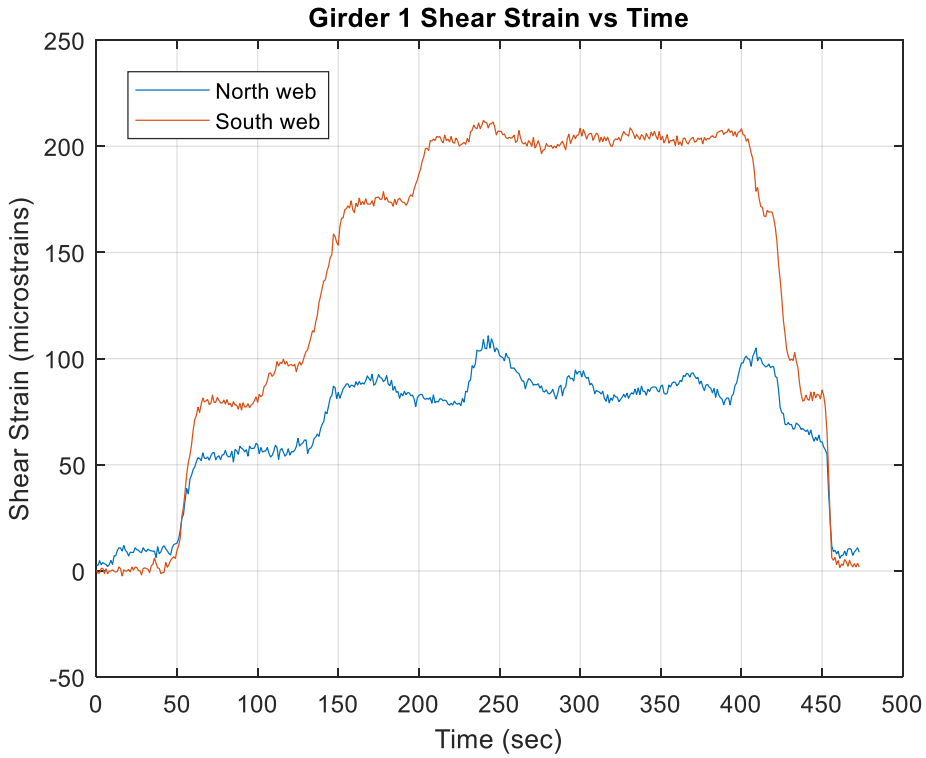

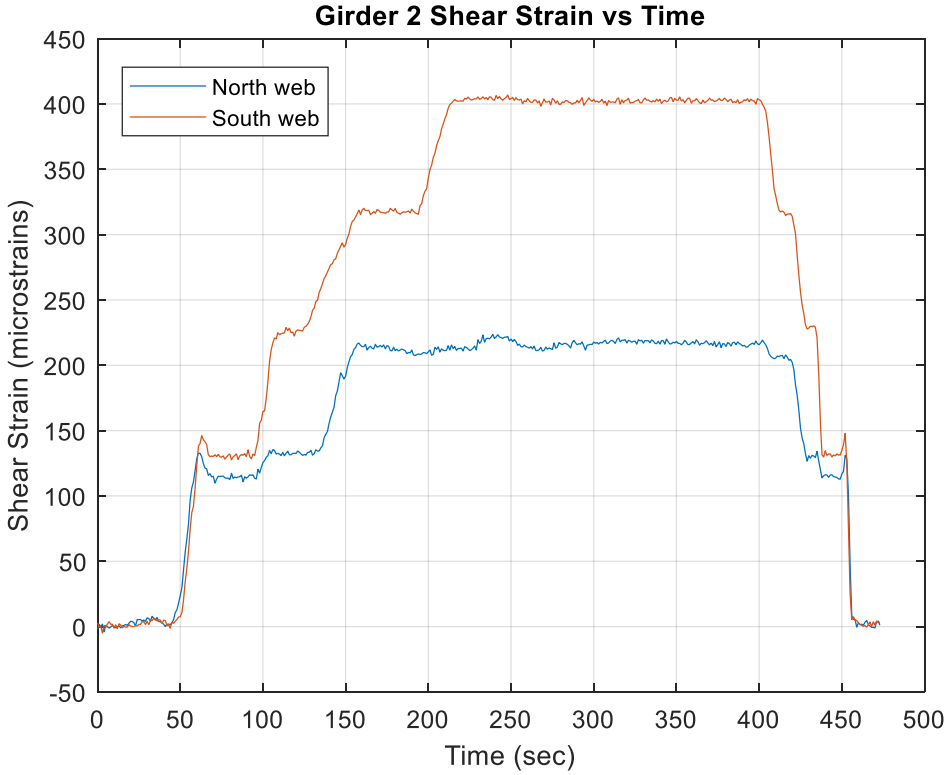

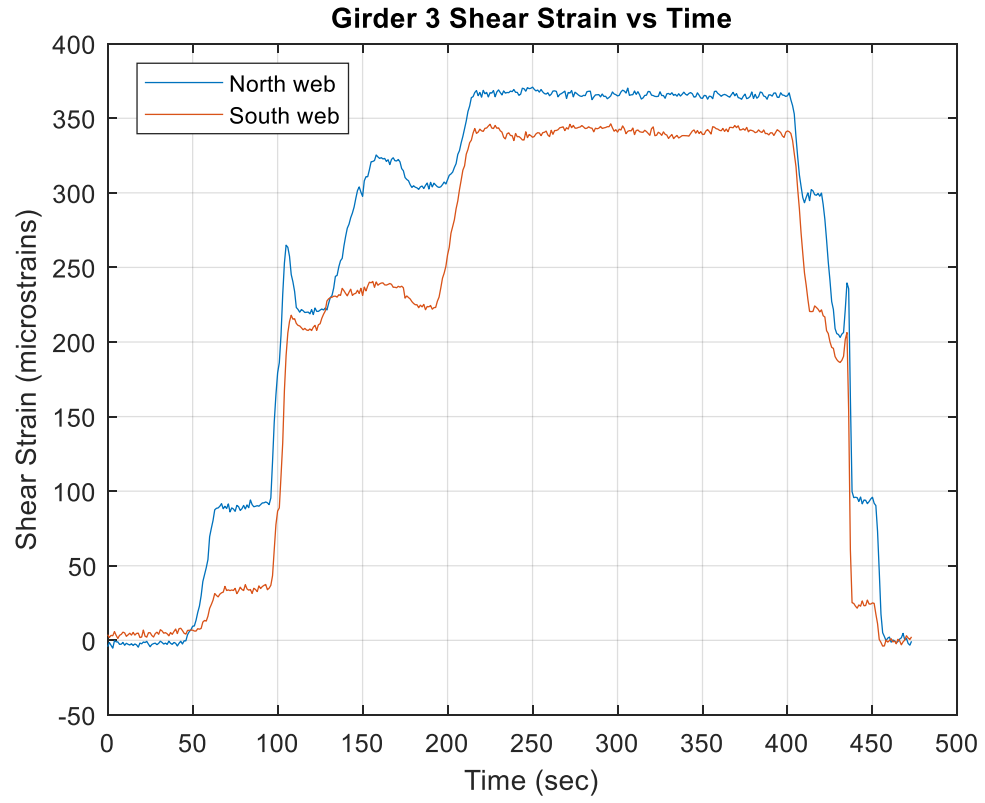
Girder 3 Shear Strain vs Time
North web
South web
Shear Strain (microstrains)
Time (sec)
400
350
300
250
200
150
100
50
0
-50
0
50
100
150
200
250
300
350
400
450
500

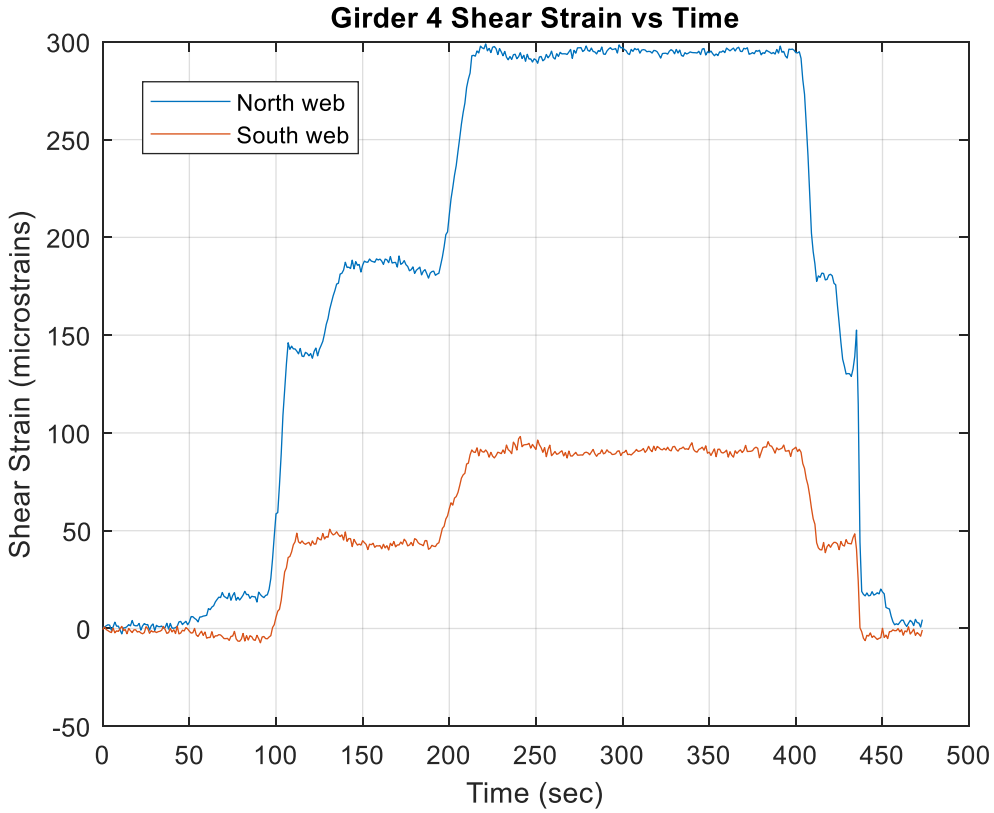
Girder 4 Shear Strain vs Time
North web
South web
Shear Strain (microstrains)
Time (sec)
300
250
200
150
100
50
0
-50
0
50
100
150
200
250
300
350
400
450
500

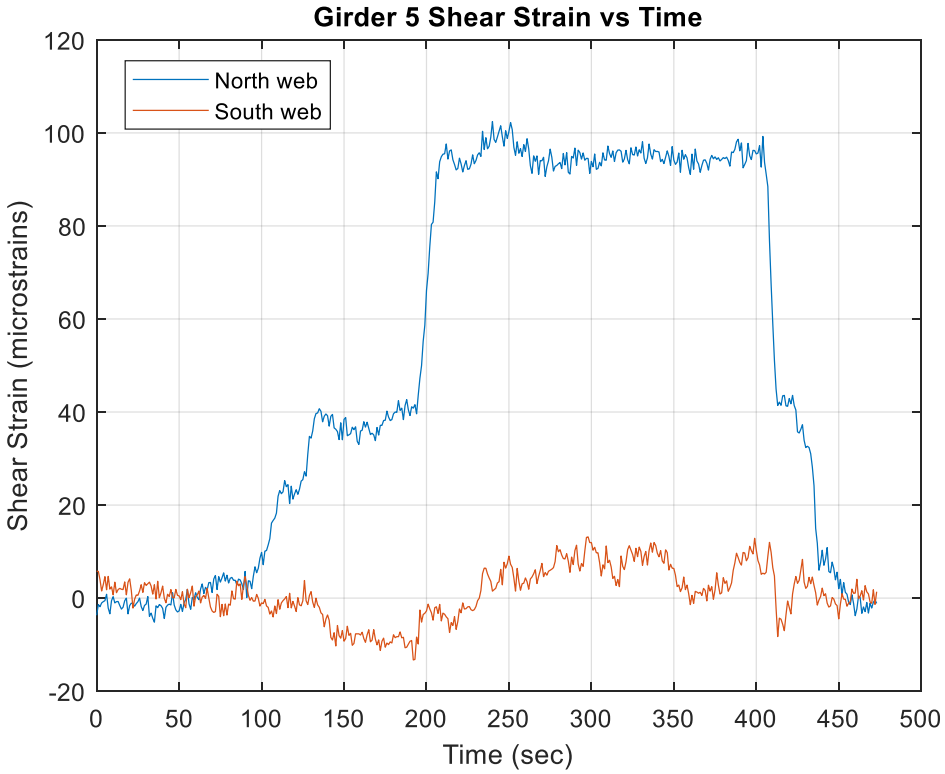

A.2.3.4 V21 Test

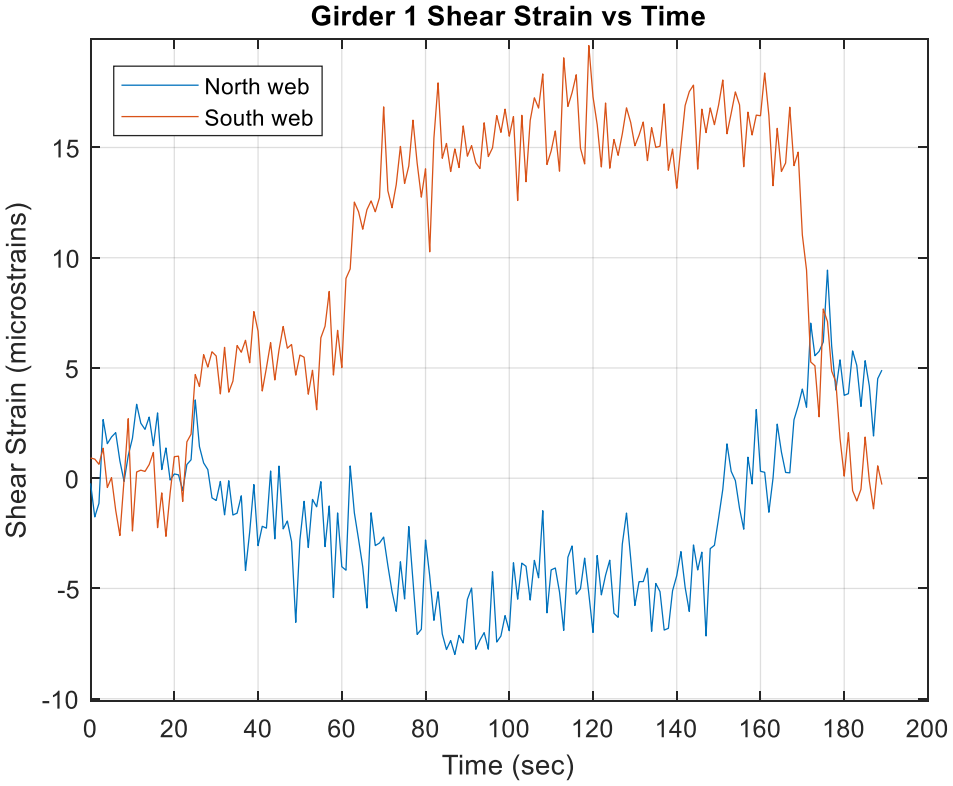

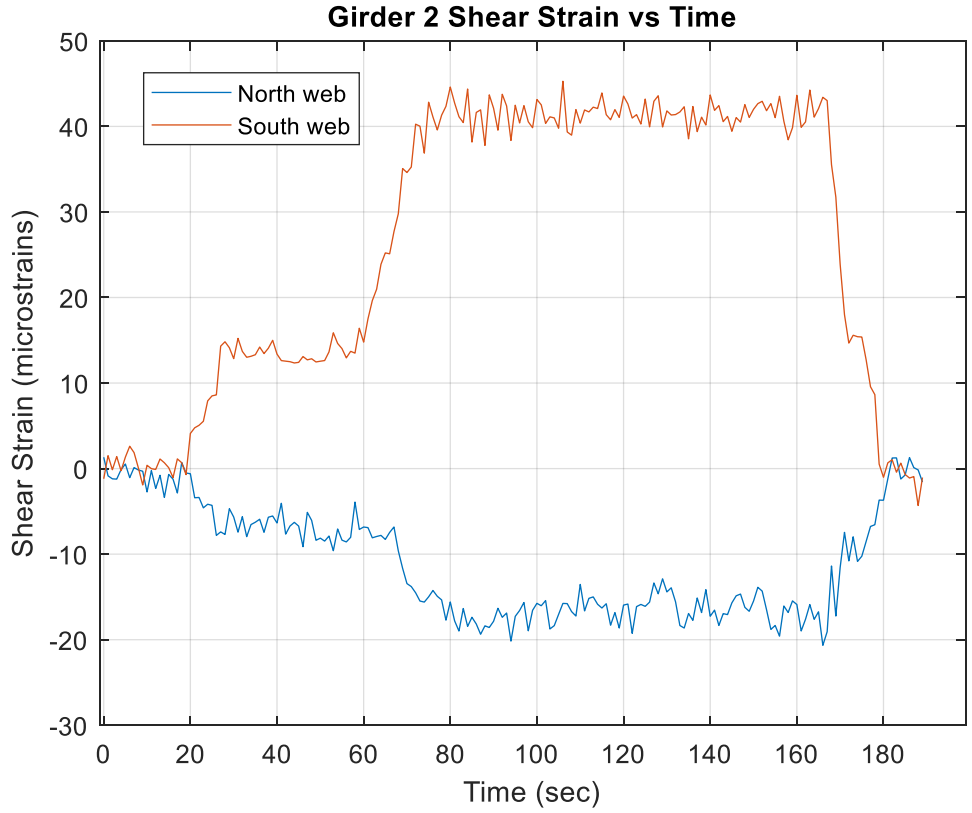
Girder 2 Shear Strain vs Time
North web
South web
Shear Strain (microstrains)
Time (sec)
50
40
30
20
10
0
-10
-20
-30
0
20
40
60
80
100
120
140
160
180

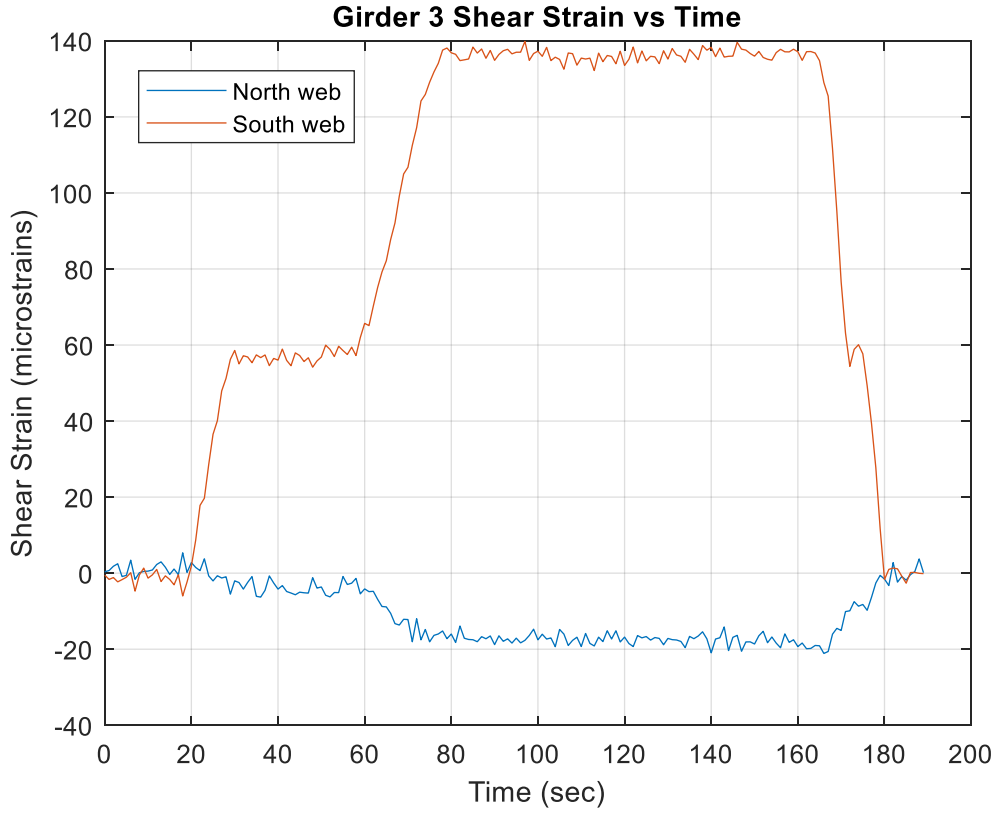
Girder 3 Shear Strain vs Time
North web
South web
Shear Strain (microstrains)
Time (sec)
140
120
100
80
60
40
20
0
-20
-40
0
20
40
60
80
100
120
140
160
180
200

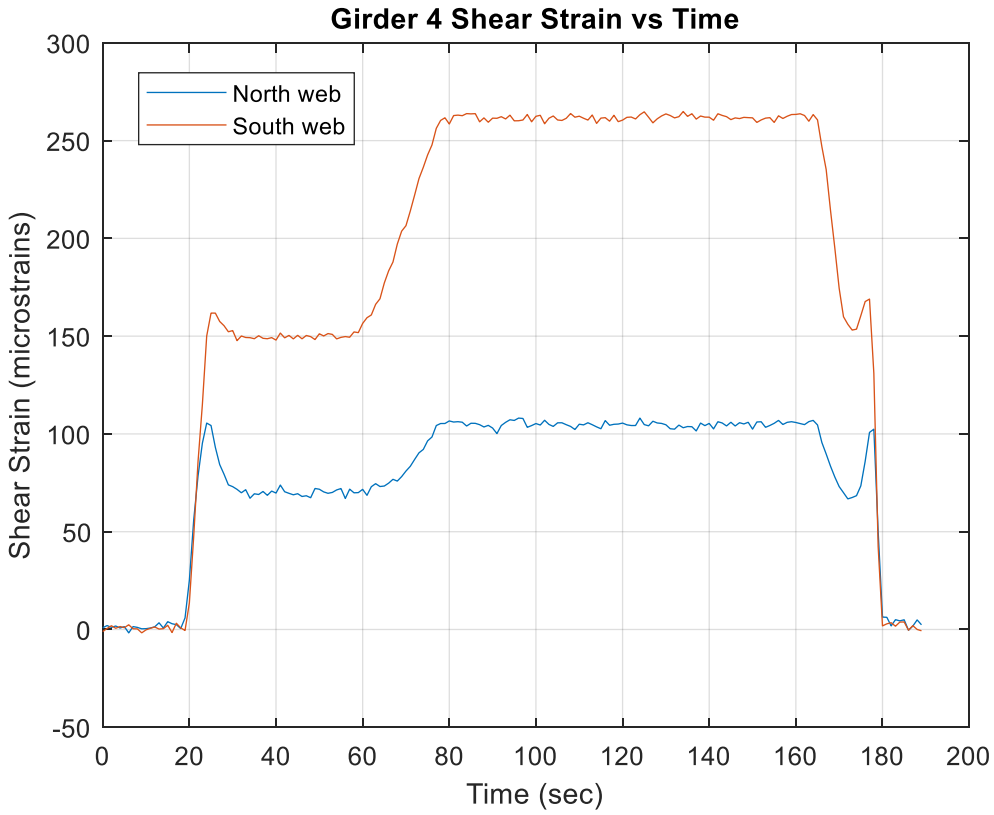
Girder 4 Shear Strain vs Time
North web
South web
Shear Strain (microstrains)
Time (sec)
300
250
200
150
100
50
0
-50
0
20
40
60
80
100
120
140
160
180
200

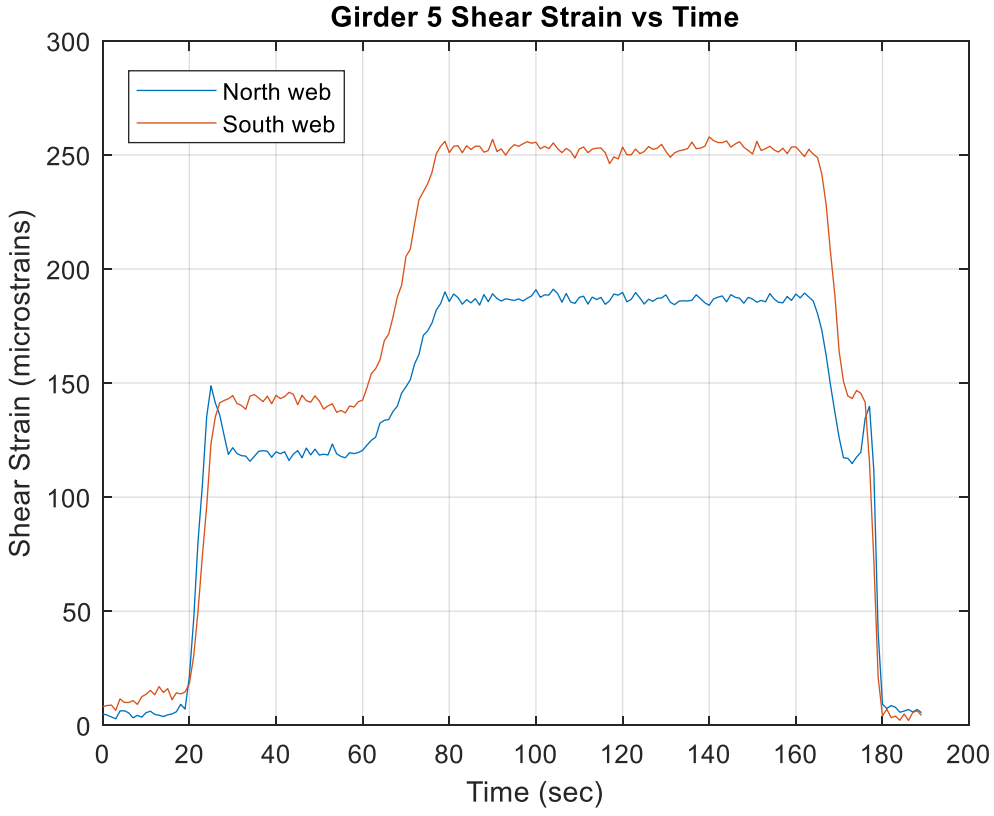
Girder 5 Shear Strain vs Time
North web
South web
Shear Strain (microstrains)
Time (sec)
300
250
200
150
100
50
0
0
20
40
60
80
100
120
140
160
180
200

A.2.3.5 V22 Test

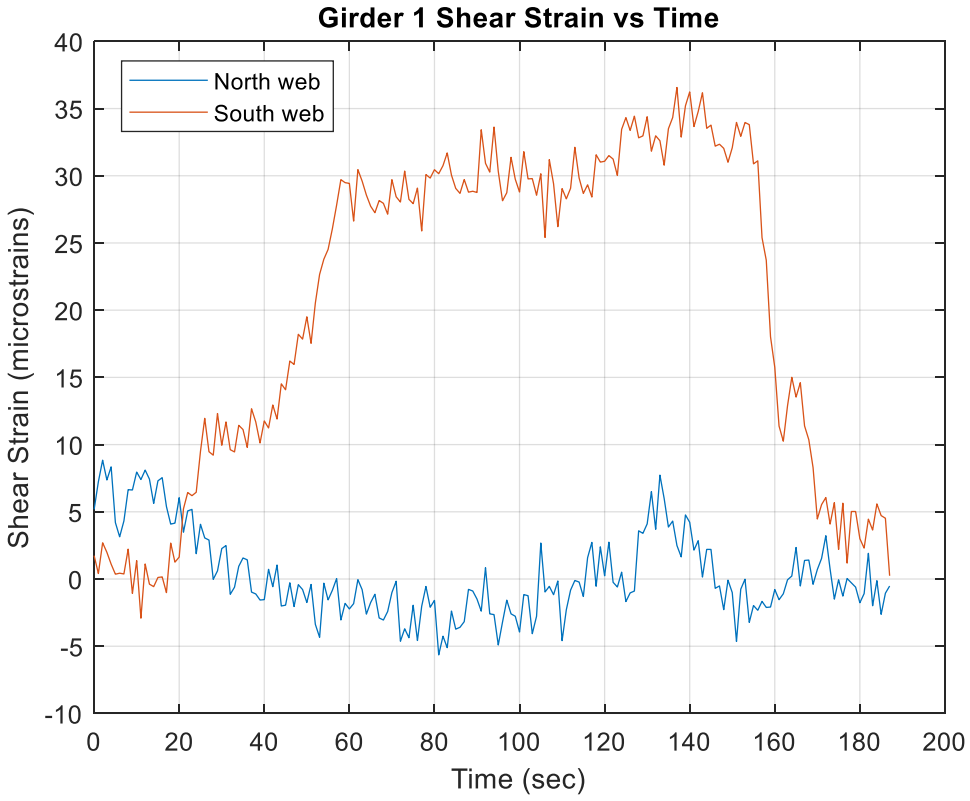

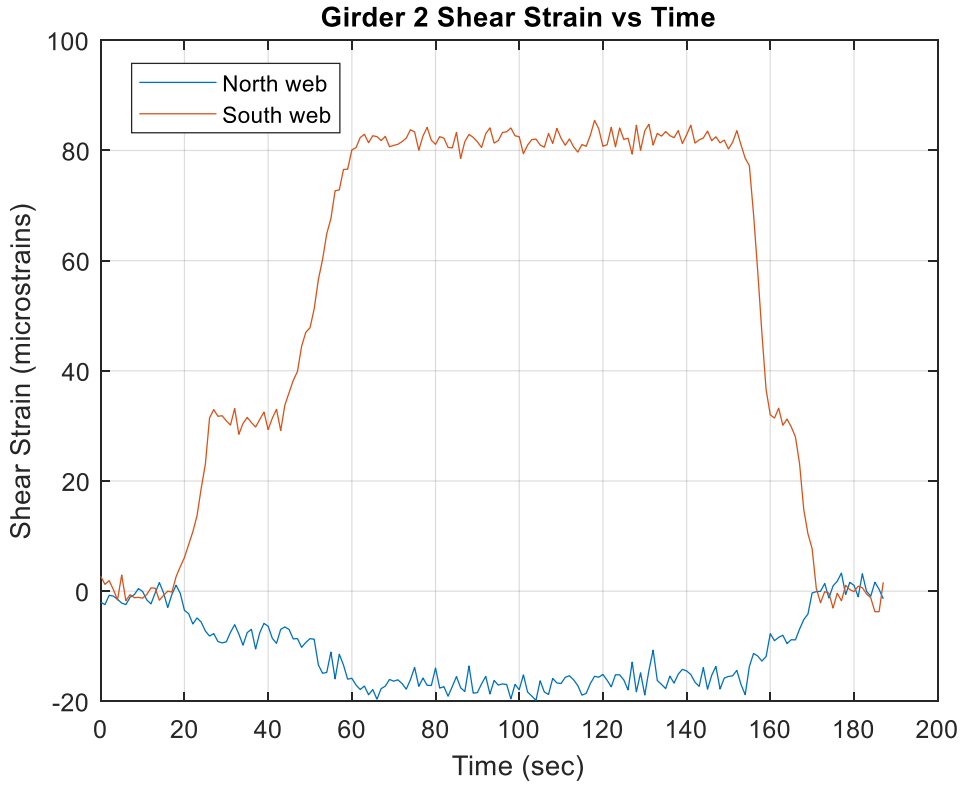

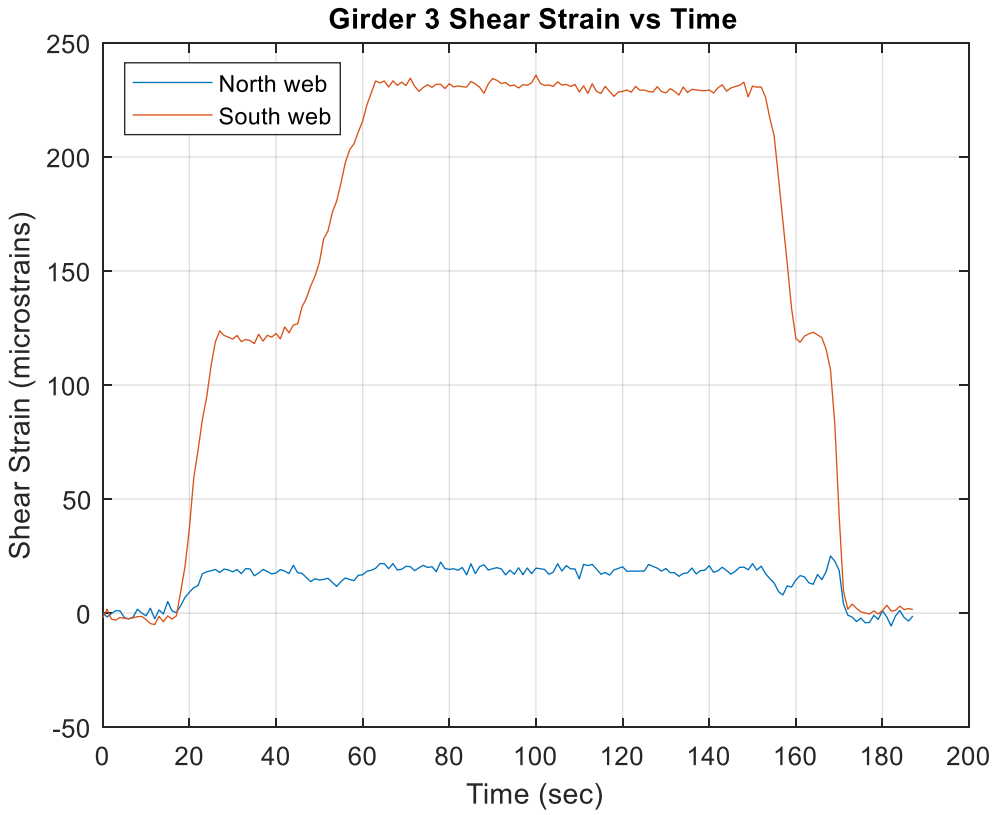
Girder 3 Shear Strain vs Time
North web
South web
Shear Strain (microstrains)
Time (sec)
250
200
150
100
50
0
-50
0
20
40
60
80
100
120
140
160
180
200

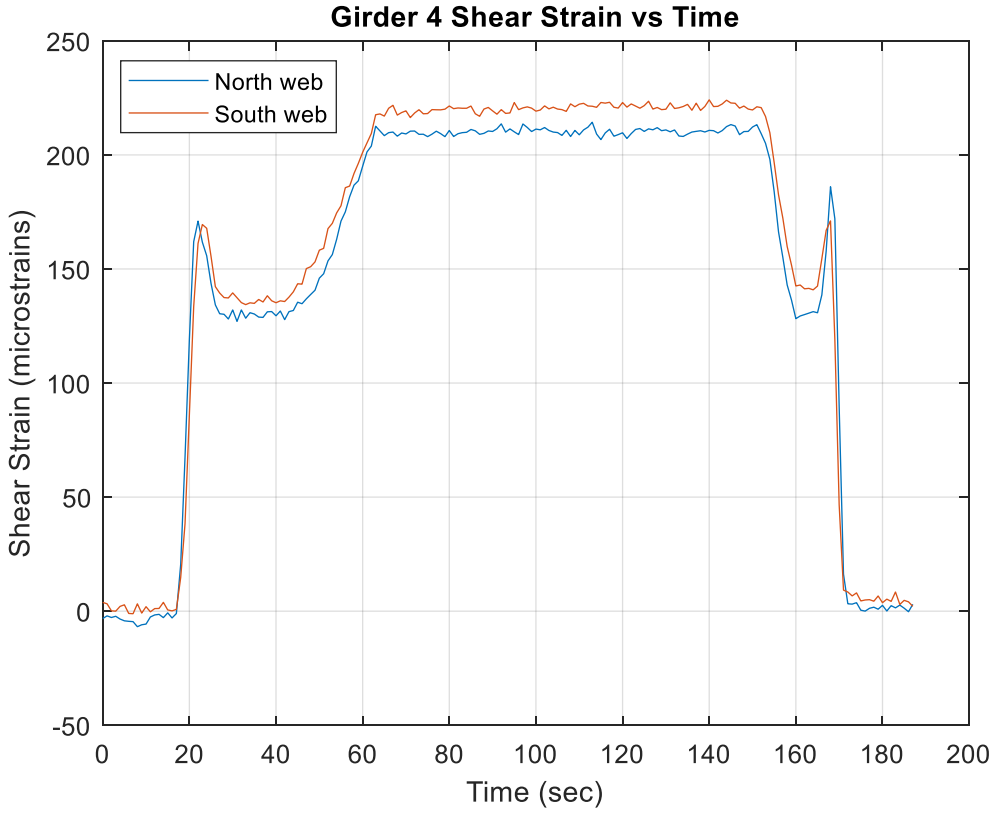
Girder 4 Shear Strain vs Time
North web
South web
Shear Strain (microstrains)
Time (sec)
250
200
150
100
50
0
-50
0
20
40
60
80
100
120
140
160
180
200

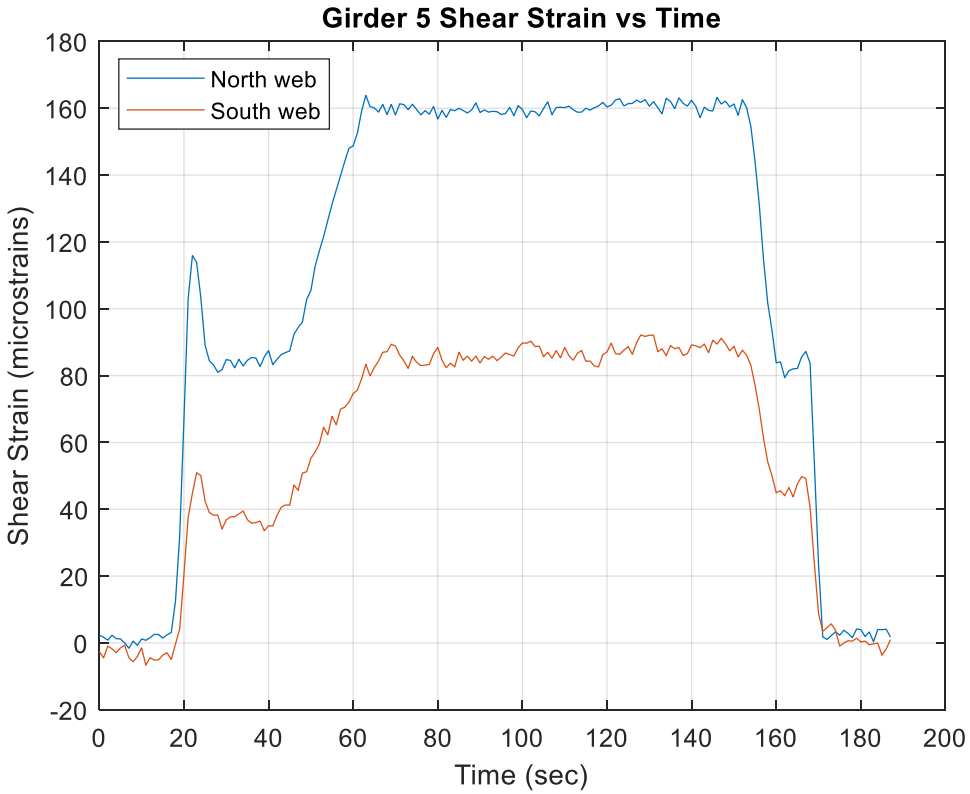

A.2.3.6 V23 Test

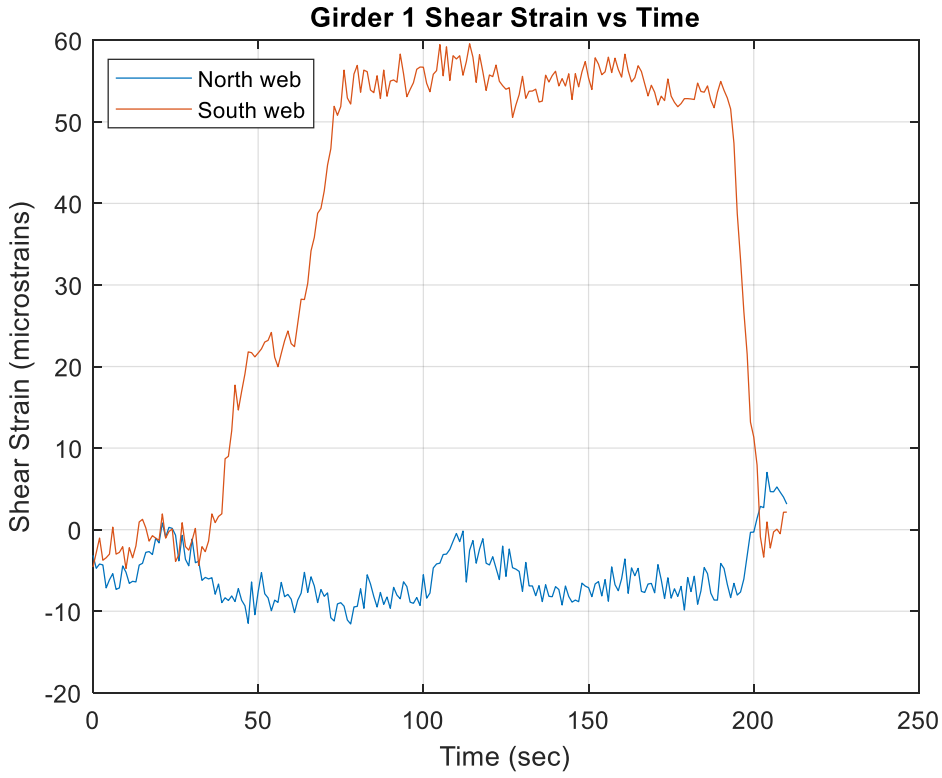

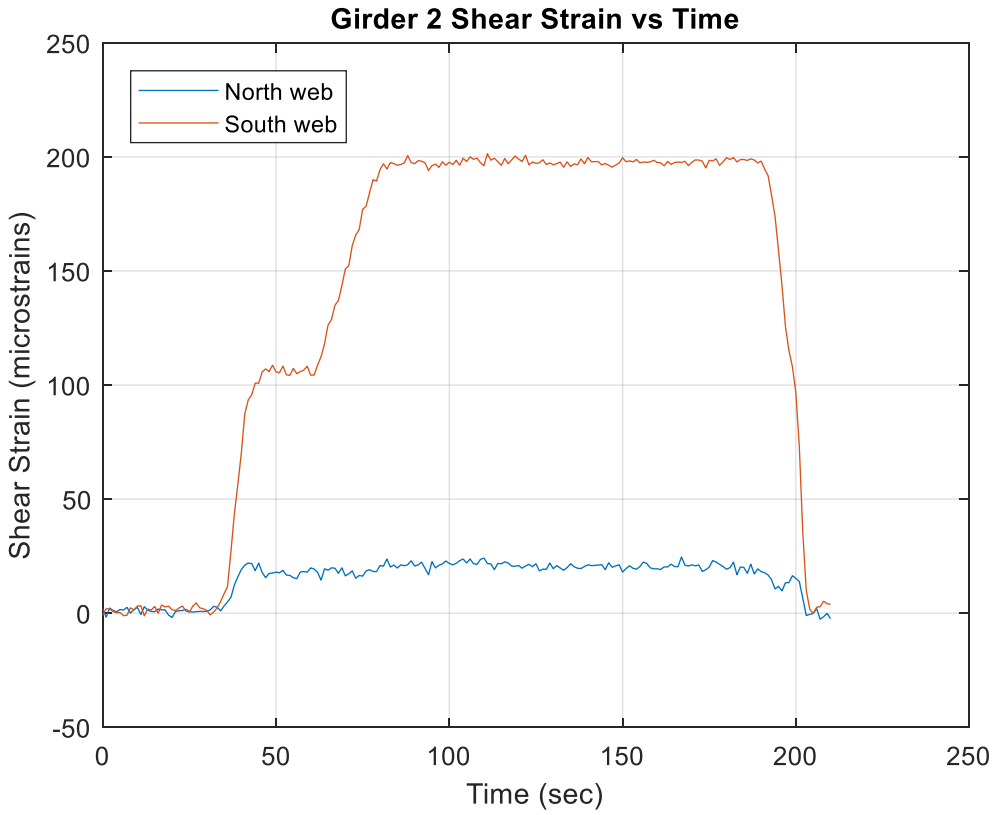
Girder 2 Shear Strain vs Time
North web
South web
Shear Strain (microstrains)
Time (sec)
250
200
150
100
50
0
-50
0
50
100
150
200
250

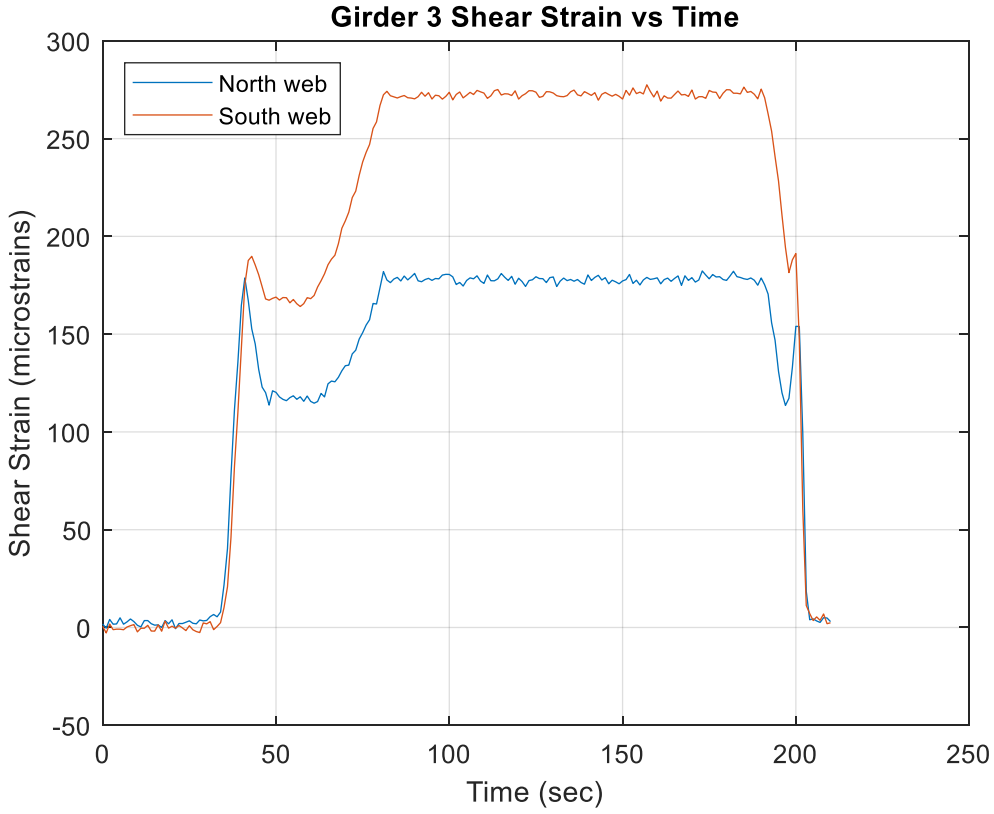
Girder 3 Shear Strain vs Time
North web
South web
Shear Strain (microstrains)
Time (sec)
300
250
200
150
100
50
0
-50
0
50
100
150
200
250

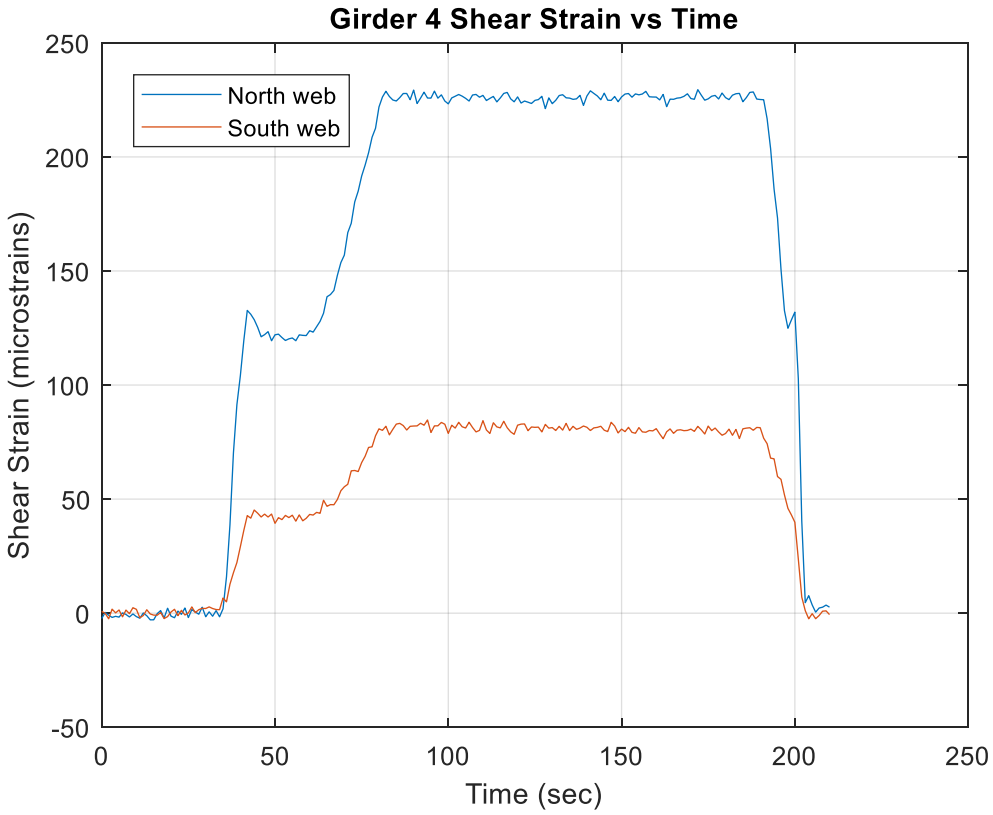
Girder 4 Shear Strain vs Time
North web
South web
Shear Strain (microstrains)
Time (sec)
250
200
150
100
50
0
-50
0
50
100
150
200
250

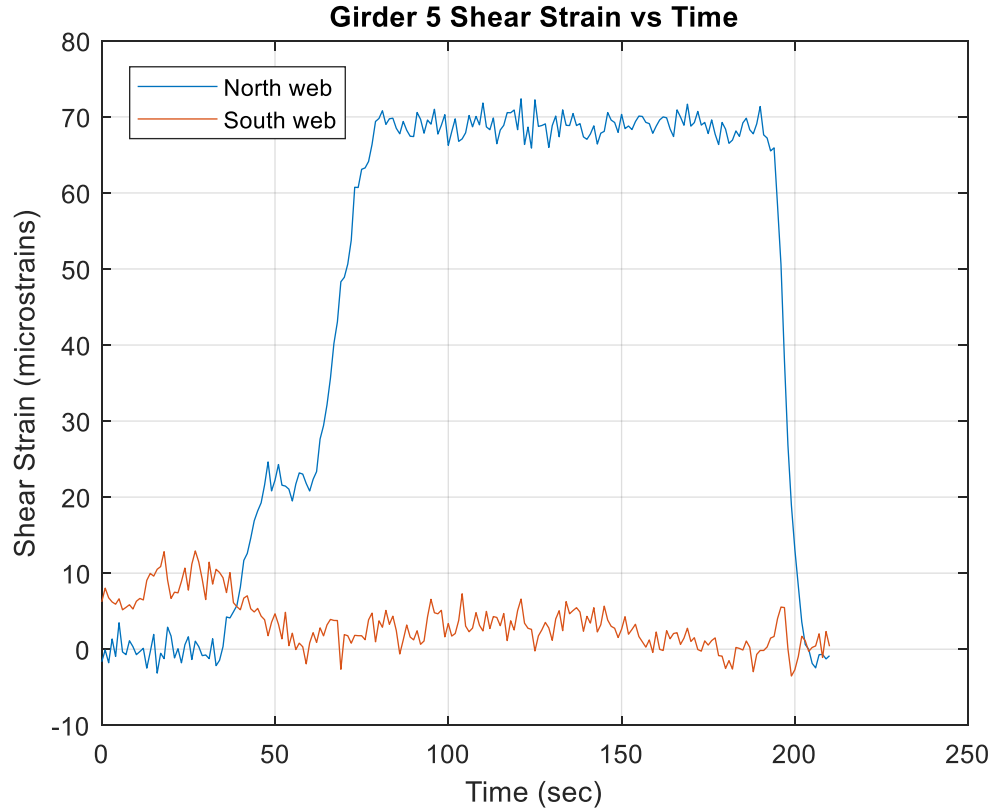
Girder 5 Shear Strain vs Time
North web
South web
Shear Strain (microstrains)
Time (sec)
80
70
60
50
40
30
20
10
0
-10
0
50
100
150
200
250

A.2.3.7 V24 Test

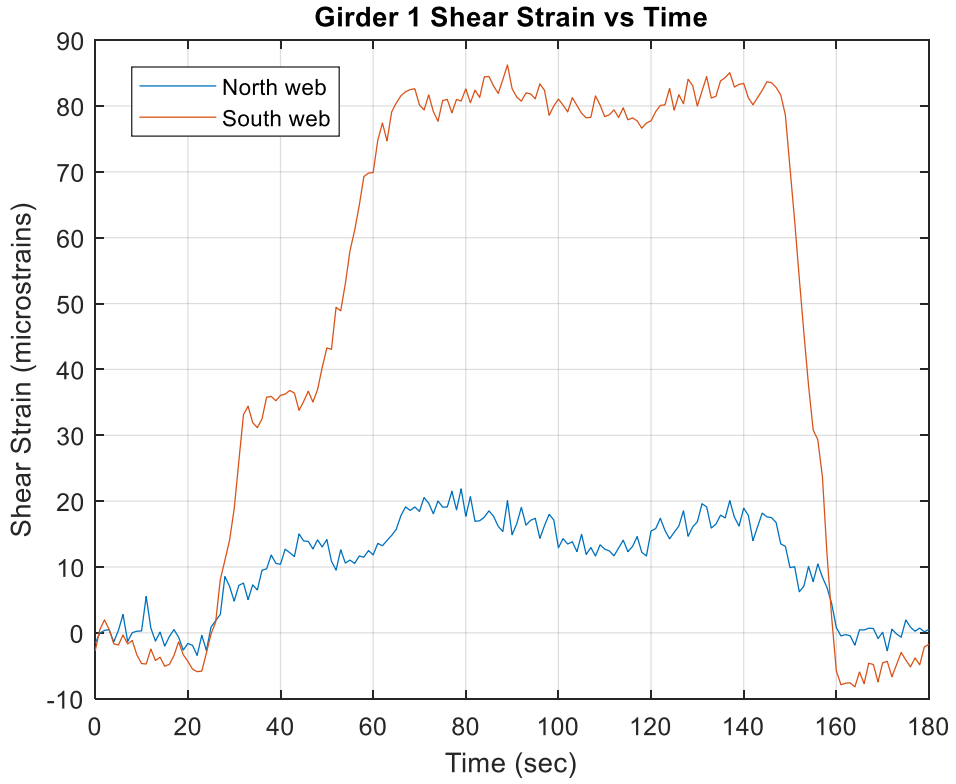

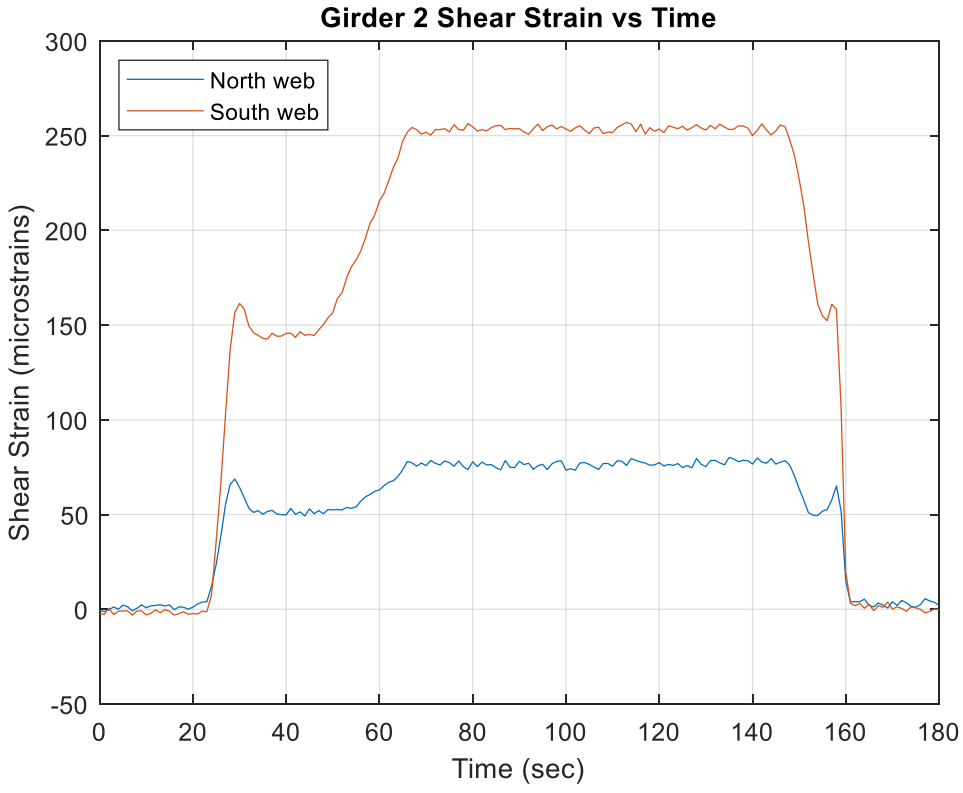

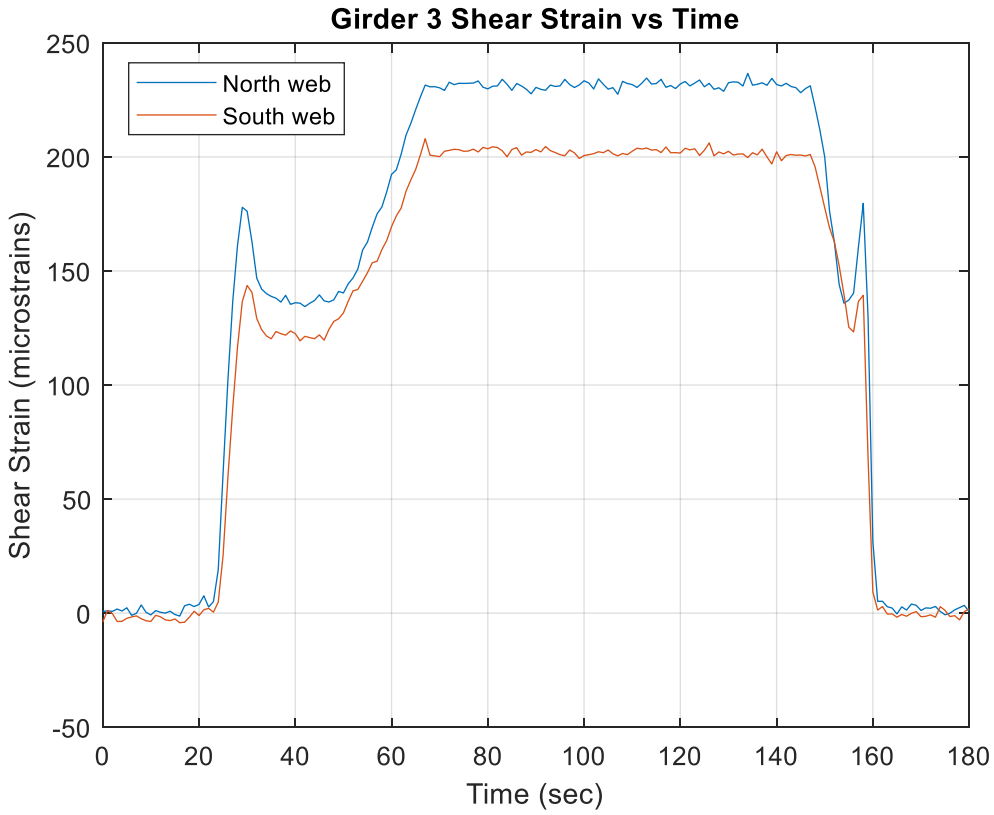
Girder 3 Shear Strain vs Time
North web
South web
Shear Strain (microstrains)
Time (sec)
250
200
150
100
50
0
-50
0
20
40
60
80
100
120
140
160
180

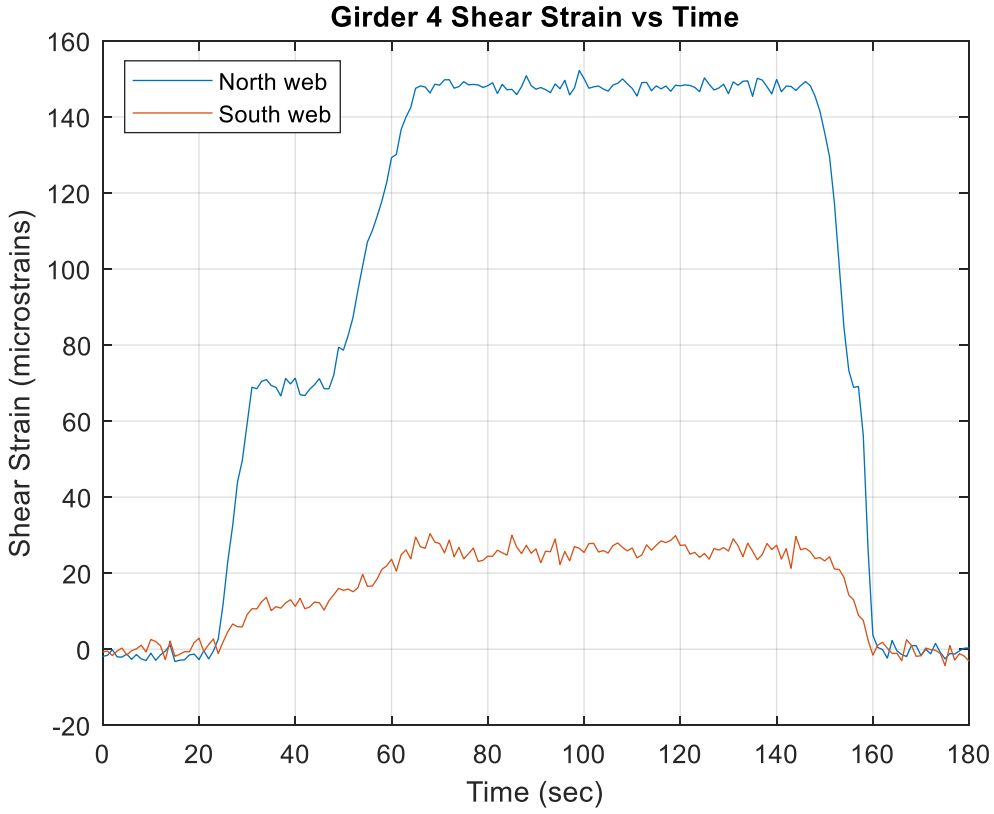
Girder 4 Shear Strain vs Time
North web
South web
Shear Strain (microstrains)
Time (sec)
160
140
120
100
80
60
40
20
0
-20
0
20
40
60
80
100
120
140
160
180

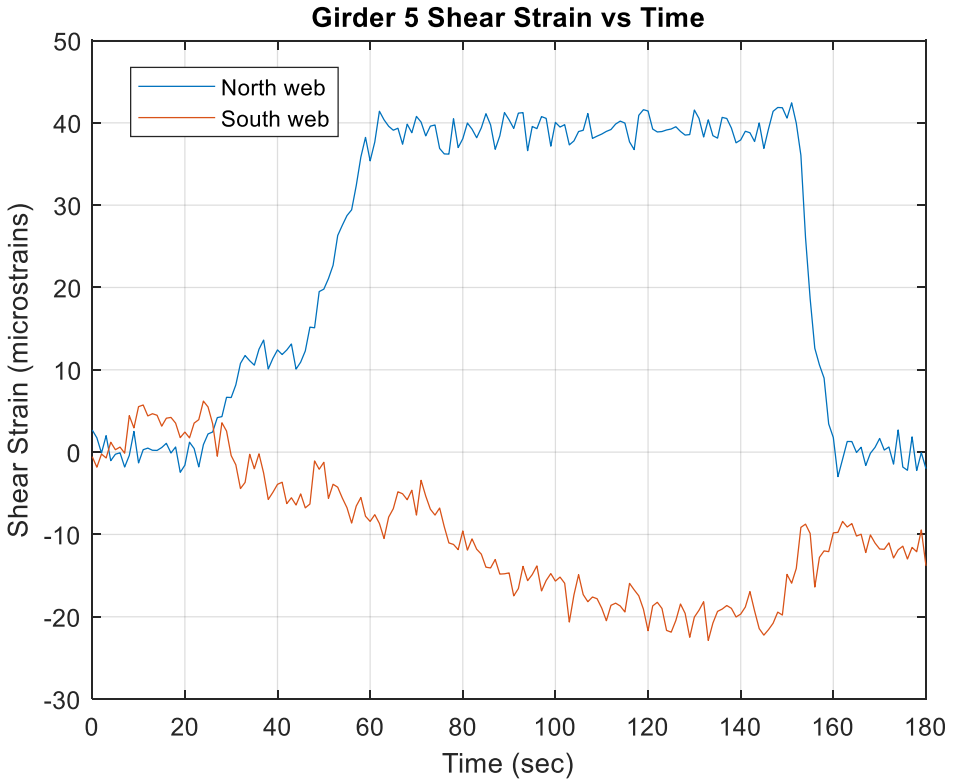

A.2.3.8 V25 Test

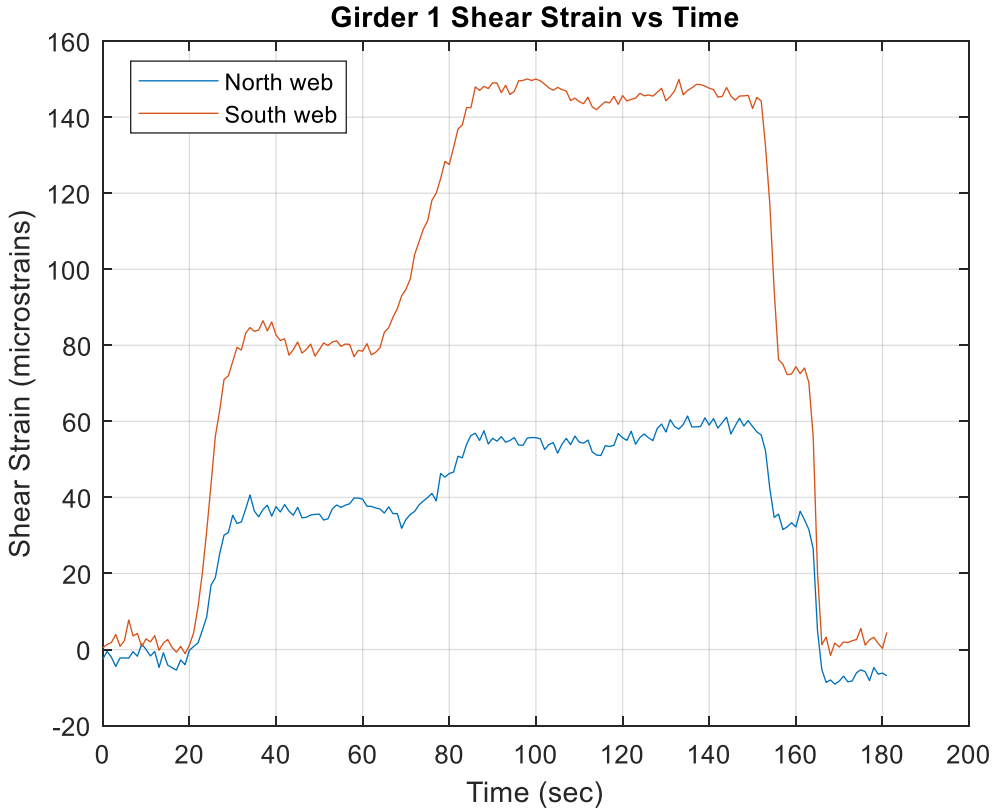

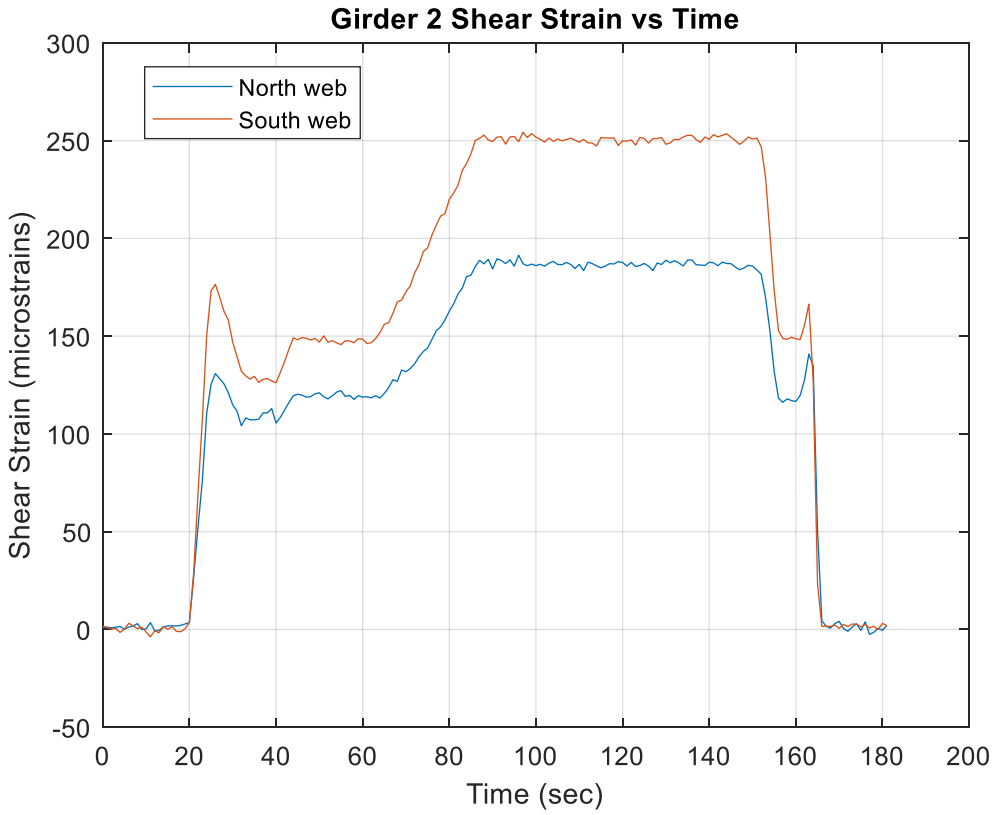
Girder 2 Shear Strain vs Time
North web
South web
Shear Strain (microstrains)
Time (sec)
300
250
200
150
100
50
0
-50
0
20
40
60
80
100
120
140
160
180
200

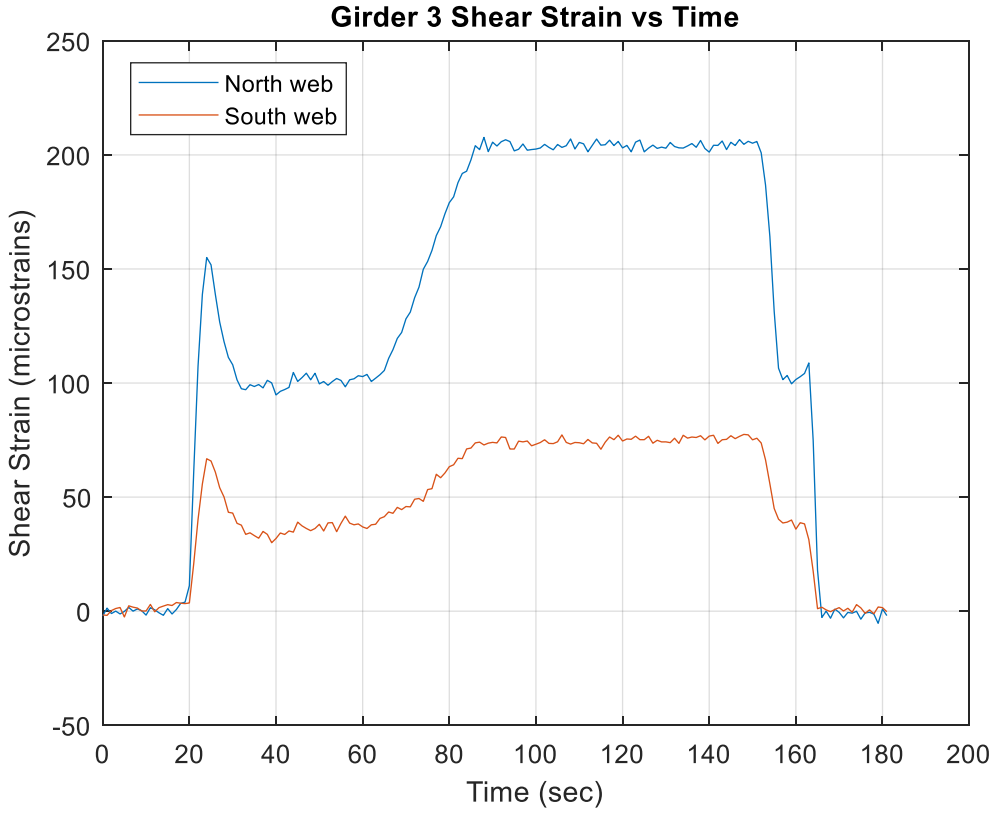
Girder 3 Shear Strain vs Time
North web
South web
Shear Strain (microstrains)
Time (sec)
250
200
150
100
50
0
-50
0
20
40
60
80
100
120
140
160
180
200

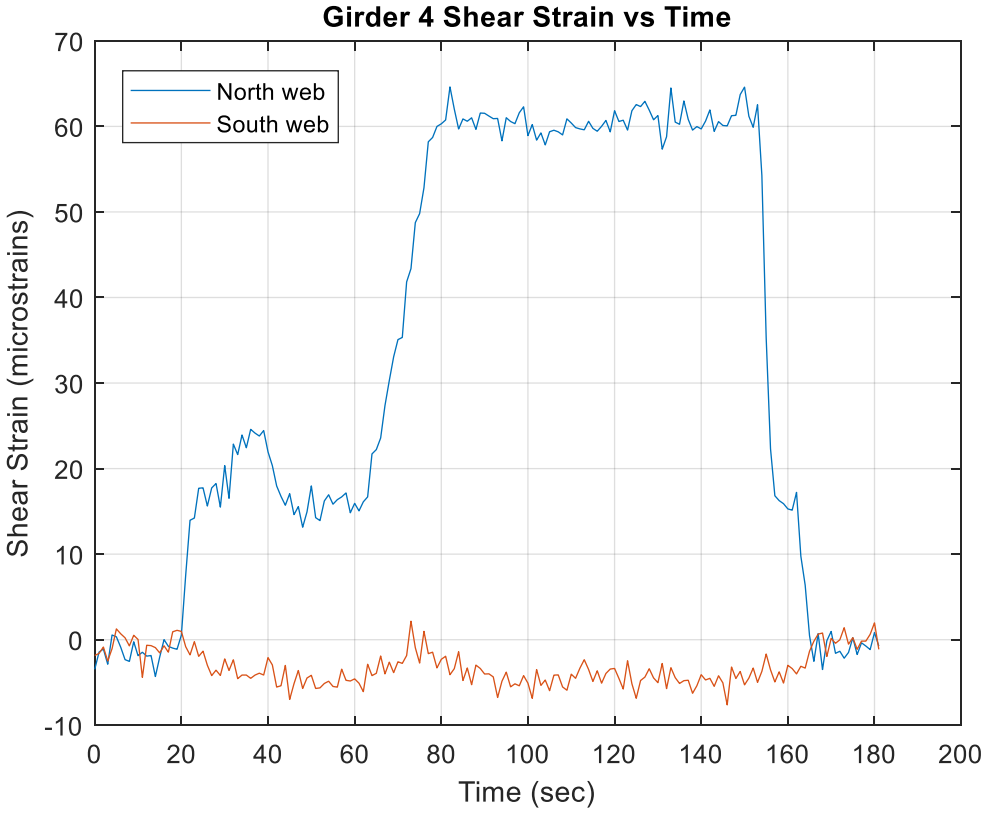
Girder 4 Shear Strain vs Time
North web
South web
Shear Strain (microstrains)
Time (sec)
70
60
50
40
30
20
10
0
-10
0
20
40
60
80
100
120
140
160
180
200

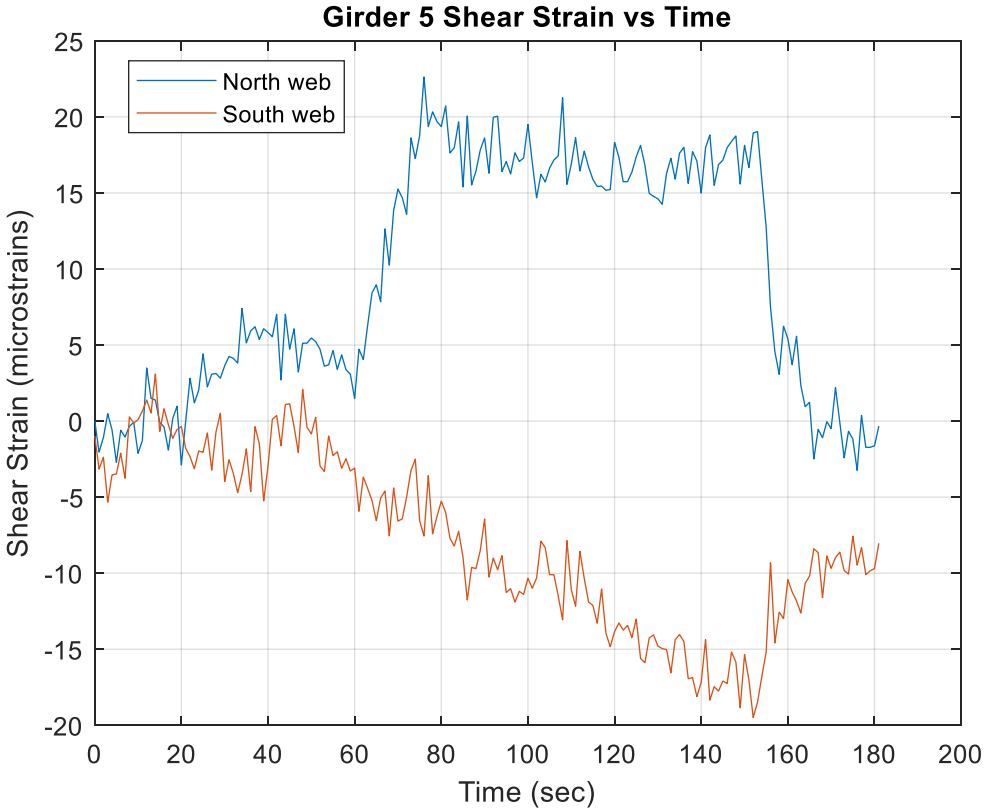
Girder 5 Shear Strain vs Time
North web
South web
Shear Strain (microstrains)
Time (sec)
25
20
15
10
5
0
-5
-10
-15
-20
0
20
40
60
80
100
120
140
160
180
200

A.3 Twin Bridge 2023

A.3.1 Instrumentation

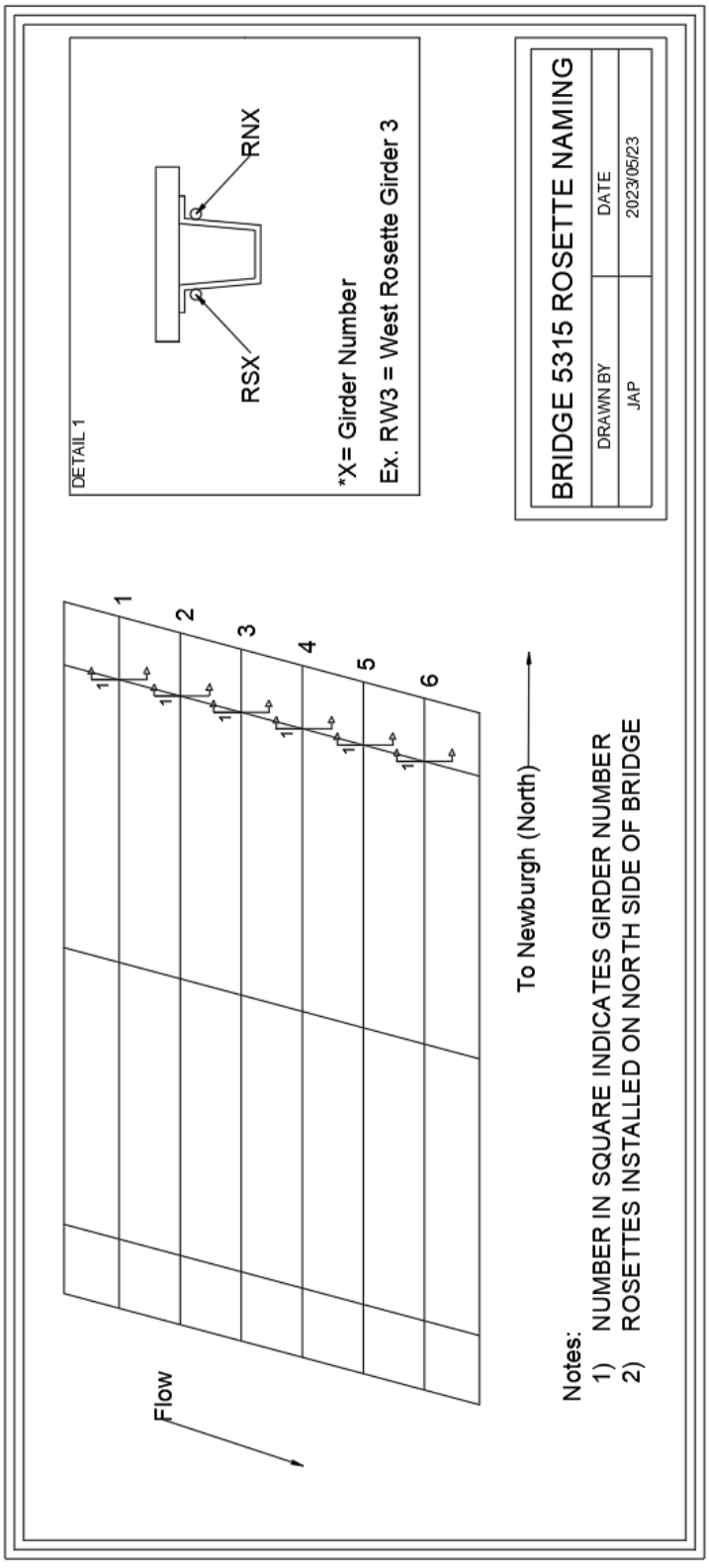

A.3.2 Loading

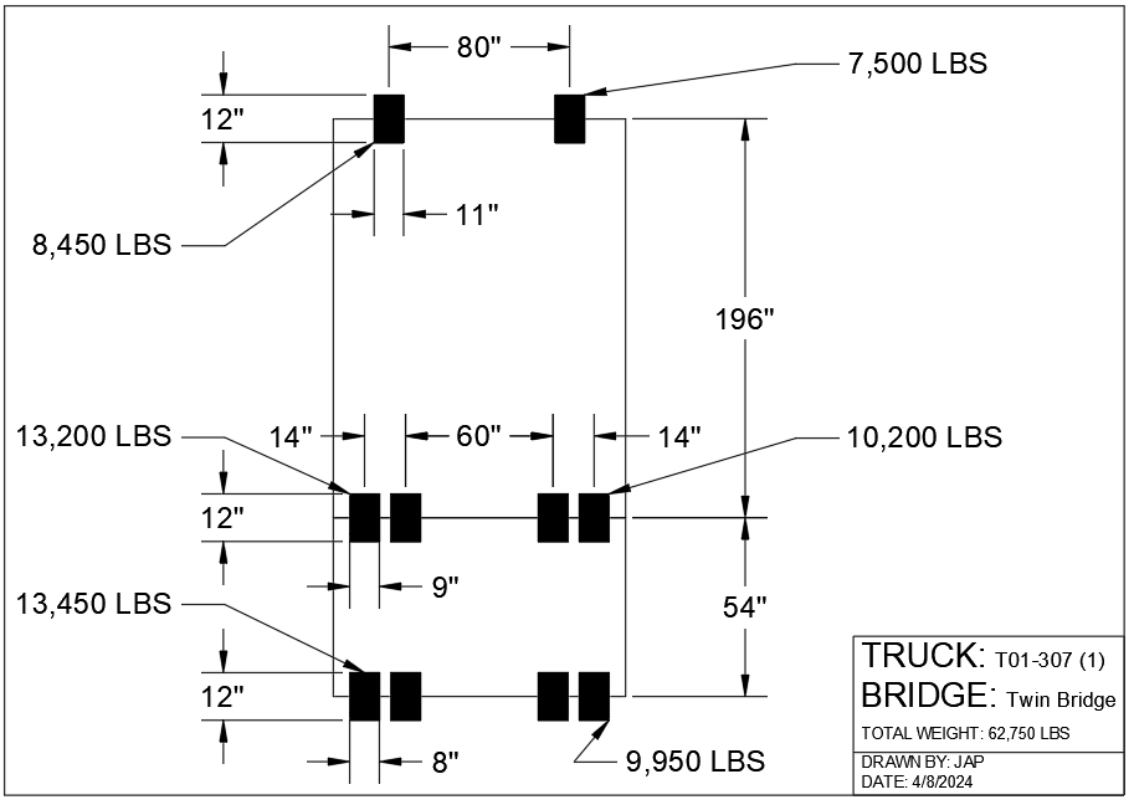
80"
7,500 LBS
12"
11"
8,450 LBS
196"
13,200 LBS
14"
60"
14"
10,200 LBS
12"
9"
13,450 LBS
54"
12"
8"
9,950 LBS
TRUCK: T01-307 (1)
BRIDGE: Twin Bridge
TOTAL WEIGHT: 62,750 LBS
DRAWN BY: JAP
DATE: 4/8/2024

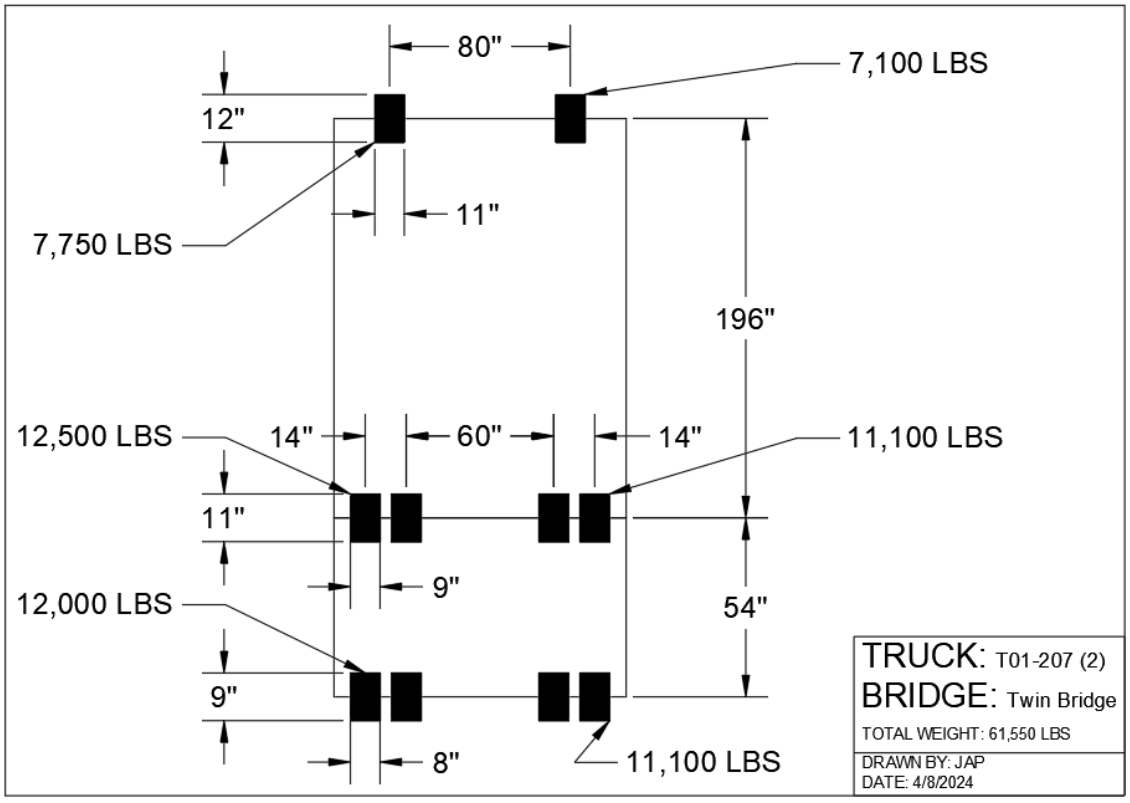
80"
7,100 LBS
12"
11"
7,750 LBS
196"
12,500 LBS
14"
60"
14"
11,100 LBS
11"
9"
12,000 LBS
54"
9"
8"
11,100 LBS
TRUCK: T01-207 (2)
BRIDGE: Twin Bridge
TOTAL WEIGHT: 61,550 LBS
DRAWN BY: JAP
DATE: 4/8/2024

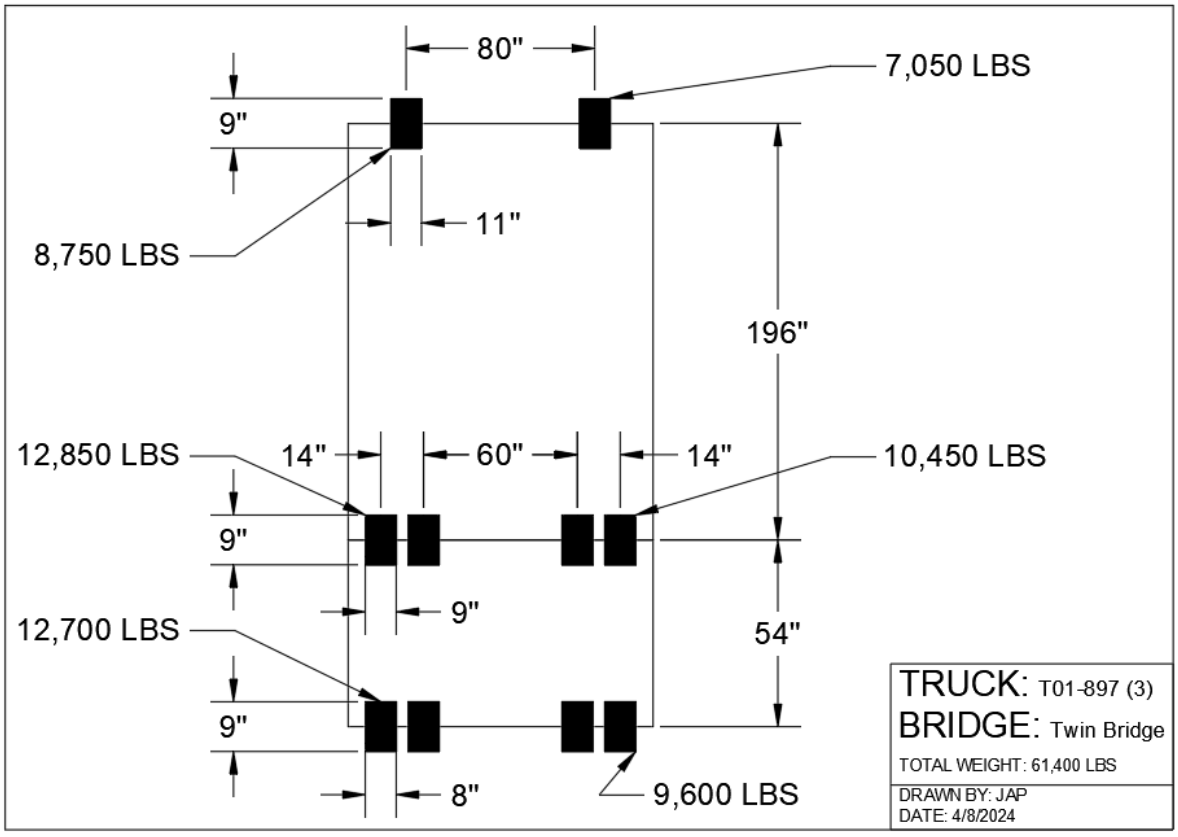
80"
7,050 LBS
9"
11"
8,750 LBS
196"
12,850 LBS
14"
60"
14"
10,450 LBS
9"
9"
12,700 LBS
54"
9"
8"
9,600 LBS
TRUCK: T01-897 (3)
BRIDGE: Twin Bridge
TOTAL WEIGHT: 61,400 LBS
DRAWN BY: JAP
DATE: 4/8/2024

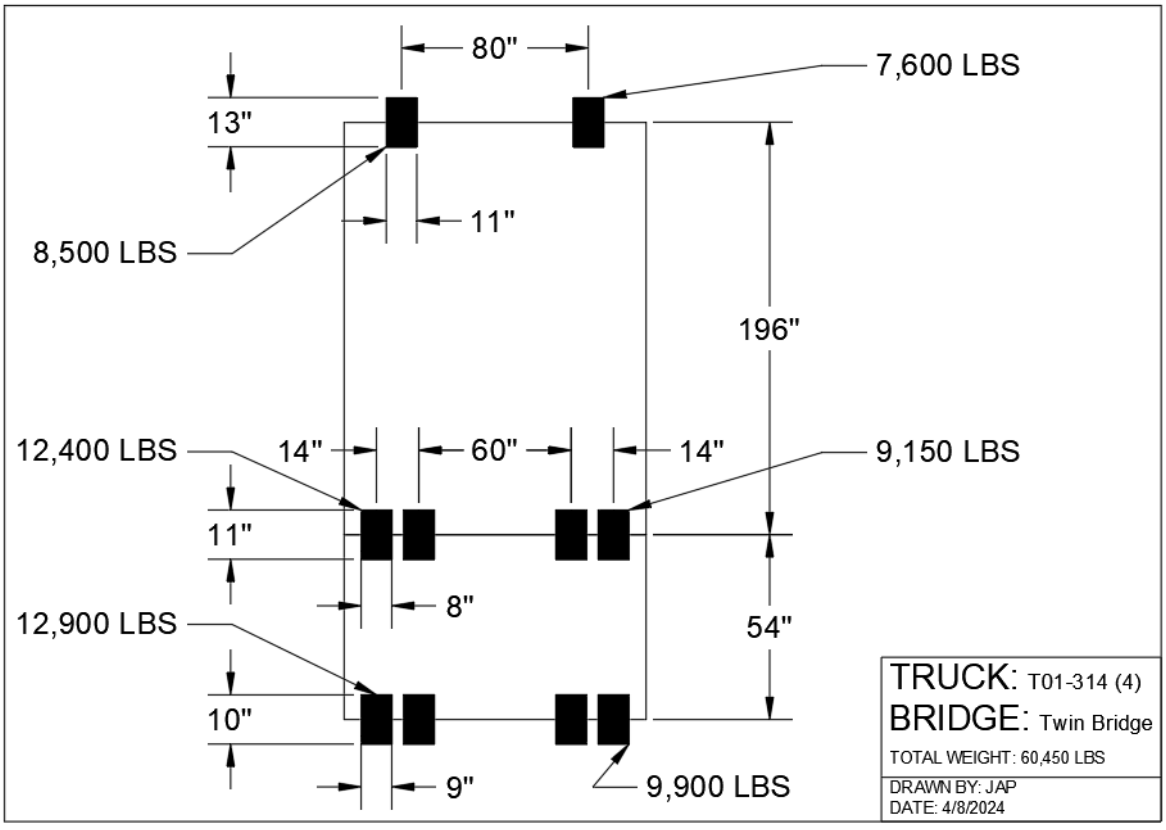
80"
7,600 LBS
13"
11"
8,500 LBS
196"
12,400 LBS
14"
60"
14"
9,150 LBS
11"
8"
12,900 LBS
54"
10"
9"
9,900 LBS
TRUCK: T01-314 (4)
BRIDGE: Twin Bridge
TOTAL WEIGHT: 60,450 LBS
DRAWN BY: JAP
DATE: 4/8/2024

A.3.3 Representative Data Plots

A.3.3.1 V41 Test

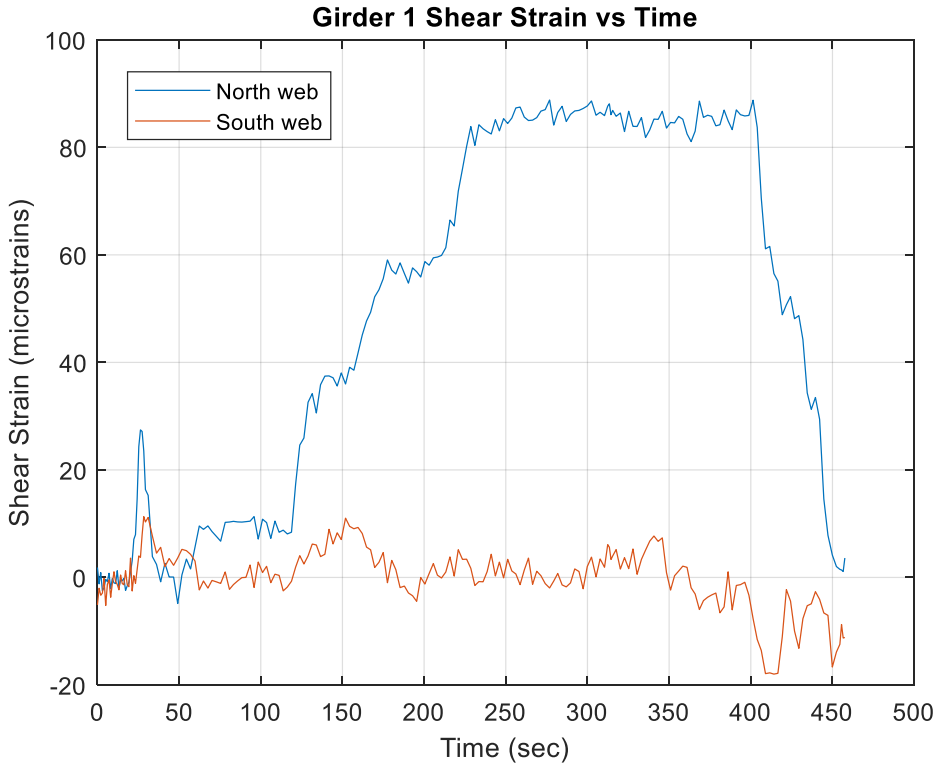

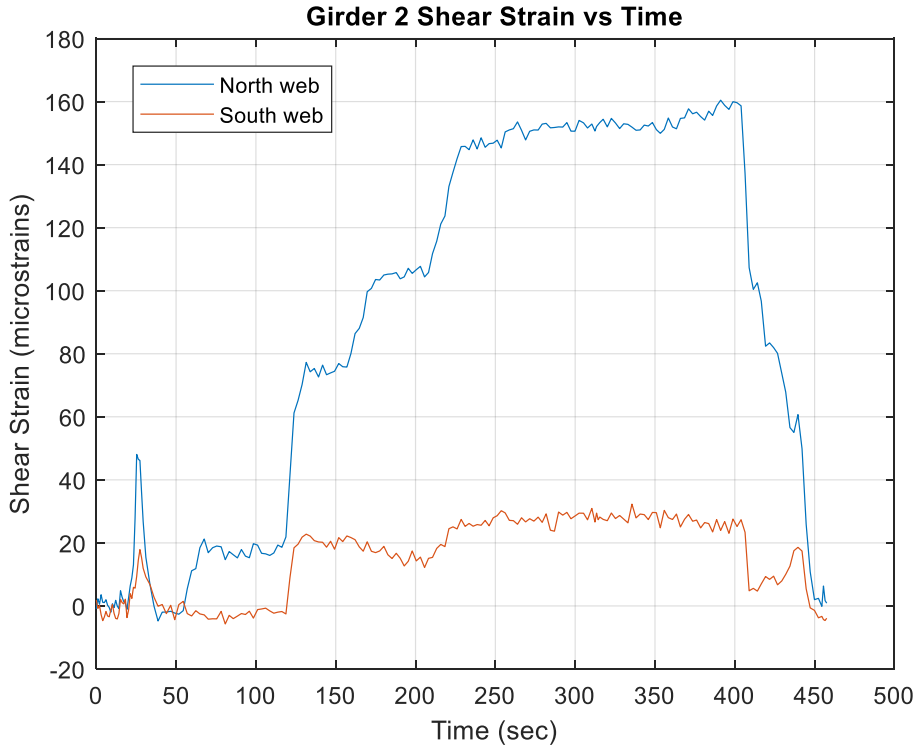

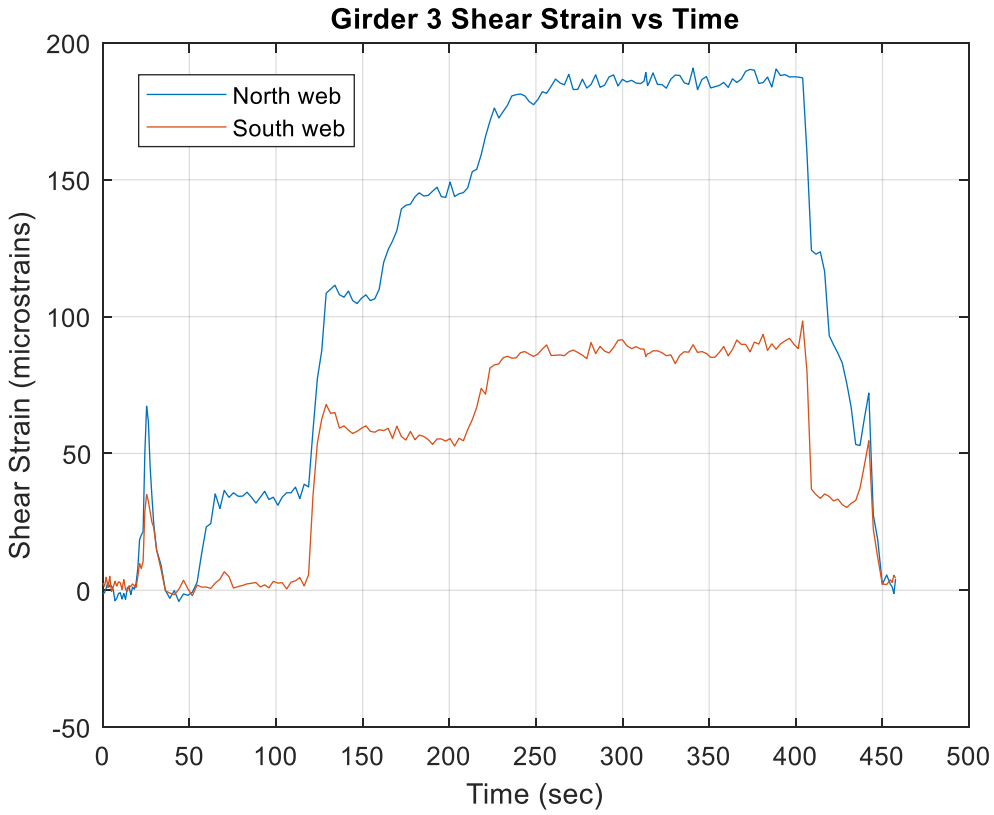
Girder 3 Shear Strain vs Time
North web
South web
Shear Strain (microstrains)
Time (sec)
200
150
100
50
0
-50
0
50
100
150
200
250
300
350
400
450
500

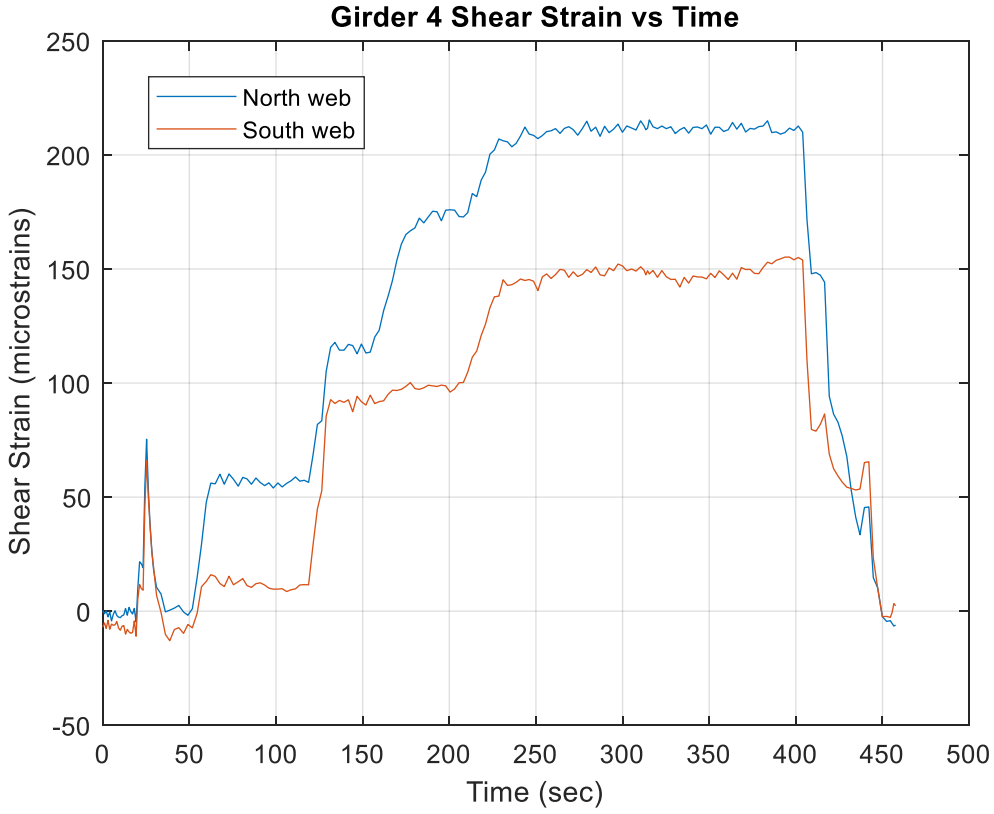
Girder 4 Shear Strain vs Time
North web
South web
Shear Strain (microstrains)
Time (sec)
250
200
150
100
50
0
-50
0
50
100
150
200
250
300
350
400
450
500

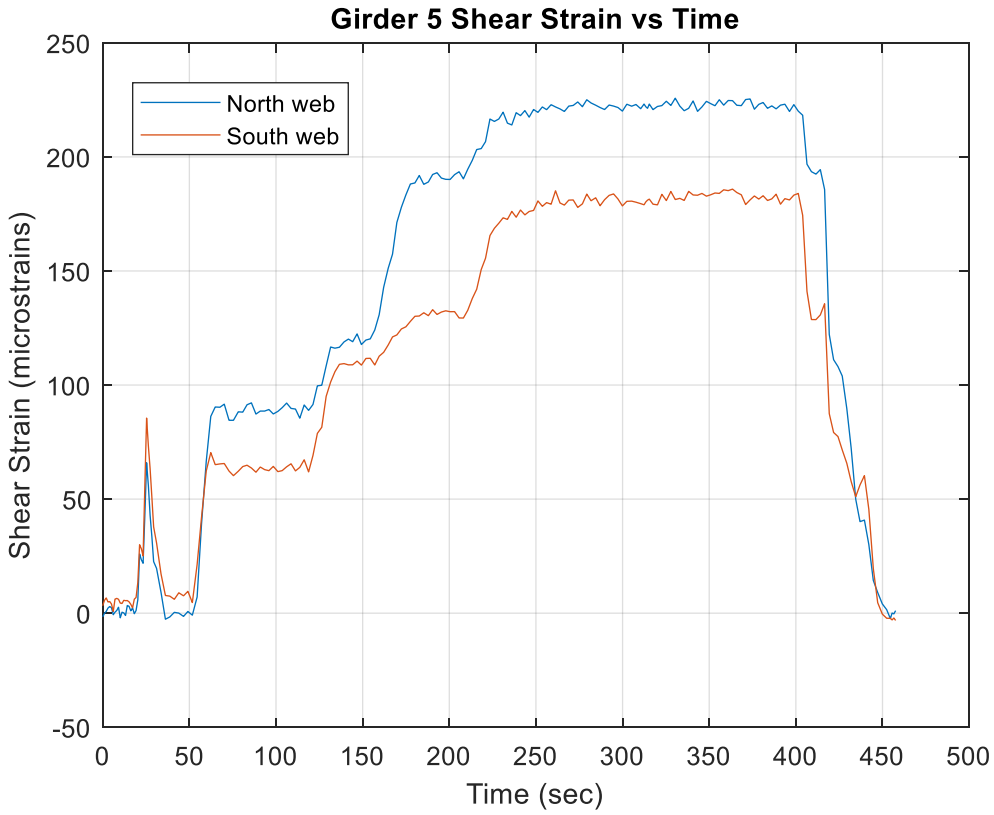
Girder 5 Shear Strain vs Time
North web
South web
Shear Strain (microstrains)
Time (sec)
250
200
150
100
50
0
-50
0
50
100
150
200
250
300
350
400
450
500

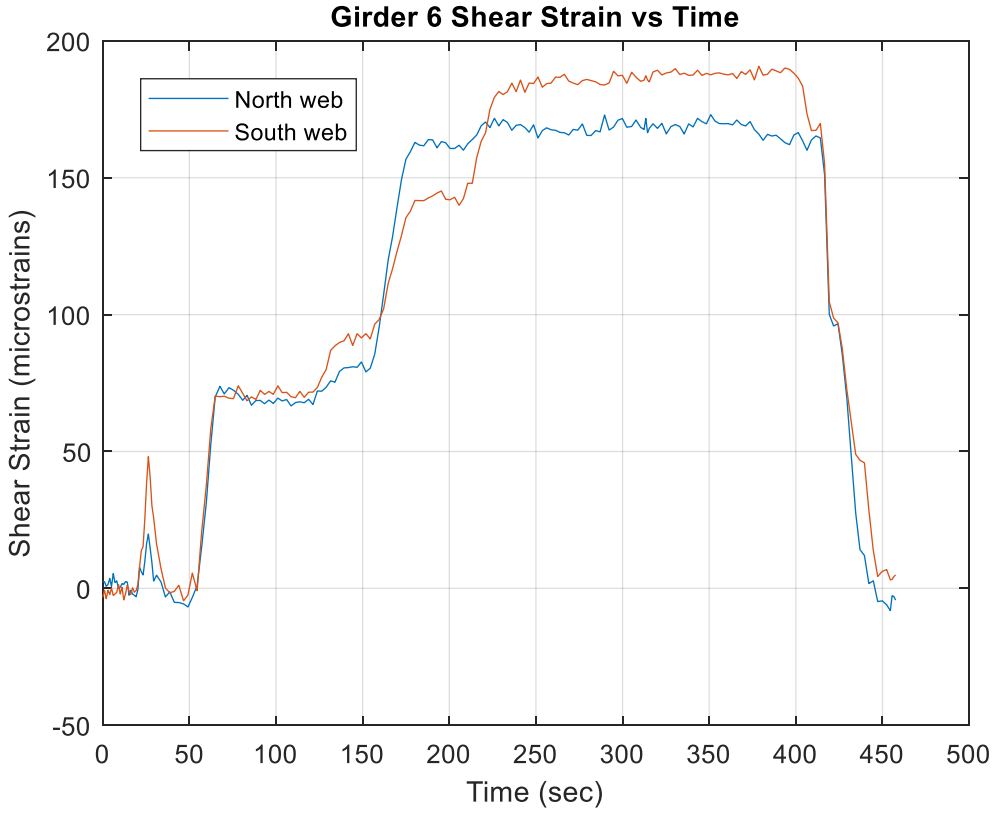
Girder 6 Shear Strain vs Time
North web
South web
Shear Strain (microstrains)
Time (sec)
200
150
100
50
0
-50
0
50
100
150
200
250
300
350
400
450
500

A.3.3.2 V42 Test

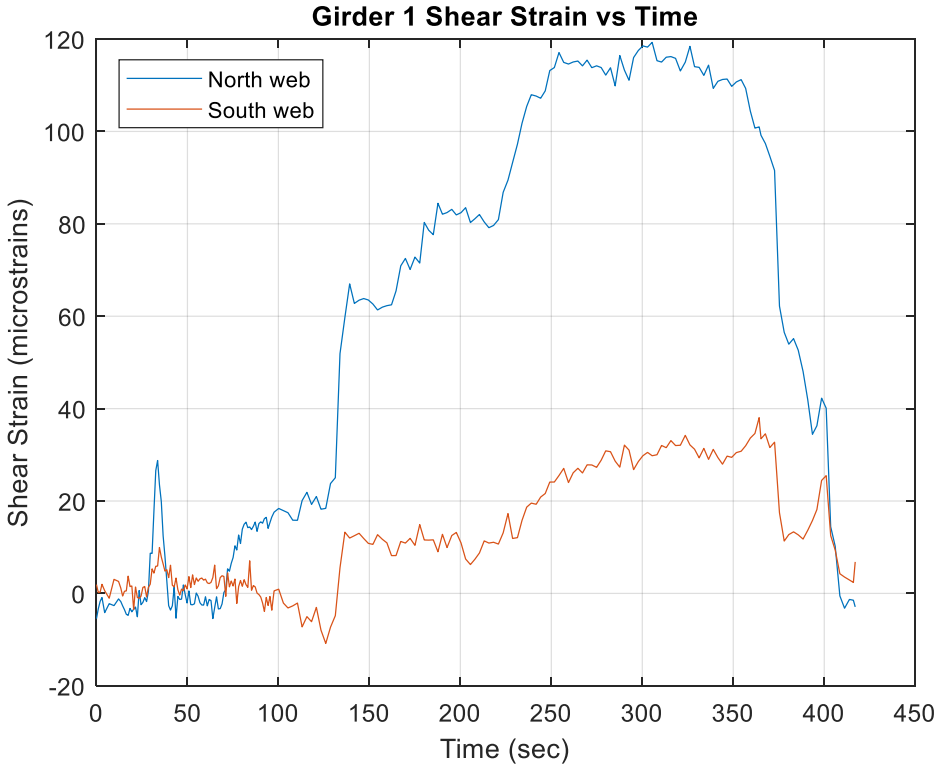

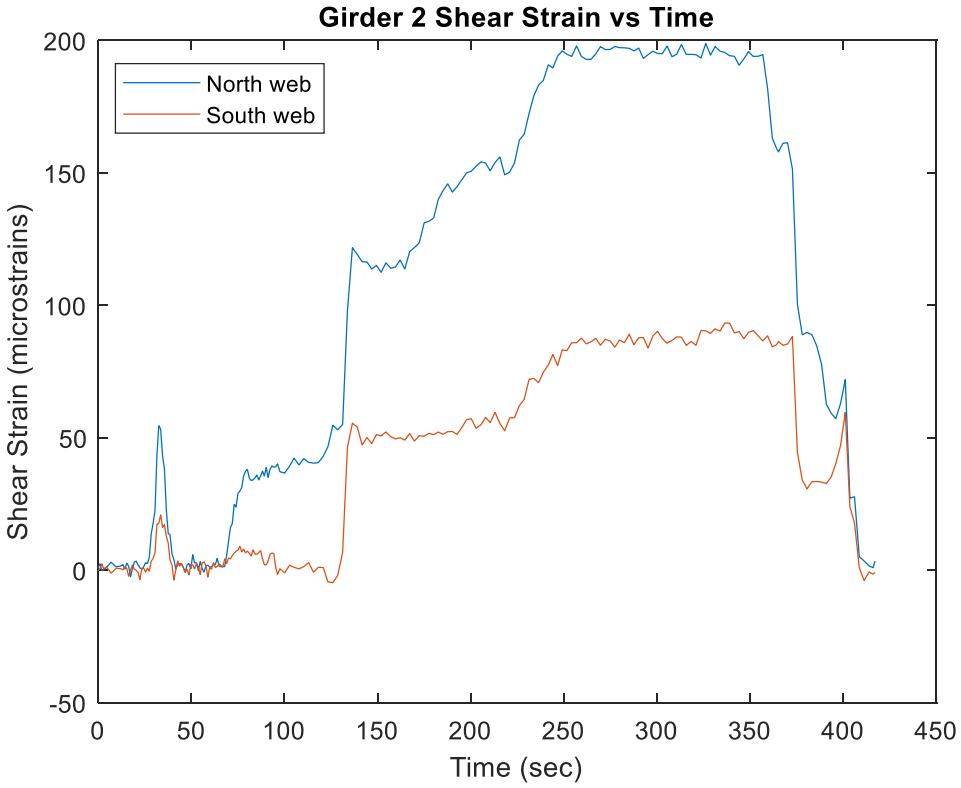

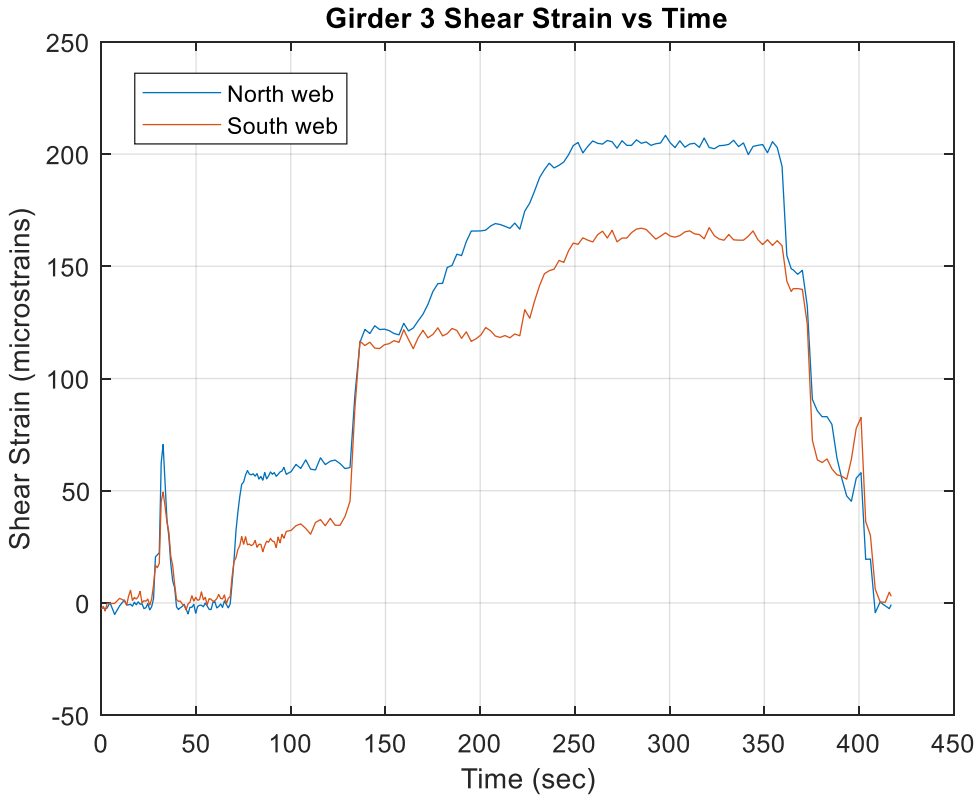
Girder 3 Shear Strain vs Time
North web
South web
Shear Strain (microstrains)
Time (sec)
250
200
150
100
50
0
-50
0
50
100
150
200
250
300
350
400
450

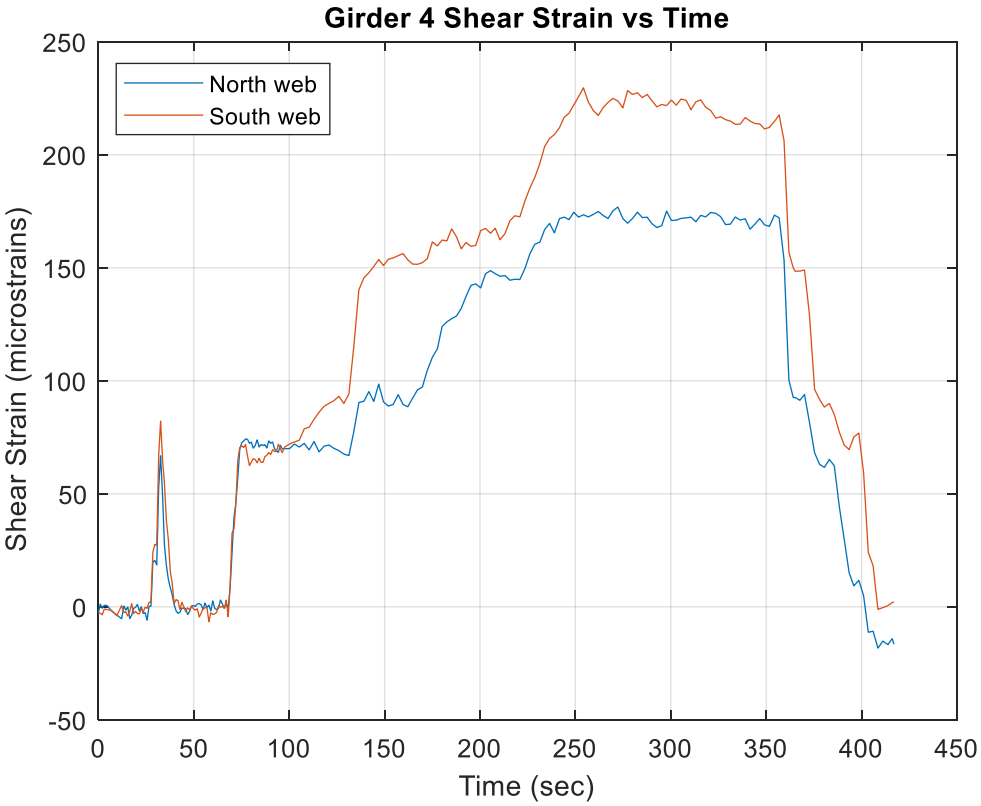
Girder 4 Shear Strain vs Time
North web
South web
Shear Strain (microstrains)
Time (sec)
250
200
150
100
50
0
-50
0
50
100
150
200
250
300
350
400
450

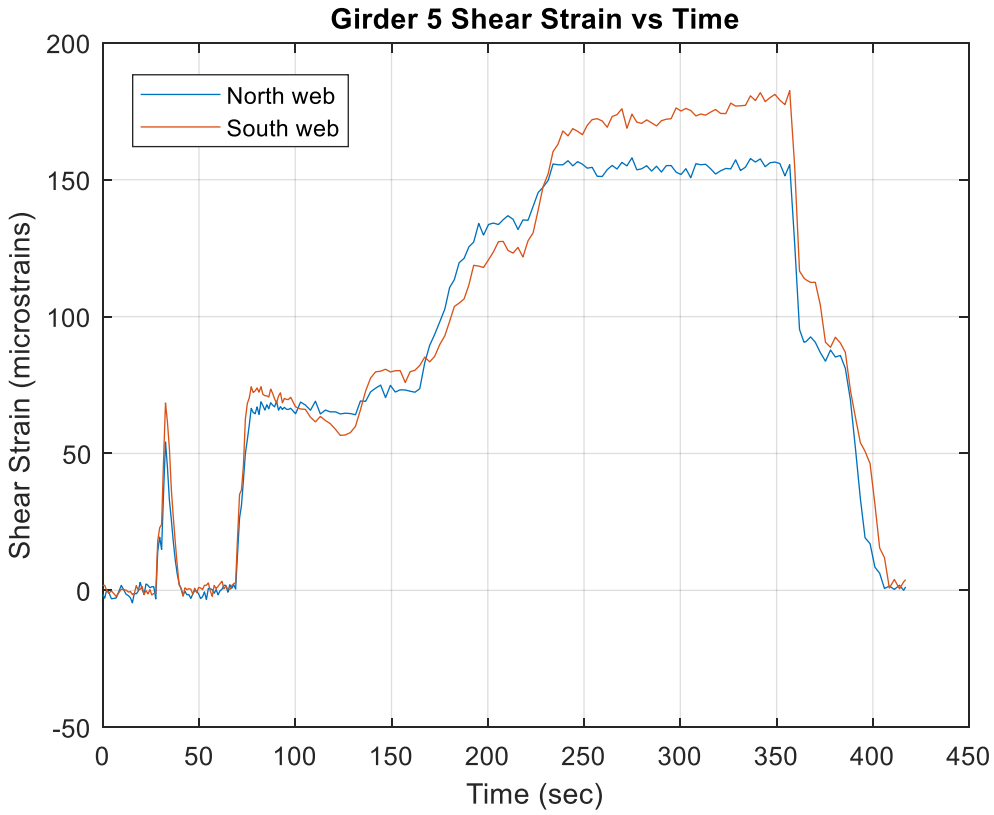
Girder 5 Shear Strain vs Time
North web
South web
Shear Strain (microstrains)
Time (sec)
200
150
100
50
0
-50
0
50
100
150
200
250
300
350
400
450

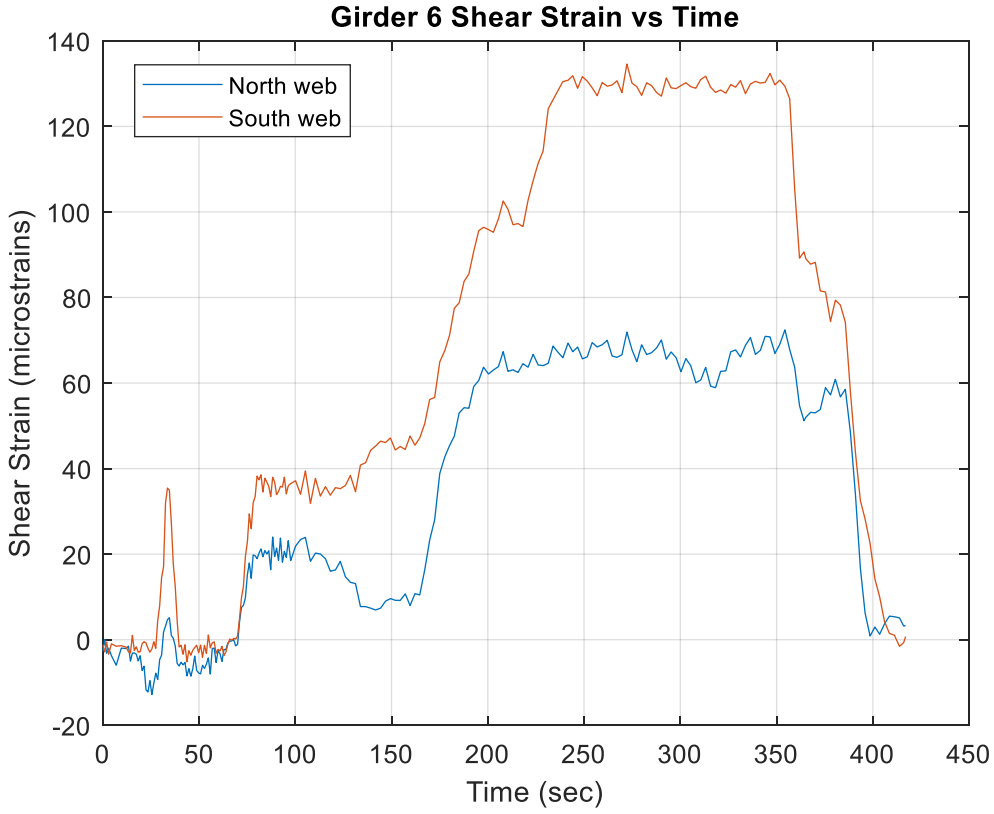
Girder 6 Shear Strain vs Time
North web
South web
Shear Strain (microstrains)
Time (sec)
140
120
100
80
60
40
20
0
-20
0
50
100
150
200
250
300
350
400
450

A.3.3.3 V43 Test

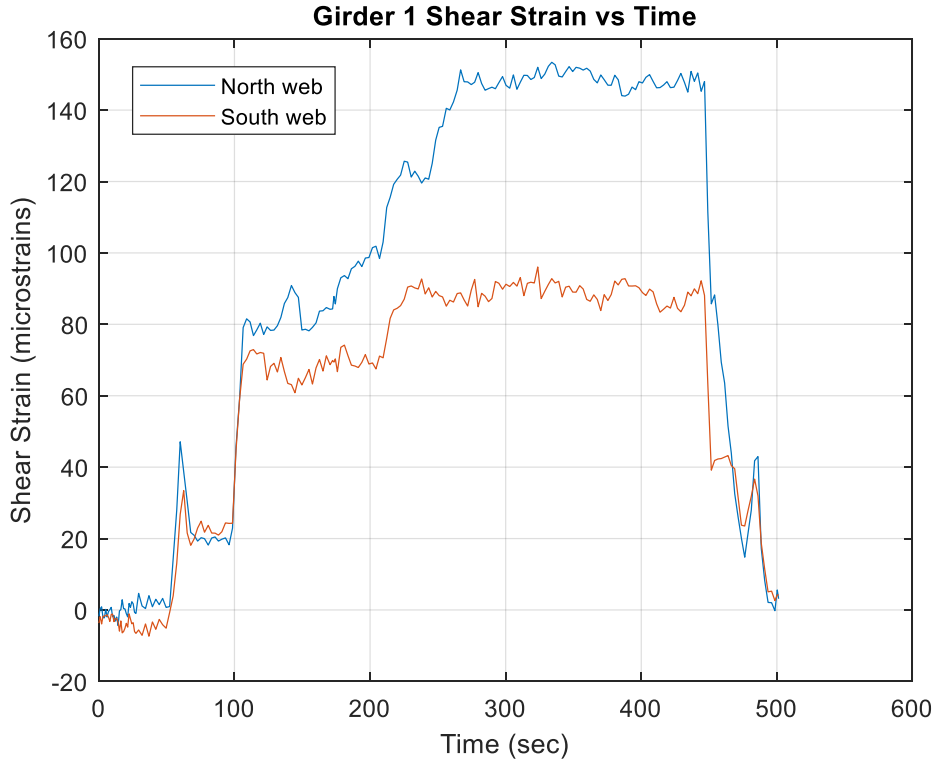

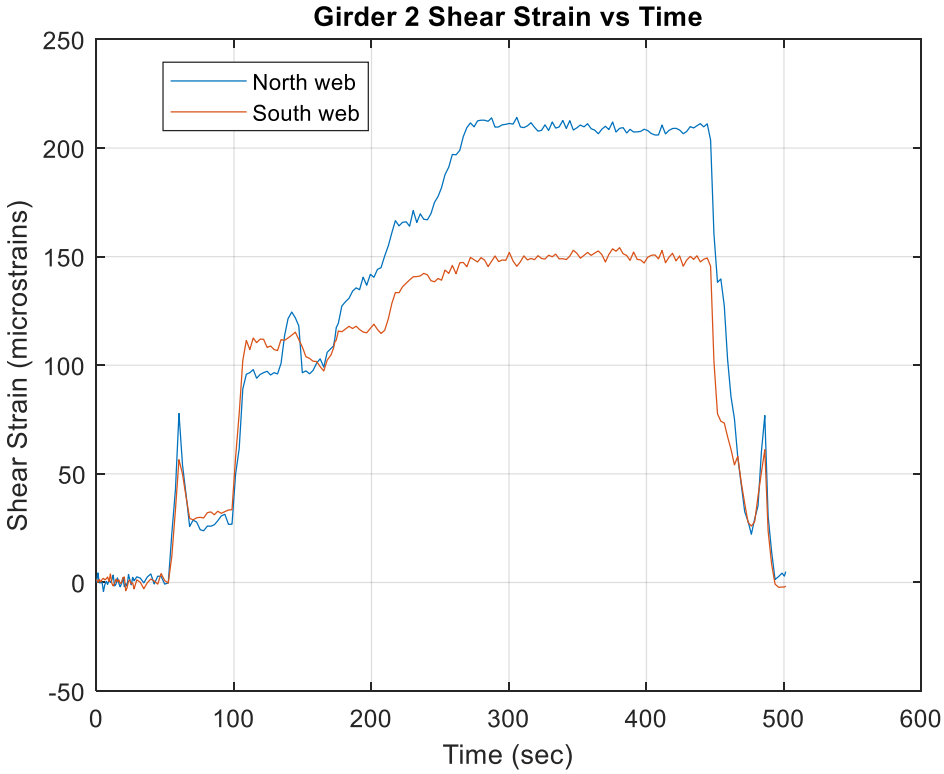

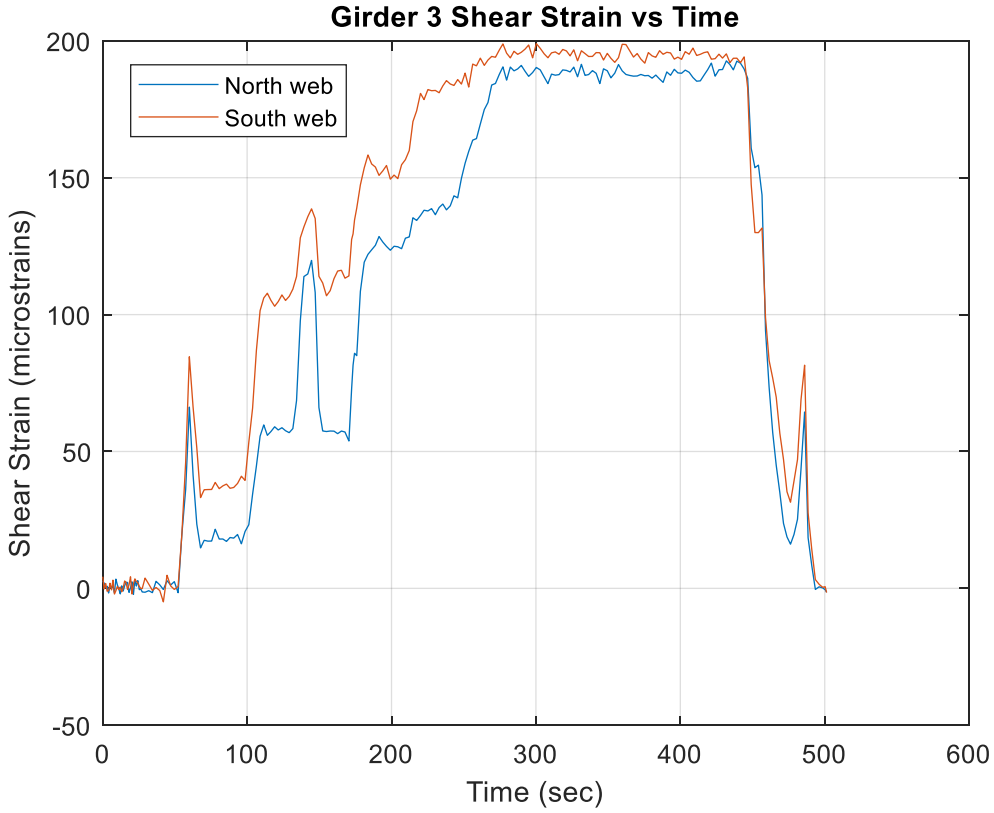
Girder 3 Shear Strain vs Time
North web
South web
Shear Strain (microstrains)
Time (sec)
200
150
100
50
0
-50
0
100
200
300
400
500
600

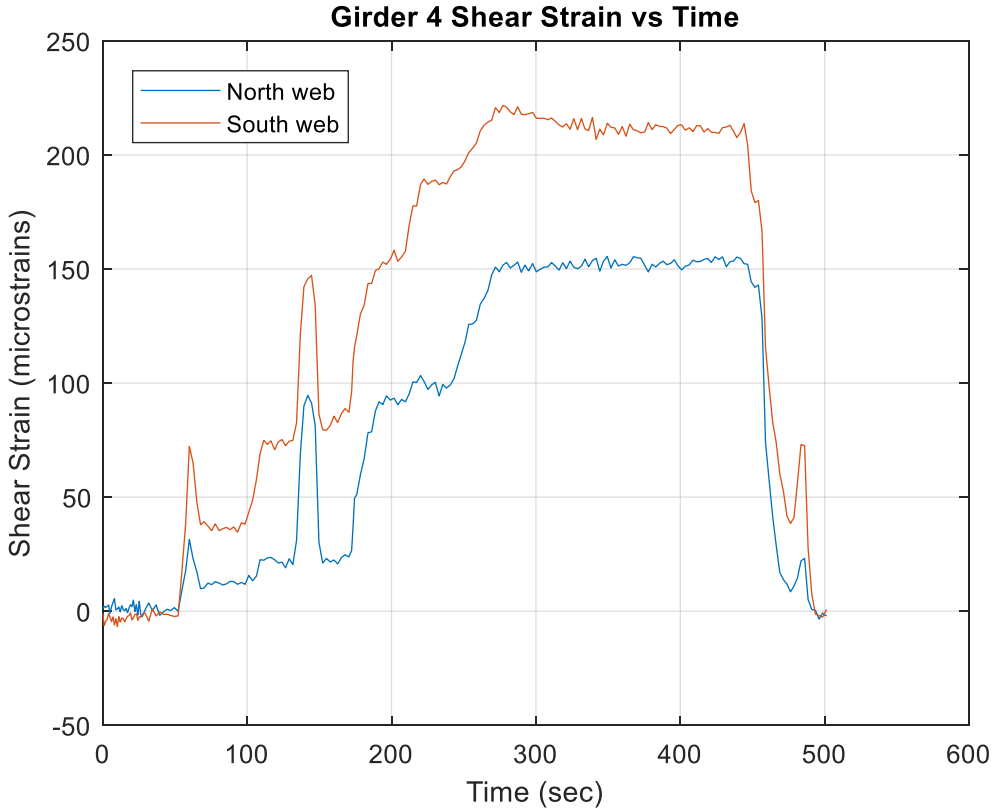
Girder 4 Shear Strain vs Time
North web
South web
Shear Strain (microstrains)
Time (sec)
250
200
150
100
50
0
-50
0
100
200
300
400
500
600

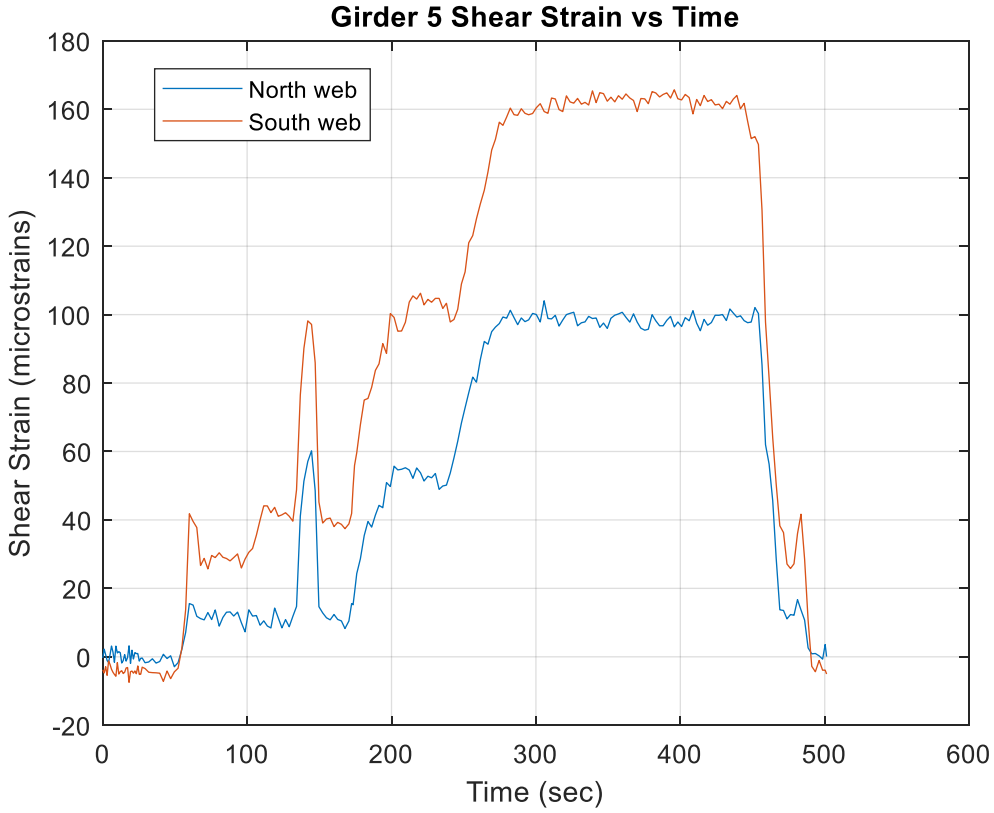
Girder 5 Shear Strain vs Time
North web
South web
Shear Strain (microstrains)
Time (sec)
180
160
140
120
100
80
60
40
20
0
-20
0
100
200
300
400
500
600

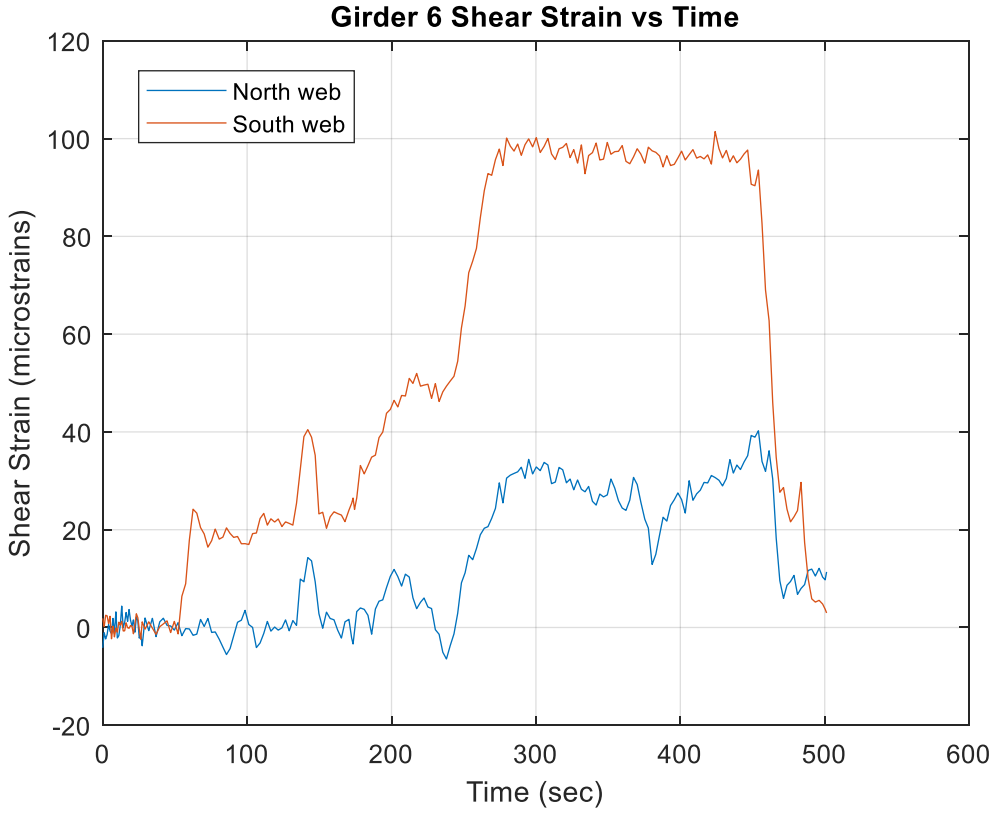
Girder 6 Shear Strain vs Time
North web
South web
Shear Strain (microstrains)
Time (sec)
120
100
80
60
40
20
0
-20
0
100
200
300
400
500
600

A.3.3.4 V21 Test

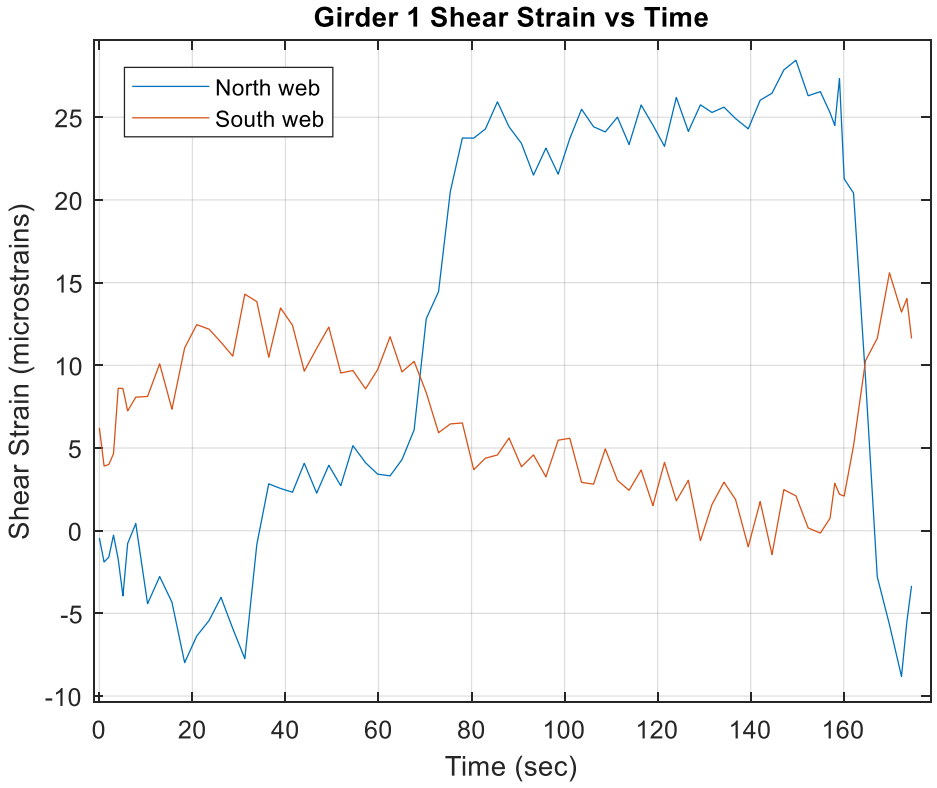

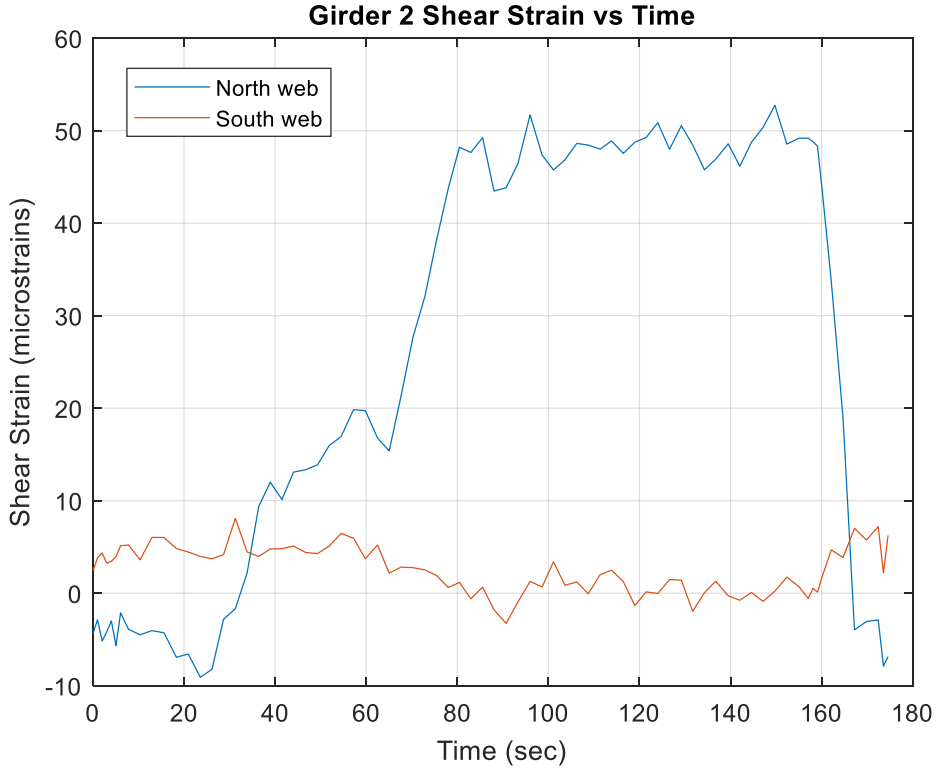

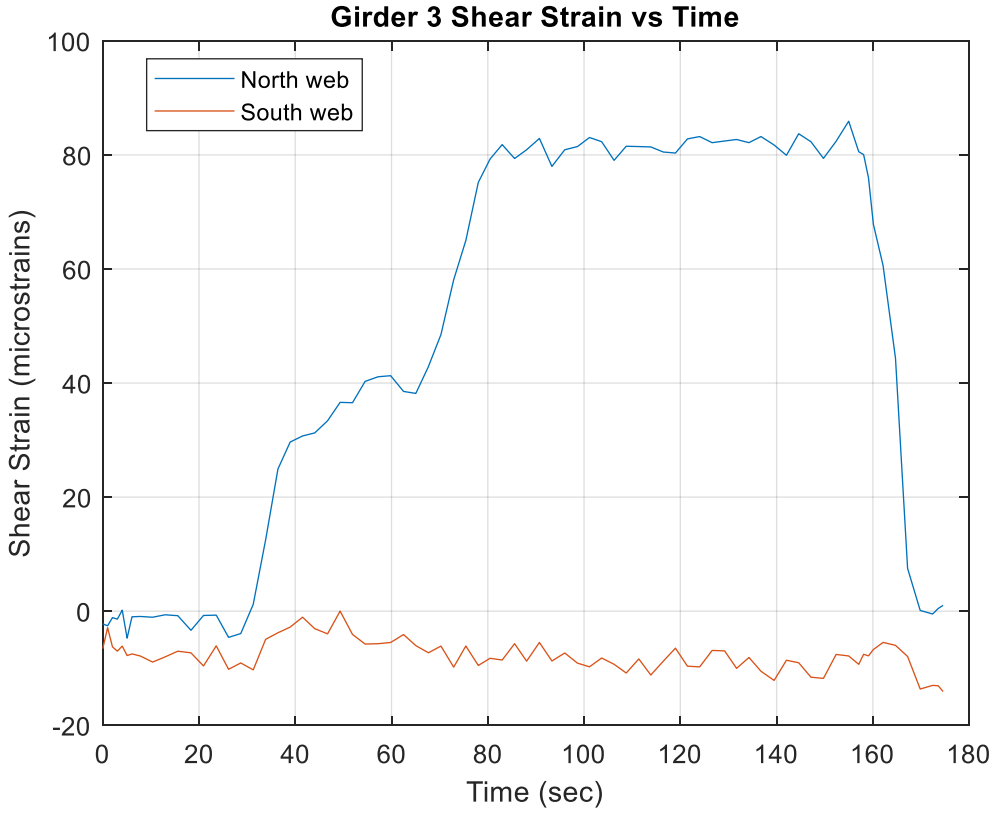
Girder 3 Shear Strain vs Time
North web
South web
Shear Strain (microstrains)
Time (sec)
100
80
60
40
20
0
-20
0
20
40
60
80
100
120
140
160
180

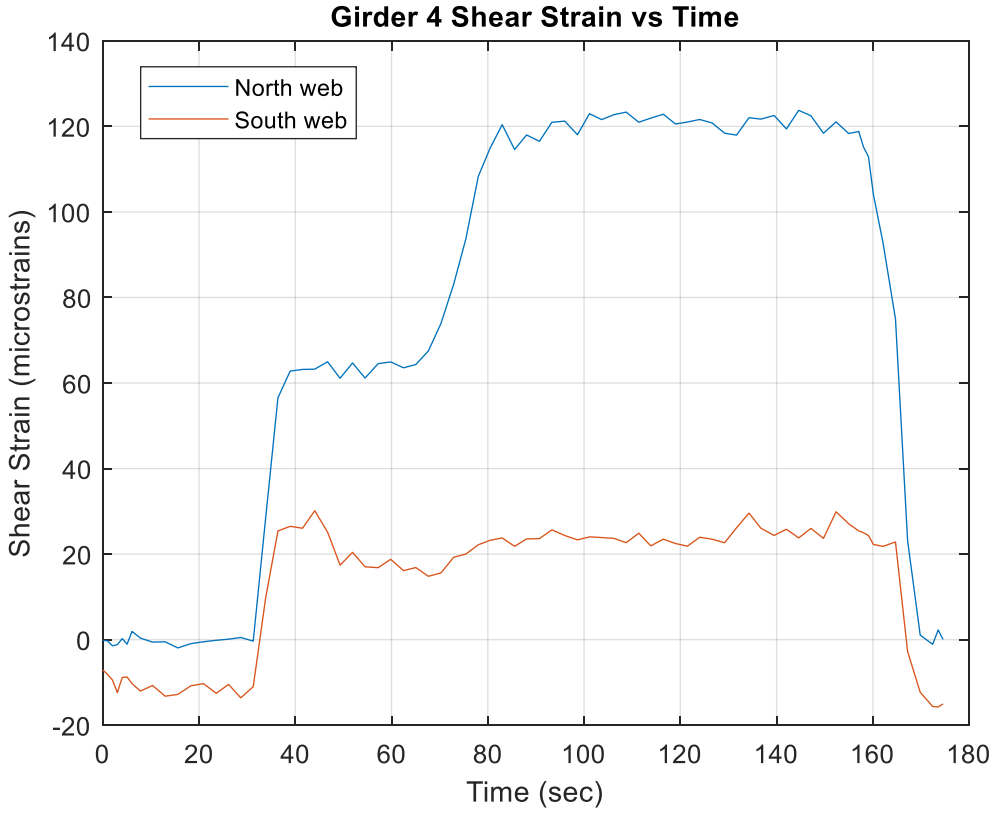
Girder 4 Shear Strain vs Time
North web
South web
Shear Strain (microstrains)
Time (sec)
140
120
100
80
60
40
20
0
-20
0
20
40
60
80
100
120
140
160
180

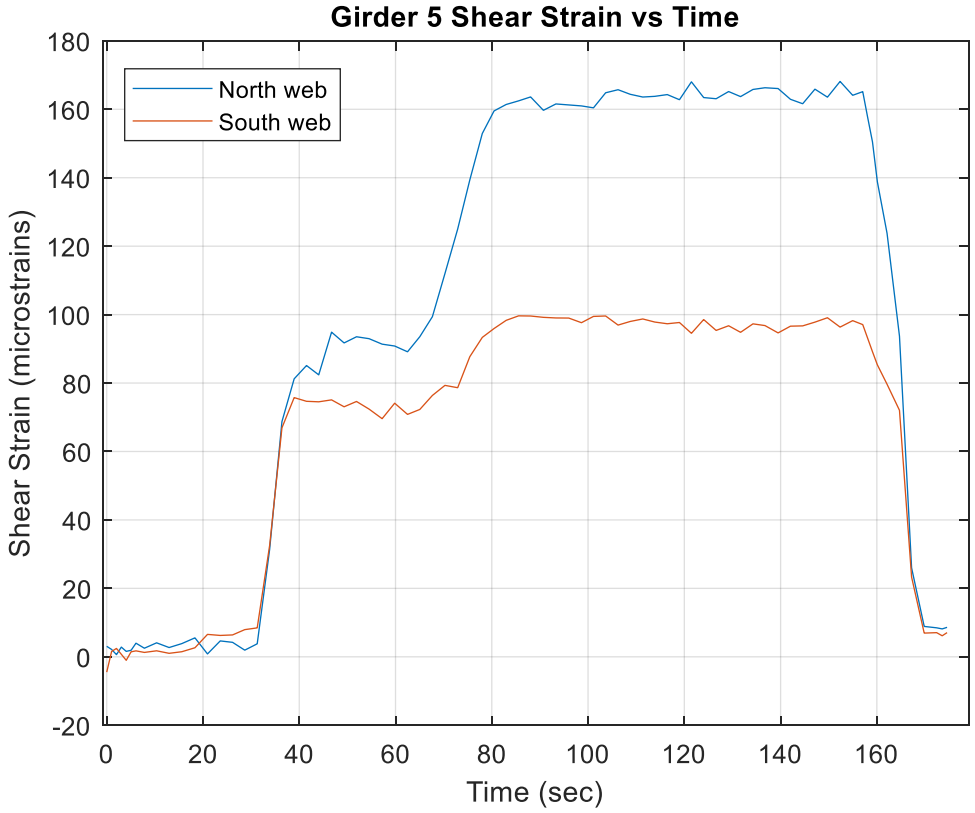
Girder 5 Shear Strain vs Time
North web
South web
Shear Strain (microstrains)
Time (sec)
180
160
140
120
100
80
60
40
20
0
-20
0
20
40
60
80
100
120
140
160

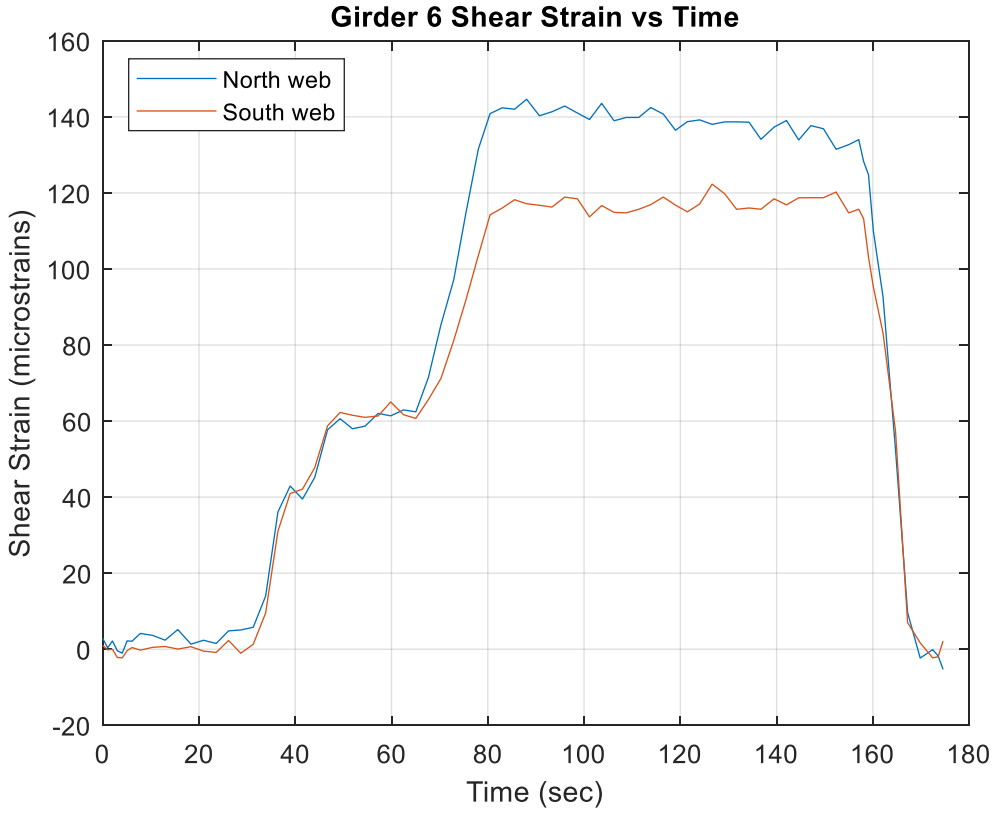
Girder 6 Shear Strain vs Time
North web
South web
Shear Strain (microstrains)
Time (sec)
160
140
120
100
80
60
40
20
0
-20
0
20
40
60
80
100
120
140
160
180

A.3.3.5 V22 Test

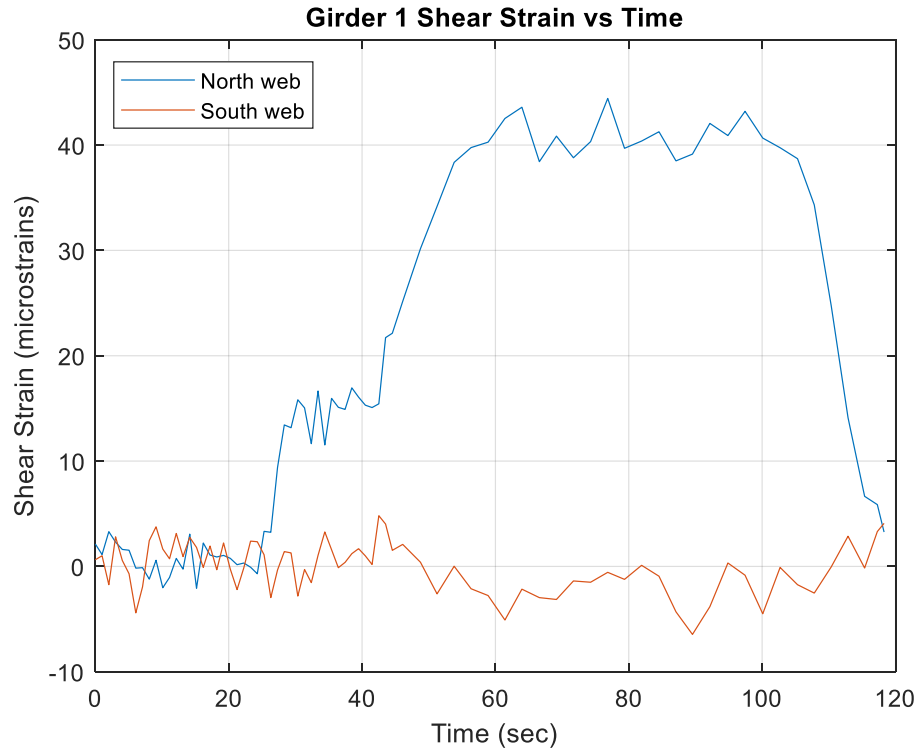

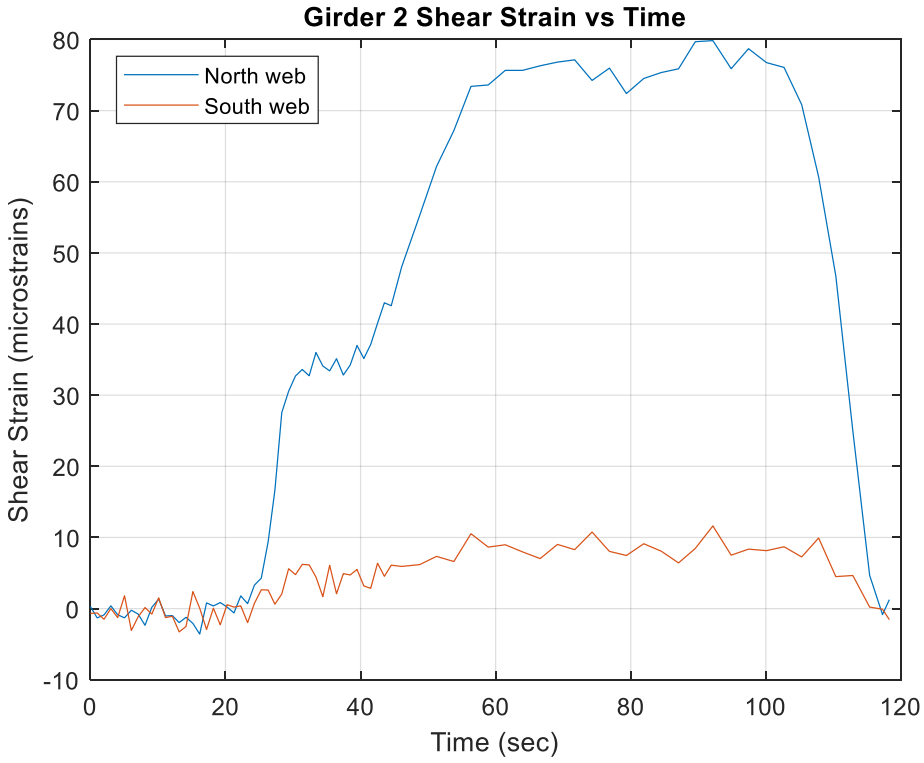

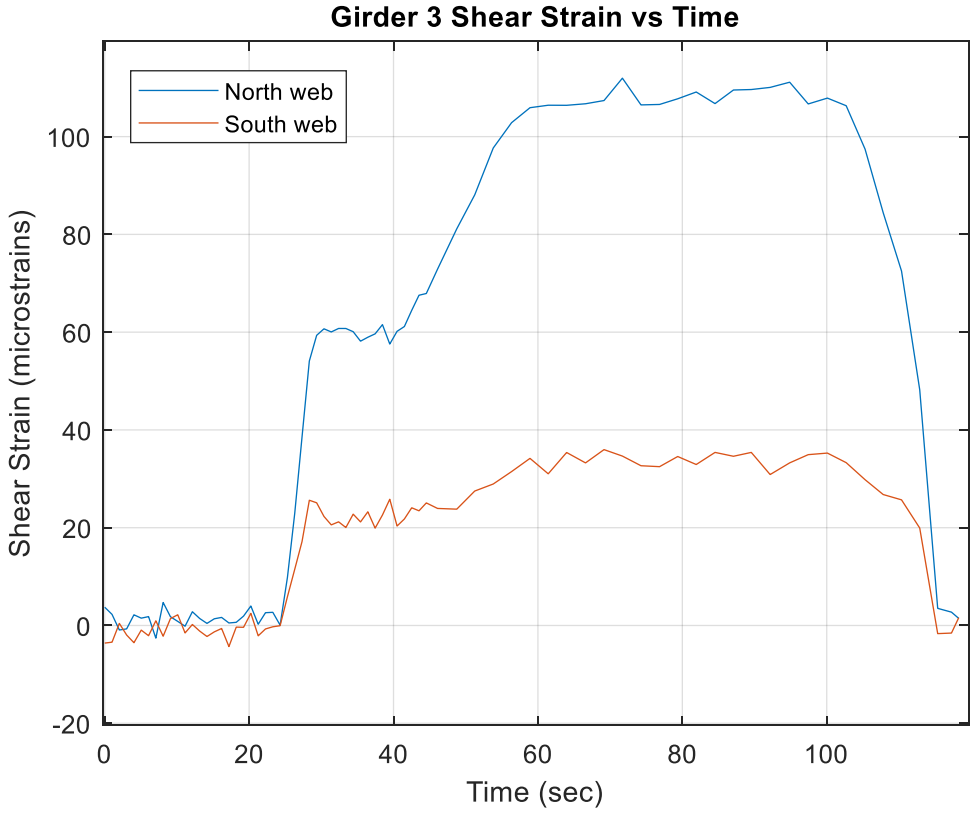
Girder 3 Shear Strain vs Time
North web
South web
Shear Strain (microstrains)
Time (sec)
-20
0
20
40
60
80
100
0
20
40
60
80
100

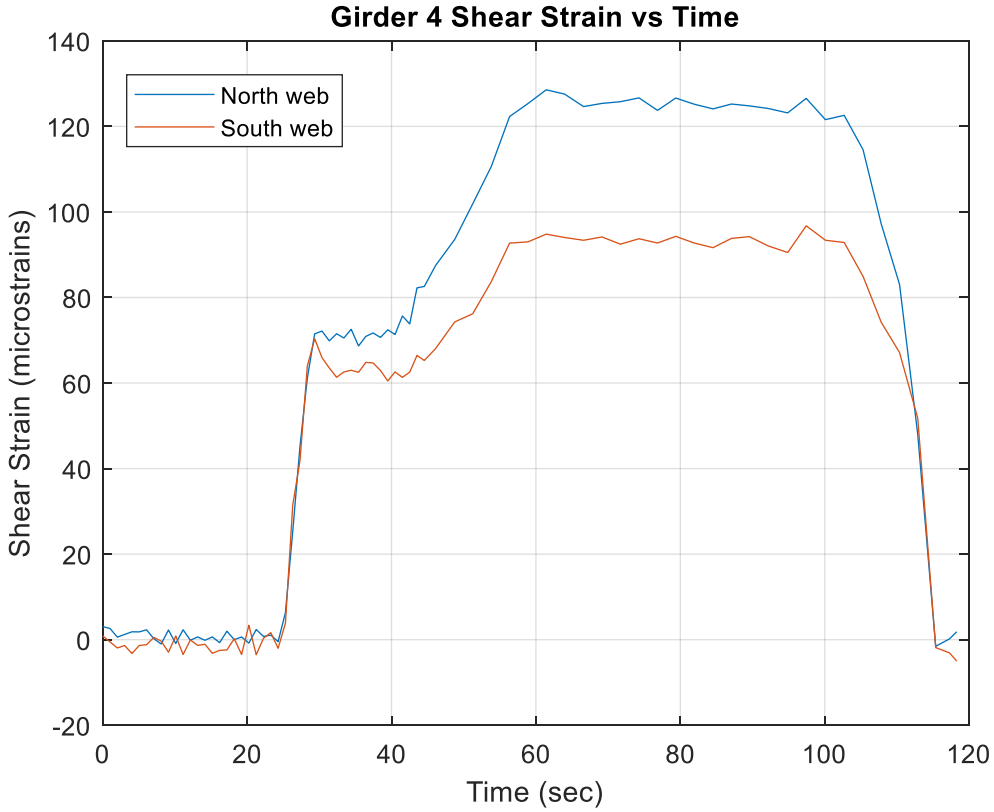
Girder 4 Shear Strain vs Time
North web
South web
Shear Strain (microstrains)
Time (sec)
-20
0
20
40
60
80
100
120
140
0
20
40
60
80
100
120

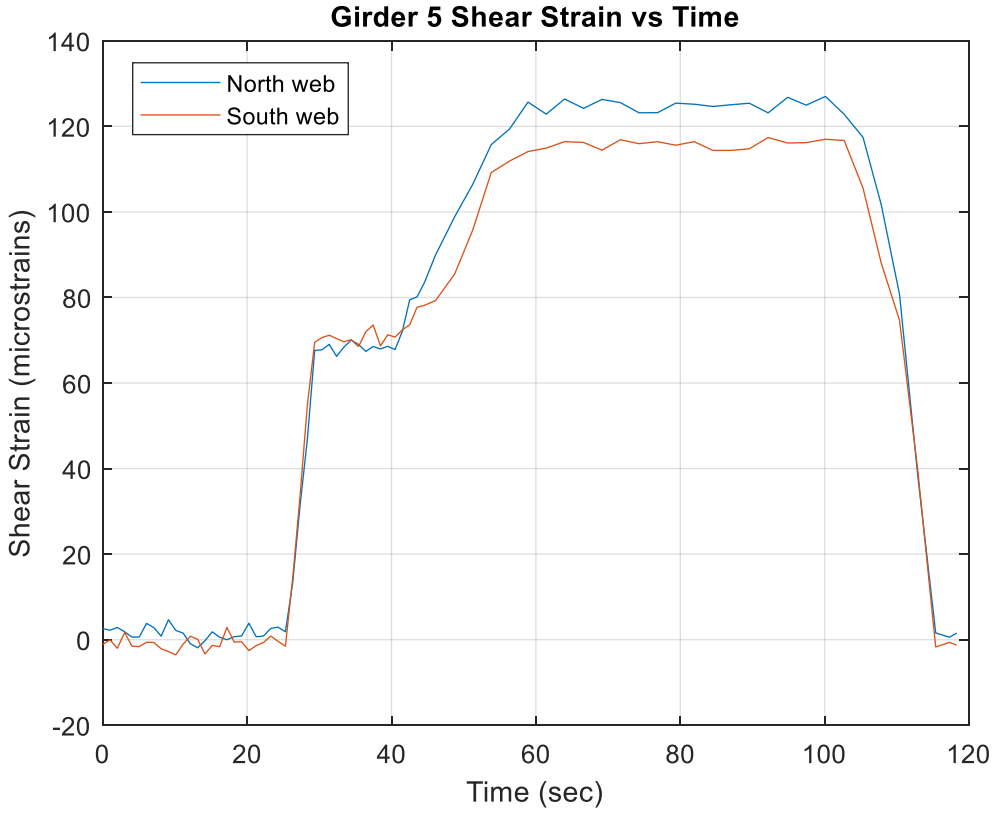
Girder 5 Shear Strain vs Time
North web
South web
Shear Strain (microstrains)
Time (sec)
140
120
100
80
60
40
20
0
-20
0
20
40
60
80
100
120

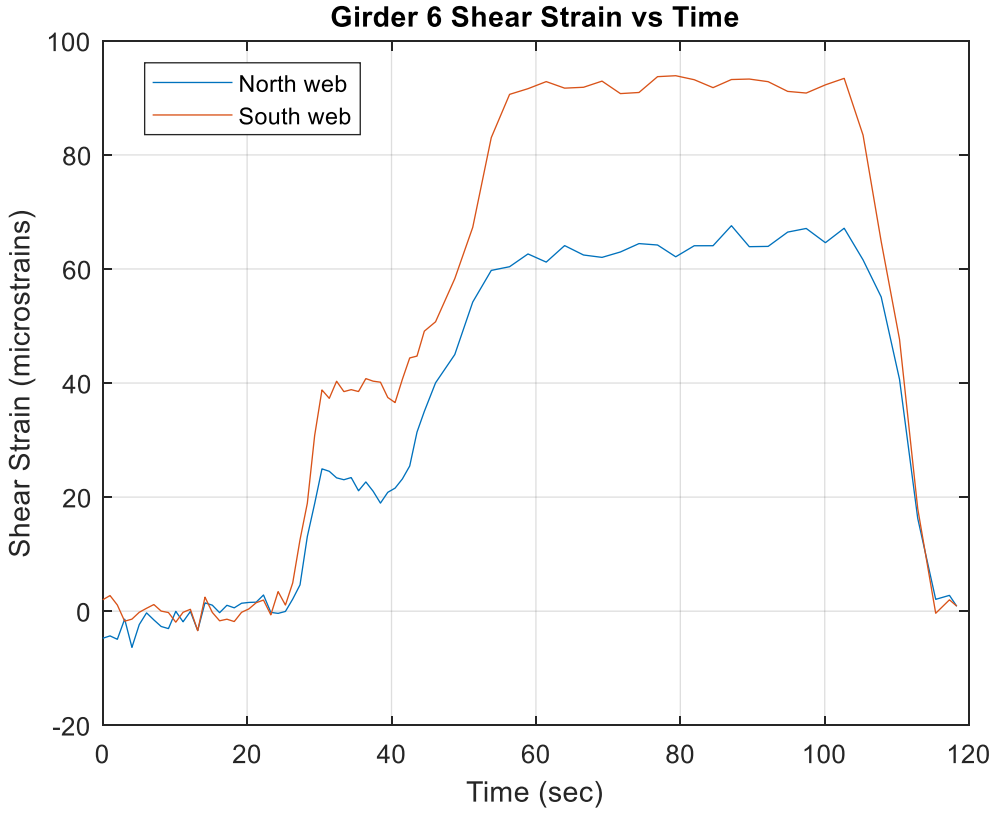
Girder 6 Shear Strain vs Time
North web
South web
Shear Strain (microstrains)
Time (sec)
100
80
60
40
20
0
-20
0
20
40
60
80
100
120

A.3.3.6 V23 Test

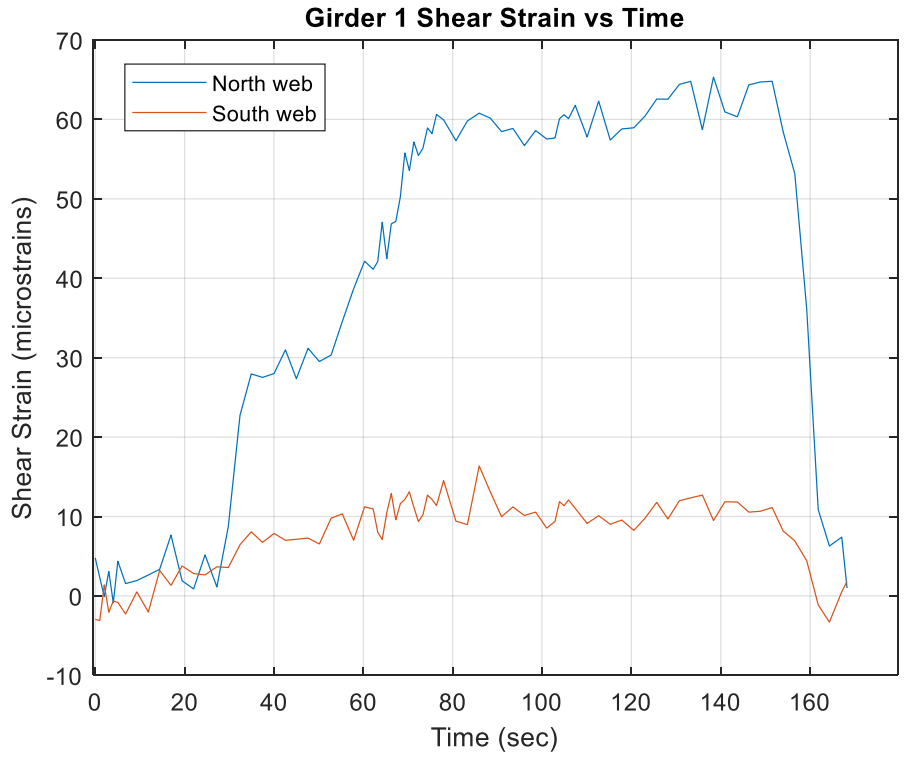

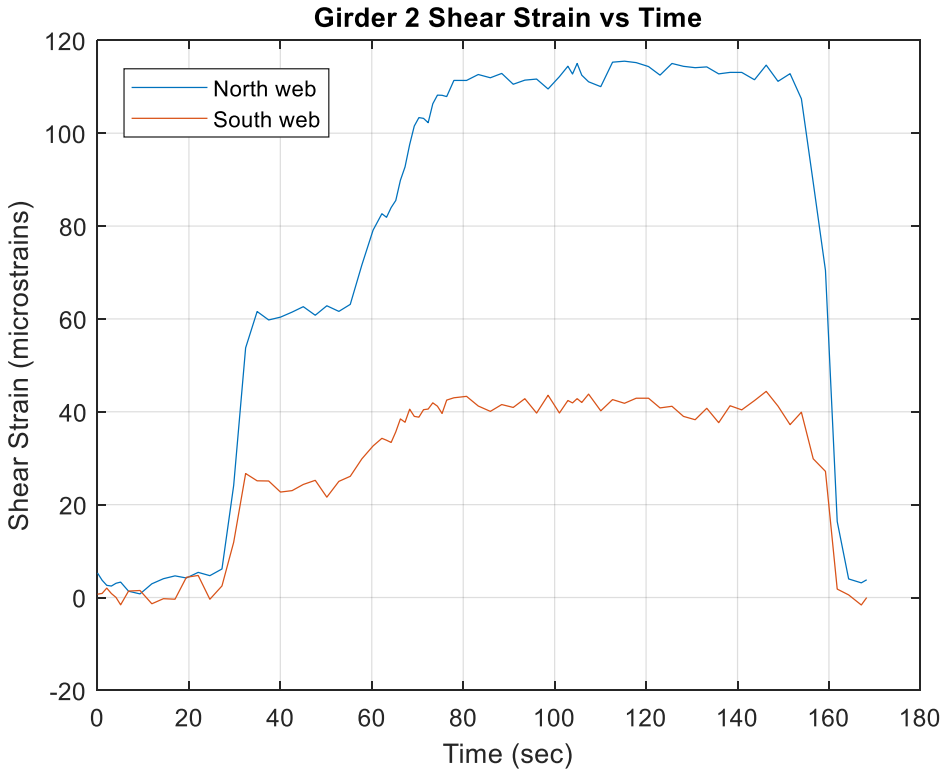

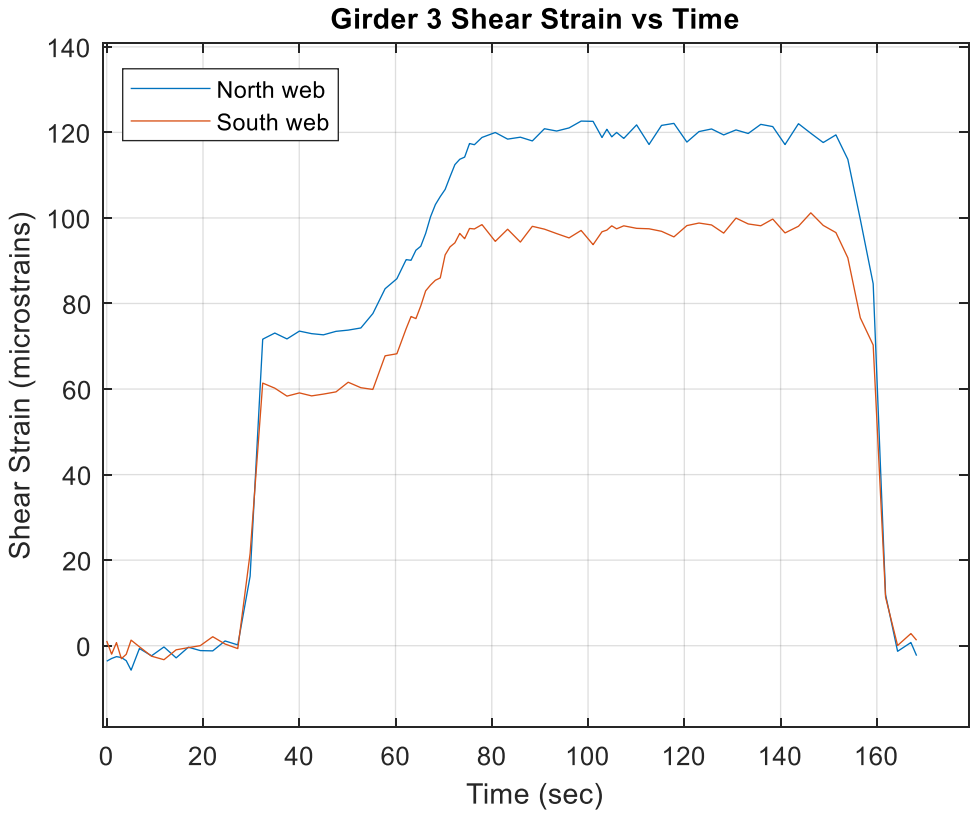
Girder 3 Shear Strain vs Time
North web
South web
Shear Strain (microstrains)
Time (sec)
140
120
100
80
60
40
20
0
0
20
40
60
80
100
120
140
160

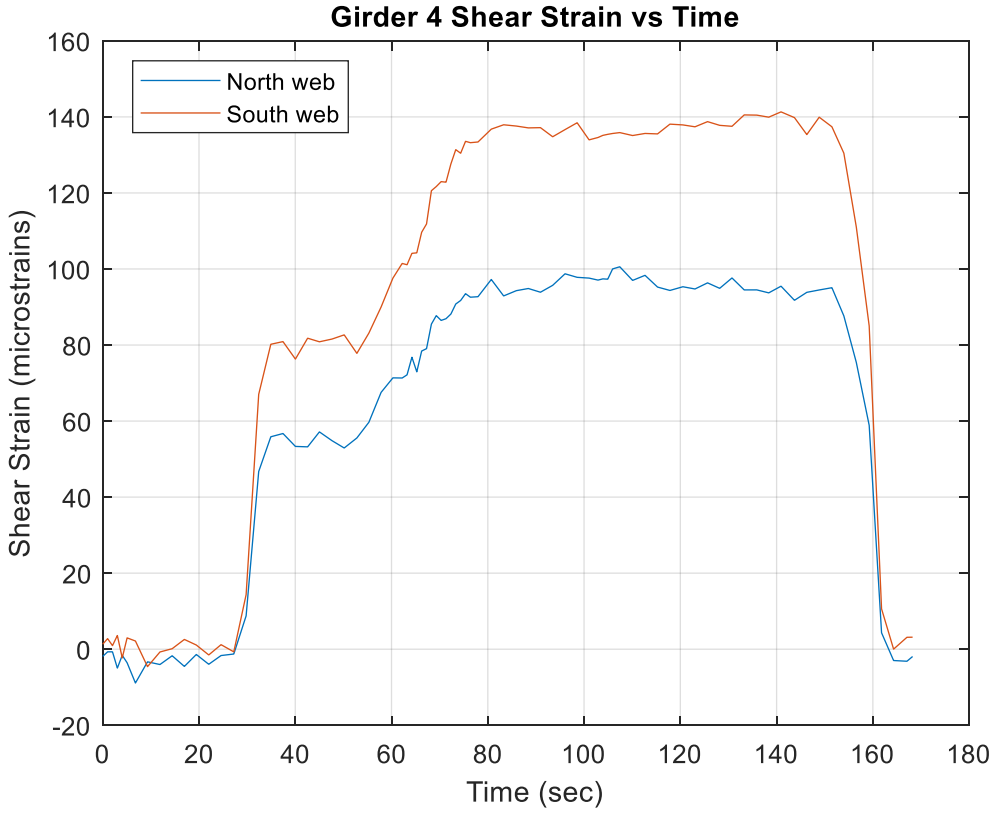
Girder 4 Shear Strain vs Time
North web
South web
Shear Strain (microstrains)
Time (sec)
160
140
120
100
80
60
40
20
0
-20
0
20
40
60
80
100
120
140
160
180

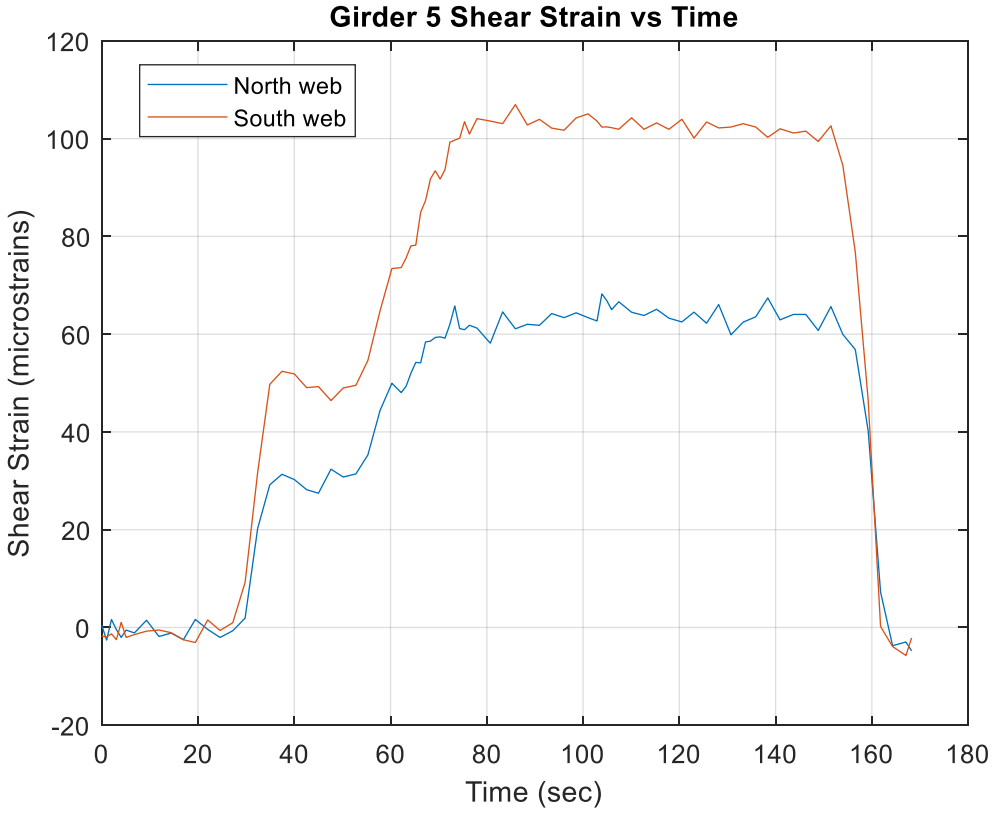
Girder 5 Shear Strain vs Time
North web
South web
Shear Strain (microstrains)
Time (sec)
120
100
80
60
40
20
0
-20
0
20
40
60
80
100
120
140
160
180

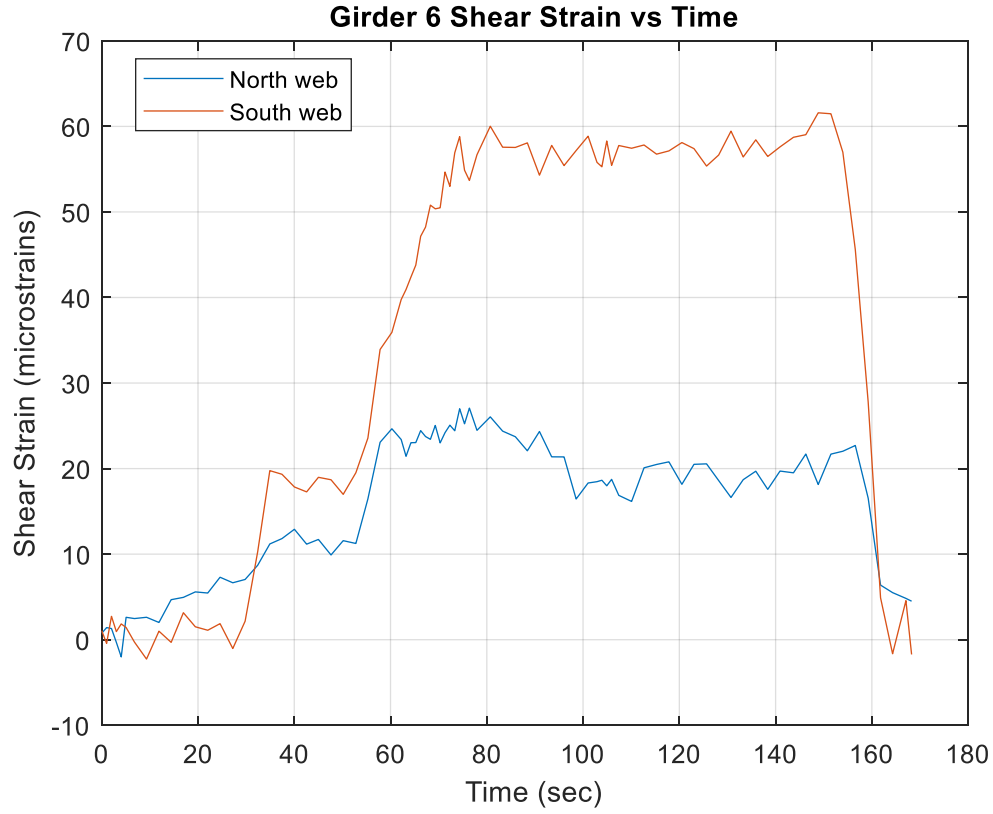
Girder 6 Shear Strain vs Time
North web
South web
Shear Strain (microstrains)
Time (sec)
70
60
50
40
30
20
10
0
-10
0
20
40
60
80
100
120
140
160
180

A.3.3.7 V24 Test

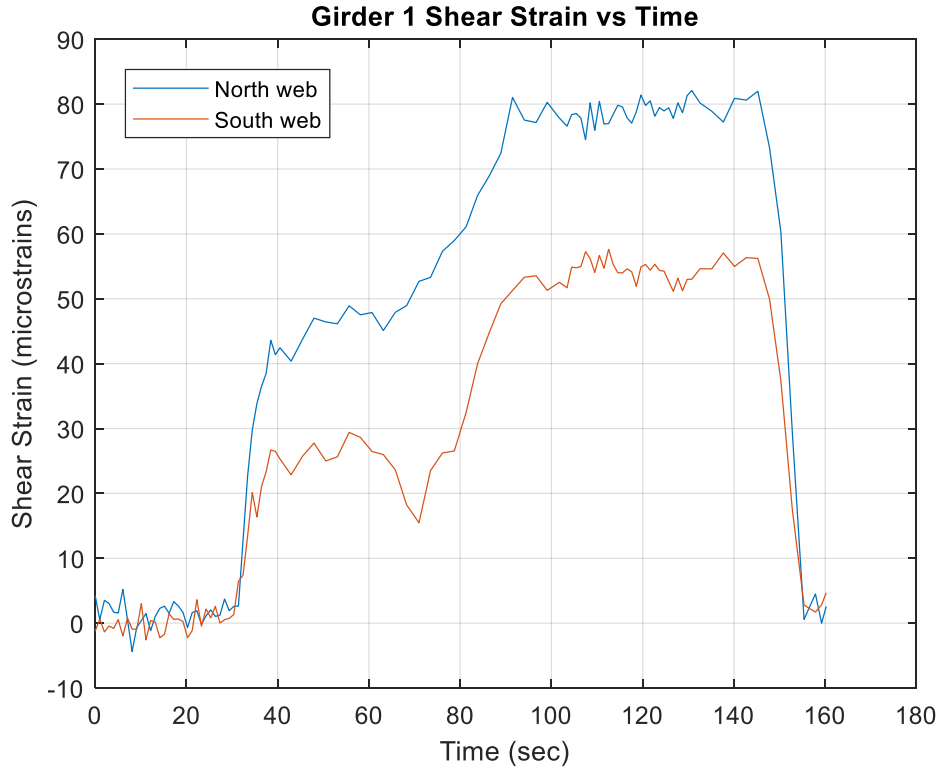

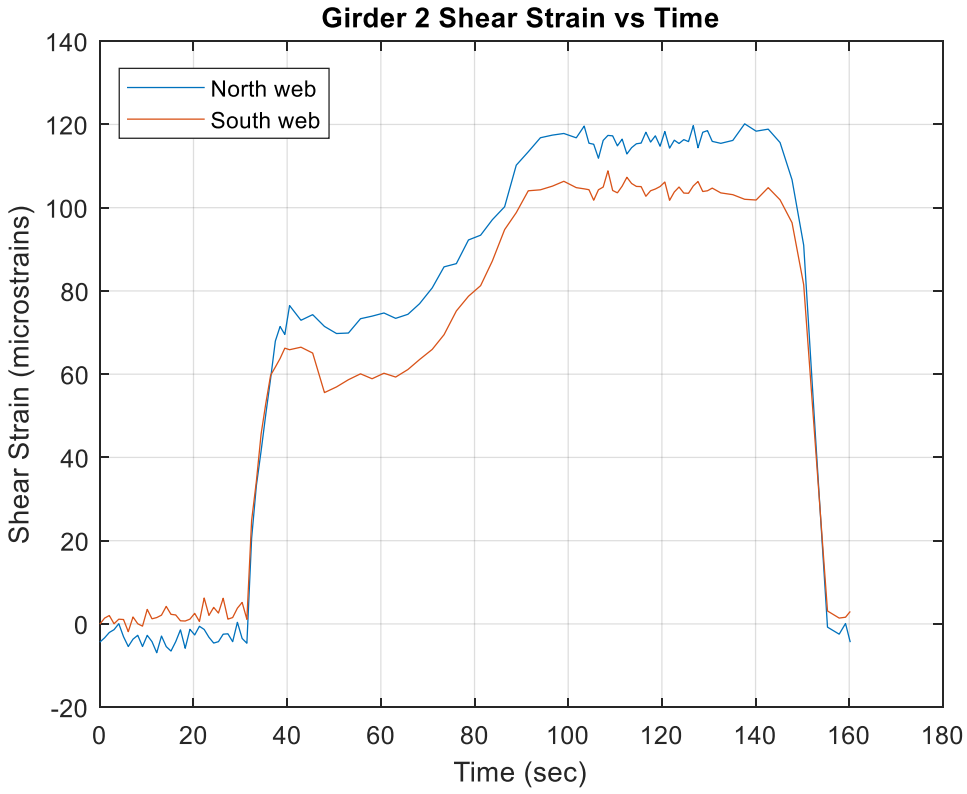

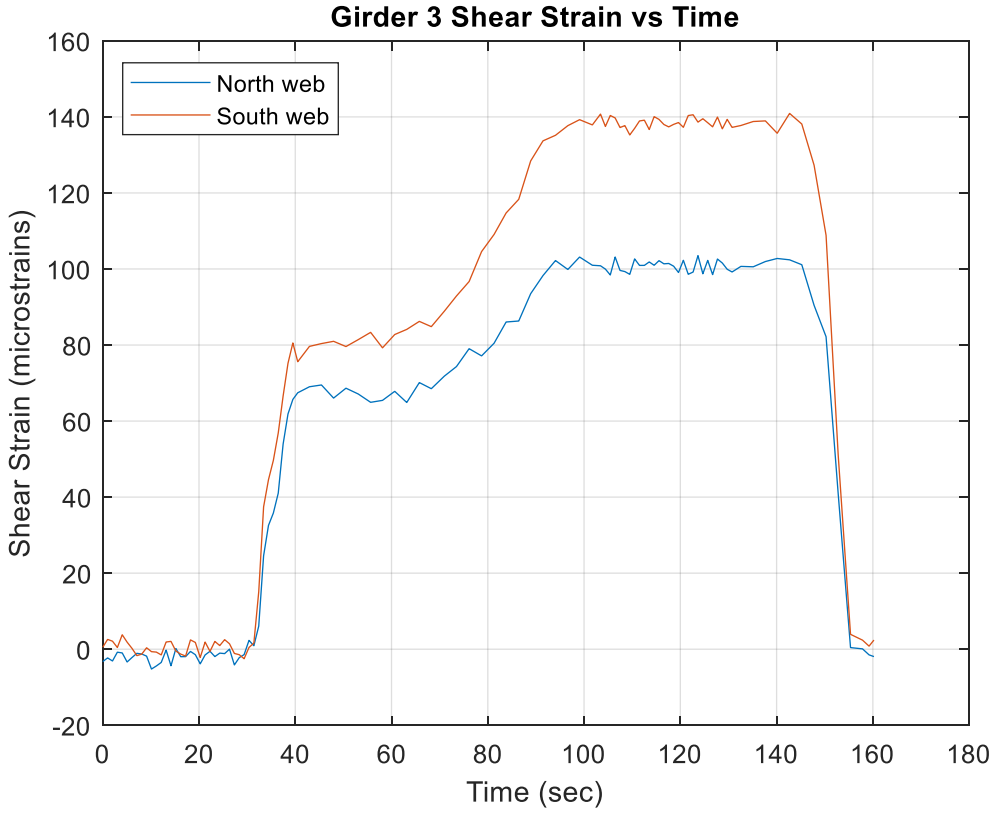
Girder 3 Shear Strain vs Time
North web
South web
Shear Strain (microstrains)
Time (sec)
160
140
120
100
80
60
40
20
0
-20
0
20
40
60
80
100
120
140
160
180

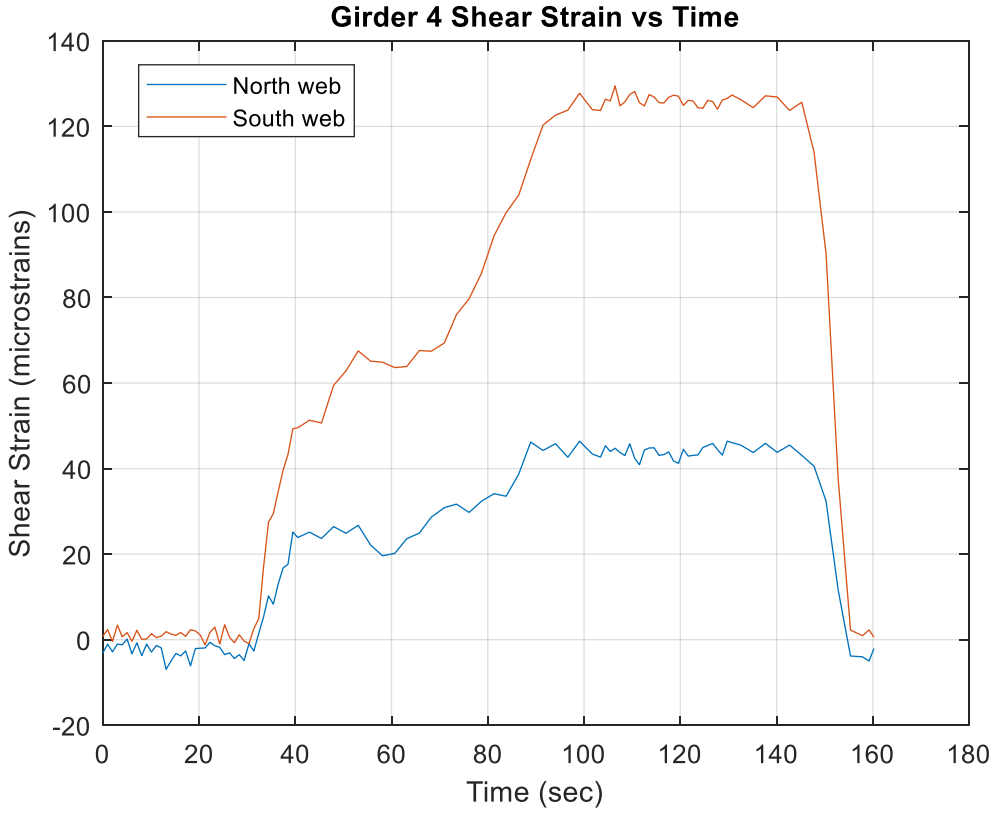
Girder 4 Shear Strain vs Time
North web
South web
Shear Strain (microstrains)
Time (sec)
140
120
100
80
60
40
20
0
-20
0
20
40
60
80
100
120
140
160
180

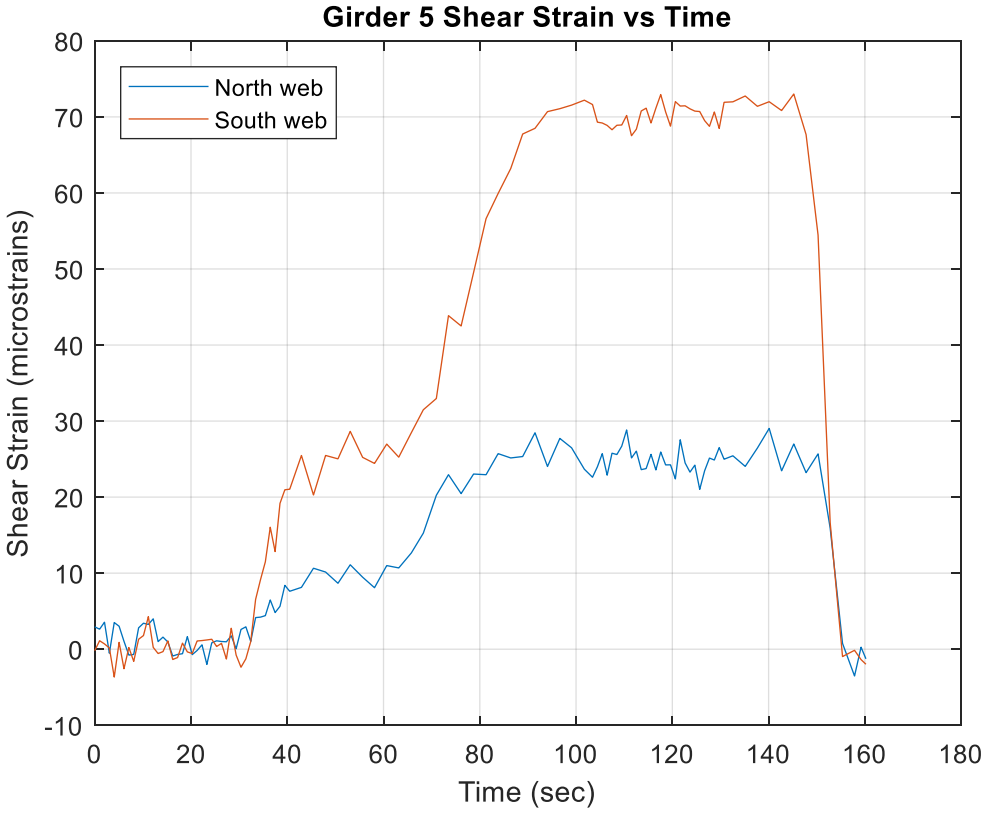
Girder 5 Shear Strain vs Time
North web
South web
Shear Strain (microstrains)
Time (sec)
80
70
60
50
40
30
20
10
0
-10
0
20
40
60
80
100
120
140
160
180

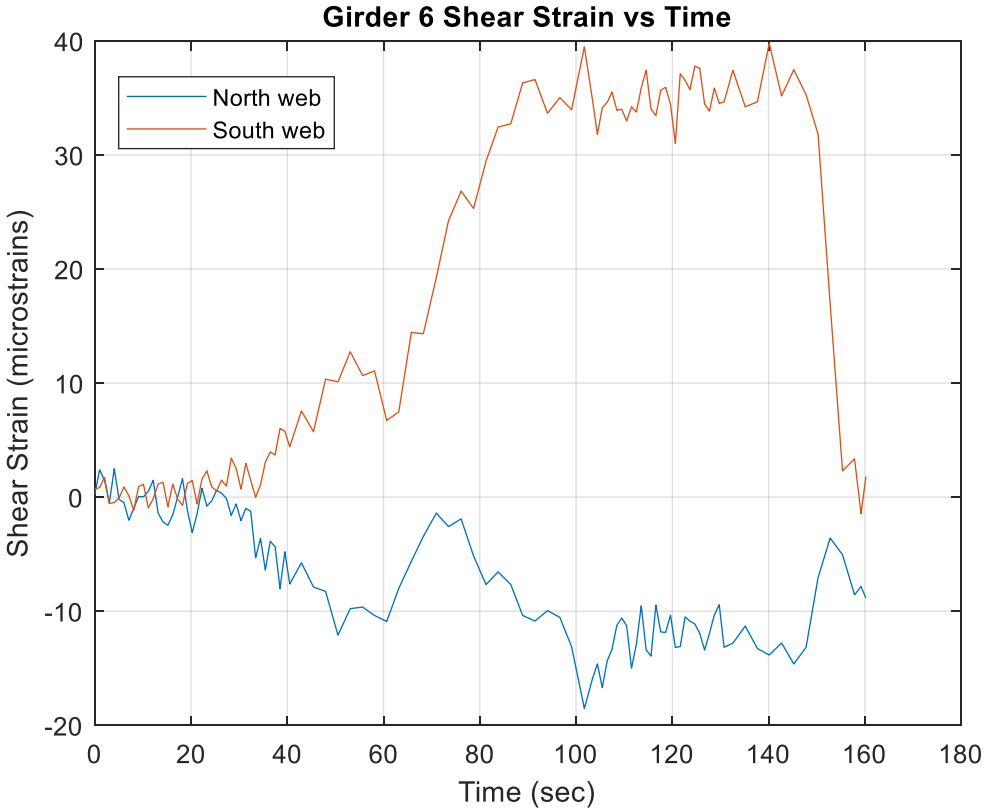
Girder 6 Shear Strain vs Time
North web
South web
Shear Strain (microstrains)
Time (sec)
40
30
20
10
0
-10
-20
0
20
40
60
80
100
120
140
160
180

A.3.3.8 V25 Test

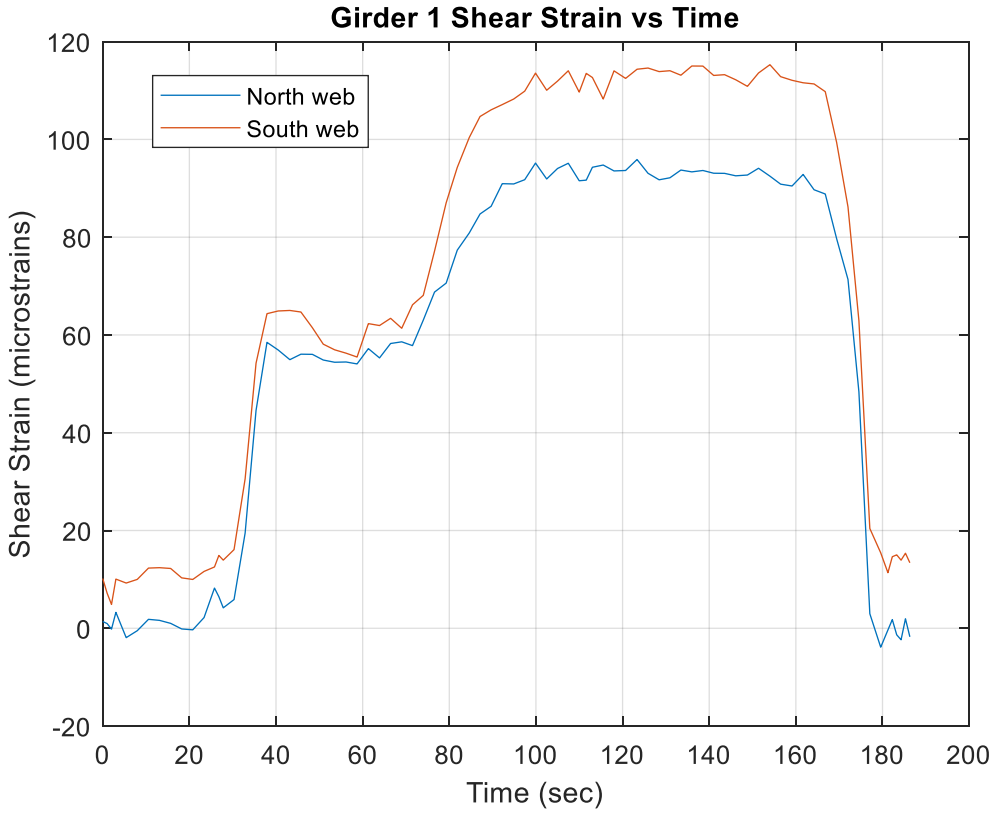

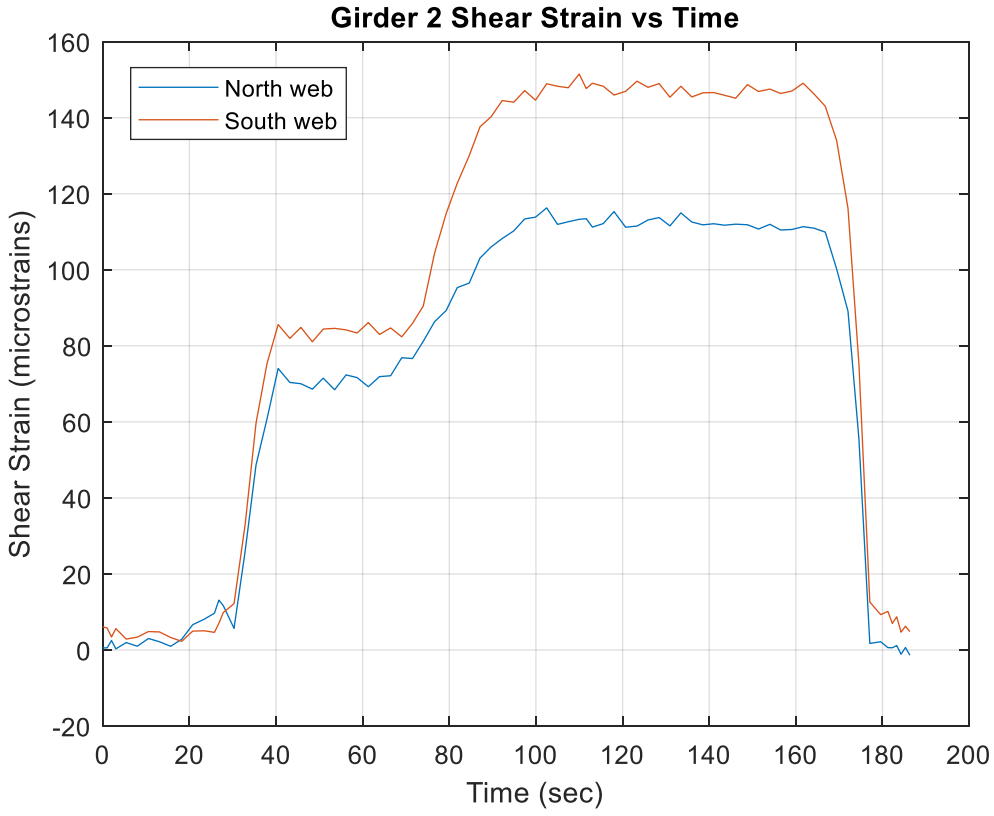

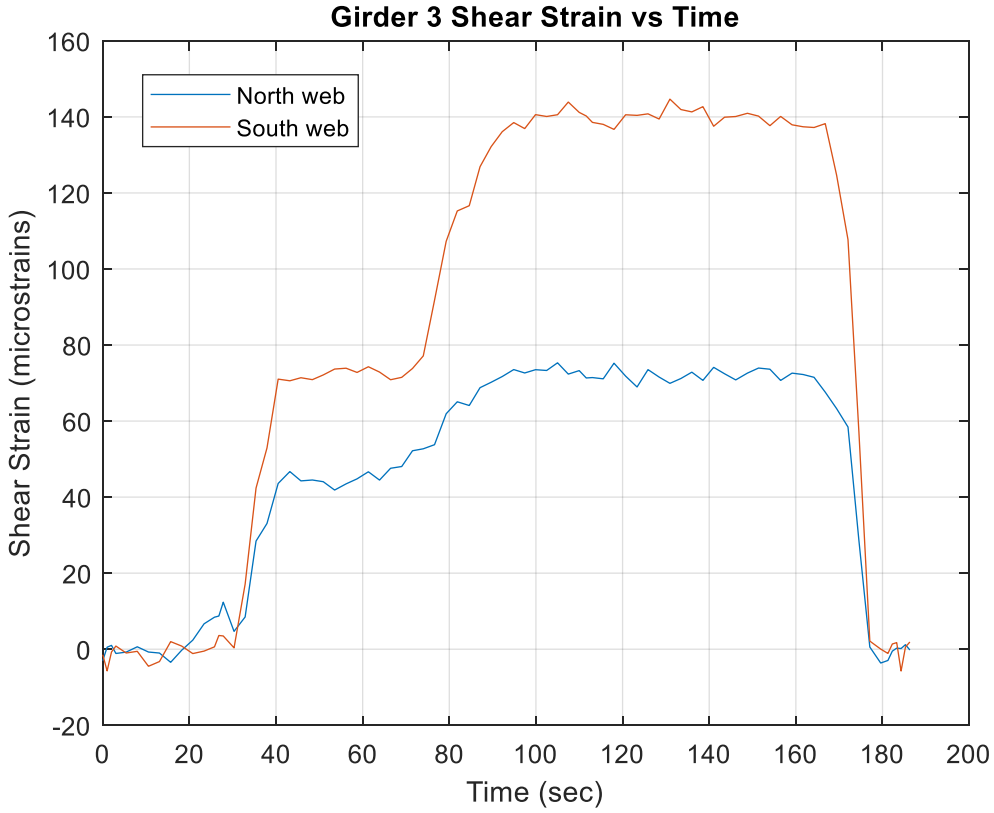
Girder 3 Shear Strain vs Time
North web
South web
Shear Strain (microstrains)
Time (sec)
160
140
120
100
80
60
40
20
0
-20
0
20
40
60
80
100
120
140
160
180
200

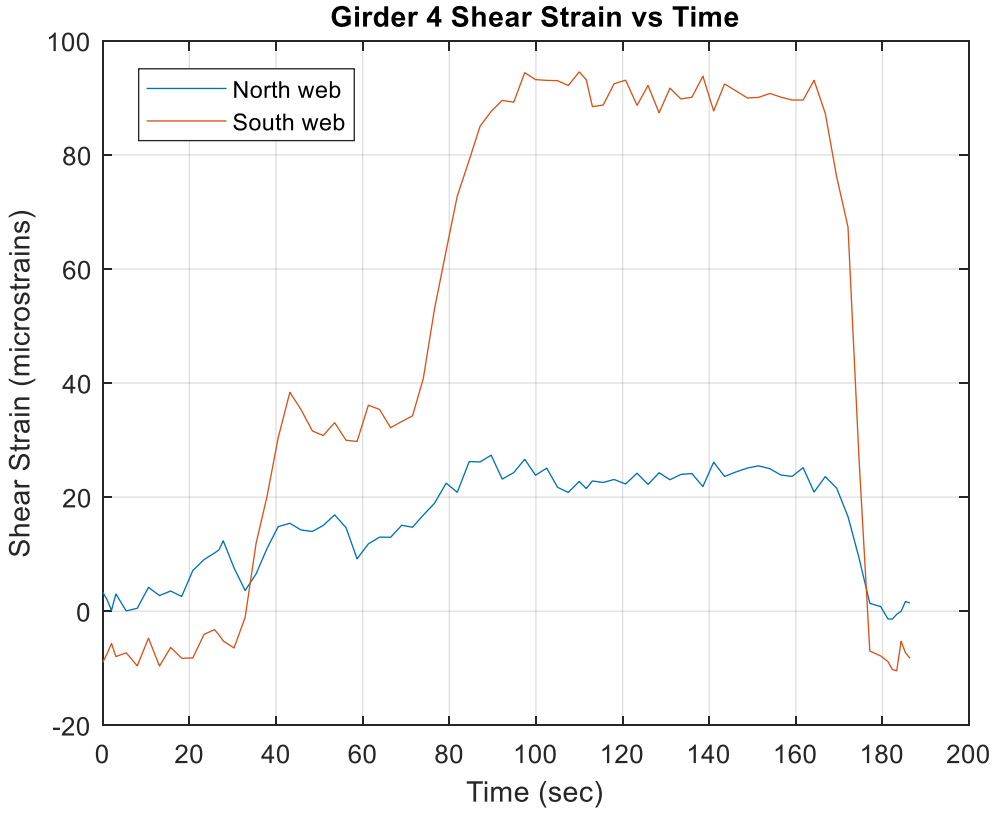
Girder 4 Shear Strain vs Time
North web
South web
Shear Strain (microstrains)
Time (sec)
100
80
60
40
20
0
-20
0
20
40
60
80
100
120
140
160
180
200

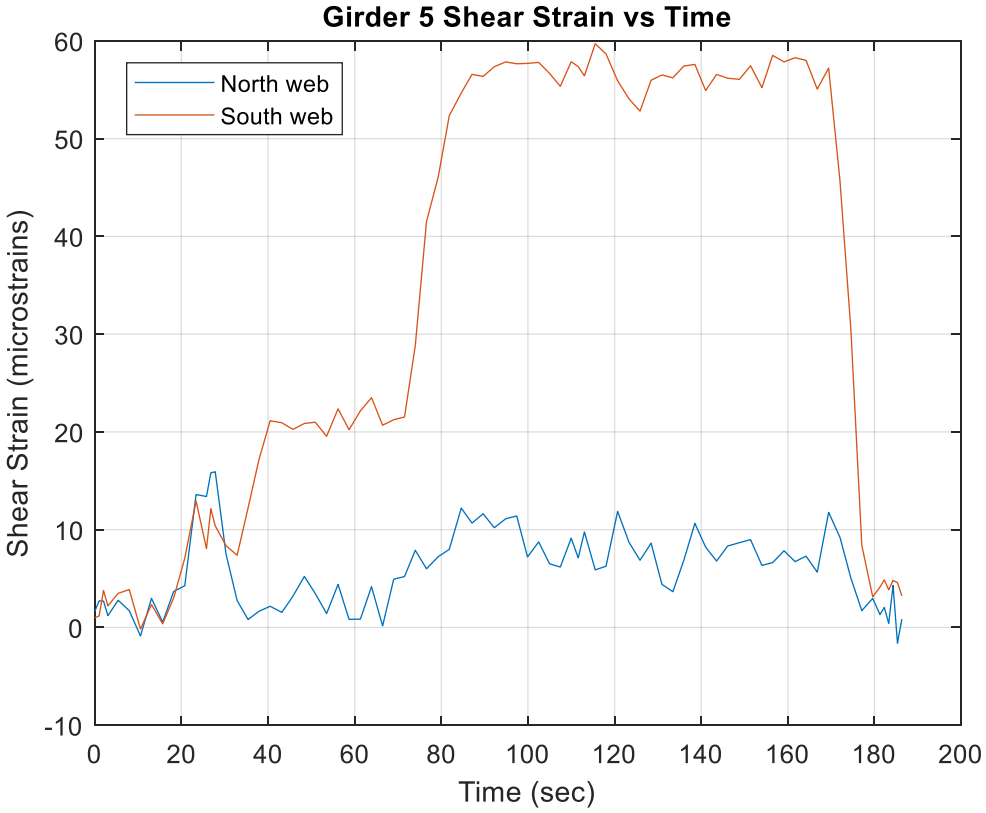
Girder 5 Shear Strain vs Time
North web
South web
Shear Strain (microstrains)
Time (sec)
60
50
40
30
20
10
0
-10
0
20
40
60
80
100
120
140
160
180
200

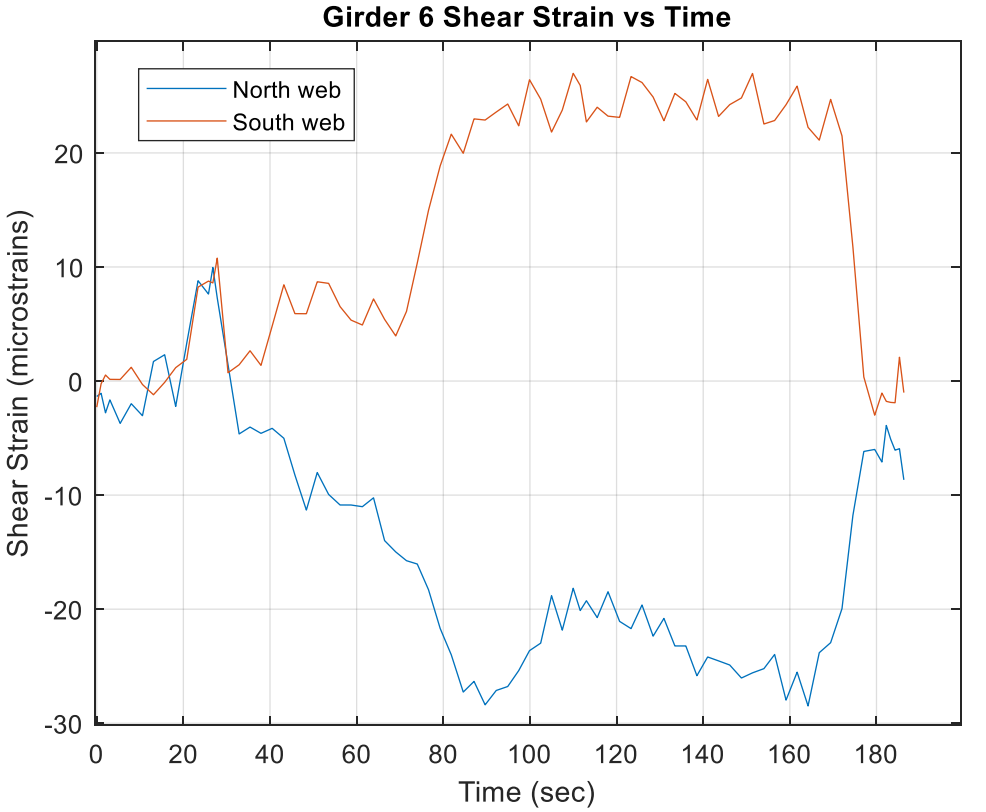
Girder 6 Shear Strain vs Time
North web
South web
Shear Strain (microstrains)
Time (sec)
20
10
0
-10
-20
-30
0
20
40
60
80
100
120
140
160
180

Appendix B: Girder Design Scripts and Functions

4/11/24 11:53 AM C:\Users\JonPinkham\Doc...\buildgirder2.m 1 of 4

```
function girder= buildgirder2(parameters)
% JP 2022 This function combines numerous functions to build the girder
% cross section based on a number of parameters and design criteria per the
% guidelines created for these girders
%% Declare Global coordinates, will be the constants so no need to use as inputs in other functions
global  Etf ttf tcore Ec S L tdeck d phi Ng fcc theta overhang bbf inp EIb
% make input structure
inp=struct;
%% Constants for the design
%Concrete compressive strength
fcc=4; %units ksi assumed constant (typical in previous designs)
% Moduli ksi from CBM paper
Etf= 3930;
Ec=1820*sqrt(fcc); % AASHTO equationfopr concrete modulus
f6w=10*0.65*0.85; % ksi web shear strength with reduction factors

%Thicknesses in
ttf= 1; % assumed constant (typical in previous designs)
%Splay Angle degrees
phi=5; % assumed constant (typical in previous designs)

%Pull variables from the parameters matrix and solve for d of girder
L=parameters(:,1)*12;%units of in
Ltod=parameters(:,2); %span to depth ratio for total depth
S=parameters(:,3)*12; % units of inches spacing
tdeck=parameters(:,4); %deck thickness units of inches
dtot=L/Ltod; %units of inches total depth of girder and deck
d=dtot-tdeck; %units of inches girder depth
Ng=parameters(:,5); % number of girders
theta= parameters(:,6);
overhang=parameters(:,7)*12; %units of inches
% Core thicnkess of web set to 0 in moment beam models (get same EI to
% apply to beam in model)
tcore=0; % not including core in design, Web is scrictly facesheets
% Core thickness for Shear model uncomment this section and comment out the
% section above
% set the thickness of the core from AIT guidance
% if d<= 30
%     tcore=0.75;
% else
%     tcore=1.5;
% end
%% Get Liove loads will not change they're based on the length
[LMu,LVu,Ldisp] = LiveLoads;
[gmint,gsint] = g;

%% First Check deflection capacity met
n=0;
j=4;
[tw] =Eweb(j);
```

```
[tbf] = Ebot(n,16);
disp=100; %initial displacement to enter the loop
while disp>L/1000
    n=n+1;% increasing bottom flange thickness
    [tbf] = Ebot(n,16);
    [Lw,Afrp] = FRPdim(tw,tbf);
    [~,~,~,~,Ictot,~,Qint,~,~] = TSA(tbf,tw, Lw);
    disp=Ldisp/EIb;
end

%% Check shear capacity
[DMunc,~,DVuc,~,~,~,~] = DeadLoads(Afrp);
Vu=gsint*LVu+DVuc;
Vr=0.75*Ictot*2*(tw-tcore)*f6w/Qint;
while Vr < Vu
    j=j+4;
    [tw] =Eweb(j);
    [tbf] = Ebot(n,16);
    [Lw,Afrp] = FRPdim(tw,tbf);
   [~,~,~,~,Ictot,~,Qint,~,~] = TSA(tbf,tw, Lw);
    [DMunc,~,DVuc,~,~,~,~] = DeadLoads(Afrp);
    Vu=gsint*LVu+DVuc;
    Vr=0.75*Ictot*2*(tw-tcore)*f6w/Qint;
end

%% Cheack Web Shear Buckling

[Nxy] = buckling2(Lw,tw);
Vrbuck=0.35*Nxy*Lw;
while Vrbuck<Vu
    j=j+4;
    [tw] =Eweb(j);
    [tbf] = Ebot(n,16);
    [Lw,Afrp] = FRPdim(tw,tbf);
    [DMunc,~,DVuc,~,~,~,~] = DeadLoads(Afrp);
    Vu=gsint*LVu+DVuc;
    [Nxy] = buckling2(Lw,tw);
    Vrbuck=0.35*Nxy*Lw;
end
%% Recheck deflection and flexure can the bf thickness decrease
%% any since tw increased and so did EI?
[Lw,Afrp] = FRPdim(tw,tbf);
 [~,~,~,~,~,~,~,~,~,~] = TSA(tbf,tw, Lw);
disp=Ldisp/EIb;
while disp<L/1000
    n=n-1;
    [tbf] = Ebot(n,16);
    [tw] =Eweb(j);
    [Lw,Afrp] = FRPdim(tw,tbf);
    [~,~,~,~,Ictot,~,Qint,~,~] = TSA(tbf,tw, Lw);
    [DMunc,~,DVuc,~,~,~,~] = DeadLoads(Afrp);
```

```
    [Nxy] = buckling2(Lw,tw);
    Vrbuck=0.35*Nxy*Lw;
    Vu=gsint*LVu+DVuc;
    Vr=0.75*Ictot*2*(tw-tcore)*f6w/Qint;
    if Vr>Vu && Vrbuck>Vu
    disp=Ldisp/EIb;
    else
        n=n+1;
        [tbf] = Ebot(n,16);
        break
    end
end

while disp>L/1000
   n=n+1;
   [tbf] = Ebot(n,16);
    [Lw,Afrp] = FRPdim(tw,tbf);
    [~,~,~,~,~,~,~,~,~] = TSA(tbf,tw, Lw);
    disp=Ldisp/EIb;
end


%% Check flexure capacity for both non composite and composite
% First non composite
[~,Inctot,ync,~,~,~,~,ntf,nbf] = TSA(tbf,tw, Lw);
[Mrnc] = flexurenc(Inctot,ync,nbf,ntf);
while Mrnc <= DMunc
   n=n+1;
   [tbf] = Ebot(n,16);
   [Lw,Afrp] = FRPdim(tw,tbf);
   [~,Inctot,ync,~,~,~,~,ntf,nbf] = TSA(tbf,tw, Lw);
    [Mrnc] = flexurenc(Inctot,ync,nbf,ntf);
    [DMunc,~,~,~,~,~,~] = DeadLoads(Afrp);
end

%second flexure composite section using moment curvature
[DMunc,DMuc,~,~,~,~,~] = DeadLoads(Afrp);
[EInc,~,ync,~,~,~,~,~,~] = TSA(tbf,tw, Lw);
Mfail = moment_curvature(tw,tbf,DMunc,EInc,ync);
Mu=gmint*LMu+DMuc;

while 0.75*Mfail <= Mu
    n=n+1;
    [tbf] = Ebot(n,16);
    [~,Afrp] = FRPdim(tw,tbf);
    [DMunc,DMuc,~,~,~,~,~] = DeadLoads(Afrp);
    [EInc,~,ync,~,~,~,~,~,~] = TSA(tbf,tw, Lw);
    Mfail = moment_curvature(tw,tbf,DMunc,EInc,ync);
    Mu=gmint*LMu+DMuc;
end
```

```
Gfs=1.5501e3; %G of web facesheets +-45 glass plies units ksi
%% final build of inp data structure with corresponding lamina properties
[tbf] = Ebot(n,16);
[ttf] = Etopf;
[tw] =Eweb(j);
TWg=bbf+2*(6.5+Lw*tand(5)-tw/cosd(5));

inp.w.tw=tw;
inp.w.Lw=Lw;
inp.dfrp=d;
inp.bf.tbf=tbf;
inp.bf.bbf=bbf;
inp.tf.ttf=1;
inp.tf.btf=13;
inp.girder.Gg=Gfs;
inp.girder.Twg=TWg;
inp.j=j;
inp.n=n;
girder=inp;
```



```
function [Lw,Afrp] = FRPdim(tw,tbf)
% JP 2022 This function will take the thicknesses of girder parts and the
% depth to determine girder dimensions such as area, length of web and
% different widths
global ttf d phi bbf btf L
btf=13; %units of inches will be constant for all girder cross sections 6.5 in per side
Lw=(d-tbf-ttf)/cosd(phi);
if L>=0 && L<60*12
    bbf=12;
elseif L>=60*12 && L<=80*12
    bbf=24;
elseif L> 80*12
    bbf=36;
end
Afrp= ttf*btf+tbf*bbf+2*Lw*tw;
```

```
function [DMunc,DMuc,DVuc,DMucx,DMuncx,DVucx,Ddisp] = DeadLoads(Afrp)
% JP 2022 This function finds the displacement at midspan, max shear, and
% max midspan moment due to dead loads with load factors applied
% Dead load types units lb/in structural and non structural
global L S tdeck Ng overhang
DCnc=115.6/(12^3)*Afrp+150/(12^3)*tdeck*S;%combination of girder and deck weight as the↙
noncomposite dead load lb/in
DCc=340/Ng/12; %combine 240 plf of curb and railing evenly distributed by all girders↙
units lb/in
DWc=144/(12^3)*S*3; %Dead load of wearing surface assume 3 inches

%% exterior dead loads
DCncx=115.6/(12^3)*Afrp+150/(12^3)*tdeck*(S/2+overhang);
DWcx= 144/(12^3)*(S/2+overhang)*3;

%% Moments structural and non structural components
DMDWc=(DWc*L^2/8)/1000; %units in-kips
DMDCnc=(DCnc*L^2/8)/1000; %units in-kips
DMDCc=((DCc)*L^2/8)/1000; %units in-kips
DMDCx=((DCc)*L^2/8)/1000;
DMDWcx=(DWcx*L^2/8)/1000;
DMDCncx=(DCncx*L^2/8)/1000;
%% Moment combinations using
DMunc=1.25*DMDCnc; %units in-kips
DMuc=1.25*DMDCc+1.5*DMDWc;%units in-kips
DMucx=1.25*DMDCx+1.5*DMDWcx;
DMuncx=1.25*DMDCncx;
%% Shears
VDCc= ((DCnc+DCc)*L/2)/1000; %units kips
VDWc= (DWc*L/2)/1000; %units kips
VDCx=((DCncx+DCc)*L/2)/1000;
VDWx=(DWcx*L/2)/1000;

%% Shear Combinations
DVuc= 1.25*VDCc+1.5*VDWc; %Units kips
DVucx=1.25*VDCx+1.5*VDWx; %units kips

%% Midspan Displacement for the unit load on all girders combined
w=((DCnc+DCc+DWc)*(Ng-2)+(DCncx+DCc+DWcx)*2)/1000; %units k/in
Ddisp=(5*w*L^4)/384; %Need to divide by EI still in units of kips*in^3 to get units of in


end
```

```
function [LMu,LVu,Ldisp] = LiveLoads
%JP 2022 Based on the bridge length L (in) the maximum possible live load moment and
%shears (kips-in and kips) are calculated following AASHTO standards using HL-93 and
Tandem
%design trucks
global L
%% Calculate the maximum moment
Mtk1= 32*L/4+40*(L/2-168)/2;
Mtk2= 50*(L/2-24)/2;
Mtrcrit=max(Mtk1,Mtk2);
Mlane=0.64/12*L^2/8;
LMu=(1.33*Mtrcrit+Mlane)*1.75;

%% Calculate the maximum shear
Vtr1=32+32*(L-168)/L+8*(L-336)/L;  %First possible max shear produced by an HL-93 truck
Vtr2=25+25*(L-48)/L; %Max shear produced by the tandem load
Vtrcrit= max(Vtr1,Vtr2); %Finding the critical truck load
Vlane= 0.64/12*L/2;
LVu=(1.33*Vtrcrit+Vlane)*1.75;

%% Midspan Displacement Assumed to be maximum
deltatk1= ((64*L^3)/48+ (80*(L/2-168)*L/2*(L^2-(L/2-168)^2-(L/2)^2))/(6*L))*1.33;
deltatk2= ((50*(L/2-24)*(3*L^2-4*((L/2-24)^2)))/24)*1.33;
deltatkcrit=max(deltatk1,deltatk2);
Ldisp=deltatkcrit; %units of kip*in^3

end
```

```
function [gmint,gsint] = g
%function [gmext,gmint,gsint,gsext] = g(S,d,L,de,theta) units of
%inches however these equations need S,L,de in feet
% JP 2022 This function determines the critical or governing girder
%distribution factors for a bridge using the AASHTO LRFD type c girder
%guidelines from section 4.6 however decision made to not use lever rule
%for the exterior girders feels unrealistic based on the field tests run
%% global variables
global S L d  theta
%% Convert the required variables to the right units and give new names so they're not
overwritten anywhere else
SL=S/12;
LL=L/12;
%% First moment interior
gmint1= ((SL/3)^0.35)*((SL*d/(12*LL^2))^0.25);
gmint2= ((SL/6.3)^0.6)*((SL*d/(12*LL^2))^0.125);
gmint=max(gmint1,gmint2);

%% Skew correction for moment
sc=1.05-0.25*tand(theta);
if sc >1.0
    sc=1.0;
else
end
gmint=sc*gmint;

%% Shear interior
gsint1=((SL/10)^0.6)*((d/(12*LL))^0.1);
gsint2=((SL/7.4)^0.8)*((d/(12*LL))^0.1);
gsint=max(gsint1,gsint2);
%% Shear exterior
%% Skew correction for shear
sc=1+(sqrt(LL*d/12)/(6*SL)*tand(theta));
gsint=gsint*sc;
end
```

```
function [tbf] = Ebot(n,j)
%JP Ebot gives the longitudinal Elastic modulus of the girder bottom flange based on
%the number of carbon ply layers n (n must be an even integer). The resulting output is
the longitudinal Elastic
%modulus of the bottom flange (ksi) to be used in transformed section
%analysis and the thickness (in.).
global inp

%% Specify the effective properties of the uni24oz
E1u= 5.34e3;  % units: ksi
E2u = 1.62e3;    % units: ksi
nu12u = 0.28;
G12u = 0.77e3;  % units: ksi
%% Specify the effective properties of Carbon
E1c= 14.37e3;  % units: ksi
E2c = 0.61e3;    % units: ksi
nu12c = 0.28;
G12c = 0.58e3;  % units: ksi
%% Specify lamina thickness
h=[.012*ones(1,j/2)]; %Assuming the thickness of each ply is 0.012 in for glass and 0.05
in for carbon
h=[h .05/2*ones(1,n) flip(h)];
%% Specify the orientations of the layers (Units: degrees)
for i=1:j/2
Theta1(1,i)=45*((-1)^(i+1));
end
ThetaArray = [Theta1 zeros(1,n) flip(Theta1)];
N = length(ThetaArray);
%% Make properties matrices
for i=1:N
    if h(i)== .012
        E1(i)= E1u;
        E2(i)= E2u;
        nu12(i)=nu12u;
        G12(i)=G12u;
    else
        E1(i)= E1c;
        E2(i)= E2c;
        nu12(i)=nu12c;
        G12(i)=G12c;
    end
end
%% Compute total laminate thickness
tbf = sum(h); %units of in
%% z locations of points where strains and stresses will be evaluated
NPoints = 500;
zpoints=linspace(-tbf/2,tbf/2,NPoints);
%% Evaluate laminate interface locations Z_k
   ZCoord(1)=-tbf/2;
   for i=1:N
       ZCoord(i+1)= ZCoord(i)+h(i);
```

```
   end
%% Calculate the reduced stiffness matrices
for k=1:N
Q{k}= ReducedStiffness(E1(1,k),nu12(1,k),E2(1,k),G12(1,k)); %units of ksi
end
%% Compute the off-axis reduced stiffness matrices
for k = 1:N
 QBar{k}=OffAxisStiffness(ThetaArray(k),cell2mat(Q([k]))); %units of ksi
end
%% Compute laminate ABD stiffness matrix
[~,~,~,~,a,~,~,~]=ComputeABD(N,QBar,ZCoord);

%%Compute laminae global properties in web
Ebfx=1/(a(1,1)*tbf); %units ksi
Ebfy=1/(a(2,2)*tbf);
Gbf=1/(a(3,3)*tbf); % units of ksi
nbf=-a(1,2)/a(1,1);

inp.bf.Ex=Ebfx;
inp.bf.Ey=Ebfy;
inp.bf.G=Gbf;
inp.bf.n=nbf;
end
```

```
function [tw,Gweb] =Eweb(j)
% JP 2022 Eweb gives the longitudinal Elastic modulus of the girder web based on
%the number of glass ply layers n (n must be an even integer). The resulting output is
the longitudinal Elastic
%modulus of the web (ksi) and shear modulus (ksi) to be used in transformed section
%analysis and design; and the thickness (in.). This does not consider the thickness of
the
%core and its material properties
global tcore inp

%% Specify the effective properties of the uni24oz
E1u= 5.34e3;  % units: ksi
E2u = 1.62e3;    % units: ksi
nu12u = 0.28;
G12u = 0.77e3;  % units: ksi
%% For shear models uncomment the core properties and include in function
% %% Specify the effective properties of the Core
% E1c= 15.95;  % units: ksi
% E2c = 15.95;    % units: ksi
% nu12c = 0.3;
% G12c = 3.19;  % units: ksi

%% Specify lamina thickness
h(1,1:j/2)= .012; % units in
%h(1,j/2+1)= tcore/2;
h= [h flip(h)];

%% Specify the orientations of the layers (Units: degrees)
ThetaArray=zeros(1,j/2);
for i=1:j/2
    ThetaArray(1,i)=45*((-1)^(i+1));
end
ThetaArray=[ThetaArray flip(ThetaArray)];
%% Determine the number of layers
N = length(ThetaArray);%% Compute total laminate thickness
%%Determine total thickness
tw = sum(h); %units of in

%% z locations of points where strains and stresses will be evaluated
NPoints = 500;
zpoints=linspace(-tw/2,tw/2,NPoints);

%% Make matrices properties
for i=1:N
    if h(i)== .012
       E1(i)= E1u;
       E2(i)= E2u;
      nu12(i)=nu12u;
      G12(i)=G12u;
%     else  % Uncomment this section for shear model with core thickness
%     included
```

```
%         E1(i)= E1c;
%         E2(i)= E2c;
%         nu12(i)=nu12c;
%         G12(i)=G12c;
    end
end

%% Evaluate laminate interface locations Z_k
   ZCoord(1)=-tw/2;
   for i=1:N
       ZCoord(i+1)= ZCoord(i)+h(i);
   end
%% Calculate the reduced stiffness matrices
for k=1:N
Q{k}= ReducedStiffness(E1(k),nu12(k),E2(k),G12(k)); %units of ksi
end



%% Compute the off-axis reduced stiffness matrices
for k = 1:N
 QBar{k}=OffAxisStiffness(ThetaArray(k),cell2mat(Q([k]))); %units of ksi
end
%% Compute laminate ABD stiffness matrix
[~,~,~,~,a,~,~,~]=ComputeABD(N,QBar,ZCoord);

%%Compute laminae global properties in web
Ewx=1/(a(1,1)*tw); %units ksi
Ewy=1/(a(2,2)*tw);
Gweb=1/(a(3,3)*tw); % units of ksi
nw=-a(1,2)/a(1,1);
inp.w.Ex=Ewx;
inp.w.Ey=Ewy;
inp.w.G=Gweb;
inp.w.n=nw;
end
```

```
function [EInc,Inctot,ync,EIc,Ictot,yc,Qint,ntf,nbf] = TSA(tbf,tw, Lw)
% JP 2022 This function does the transformed section analysis for the
% noncomposite and composite cross sections for the girders all variables
% units are ksi and inches coming in as inputs and will have outputs in
% units of inches and ksi.
global inp Etf ttf  Ec S  tdeck d phi overhang bbf btf EIb Ng tcore
% extract moduli
Ebf=inp.bf.Ex;
Ew=inp.w.Ex;

%% Modular ratios
nbf=Ebf/Ec;
nw=Ew/Ec;
ntf=Etf/Ec;

%% Non composite section
Abf=nbf*bbf*tbf;
ybf=tbf/2;
Ibf=nbf/12*bbf*tbf^3;
Aw=2*nw*Lw*tw;
yw=tbf+Lw/2*cosd(phi);
Iw=2*(nw*tw*Lw/12*((Lw*cosd(phi))^2+(nw*tw*sind(phi))^2));
Atf=ntf*btf*ttf;
ytf=d-ttf/2;
Itf=ntf/12*btf*ttf^3;

Aync=Abf*ybf+Aw*yw+Atf*ytf;
Anc=Abf+Aw+Atf;
ync=Aync/Anc;
Inc=Ibf+Iw+Itf;
PAnc=Abf*(ybf-ync)^2+Aw*(yw-ync)^2+Atf*(ytf-ync)^2;
EInc=Ec*(Inc+PAnc);
Inctot=EInc/Ec;

%% Find Girder properties for beam profile in ABAQUS J,I12,I22
I2bf=nbf*bbf^3*tbf/12;
I2w=2*nw*tw^3*Lw/12;
I2tf=2*ntf*btf^3*ttf/12;
dtf=btf/2+bbf/2-tw/cosd(phi)+Lw*sind(5); %distance CG tf to ybar
dw=bbf/2-(tw/2)/cosd(phi)+Lw/2*sind(phi); %distance CG web to ybar
PA2=Aw*dw^2+Atf*dtf^2;
Inc2=I2bf+I2w+I2tf+PA2; % Value for I22

tfs=tw-tcore; %Thickenss of facesheets in the web
J=2*bbf^2*d^2*tfs^2/(bbf*tfs+d*tfs);% J for a thin walled rectangular section that has↙
the thinkness of both web facesheets

%find I12
Inc12=0;
```

```
%% Composite section interior
Aconc=S*tdeck;
yconc= d+tdeck/2;
Iconc=1/12*S*tdeck^3;


Ayc=Aync+Aconc*yconc;
Ac=Anc+Aconc;
yc=Ayc/Ac;
Ic=Inc+Iconc;
PAc= Abf*(ybf-yc)^2+Aw*(yw-yc)^2+Atf*(ytf-yc)^2+Aconc*(yconc-yc)^2;
EIc=Ec*(Ic+PAc);
Ictot=EIc/Ec; %units in^4

ywbf=(Abf*ybf+Aw*yw)/(Abf+Aw);
ybar=yc-ywbf;
Qint=(Abf+Aw)*ybar; % units in^3



%% composite section exterior
Aconcx=(S/2+overhang)*tdeck;
Iconcx=1/12*(S/2+overhang)*tdeck^3;

Aycx=Aync+Aconcx*yconc;
Acx=Anc+Aconcx;
ycx=Aycx/Acx;
Icx=Inc+Iconcx;
PAcx=Abf*(ybf-ycx)^2+Aw*(yw-ycx)^2+Atf*(ytf-ycx)^2+Aconcx*(yconc-ycx)^2;
EIcx=Ec*(Icx+PAcx);
Icxtot=EIcx/Ec;



%%Composite Section Entire Bridge
Aconcb= tdeck*(S*(Ng-1)+2*overhang);
Acurb=2*20*12.25;
Abfb=Ng*Abf;
Awb=Ng*Aw;
Atfb=Ng*Atf;
ycurb=d+tdeck+12.25/2;

Ayb=Aconcb*yconc+Acurb*ycurb+Abfb*ybf+Awb*yw+Atfb*ytf;
Ab=Aconcb+Acurb+Abfb+Atfb+Awb;
yb=Ayb/Ab;

Iconcb=1/12*((Ng-1)*S+2*overhang)*tdeck^3;
Icurb=1/12*40*12^3;

Ib=Iconcb+Icurb+Ng*(Inc);
```

```
PAb=Aconcb*(yconc-yb)^2+Acurb*(ycurb-yb)^2+Abfb*(ybf-yb)^2+Awb*(yw-yb)^2+Atfb*(ytf-yb)^2;

EIb=Ec*(Ib+PAb);

%% Q for location 1 in below top of web
Lwu=Lw-(1/cosd(phi)); % length of web under the location for Q calculation
Awu=Lwu*tw*nw*2; % web area under
ywu=tbf+Lw*cosd(phi)/2; % neutral axis of web area under
ywbfu=(Abf*ybf+Awu*ywu)/(Abf+Awu);
ybaru=yc-ywbfu;
Qintr=(Abf+Awu)*ybaru;

ybarx=ycx-ywbfu;
Qxr=(Abf+Awu)*ybarx;

inp.Ec=Ec;
inp.Q.Qx=Qxr;
inp.Q.Qint=Qintr;
inp.I.Iint=Ictot;
inp.I.Ix=Icxtot;
inp.SE.SEint=Ec*Ictot/yc;
inp.SE.SEx=Ec*Icxtot/ycx;
inp.girder.y=ync;
inp.girder.yc=yc;
inp.girder.A=Anc;
inp.girder.J=J;
inp.girder.I11=Inctot;
inp.girder.I22=Inc2;
inp.girder.I12=Inc12;
end
```

```
function [Nxy] = buckling2(Lw,tw)
% JP 2022, This function uses the buckling data from testing to interpolate
% Nxy values for a certion web height, web thickness and core thickness
global tcore d
tfs=(tw-tcore)/2; %tcore is set to zero not including in laminate analysis
% Since the thickness of the core is not included in the design yet one is
% and web properties needed for the buckling values of N assume a reasonable
% core thickness. Assumption based on information from AIT bridges
if d<= 30
    tcoreassumed=0.75;
else
    tcoreassumed=1.5;
end
%t_tot=tw;
t_tot=tcoreassumed+2*tfs;
r=tcoreassumed/t_tot;
%% round to bounds for tfs and Lw
tfslow=0.12*floor(tfs/0.12);
Lwlow=12*floor(Lw/12);

%% Use these bounds to open correct lower bound plot and interpolate Nxy
%% between certain face sheet thickness data points
if Lw>=0 && Lw<24
    dat1=load('h24data.mat');
   dat2= load('h36data.mat');
   Lwlow=24;
elseif Lw>=24 && Lw<36
   dat1=load('h24data.mat');
   dat2= load('h36data.mat');
elseif Lw>= 36 && Lw<48
    dat1=load('h36data.mat');
    dat2=load('h48data.mat');
elseif Lw>= 48 && Lw<60
    dat1=load('h48data.mat');
    dat2=load('h60data.mat');
elseif Lw>= 60
    dat1=load('h60data.mat');
    dat2=load('h72data.mat');

end



if tfs>=0 && tfs<0.12
    xy1=dat1.dat.t12;
    xy2=dat1.dat.t24;
    xy3=dat2.dat.t12;
    xy4=dat2.dat.t24;
    tfslow=0.12;
elseif tfs>= 0.12 && tfs<0.24
    xy1=dat1.dat.t12;
```

```
    xy2=dat1.dat.t24;
    xy3=dat2.dat.t12;
    xy4=dat2.dat.t24;
elseif tfs>= 0.24 && tfs<0.36
   xy1=dat1.dat.t24;
    xy2=dat1.dat.t36;
    xy3=dat2.dat.t24;
    xy4=dat2.dat.t36;
elseif tfs>= 0.36 && tfs<0.48
   xy1=dat1.dat.t36;
    xy2=dat1.dat.t48;
    xy3=dat2.dat.t36;
    xy4=dat2.dat.t48;
elseif tfs>= 0.48 && tfs<0.60
   xy1=dat1.dat.t48;
    xy2=dat1.dat.t60;
    xy3=dat2.dat.t48;
    xy4=dat2.dat.t60;
elseif tfs>= 0.60 && tfs<0.72
   xy1=dat1.dat.t60;
    xy2=dat1.dat.t72;
    xy3=dat2.dat.t60;
    xy4=dat2.dat.t72;
elseif tfs>= 0.72
   xy1=dat1.dat.t72;
    xy2=dat1.dat.t84;
    xy3=dat2.dat.t72;
    xy4=dat2.dat.t84;
end

x1=xy1(:,1);
y1=xy1(:,2);
if r>x1(9)
    m=(y1(9)-y1(8))/(x1(9)-x1(8));
    Nxy1=m*(r-x1(9))+y1(9);
else
Nxy1=interp1(x1,y1,r);
end


x2=xy2(:,1);
y2=xy2(:,2);
if r>x2(9)
    m=(y2(9)-y2(8))/(x2(9)-x2(8));
    Nxy2=m*(r-x2(9))+y2(9);
else
Nxy2=interp1(x2,y2,r);
end

Nxylower=((Nxy2-Nxy1)/0.12)*(tfs-tfslow)+Nxy1;
```

```
x3=xy3(:,1);
y3=xy3(:,2);
if r>x3(9)
    m=(y3(9)-y3(8))/(x3(9)-x3(8));
    Nxy3=m*(r-x3(9))+y3(9);
else
Nxy3=interp1(x3,y3,r);
end


x4=xy4(:,1);
y4=xy4(:,2);
if r>x4(9)
    m=(y4(9)-y4(8))/(x4(9)-x4(8));
    Nxy4=m*(r-x4(9))+y4(9);
else
Nxy4=interp1(x4,y4,r);
end

Nxyupper=((Nxy4-Nxy3)/0.12)*(tfs-tfslow)+Nxy3;

%% Interpolate between the upper and lower Nxy for the certain Lw for the actual Lw
Nxy=((Nxyupper-Nxylower)/12)*(Lw-Lwlow)+Nxylower;
```



```
function [Mrnc] = flexurenc(Inc,ync,nbf,ntf)
% JP 2022 This function determiens the non composite flexural capacity
% constants the non reduced values reported by manufacturer in the
% calculations package for HGMB AIT
%Global variables
global Etf d inp
Ebf=inp.bf.Ex;

eltbfnr= 0.0101; %non reduced tensile strain in botom flange assuming its of carbon
elctfnr= 0.01945; %non reduced compressive strain in top flange
%reduce ultimate tensile and compressive strains
eltbf=0.832*0.85*eltbfnr; %assuming carbin used in bf
elctf=0.857*0.65*elctfnr;  %assuming glass used in tf

Mneg=Etf*elctf*Inc/(ntf*(d-ync));
Mpos= Ebf*eltbf*Inc/(nbf*ync);
Mn=min(Mneg,Mpos);

Mrnc=0.75*Mn; %reducing using the resistance factor provided in the code
```

```
function Mfail = moment_curvature(tw,tbf,DMunc,EInc,ync)

% This function performs a moment-curvature analysis on a CT girder to
% determine the moment at which it will fail. It assumes as linear elastic
% resposne of FRP and a nonlinear constitutive response of concrete
% described in compression by the Hognestad constitutive curve

%% Initialization %%

% Declare global variables (makes them available to all functions so they
% do not need to be passed as inputs)
global  Etf  Ec  alpha  bc d ttf epsfail phi S D bbf
global  dw  kcurrent fpc fail antype btf eps0 tdeck fcc tweb

tweb=tw;
% Ignore this
x = [20];
for jj = 1:length(x)
antype = 1;

% Locked-in strain due to the weight of wet concrete - this may or may not
% be something that needs to be dealt with. Bill will probably say yes but
% it is worth discussion
eps0 = DMunc*ync/EInc;


%% Geometry and Material Properties %%

% Carbon rupture strain (F1t/E1) Assumed from HGMB properties
epsfail = 0.832*0.85*145.8/14.37e3;


% Total depth
D = d+tdeck;

% Web depth
dw = d-tbf-ttf;
% Top flange width (in)

% Deck width (in)
bc = S;
% Web splay angle
alpha = phi;
% Concrete compressive strength (ksi)
fpc = fcc;
% Concrete MOE (ksi)
Ec = 1820*sqrt(fpc);

%% Analysis %%

% Create a vector of curvature values for which moment values will be
```

```
% calculated (1/in)
k = 0:5*10^-4:5e-3;
% Mark that failure has not yet occured
fail = 0;
% Count the first iteration
ii = 1;
% Craete a handle to the function that sums internal forces
fun = @getybar;

% While the section has not yet failed
while fail == 0
%     Pass in the current curvature
    kcurrent = k(ii);
%     Find the neutral axis height at which internal forces are in
%     equilibrium
    ybar(ii) = fminsearch(fun,d);
%     Calculate the moment
    M(ii) = getM(ybar(ii),tbf,tw);
%     Count the iteration
    ii = ii+1;
end

%% Post-Processing %%

% In case M is negative, find the positive
M = abs(M);
% THe section fails at the largest M
Mfail(jj+1) = max(M);
end

% Plot if you want. Does not need to be done
%figure; plot(Mfail)

%figure;plot(k(1:length(M)),M)
%figure;plot(k(1:length(ybar)),ybar)
```

```
function residual = getybar(ybar)

% This function performs an approximate nonlinaer analysis of a CT girder
% section under a given curvature and outputs the residual force. This
% residual is used as an error value in an optimization algorithm designed
% to find the neutral axis height at which internal forces are in
% equilibrium.

% Collect global variables
global D inp Etf ttf alpha bc bbf btf dw kcurrent fpc antype eps0 d
global tweb
tbf=d-ttf-dw;

Ebf=inp.bf.Ex;
Ew=inp.w.Ex;

% Discretize the section into 100 vertical slices, each one "dy" in height
dy = D/1000;
ynow = 0;
yhat = 0:dy:D;
% Preallocate memory to hold the force acting on each slice
F = zeros(size(yhat));

% For each clice in the discretized section
for ii = 1:length(yhat)
%     Calculate the strain in the current slice based on its distance from
%     the current neutral axis, the curvature, and any locked-in strain
    eps = (kcurrent+(eps0/ybar))*(ybar-ynow);
%     Depending on the location of the slice within the section, calculate
%     the area of the slice (dy*width at the current height) and multiply
%     by the stress (using the strain and an appropriate constitutive
%     model) to find the force at the slice center

%         Bottom Flange - stress = E*eps
    if ynow <= tbf
        b = bbf;
        A = b*dy;
        F(ii) = A*eps*Ebf;

%         Web - stress = E*eps
    elseif ynow <= tbf+dw
        b = 2*tweb/cosd(alpha);
        A = b*dy;
        F(ii) = A*eps*Ew;

%         Top flange - stress = E*eps
    elseif ynow <= tbf+dw+ttf
        b = btf;
        A = b*dy;
        F(ii) = A*eps*Etf;
```

```
%         Deck - stress = f(eps), f = Hognestad curve
    else
        b = bc;
        A = b*dy;
        fc = concstress(eps);
        F(ii) = fc*A;
    end
%     Move to the next slice
    ynow = ynow+dy;
end
% Find the residual by summing the force contribution from each slice
residual = abs(sum(F));
```

```
function M = getM(ybar,tbf,tw)

% This function performs an approximate nonlinaer analysis of a CT girder
% section under a given curvature and outputs the internal moment. This
% relies on the previously determined neutral axis height that ensures
% internal force equilibrium

% Collect global variables
global D  Etf ttf alpha inp
global bc bbf btf dw kcurrent fpc antype fail epsfail eps0

Ebf=inp.bf.Ex;
Ew=inp.w.Ex;

% Discretize the section into 1000 vertical slices, each one "dy" in height
dy = D/1000;
ynow = 0;
yhat = 0:dy:D;
% Preallocate memory to hold the force, strain, and moment in each slice
F = zeros(size(yhat));
Mvec = F;
eps = F;
% For each clice in the discretized section
for ii = 1:length(yhat)
%     Calculate the strain in the current slice based on its distance from
%     the current neutral axis, the curvature, and any locked-in strain
    eps(ii) = (kcurrent+(eps0/ybar))*(ybar-ynow);
%     Depending on the location of the slice within the section, calculate
%     the area of the slice (dy*width at the current height) and multiply
%     by the stress (using the strain and an appropriate constitutive
%     model) to find the force at the slice center

%         Bottom Flange - stress = E*eps
    if ynow <= tbf
        b = bbf;
        A = b*dy;
        F(ii) = A*eps(ii)*Ebf;
%         Check to make sure the strain in the bottom flange is less than
%         the carbon rupture strain. If it is equal to or higher, throw a
%         flag whcih will end the analysis
        if eps(ii) > epsfail
            fail = 1;
        end

 %         Web - stress = E*eps
    elseif ynow <= tbf+dw
        b = 2*tw/cosd(alpha);
        A = b*dy;
        F(ii) = A*eps(ii)*Ew;

%         Top flange - stress = E*eps
```

```
    elseif ynow <= tbf+dw+ttf
        b = btf;
        A = b*dy;
        F(ii) = A*eps(ii)*Etf;

%         Deck - stress = f(eps), f = Hognestad curve
    else
        b = bc;
        A = b*dy;
        fc = concstress(eps(ii));
        F(ii) = fc*A;
    end
%     Calculate the contribution to internal moment from the current slice
%     by multiplying the force times the distance to the top of the section
    Mvec(ii) = F(ii)*(D-ynow);
%     Move to the next slice
    ynow = ynow+dy;
end
% Find the total internal moment
M = sum(Mvec);
```

Appendix C: Parametric Model Scripts and Functions

C.1 Moment Parametric Model

4/11/24 2:33 PM C:\Users\JonPinkham\Docu...\Girderscript.m 1 of 2

```
%% This script runs the varying parameters that are desired to be inspected
% %and give the output of girder designs and the results of Fe analysis


%% Ranges for Parameters
tic
L= 40:10:80;
Ld=18;
Ng= [5];
tdeck=[7 8 9];
theta=[0];
p=[];
for k=1:length(theta)
    for i=1:length(L)
        for j=1:length(Ld)
            for m=1:length(Ng)
                for n=1:length(tdeck)
                    [parameters] = parameter(L(i),Ld(j),Ng(m),theta(k),tdeck(n));
                    p=[p ; parameters];
                end
            end
        end
    end
end
%% standrd Bridge [60 18 6 8 5 0 3];
% # of lanes loaded either 2 or 1
lns=1;

for t=1
    if lns(t)== 1
        y=6;
    else
        y=4;
    end
    %y=1; %%%%% Remove this for any parametric studies
for i=1:size(p,1)
    inputs=p(i,:);
    girder(i)= buildgirder2(inputs);
    [longstrains,rxns,rxnsA,m,dist,longpos] = CT_Parameter_Beam2(inputs,girder(i),0.04,y,↙
lns(t));
    for j=1:size(longstrains,1)
    %Reactions(j,:)=getRs(inputs,girder(i),gammaxyminus(j,:),gammaxyplus(j,:));
    [Moments(j,:),MDFs(j,:)]=getMDFs(inputs,girder(i),longstrains(j,:),lns(t));
%     VDFs(j,:)=GetVDFs(inputs,rxns(j,:),lns(t));
    end
    Ng=inputs(1,5);
    MDFint1=MDFs(1:end, 2:Ng-1);
    MDFext1=[MDFs(1:end,1), MDFs(1:end,Ng)];
    longsint1=longstrains(1:end, 2:Ng-1);
    longsext1=[longstrains(1:end,1), longstrains(1:end,Ng)];
```

```
    MDFint2=max(MDFint1);
    MDFext2=max(MDFext1);
    longsint2=max(longsint1);
    longsext2=max(longsext1);

    MDFint(i)=max(MDFint2);
    MDFext(i)=max(MDFext2);
    longsint(i)=max(longsint2);
    longsext(i)=max(longsext2);
    %% Define file location for excel sheet
    filename= 'C:\Users\JonPinkham\OneDrive - University of Maine↙
System\Documents\Parametric\Results.xlsx';
    runs=size(p,1);
    xlRange=strcat('A',num2str(310+i)); %where in excel to start data from
    sheet=2; %define sheet in excel to put data


    %% Build the output vector
    td=inputs(1,4); % deck thickness
    dfrp=girder(i).dfrp;
    ync=girder(i).girder.y; % NA of girder itself
    Inc=girder(i).girder.I11; % NC moment of inertia for girder section
    A=girder(i).girder.A; % girder cross sectional area
    eg=dfrp+td/2-ync; % distance between center of gravities of deck and basic beam
    Kg=Inc+A*(eg^2);
    ohang=inputs(1,7); % overhang ft.
    Lw=girder(i).w.Lw; % length of web (inches)
    bbf=girder(i).bf.bbf; % width of bottom flange (inches)
    tw=girder(i).w.tw; % web thickness (inches)
    de= ohang-((20+bbf/2+Lw*sind(5)-tw/2)/12); % distance from center of web at top of↙
girder to curb inside edge (ft)
    Twg=girder(i).girder.Twg;

    A=[inputs, Kg, de, dfrp, MDFint(i),MDFext(i),longsint(i),longsext(i), bbf, Twg];
    xlswrite(filename,A,sheet,xlRange) % Write data into excel in specified location
%
%
  clearvars MDFint2 MDFint1 MDFext1 MDFext2 VDFint1 VDFint2 VDFext1 VDFext2 MDFs VDFs↙
Moments longsext1 longsext2 longsint1 longsint2
  clearvars rint1 rext1 rint2 rext2
end
end

time5=toc;
```

```
function [longstrains,rxns,rxnsA,m,dist,longpos] = CT_Parameter_Beam2(inputs,girder,x,y,↙
lns)
% This function submits parameters to ABAQUS for analysis. The purpose of
% this analysis is to generate results for use in determining CT girder
% distribution factors.

% Schanck 2022

%% Initialization %%

% These variables are changed to alter various dimensional parameters in
% the model


% Span length (in)
span = inputs(1,1)*12;
% Girder spacing (in)
spacing = inputs(3)*12;
% Girder depth (in)
depth = girder.dfrp;
% Offset to Account for splay angle (in)
splay = girder.dfrp*tand(5);
%Number of girders
Ng=inputs(1,5);
%Overhang
overhang=inputs(7)*12;
%Total deck width
Bbridge=spacing*(Ng-1)+2*overhang;
% Minimum transverse offset lane load can start from the edge of curb
% note lane can start right at edge but the truck inside the lane can not
% get any closer than 24 inches to the lane edge
Mintransverse=0;
%Maximum transverse distance from outer edge that the outside load path can
%start
Maxtransverse=Bbridge-(24*12)-40;
%stepsize for transverse loading
center=(Maxtransverse+Mintransverse)/2-1.0;
stepa=(center-Mintransverse)/(y/2);
stepb=(Maxtransverse-center)/(y/2);
stepo=(center-Mintransverse)/(y);

% Skew Angle (Degrees)
theta = inputs(1,6);

% Distance from edge of imaginery curb (20 in) to outside of first lane load (in)
if theta == 0 % Take advantage of symmetry only run load on one side
    dist = [Mintransverse:stepo:center];
    %dist=Mintransverse;
else % for a skewed bridge run loadings all the way across
    dist=[Mintransverse:stepa:center center+2 center+stepb:stepb:Maxtransverse];
end
```

```
%dist=center;


% Bottom flange width (in)
BF = girder.bf.bbf;
% Top flange width (in)
TF = girder.tf.btf;


% BF E1 (ksi)
E1BF = girder.bf.Ex;
% BF E2 (ksi)
E2BF = girder.bf.Ey;
% BF Poissons
nuBF = girder.bf.n;
% BF G (ksi)
GBF = girder.bf.G;
% BF Thickness (in)
tBF = girder.bf.tbf;



% Web E1 (ksi)
E1W = girder.w.Ex;
% Web E2 (ksi)
E2W = girder.w.Ey;
% Web Poissons
nuW = girder.w.n;
% Web G (ksi)
GW = girder.w.G;
% Web Thickness (in)
tW = girder.w.tw;

% TF E1 (ksi)
E1TF = girder.tf.Ex;
% TF E2 (ksi)
E2TF = girder.tf.Ey;
% TF Poissons
nuTF = girder.tf.n;
% TF G (ksi)
GTF = girder.tf.G;
% TF Thickness (in)
tTF = girder.tf.ttf;


%%%%%%%%%%%%%%%%%% EDITED TO INCORPORATE CRACKED DECK %%%%%%%%%%%
% Concrete Thickness (in)
tc = inputs(4);
% Concrete E (ksi)
Ec = 3640;
```

```
% Concrete E CRACKED (ksi)
if tc== 7
Ec_cr = 772;
elseif tc==8
Ec_cr = 742;
elseif tc==9
Ec_cr = 711;
elseif tc==10
Ec_cr = 680;
end
%%%%%%%%%%%%%%%%%%%%%%%%%%%%%%%%%%%%%%%%%%%%%%%%%%%%%%%%%%%%%%%%%%%%%%%


%OH
OH=overhang-BF/2-TF/2-splay;
% Mesh size for Girders and deck (in)
mesh_size = 1/x;

% Fraction of Girder Sampled for Max Moment
L = 0.3;

% Girder Elastic Modulus (ksi)
Eg = 3640;
Gg = girder.girder.Gg; %Same as G for +-45 web facesheets

yc=girder.girder.yc; %composite section NA used to interpolate longitudinal strains
ybar = girder.girder.y;%non composite NA for just girder used for offset location of beam
element

A = girder.girder.A;
Ixx = girder.girder.I11;
Ixy = girder.girder.I12;
Iyy = girder.girder.I22;
J = girder.girder.J;

LC=[1 2]; % two loading conditions 1 is HL-93 truck; 2 is tandem axles
m=1; %counter
longstrains=[];
    rxns=[];
    rxnsA=[];
for t=1%:2

    if LC(t)==1
        if theta>= 0 && theta<=20
            longpos= span/2-144; %[span/2-168:24:span/2-120];
        elseif theta>20 && theta<=45
            longpos=span/2-168;% [span/2-192:24:span/2-144];
        elseif theta>45
            longpos=span/2-192; %[span/2-228:24:span/2-180];

        end
```

```
elseif LC(t)==2
    if theta>= 0 && theta<=15
        longpos=span/2-36; %[span/2-60:24:span/2-12];
    elseif theta>15 && theta<=45
        longpos=span/2-60; %[span/2-84:24:span/2-36];
    elseif theta>45
        longpos=span/2-84; %[span/2-108:24:span/2-60];
    end
end

   %Jvec=[0.5*J 0.75*J J 1.5*J 2*J];

%for j=1:length(Jvec)
for l=1:length(longpos)
    for i=1:length(dist)

        %Logic for if the HL-93 truck will completely fit on bridge or not
        effectivelength=346+92*tand(theta)+longpos(l);
        if effectivelength<span
            fulltruck=1; %true full truck will fit
        else
            fulltruck=0; % false won't fit use two rear axles only
        end

        if ((Ng-1)*spacing+2*OH+BF+TF)/2 > 144
            lanewidth = 120;
        else
            lanewidth = ((Ng-1)*spacing+2*OH+BF+TF)/2-24;
        end

        % Truck Loads zeroed for appropriate load scenario
        if lns == 2
            lane2 = 4.444e-4;
            rear2 = 0.1064;
            front2 = .0266;
            tan2 = 0.0831;
            lane1 = 4.444e-4;
            rear1 = 0.1064;
            front1 = .0266;
            tan1 = 0.0831;
        elseif lns == 1 && dist(i)<=center+1
            lane2 =1e-15;
            rear2 = 1e-15;
            front2 = 1e-15;
            tan2 = 1e-15;
            lane1 = 4.444e-4;
            rear1 = 0.1064;
            front1 = .0266;
            tan1 = 0.0831;
        elseif lns == 1 && dist(i)>center+1
```

```
                lane1 =1e-15;
                rear1 = 1e-15;
                front1 = 1e-15;
                tan1 = 1e-15;
                lane2 = 4.444e-4;
                rear2 = 0.1064;
                front2 = .0266;
                tan2 = 0.0831;
            end

            ln1= dist(i); % Value of d for input files offset from curb edge to start↙
firts lane load
            le1=24; % value for a (in) to start the uniform 10 ft load lane 1
            t1=48; % value for b (in) to start position of truck 1 in lane 1
            t2=24; % value for c (in) to start positions of truck 2 in lane 2
            le2=0; % value for e (in) to start the uniform 10 ft load lane 2

            if ln1 == Mintransverse
                le1=0; % value for a (in) to start the uniform 10 ft load lane 1
                t1=24; % value for b (in) to start position of truck 1 in lane 1
                t2=24; % value for c (in) to start positions of truck 2 in lane 2
                le2=0; % value for e (in) to start the uniform 10 ft load lane 2
            elseif ln1 == Maxtransverse
                le2=24; % value for e (in) to start the uniform 10 ft load lane 2
                le1=24; % value for a (in) to start the uniform 10 ft load lane 1
                t1=48; % value for b (in) to start position of truck 1 in lane 1
                t2=48; % value for c (in) to start positions of truck 2 in lane 2
            end

            % Record the initiation directory
            starter = pwd;

            if Ng == 4 && LC(t) == 1 && fulltruck==1
                inploc = 'C:\Users\JonPinkham\Documents\MATLAB\Girder Design';
                inpfile = 'C:\Users\JonPinkham\Documents\MATLAB\Girder↙
Design\Setup_4_Skew.py';
                file = 'Setup_4_Skew.py';
            elseif Ng == 5 && LC(t) == 1 && fulltruck==1
                inploc = 'C:\Users\JonPinkham\Documents\MATLAB\Girder Design';
                inpfile = 'C:\Users\JonPinkham\Documents\MATLAB\Girder↙
Design\Setup_5_Skew.py';
                file = 'Setup_5_Skew.py';
            elseif Ng == 6 && LC(t) == 1 && fulltruck==1
                inploc = 'C:\Users\JonPinkham\Documents\MATLAB\Girder Design';
                inpfile = 'C:\Users\JonPinkham\Documents\MATLAB\Girder↙
Design\Setup_6_Skew.py';
                file = 'Setup_6_Skew.py';
            elseif Ng == 4 && LC(t) == 1 && fulltruck==0
                inploc = 'C:\Users\JonPinkham\Documents\MATLAB\Girder Design';
                inpfile = 'C:\Users\JonPinkham\Documents\MATLAB\Girder↙
Design\Setup_4_Skew_Reartruck.py';
```

```
            file = 'Setup_4_Skew_Reartruck.py';
        elseif Ng == 5 && LC(t) == 1 && fulltruck==0
            inploc = 'C:\Users\JonPinkham\Documents\MATLAB\Girder Design';
            inpfile = 'C:\Users\JonPinkham\Documents\MATLAB\Girder↙
Design\Setup_5_Skew_Reartruck.py';
            file = 'Setup_5_Skew_Reartruck.py';
        elseif Ng == 6 && LC(t) == 1 && fulltruck==0
            inploc = 'C:\Users\JonPinkham\Documents\MATLAB\Girder Design';
            inpfile = 'C:\Users\JonPinkham\Documents\MATLAB\Girder↙
Design\Setup_6_Skew_Reartruck.py';
            file = 'Setup_6_Skew_Reartruck.py';
        end


        if Ng == 4 && LC(t) == 2
            inploc = 'C:\Users\JonPinkham\Documents\MATLAB\Girder Design';
            inpfile = 'C:\Users\JonPinkham\Documents\MATLAB\Girder↙
Design\Setup_4_Skew_Tandem.py';
            file = 'Setup_4_Skew_Tandem.py';
        elseif Ng == 5 && LC(t) == 2
            inploc = 'C:\Users\JonPinkham\Documents\MATLAB\Girder Design';
            inpfile = 'C:\Users\JonPinkham\Documents\MATLAB\Girder↙
Design\Setup_5_Skew_Tandem.py';
            file = 'Setup_5_Skew_Tandem.py';
        elseif Ng == 6 && LC(t) == 2
            inploc = 'C:\Users\JonPinkham\Documents\MATLAB\Girder Design';
            inpfile = 'C:\Users\JonPinkham\Documents\MATLAB\Girder↙
Design\Setup_6_Skew_Tandem.py';
            file = 'Setup_6_Skew_Tandem.py';
        end



        %% Alter Python Script %%

        % Open Python script
        fid = fopen(inpfile,'r+');
        % Read first line
        tline = fgetl(fid);

        % Copy all lines of the ".py" file to a cell structure named "fc" (file
        % content)
        ii = 1;
        fc{ii} = tline;
        while ischar(tline)
            ii = ii+1;
            tline = fgetl(fid);
            fc{ii} = tline;
        end
        % Close ".py" file
```

```
fclose(fid);


% Search for unique keyword phrase coresponding to a variable parameter in
% the ".py" file and update the associated value
for ii = 1:length(fc)
    if ~isempty(strfind(fc{ii},'# Distance between'))
        fc{ii+1} = sprintf('dist = %.5E',dist(i));
    elseif ~isempty(strfind(fc{ii},'# Span length'))
        fc{ii+1} = sprintf('span = %.5E',span);
    elseif ~isempty(strfind(fc{ii},'# Girder spacing'))
        fc{ii+1} = sprintf('spacing = %.5E',spacing);
    elseif ~isempty(strfind(fc{ii},'# Girder Depth'))
        fc{ii+1} = sprintf('depth = %.5E',depth);
    elseif ~isempty(strfind(fc{ii},'# Offset to Account for splay angle↙
(in)'))
        fc{ii+1} = sprintf('splay = %.5E',splay);
    elseif ~isempty(strfind(fc{ii},'# Deck overhang'))
        fc{ii+1} = sprintf('OH = %.5E',OH);
    elseif ~isempty(strfind(fc{ii},'# Bottom Flange Width'))
        fc{ii+1} = sprintf('BF = %.5E',BF);
    elseif ~isempty(strfind(fc{ii},'# Top Flange Width'))
        fc{ii+1} = sprintf('TF = %.5E',TF);
    elseif ~isempty(strfind(fc{ii},'# Longitudinal position'))
        fc{ii+1} = sprintf('Zpos = %.5E',longpos(l));
    elseif ~isempty(strfind(fc{ii},'# Bottom flange thickness'))
        fc{ii+1} = sprintf('BFthick = %.5E',BFthick);
    elseif ~isempty(strfind(fc{ii},'# Web thickness'))
        fc{ii+1} = sprintf('Wthick = %.5E',Wthick);

    elseif ~isempty(strfind(fc{ii},'# BF E1 (ksi)'))
        fc{ii+1} = sprintf('E1BF = %.5E',E1BF);
    elseif ~isempty(strfind(fc{ii},'# BF E2 (ksi)'))
        fc{ii+1} = sprintf('E2BF = %.5E',E2BF);
    elseif ~isempty(strfind(fc{ii},'# BF Poissons'))
        fc{ii+1} = sprintf('nuBF = %.5E',nuBF);
    elseif ~isempty(strfind(fc{ii},'# BF G (ksi)'))
        fc{ii+1} = sprintf('GBF = %.5E',GBF);
    elseif ~isempty(strfind(fc{ii},'# BF Thickness (in)'))
        fc{ii+1} = sprintf('tBF = %.5E',tBF);
    elseif ~isempty(strfind(fc{ii},'# Web E1 (ksi)'))
        fc{ii+1} = sprintf('E1W = %.5E',E1W);
    elseif ~isempty(strfind(fc{ii},'# Web E2 (ksi)'))
        fc{ii+1} = sprintf('E2W = %.5E',E2W);
    elseif ~isempty(strfind(fc{ii},'# Web Poissons'))
        fc{ii+1} = sprintf('nuW = %.5E',nuW);
    elseif ~isempty(strfind(fc{ii},'# Web G (ksi)'))
        fc{ii+1} = sprintf('GW = %.5E',GW);
    elseif ~isempty(strfind(fc{ii},'# Web Thickness (in)'))
        fc{ii+1} = sprintf('tW = %.5E',tW);
    elseif ~isempty(strfind(fc{ii},'# TF E1 (ksi)'))
```

```
                fc{ii+1} = sprintf('E1TF = %.5E',E1TF);
            elseif ~isempty(strfind(fc{ii},'# TF E2 (ksi)'))
                fc{ii+1} = sprintf('E2TF = %.5E',E2TF);
            elseif ~isempty(strfind(fc{ii},'# TF Poissons'))
                fc{ii+1} = sprintf('nuTF = %.5E',nuTF);
            elseif ~isempty(strfind(fc{ii},'# TF G (ksi)'))
                fc{ii+1} = sprintf('GTF = %.5E',GTF);
            elseif ~isempty(strfind(fc{ii},'# TF Thickness (in)'))
                fc{ii+1} = sprintf('tTF = %.5E',tTF);
            elseif ~isempty(strfind(fc{ii},'# Concrete E (ksi)'))
                fc{ii+1} = sprintf('Ec = %.5E',Ec);
            elseif ~isempty(strfind(fc{ii},'# Concrete E Cracked (ksi)'))
                fc{ii+1} = sprintf('Ec_cr = %.5E',Ec_cr);
            elseif ~isempty(strfind(fc{ii},'# Concrete Thickness (in)'))
                fc{ii+1} = sprintf('tc = %.5E',tc);
            elseif ~isempty(strfind(fc{ii},'# Mesh size (in)'))
                fc{ii+1} = sprintf('mshsize = %.5E',mesh_size);
            elseif ~isempty(strfind(fc{ii},'# Fraction of Girder Sampled for Max↙
moment'))
                fc{ii+1} = sprintf('L = %.5E',L);
            elseif ~isempty(strfind(fc{ii},'# Girder Elastic Modulus (ksi)'))
                fc{ii+1} = sprintf('Eg = %.5E',Eg);
            elseif ~isempty(strfind(fc{ii},'# Girder centroid (in)'))
                fc{ii+1} = sprintf('ybar = %.5E',ybar);
            elseif ~isempty(strfind(fc{ii},'# Girder Shear Modulus'))
                fc{ii+1} = sprintf('Gg = %.5E',Gg);
            elseif ~isempty(strfind(fc{ii},'# Girder Area (in2)'))
                fc{ii+1} = sprintf('A = %.5E',A);
            elseif ~isempty(strfind(fc{ii},'# Girder Ixx'))
                fc{ii+1} = sprintf('Ixx = %.5E',Ixx);
            elseif ~isempty(strfind(fc{ii},'# Girder Ixy'))
                fc{ii+1} = sprintf('Ixy = %.5E',Ixy);
            elseif ~isempty(strfind(fc{ii},'# Girder Iyy'))
                fc{ii+1} = sprintf('Iyy = %.5E',Iyy);
            elseif ~isempty(strfind(fc{ii},'# Girder J'))
                fc{ii+1} = sprintf('Izz = %.5E',J);
            elseif ~isempty(strfind(fc{ii},'# Skew Angle'))
                fc{ii+1} = sprintf('thetad = %.5E',theta);
            elseif ~isempty(strfind(fc{ii},'#Available Lane Width'))
                fc{ii+1} = sprintf('lanewidth = %.5E',lanewidth);
            elseif ~isempty(strfind(fc{ii},'# Truck 1'))
                fc{ii+1} = sprintf('lane1 = %.5E',lane1);
                fc{ii+2} = sprintf('rear1 = %.5E',rear1);
                fc{ii+3} = sprintf('front1 = %.5E',front1);
                fc{ii+4} = sprintf('tan1 = %.5E',tan1);
            elseif ~isempty(strfind(fc{ii},'# Truck 2'))
                fc{ii+1} = sprintf('lane2 = %.5E',lane2);
                fc{ii+2} = sprintf('rear2 = %.5E',rear2);
                fc{ii+3} = sprintf('front2 = %.5E',front2);
                fc{ii+4} = sprintf('tan2 = %.5E',tan2);
            elseif ~isempty(strfind(fc{ii},'# Variables For Transverse Placing of↙
```

```
Trucks and Uniform Lane Loads'))
                    fc{ii+1} = sprintf('a = %.5E',le1);
                    fc{ii+2} = sprintf('b = %.5E',t1);
                    fc{ii+3} = sprintf('c = %.5E',t2);
                    fc{ii+4} = sprintf('d = %.5E',ln1);
                    fc{ii+5} = sprintf('e = %.5E',le2);


                end
            end

            newcell = fc;



            % Reopen ".fid" file, erase content for overwriting, then rewrite with
            % updated file contained in "fc" (NOTE: if this process is halted before
            % the complete, new ".py" file is written, ABAQUS will throw an error)
            fid = fopen(inpfile,'w');
            for ii = 1:length(newcell)+1
                if newcell{ii+1} == -1
                    fprintf(fid,'%s',newcell{ii});
                    break
                else
                    fprintf(fid,'%s\r\n',newcell{ii});
                end
            end

            % Close file
            fclose(fid);

            %% Run Analysis %%


            delete('G1M.csv')
            delete('G2M.csv')
            delete('G3M.csv')
            delete('G4M.csv')
            delete('G5M.csv')
            delete('G6M.csv')
            % delete('Sideplus.csv')
            % delete('Sideminus.csv')
            delete('Rxn.csv')
            delete('RxnA.csv')
            % Write the console command to run the .py script without opening an
            % instance of the ABAQUS GUI
            cmd_str = sprintf('abaqus cae noGUI=%s',file);
            %cmd_str = sprintf('abaqus cae script=%s',file);
            % Run the above command through MATLAB's console shell
            try
                try
```

```
status = system(cmd_str);
X = (-5*span*L/10:span*L/10:5*span*L/10);
xq=(X(1):span/100:X(end));
G1 = readmatrix('G1M.csv','Range','5:7');
G1(isnan(G1)) = [];
G1(G1==0) = [];
G1 = G1(2:end);
G1(G1 > 1.0) = [];
y1 = spline(X,G1,xq);
eps1 = max(y1);

G2 = readmatrix('G2M.csv','Range','5:7');

G2(isnan(G2)) = [];
G2(G2==0) = [];
G2(G2 > 1.0) = [];
G2 = G2(2:end);

y2 = spline(X,G2,xq);
eps2 = max(y2);

G3 = readmatrix('G3M.csv','Range','5:7');
G3(isnan(G3)) = [];
G3(G3==0) = [];
G3(G3 > 1.0) = [];
G3 = G3(2:end);

y3 = spline(X,G3,xq);
eps3 = max(y3);

G4 = readmatrix('G4M.csv','Range','5:7');
G4(isnan(G4)) = [];
G4(G4==0) = [];
G4(G4 > 1.0) = [];
G4 = G4(2:end);

y4 = spline(X,G4,xq);
eps4 = max(y4);
longs = [eps1,eps2,eps3,eps4];
if Ng == 5
    G5 = readmatrix('G5M.csv','Range','5:7');
    G5(isnan(G5)) = [];
    G5(G5==0) = [];
    G5(G5 > 1.0) = [];
    G5 = G5(2:end);
    y5 = spline(X,G5,xq);
    eps5 = max(y5);
    longs = [longs,eps5];
elseif Ng == 6
    G5 = readmatrix('G5M.csv','Range','5:7');
    G5(isnan(G5)) = [];
```

```
        G5(G5==0) = [];
        G5(G5 > 1.0) = [];
        G5 = G5(2:end);
        y5 = spline(X,G5,xq);
        eps5 = max(y5);
        G6 = readmatrix('G6M.csv','Range','5:7');
        G6(isnan(G6)) = [];
        G6(G6==0) = [];
        G6(G6 > 1.0) = [];
        G6 = G6(2:end);
        y6 = spline(X,G6,xq);
        eps6 = max(y6);
        longs = [longs,eps5,eps6];
    end
    rx = readmatrix('Rxn.csv','Delimiter',' ');
    rx = rx(end,:);
    rx(isnan(rx)) = [];

    % Eliminate zero padding
    rx(rx == 0) = [];
    % Calculate engineering shear strains
    rxnsit = rx(2:end);

    rxA = readmatrix('RxnA.csv','Delimiter',' ');
    rxA = rxA(end,:);
    rxA(isnan(rxA)) = [];
    % Eliminate zero padding
    rxA(rxA == 0) = [];
    % Calculate engineering shear strains
    rxnsAit = rxA(2:end);


catch
    status = system(cmd_str);
    X = (-5*span*L/10:span*L/10:5*span*L/10);
    xq=(X(1):span/100:X(end));
    G1 = readmatrix('G1M.csv','Range','5:7');
    G1(isnan(G1)) = [];
    G1(G1==0) = [];
    G1 = G1(2:end);
    G1(G1 > 1.0) = [];
    y1 = spline(X,G1,xq);
    eps1 = max(y1);

    G2 = readmatrix('G2M.csv','Range','5:7');

    G2(isnan(G2)) = [];
    G2(G2==0) = [];
    G2(G2 > 1.0) = [];
    G2 = G2(2:end);
```

```
y2 = spline(X,G2,xq);
eps2 = max(y2);

G3 = readmatrix('G3M.csv','Range','5:7');
G3(isnan(G3)) = [];
G3(G3==0) = [];
G3(G3 > 1.0) = [];
G3 = G3(2:end);

y3 = spline(X,G3,xq);
eps3 = max(y3);

G4 = readmatrix('G4M.csv','Range','5:7');
G4(isnan(G4)) = [];
G4(G4==0) = [];
G4(G4 > 1.0) = [];
G4 = G4(2:end);

y4 = spline(X,G4,xq);
eps4 = max(y4);
longs = [eps1,eps2,eps3,eps4];
if Ng == 5
    G5 = readmatrix('G5M.csv','Range','5:7');
    G5(isnan(G5)) = [];
    G5(G5==0) = [];
    G5(G5 > 1.0) = [];
    G5 = G5(2:end);
    y5 = spline(X,G5,xq);
    eps5 = max(y5);
    longs = [longs,eps5];
elseif Ng == 6
    G5 = readmatrix('G5M.csv','Range','5:7');
    G5(isnan(G5)) = [];
    G5(G5==0) = [];
    G5(G5 > 1.0) = [];
    G5 = G5(2:end);
    y5 = spline(X,G5,xq);
    eps5 = max(y5);
    G6 = readmatrix('G6M.csv','Range','5:7');
    G6(isnan(G6)) = [];
    G6(G6==0) = [];
    G6(G6 > 1.0) = [];
    G6 = G6(2:end);
    y6 = spline(X,G6,xq);
    eps6 = max(y6);
    longs = [longs,eps5,eps6];
end
rx = readmatrix('Rxn.csv','Delimiter',' ');
rx = rx(end,:);
rx(isnan(rx)) = [];
```

```
                    % Eliminate zero padding
                    rx(rx == 0) = [];
                    % Calculate engineering shear strains
                    rxnsit = rx(2:end);

                    rxA = readmatrix('RxnA.csv','Delimiter',' ');
                    rxA = rxA(end,:);
                    rxA(isnan(rxA)) = [];
                    % Eliminate zero padding
                    rxA(rxA == 0) = [];
                    % Calculate engineering shear strains
                    rxnsAit = rxA(2:end);
                end
            catch
                dout =  dist(i);
                Longout=longpos(1);
                save('Errout','dout','Longout','inputs');
            end

            %% Read Output Files %%

            for c=1:length(longs)
                long(c)=longs(c)*yc/(yc-ybar);
            end
            longstrains=[longstrains; long];
            rxns=[rxns;rxnsit];
            rxnsA=[rxnsA;rxnsAit];

            %J_used(m)=Jvec(j);

            m=m+1;
            %end
        end
    end
end
m=m-1;

% Return to initialization directory
cd(starter)
```

```
function [M,MDF] = getMDFs(inputs,girder,flexstrains,lns)
% 2022 JP
% This function finds the moments and MDFs using girder properties and
% output longitudinal strains from moment models
Ng=inputs(1,5);
%% calculate MDF and moments from the strains

SEint=girder.SE.SEint;
SEx=girder.SE.SEx;
M=zeros(1,Ng);
MDF=zeros(1,Ng);
for i=2:Ng-1
    M(1,i)=flexstrains(1,i)*SEint;

end
M(1,1)=flexstrains(1,1)*SEx;
M(1,Ng)=flexstrains(1,Ng)*SEx;

Mtot=sum(M);
if lns == 2
    X=2;
else
    X= 1.2;
end

for i=2:Ng-1
 MDF(1,i)=X*M(1,i)/Mtot;
end
MDF(1,1)=X*M(1,1)/Mtot;
MDF(1,Ng)=X*M(1,Ng)/Mtot;
end
```

C.2 Shear Parametric Model

4/11/24 2:47 PM C:\Users\JonPinkham...\Girderscriptshear.m 1 of 3

```
%% This script runs the varying parameters that are desired to be inspacted and give the
output of girder designs and the results of Fe analysis


%% Ranges for Parameters
tic
L= [60 80];
Ld=16:20;
Ng= 5;
tdeck=8;
theta=0;
p=[];
for k=1:length(theta)
    for i=1:length(L)
        for j=1:length(Ld)
            for m=1:length(Ng)
                for n=1:length(tdeck)
                    [parameters] = parameter(L(i),Ld(j),Ng(m),theta(k),tdeck(n));
                    p=[p ; parameters];
                end
            end
        end
    end
end
%% standrd Bridge [60 18 6 8 5 0 3];
% # of lanes loaded
lns=2;
% Load case 1= HL-93 2= Tandem
%LC=[1];
y=[4]; % Constant 5 transverse locations run across the bridge for single and two lane
for t=1
for i=1:size(p,1)
    inputs=p(i,:);
    girder(i)= buildgirdershear(inputs);
    [shearstrains,rxns,m,dist,longpos] = CT_Parameter_Shear(inputs,girder(i),40,y,lns
(t));
    for j=1:m
    VDFs(j,:)=GetVDFs(inputs,rxns(j,:),lns(t));
    end
    Ng=inputs(1,5);
    VDFint1=VDFs(:,2:Ng-1);
    VDFext1=[VDFs(:,1),VDFs(:,Ng)];
    rint1=rxns(:,2:Ng-1);
    rext1=[rxns(:,1),rxns(:,Ng)];


    VDFinttr=max(VDFint1(1:m/2,:));
    VDFexttr=max(VDFext1(1:m/2,:));
    rinttr=max(rint1(1:m/2,:));
    rexttr=max(rext1(1:m/2,:));
```

```
    VDFinttan=max(VDFint1(m/2+1:m,:));
    VDFexttan=max(VDFext1(m/2+1:m,:));
    rinttan=max(rint1(m/2+1:m,:));
    rexttan=max(rext1(m/2+1:m,:));

    VDFint2=[max(VDFinttr),max(VDFinttan)];
    VDFext2=[max(VDFexttr),max(VDFexttan)];
    rint2=[max(rinttr),max(rinttan)];
    rext2=[max(rexttr),max(rexttan)];

    VDFint(i,t)=max(VDFint2);
    if VDFint(i,t)== max(VDFinttr)
        govint={'truck'};
    else
        govint={'tandem'};
    end
    [x,y]=find(VDFs==VDFint(i,t));
    strainsint=shearstrains(x,2*y-1:2*y);
    strain1=max(abs(strainsint));
    ratioint(i,t)=strain1*2/(strainsint(1)-strainsint(2));


    VDFext(i,t)=max(VDFext2);
    if VDFext(i,t)== max(VDFexttr)
        govext={'truck'};
    else
        govext={'tandem'};
    end
    [x,y]=find(VDFs==VDFext(i,t));
    strainsext=shearstrains(x,2*y-1:2*y);
    strain1=max(abs(strainsext));
    ratioext(i,t)=strain1*2/(strainsext(1)-strainsext(2));
    rint(i,t)=max(rint2);
    rext(i,t)=max(rext2);
    filename=  'C:\Users\JonPinkham\OneDrive - University of Maine
System\Desktop\ShearParametric\Results.xlsx'; %'C:\Users\JonPinkham\OneDrive - University
of Maine System\Documents\Parametric studies\Results.xlsx';
    runs=size(p,1);
    xlRange=strcat('A',num2str(93+i));
    sheet=3;

%% Build the output vector
    td=inputs(1,4); % deck thickness
    dfrp=girder(i).dfrp;
    ync=girder(i).girder.y; % NA of girder itself
    Inc=girder(i).girder.I11; % NC moment of inertia for girder section
    A=girder(i).girder.A; % girder cross sectional area
    eg=dfrp+td/2-ync; % distance between center of gravities of deck and basic beam
    Kg=Inc+A*(eg^2);
    ohang=inputs(1,7); % overhang ft.
    Lw=girder(i).w.Lw; % length of web (inches)
```

```
    bbf=girder(i).bf.bbf; % width of bottom flange (inches)
    tw=girder(i).w.tw; % web thickness (inches)
    de= ohang-((20+bbf/2+Lw*sind(5)-tw/2)/12); % distance from center of web at top of girder to curb inside edge (ft)
    Twg=girder(i).girder.Twg;

    A=[inputs(1,1), inputs(1,2), inputs(1,3), inputs(1,4), inputs(1,5), inputs(1,6), inputs(1,7), Kg, de, dfrp,VDFint(i,t),VDFext(i,t), rint(i,t), rext(i,t),ratioint(i,t), ratioext(i,t), bbf, Twg, govint, govext];
    xlswrite(filename,A,sheet,xlRange)
%
%
  clearvars  VDFint1 VDFint2 VDFext1 VDFext2 VDFs
  clearvars rint1 rext1 rint2 rext2 shearstrains strainsint strainext
end
end
time5=toc;
```

```
function [shearstr,rxns,m,dist,longpos] = CT_Parameter_Shear(inputs,girder,x,y,lns)
% This function submits parameters to ABAQUS for analysis. The purpose of
% this analysis is to generate results for use in determining CT girder
% distribution factors.

% Schanck 2022
% Pinkham 2023 modifications
%% Notes
% These setup files currently not fully capable of performing skewed bridge
% analysis straight bridge only.

%% Initialization %%

% These variables are changed to alter various dimensional parameters in
% the model

% Span length (in)
span = inputs(1,1)*12;
% Girder spacing (in)
spacing = inputs(3)*12;
% Girder depth (in)
depth = girder.dfrp;
% Offset to Account for splay angle (in)
splay = girder.dfrp*tand(5);
%Number of girders
Ng=inputs(1,5);
%Overhang
overhang=inputs(7)*12;
%Total deck width
Bbridge=spacing*(Ng-1)+2*overhang;
% Minimum transverse offset lane load can start from the edge of curb
% note lane can start right at edge but the truck inside the lane can not
% get any closer than 24 inches to the lane edge
Mintransverse=0;
%Maximum transverse distance from outer edge that the outside load path can
%start
Maxtransverse=Bbridge-(24*12)-40;
%stepsize for transverse loading
center=(Maxtransverse+Mintransverse)/2-1.0;
stepa=(center-Mintransverse)/(y/2);
stepb=(Maxtransverse-center)/(y/2);
stepo=(center-Mintransverse)/(y);

% Skew Angle (Degrees)
theta = inputs(1,6);

% Distance from edge of imaginery curb (20 in) to outside of first lane load (in)
if theta == 0 % Take advantage of symmetry only run load on one side
    dist = [Mintransverse:stepo:center];
else % for a skewed bridge run loadings all the way across
    dist=[Mintransverse:stepa:center center+1 center+stepb:stepb:Maxtransverse];
```

```
end

% Bottom flange width (in)
BF = girder.bf.bbf;
% Top flange width (in)
TF = girder.tf.btf;


% BF E1 (ksi)
E1BF = girder.bf.Ex;
% BF E2 (ksi)
E2BF = girder.bf.Ey;
% BF Poissons
nuBF = girder.bf.n;
% BF G (ksi)
GBF = girder.bf.G;
% BF Thickness (in)
tBF = girder.bf.tbf;

% Web E1 (ksi)
E1W = girder.w.Ex;
% Web E2 (ksi)
E2W = girder.w.Ey;
% Web Poissons
nuW = girder.w.n;
% Web G (ksi)
GW = girder.w.G;
% Web Thickness (in)
tW = girder.w.tw;

%% Web without core properties constant except thickness, assumed always +-45 GFRP just↙
with varying thickness
% Radial E1 (ksi)
E1Wt = 2228.4;
% Radial E2 (ksi)
E2Wt = 2228.4;
% Radial Poissons
nuWt = 0.447;
% Radial G (ksi)
GWt = 1.5501e3;
% Radial Thickness (in)
tWt = girder.rad.tw;

% TF E1 (ksi)
E1TF = girder.tf.Ex;
% TF E2 (ksi)
E2TF = girder.tf.Ey;
% TF Poissons
nuTF = girder.tf.n;
% TF G (ksi)
GTF = girder.tf.G;
```

```
% TF Thickness (in)
tTF = girder.tf.ttf;


%%%%%%%%%%%%%%%%%% EDITED TO INCORPORATE CRACKED DECK %%%%%%%%%%%%
% Concrete Thickness (in)
tc = inputs(4);
% Concrete E (ksi)
Ec = 3640;
% Concrete E CRACKED (ksi)
if tc== 7
Ec_cr = 772;
elseif tc==8
Ec_cr = 742;
elseif tc==9
Ec_cr = 711;
elseif tc==10
Ec_cr = 680;
end
%%%%%%%%%%%%%%%%%%%%%%%%%%%%%%%%%%%%%%%%%%%%%%%%%%%%%%%%%%%%%%%%%%%%%%%



% Mesh size for Girders and deck (in)
%mesh_size = depth/x;
%mesh_size = x;
mesh_size = span/x;

LC=[1 2]; % two loading conditions 1 is HL-93 truck; 2 is tandem axles
m=1; %counter
shearstr=[];
    rxns=[];

for t=1:2

longpos=depth;

    for l=1:length(longpos)
        for i=1:length(dist)

            %Logic for if the HL-93 truck will completely fit on bridge or not
            effectivelength=346+92*tand(theta)+longpos(l);
            if effectivelength<span
                fulltruck=1; %true full truck will fit
            else
                fulltruck=0; % false won't fit use two rear axles only
            end

            if ((Ng-1)*spacing+2*overhang)/2 > 144
                lanewidth = 120;
            else
```

```
        lanewidth = ((Ng-1)*spacing+2*overhang)/2-24;
    end

    % Truck Loads zeroed for appropriate load scenario
    if lns == 2
        lane2 = 4.444e-4;
        rear2 = 0.1064;
        front2 = .0266;
        tan2 = 0.0831;
        lane1 = 4.444e-4;
        rear1 = 0.1064;
        front1 = .0266;
        tan1 = 0.0831;
    elseif lns == 1 && dist(i)<=center+1
        lane2 =1e-15;
        rear2 = 1e-15;
        front2 = 1e-15;
        tan2 = 1e-15;
        lane1 = 4.444e-4;
        rear1 = 0.1064;
        front1 = .0266;
        tan1 = 0.0831;
    elseif lns == 1 && dist(i)>center+1
        lane1 =1e-15;
        rear1 = 1e-15;
        front1 = 1e-15;
        tan1 = 1e-15;
        lane2 = 4.444e-4;
        rear2 = 0.1064;
        front2 = .0266;
        tan2 = 0.0831;
    end

    ln1= dist(i); % Value of d for input files offset from curb edge to start↙
firts lane load
    le1=24; % value for a (in) to start the uniform 10 ft load lane 1
    t1=48; % value for b (in) to start position of truck 1 in lane 1
    t2=24; % value for c (in) to start positions of truck 2 in lane 2
    le2=0; % value for e (in) to start the uniform 10 ft load lane 2

    if ln1 == Mintransverse
        le1=0; % value for a (in) to start the uniform 10 ft load lane 1
        t1=24; % value for b (in) to start position of truck 1 in lane 1
        t2=24; % value for c (in) to start positions of truck 2 in lane 2
        le2=0; % value for e (in) to start the uniform 10 ft load lane 2
    elseif ln1 == Maxtransverse
        le2=24; % value for e (in) to start the uniform 10 ft load lane 2
        le1=24; % value for a (in) to start the uniform 10 ft load lane 1
        t1=48; % value for b (in) to start position of truck 1 in lane 1
        t2=48; % value for c (in) to start positions of truck 2 in lane 2
    end
```

```
            % Record the initiation directory
            starter = pwd;

            if Ng == 5 && LC(t) == 1 && fulltruck==1
                inploc = 'C:\Users\JonPinkham\Desktop\ShearParametric';
                inpfile = 'C:\Users\JonPinkham\Desktop\ShearParametric\setup5.py';
                file = 'setup5.py';
            elseif Ng == 6 && LC(t) == 1 && fulltruck==1
                inploc = 'C:\Users\JonPinkham\Desktop\ShearParametric';
                inpfile = 'C:\Users\JonPinkham\Desktop\ShearParametric\setup6.py';
                file = 'setup6.py';

                %Should not be any issues with truck fitting on a bridge as
                %long as no skew and over 40 ft and do not exceed a
                %longitudinal position of 134 inches which is quite far out
                % from the abutment and not a maximized shear position most
                % likely.
%             elseif Ng == 5 && LC(t) == 1 && fulltruck==0
%                 inploc = 'C:\Users\JonPinkham\OneDrive - University of Maine↙
System\Documents\MATLAB\Girder Design';
%                 inpfile = 'C:\Users\JonPinkham\OneDrive - University of Maine↙
System\Documents\MATLAB\Girder Design\Setup_4_Skew_Reartruck.py';
%                 file = 'Setup_4_Skew_Reartruck.py';
%             elseif Ng == 6 && LC(t) == 1 && fulltruck==0
%                 inploc = 'C:\Users\JonPinkham\OneDrive - University of Maine↙
System\Documents\MATLAB\Girder Design';
%                 inpfile = 'C:\Users\JonPinkham\OneDrive - University of Maine↙
System\Documents\MATLAB\Girder Design\Setup_5_Skew_Reartruck.py';
%                 file = 'Setup_5_Skew_Reartruck.py';
            end


            if Ng == 5 && LC(t) == 2
                inploc = 'C:\Users\JonPinkham\Desktop\ShearParametric';
                inpfile = 'C:\Users\JonPinkham\Desktop\ShearParametric\setup5_tan.py';
                file = 'setup5_tan.py';
            elseif Ng == 6 && LC(t) == 2
                inploc = 'C:\Users\JonPinkham\Desktop\ShearParametric';
                inpfile = 'C:\Users\JonPinkham\Desktop\ShearParametric\setup6_tan.py';
                file = 'setup6_tan.py';

            end

            %% Alter Python Script %%

            % Open Python script
            fid = fopen(inpfile,'r+');
            % Read first line
            tline = fgetl(fid);
```

```
% Copy all lines of the ".py" file to a cell structure named "fc" (file
% content)
ii = 1;
fc{ii} = tline;
while ischar(tline)
    ii = ii+1;
    tline = fgetl(fid);
    fc{ii} = tline;
end
% Close ".py" file
fclose(fid);


% Search for unique keyword phrase coresponding to a variable parameter in
% the ".py" file and update the associated value
for ii = 1:length(fc)
    if ~isempty(strfind(fc{ii},'# Distance between'))
        fc{ii+1} = sprintf('dist = %.5E',dist(i));
    elseif ~isempty(strfind(fc{ii},'# Span length'))
        fc{ii+1} = sprintf('span = %.5E',span);
    elseif ~isempty(strfind(fc{ii},'# Girder spacing'))
        fc{ii+1} = sprintf('spacing = %.5E',spacing);
    elseif ~isempty(strfind(fc{ii},'# Girder Depth'))
        fc{ii+1} = sprintf('depth = %.5E',depth);
    elseif ~isempty(strfind(fc{ii},'# Offset to Account for splay angle↙
(in)'))
        fc{ii+1} = sprintf('splay = %.5E',splay);
    elseif ~isempty(strfind(fc{ii},'# Deck overhang'))
        fc{ii+1} = sprintf('OH = %.5E',overhang);
    elseif ~isempty(strfind(fc{ii},'# Bottom Flange Width'))
        fc{ii+1} = sprintf('BF = %.5E',BF);
    elseif ~isempty(strfind(fc{ii},'# Top Flange Width'))
        fc{ii+1} = sprintf('TF = %.5E',TF);
    elseif ~isempty(strfind(fc{ii},'# Longitudinal position'))
        fc{ii+1} = sprintf('Zpos = %.5E',longpos(l));


    elseif ~isempty(strfind(fc{ii},'# BF E1 (ksi)'))
        fc{ii+1} = sprintf('E1BF = %.5E',E1BF);
    elseif ~isempty(strfind(fc{ii},'# BF E2 (ksi)'))
        fc{ii+1} = sprintf('E2BF = %.5E',E2BF);
    elseif ~isempty(strfind(fc{ii},'# BF Poissons'))
        fc{ii+1} = sprintf('nuBF = %.5E',nuBF);
    elseif ~isempty(strfind(fc{ii},'# BF G (ksi)'))
        fc{ii+1} = sprintf('GBF = %.5E',GBF);
    elseif ~isempty(strfind(fc{ii},'# BF Thickness (in)'))
        fc{ii+1} = sprintf('tBF = %.5E',tBF);
    elseif ~isempty(strfind(fc{ii},'# Web E1 (ksi)'))
        fc{ii+1} = sprintf('E1W = %.5E',E1W);
    elseif ~isempty(strfind(fc{ii},'# Web E2 (ksi)'))
        fc{ii+1} = sprintf('E2W = %.5E',E2W);
```

```
elseif ~isempty(strfind(fc{ii},'# Web Poissons'))
    fc{ii+1} = sprintf('nuW = %.5E',nuW);
elseif ~isempty(strfind(fc{ii},'# Web G (ksi)'))
    fc{ii+1} = sprintf('GW = %.5E',GW);
elseif ~isempty(strfind(fc{ii},'# Web Thickness (in)'))
    fc{ii+1} = sprintf('tW = %.5E',tW);

elseif ~isempty(strfind(fc{ii},'# Radial E1'))
    fc{ii+1} = sprintf('E1Wt = %.5E',E1Wt);
elseif ~isempty(strfind(fc{ii},'# Radial E2'))
    fc{ii+1} = sprintf('E2Wt = %.5E',E2Wt);
elseif ~isempty(strfind(fc{ii},'# Radial nu'))
    fc{ii+1} = sprintf('nuWt = %.5E',nuWt);
elseif ~isempty(strfind(fc{ii},'# Radial G'))
    fc{ii+1} = sprintf('GWt = %.5E',GWt);
elseif ~isempty(strfind(fc{ii},'# Radial thickness'))
    fc{ii+1} = sprintf('tWt = %.5E',tWt);


elseif ~isempty(strfind(fc{ii},'# TF E1 (ksi)'))
    fc{ii+1} = sprintf('E1TF = %.5E',E1TF);
elseif ~isempty(strfind(fc{ii},'# TF E2 (ksi)'))
    fc{ii+1} = sprintf('E2TF = %.5E',E2TF);
elseif ~isempty(strfind(fc{ii},'# TF Poissons'))
    fc{ii+1} = sprintf('nuTF = %.5E',nuTF);
elseif ~isempty(strfind(fc{ii},'# TF G (ksi)'))
    fc{ii+1} = sprintf('GTF = %.5E',GTF);
elseif ~isempty(strfind(fc{ii},'# TF Thickness (in)'))
    fc{ii+1} = sprintf('tTF = %.5E',tTF);
elseif ~isempty(strfind(fc{ii},'# Concrete E (ksi)'))
    fc{ii+1} = sprintf('Ec = %.5E',Ec);
elseif ~isempty(strfind(fc{ii},'# Concrete E Cracked (ksi)'))
    fc{ii+1} = sprintf('Ec_cr = %.5E',Ec_cr);
elseif ~isempty(strfind(fc{ii},'# Concrete Thickness (in)'))
    fc{ii+1} = sprintf('tc = %.5E',tc);
elseif ~isempty(strfind(fc{ii},'# Mesh size (in)'))
    fc{ii+1} = sprintf('mshsize = %.5E',mesh_size);
elseif ~isempty(strfind(fc{ii},'# Skew Angle'))
    fc{ii+1} = sprintf('thetad = %.5E',theta);
elseif ~isempty(strfind(fc{ii},'#Available Lane Width'))
    fc{ii+1} = sprintf('lanewidth = %.5E',lanewidth);
elseif ~isempty(strfind(fc{ii},'# Truck 1'))
    fc{ii+1} = sprintf('lane1 = %.5E',lane1);
    fc{ii+2} = sprintf('rear1 = %.5E',rear1);
    fc{ii+3} = sprintf('front1 = %.5E',front1);
    fc{ii+4} = sprintf('tan1 = %.5E',tan1);
elseif ~isempty(strfind(fc{ii},'# Truck 2'))
    fc{ii+1} = sprintf('lane2 = %.5E',lane2);
    fc{ii+2} = sprintf('rear2 = %.5E',rear2);
    fc{ii+3} = sprintf('front2 = %.5E',front2);
    fc{ii+4} = sprintf('tan2 = %.5E',tan2);
```

```
            elseif ~isempty(strfind(fc{ii},'# Variables For Transverse Placing of
Trucks and Uniform Lane Loads'))
                fc{ii+1} = sprintf('a = %.5E',le1);
                fc{ii+2} = sprintf('b = %.5E',t1);
                fc{ii+3} = sprintf('c = %.5E',t2);
                fc{ii+4} = sprintf('d = %.5E',ln1);
                fc{ii+5} = sprintf('e = %.5E',le2);


            end
        end

        newcell = fc;


        % Reopen ".fid" file, erase content for overwriting, then rewrite with
        % updated file contained in "fc" (NOTE: if this process is halted before
        % the complete, new ".py" file is written, ABAQUS will throw an error)
        fid = fopen(inpfile,'w');
        for ii = 1:length(newcell)+1
            if newcell{ii+1} == -1
                fprintf(fid,'%s',newcell{ii});
                break
            else
                fprintf(fid,'%s\r\n',newcell{ii});
            end
        end

        % Close file
        fclose(fid);

        %% Run Analysis %%

        delete('gird1.csv')
        delete('gird2.csv')
        delete('gird3.csv')
        delete('gird4.csv')
        delete('gird5.csv')
        delete('gird6.csv')
        delete('shearstrains.csv')
        % Write the console command to run the .py script without opening an
        % instance of the ABAQUS GUI
        cmd_str = sprintf('abaqus cae noGUI=%s',file);
        %cmd_str = sprintf('abaqus cae script=%s',file); % Run this is
        %you want it to open model in ABAQUS GUI to check model
        % Run the above command through MATLAB's console shell
        try
            try
                status = system(cmd_str);

                G1 = readmatrix('gird1.csv');
```

```
G1(isnan(G1)) = [];
G1(G1==0) = [];
G1(G1==26)=[];
G1(G1==27)=[];
G1(G1==33)=[];
G1(G1==36)=[];
G1(G1==39)=[];
G1(G1==40)=[];
G1(G1==45)=[];
G1 = G1(2:end);
R1=sum(G1);

G2 = readmatrix('gird2.csv');

G2(isnan(G2)) = [];
G2(G2==0) = [];
G2(G2==26)=[];
G2(G2==27)=[];
G2(G2==33)=[];
G2(G2==36)=[];
G2(G2==39)=[];
G2(G2==40)=[];
G2(G2==45)=[];
G2 = G2(2:end);
R2=sum(G2);



G3 = readmatrix('gird3.csv');
G3(isnan(G3)) = [];
G3(G3==0) = [];
G3(G3==26)=[];
G3(G3==27)=[];
G3(G3==33)=[];
G3(G3==36)=[];
G3(G3==39)=[];
G3(G3==40)=[];
G3(G3==45)=[];
G3 = G3(2:end);
R3=sum(G3);

G4 = readmatrix('gird4.csv');
G4(isnan(G4)) = [];
G4(G4==0) = [];
G4(G4==26)=[];
G4(G4==27)=[];
G4(G4==33)=[];
G4(G4==36)=[];
G4(G4==39)=[];
G4(G4==40)=[];
G4(G4==45)=[];
```

```
G4 = G4(2:end);
R4=sum(G4);

rxnsit = [R1,R2,R3,R4];

if Ng == 5
    G5 = readmatrix('gird5.csv');
    G5(isnan(G5)) = [];
    G5(G5==0) = [];
    G5(G5==26)=[];
    G5(G5==27)=[];
    G5(G5==33)=[];
    G5(G5==36)=[];
    G5(G5==39)=[];
    G5(G5==40)=[];
    G5(G5==45)=[];
    G5 = G5(2:end);
    R5=sum(G5);
    rxnsit = [rxnsit,R5];
elseif Ng == 6
    G5 = readmatrix('gird5.csv');
    G5(isnan(G5)) = [];
    G5(G5==0) = [];
    G5(G5==26)=[];
    G5(G5==27)=[];
    G5(G5==33)=[];
    G5(G5==36)=[];
    G5(G5==39)=[];
    G5(G5==40)=[];
    G5(G5==45)=[];
    G5 = G5(2:end);
    R5=sum(G5);

    G6 = readmatrix('gird6.csv');
    G6(isnan(G6)) = [];
    G6(G6==0) = [];
    G6(G6==26)=[];
    G6(G6==27)=[];
    G6(G6==33)=[];
    G6(G6==36)=[];
    G6(G6==39)=[];
    G6(G6==40)=[];
    G6(G6==45)=[];
    G6 = G6(2:end);
    R6=sum(G6);

    rxnsit = [rxnsit,R5,R6];
end
shearstrainsit=readmatrix('shearstrains.csv','Range','5:7');
shearstrainsit(isnan(shearstrainsit))=[];
shearstrainsit(shearstrainsit==0)=[];
```

```
    shearstrainsit(shearstrainsit>=1)=[];

catch
    status = system(cmd_str);

     G1 = readmatrix('gird1.csv');
    G1(isnan(G1)) = [];
    G1(G1==0) = [];
    G1(G1==26)=[];
    G1(G1==27)=[];
    G1(G1==33)=[];
    G1(G1==36)=[];
    G1(G1==39)=[];
    G1(G1==40)=[];
    G1(G1==45)=[];
    G1 = G1(2:end);
    R1=sum(G1);

    G2 = readmatrix('gird2.csv');

    G2(isnan(G2)) = [];
    G2(G2==0) = [];
    G2(G2==26)=[];
    G2(G2==27)=[];
    G2(G2==33)=[];
    G2(G2==36)=[];
    G2(G2==39)=[];
    G2(G2==40)=[];
    G2(G2==45)=[];
    G2 = G2(2:end);
    R2=sum(G2);



    G3 = readmatrix('gird3.csv');
    G3(isnan(G3)) = [];
    G3(G3==0) = [];
    G3(G3==26)=[];
    G3(G3==27)=[];
    G3(G3==33)=[];
    G3(G3==36)=[];
    G3(G3==39)=[];
    G3(G3==40)=[];
    G3(G3==45)=[];
    G3 = G3(2:end);
    R3=sum(G3);

    G4 = readmatrix('gird4.csv');
    G4(isnan(G4)) = [];
    G4(G4==0) = [];
    G4(G4==26)=[];
```

```
G4(G4==27)=[];
G4(G4==33)=[];
G4(G4==36)=[];
G4(G4==39)=[];
G4(G4==40)=[];
G4(G4==45)=[];
G4 = G4(2:end);
R4=sum(G4);

rxnsit = [R1,R2,R3,R4];

if Ng == 5
    G5 = readmatrix('gird5.csv');
    G5(isnan(G5)) = [];
    G5(G5==0) = [];
    G5(G5==26)=[];
    G5(G5==27)=[];
    G5(G5==33)=[];
    G5(G5==36)=[];
    G5(G5==39)=[];
    G5(G5==40)=[];
    G5(G5==45)=[];
    G5 = G5(2:end);
    R5=sum(G5);
    rxnsit = [rxnsit,R5];
elseif Ng == 6
    G5 = readmatrix('gird5.csv');
    G5(isnan(G5)) = [];
    G5(G5==0) = [];
    G5(G5==26)=[];
    G5(G5==27)=[];
    G5(G5==33)=[];
    G5(G5==36)=[];
    G5(G5==39)=[];
    G5(G5==40)=[];
    G5(G5==45)=[];
    G5 = G5(2:end);
    R5=sum(G5);

    G6 = readmatrix('gird6.csv');
    G6(isnan(G6)) = [];
    G6(G6==0) = [];
    G6(G6==26)=[];
    G6(G6==27)=[];
    G6(G6==33)=[];
    G6(G6==36)=[];
    G6(G6==39)=[];
    G6(G6==40)=[];
    G6(G6==45)=[];
    G6 = G6(2:end);
    R6=sum(G6);
```

```
                    rxnsit = [rxnsit,R5,R6];
                end
                shearstrainsit=readmatrix('shearstrains.csv','Range','5:7');
                shearstrainsit(isnan(shearstrainsit))=[];
                shearstrainsit(shearstrainsit==0)=[];
                shearstrainsit(shearstrainsit>=1)=[];

            end
        catch
            dout =  dist(i);
            Longout=longpos(1);
            save('Errout','dout','Longout','inputs');
        end

        %% Read Output Files %%
        rxns=[rxns;rxnsit];
        shearstr=[shearstr;shearstrainsit];
        m=m+1;

    end
  end
end
m=m-1;

% Return to initialization directory
cd(starter)
```



```
function [VDF] = GetVDFs(inputs, rxns,lns)
%JP 2022 this function calculates the shear distribution factors for each
%girder on the end with maximized shear loading
Ng=inputs(1,5);
%% calculate VDF from the reactions
Rtot=sum(rxns);
if lns == 2
    X=2;
else
    X= 1.2;
end
VDF=zeros(1,Ng);
for i=2:Ng-1
    VDF(1,i)=X*rxns(1,i)/Rtot;
end
VDF(1,1)=X*rxns(1,1)/Rtot;
VDF(1,Ng)=X*rxns(1,Ng)/Rtot;
end
```

Transportation Infrastructure Durability Center
AT THE UNIVERSITY OF MAINE

35 Flagstaff Road
Orono, Maine 04469
tidc@maine.edu
207.581.4376

www.tidc-utc.org